Towards Modeling Phosphate Slurry Flow Using CFD technique

Marwane Elkarii

PSL UNIVERSITÉ PARIS

MOHAMMED VI POLYTECHNIC UNIVERSITY

THÈSE DE DOCTORAT

DE L'UNIVERSITÉ PSL

Préparée dans le cadre d'une cotutelle entre MINES Paris et l'Université Mohammed VI Polytechnique

Vers la modélisation d'un écoulement de pulpe de phosphate à l'aide de la technique CFD

Towards Modeling a Phosphate Slurry Flow Using CFD technique

Soutenue par

Marwane Elkarii

Le 07 Juillet 2023

École doctorale n°621

Ingénierie des Systèmes, Matériaux, Mécanique, Énergétique

Spécialité

Énergétique et Génie des Procédés

Composition du jury :

Zoubida Mghazli Professeure, Faculté des Sciences, Université Ibn Tofaïl, Maroc	*Présidente*
Jean-Philippe Passarello Professeur des universités, Université Sorbonne Paris Nord, France	*Rapporteur*
Mohammed Seaid Associate professor, Université de Durham, Royaume-Uni	*Rapporteur*
Radouan Boukharfane Professeur Assistant, Université Mohammed VI Polytechnique, Maroc	*Examinateur*
Saad Benjelloun Professeur Assistant, Université Mohammed VI Polytechnique, Maroc	*Co-directeur*
Chakib Bouallou Professeur, Mines Paris, France	*Directeur de thèse*

MINES PARIS | PSL

In memory of my dear father Elmostafa, I dedicate this thesis,
To you, Dad, with eternal love and gratitude,
I miss you more than words can express. Every step of this academic journey has reminded me of how proud you would have been of me. I so wished to share this precious moment with you, but unfortunately, destiny had other plans. Despite the bitterness of not being able to physically share this chapter of my life with you, I know you are always with me in spirit. I will strive to honor your memory by giving my best and pursuing my aspirations.
I miss you, dear Dad. I dedicate this thesis to your memory, hoping it reflects a fragment of the love and admiration I hold for you.
May God have mercy on your soul.
With all my love,
Your son Marwane.

Acknowledgment

I extend my deepest gratitude to my thesis advisor, Pr. Chakib Bouallou, for warmly welcoming me to the Energy Efficiency of Systems (CES) Center at MINES Paris. I am profoundly thankful for his patience in integrating me into his team, introducing me to the world of scientific research, and expertly guiding my work. His invaluable advice and unwavering support throughout this journey have been instrumental, and I am truly appreciative.

My gratitude also extends to my co-advisors for this thesis: (i) Saad Benjelloun, for his co-supervision and collaboration, and for welcoming me into his research team at the MSDA laboratory. I want to convey my deep appreciation for his assistance, guidance, and support, and (ii) Radouan Boukharfane, without whom this challenging journey would never have taken place. I am profoundly and sincerely thankful for all the invaluable contributions you've made through our countless lengthy discussions, your insightful advice, unwavering guidance, and the generous sharing of your profound knowledge and skills. Your steadfast support and availability during hard times have left an indelible mark on me. Thank you very much for accompanying me throughout these years, both professionally and personally.

I express my heartfelt gratitude to Mr. Jean Philippe Passarello and Mr. Mohammed Seaid for graciously agreeing to serve as reviewers for this thesis. I sincerely thank them for dedicating their time to meticulously review and correct the manuscript. Their participation in my defense jury is an esteemed honor. I am also grateful to Mrs. Zoubida Mghazli for agreeing to preside over the committee and for her thorough examination of the manuscript. Her presence is truly appreciated.

A very special thanks goes to my mother, Aicha, whose unwavering support has been my bedrock throughout this journey. Her constant presence, encouragement, and upliftment have been invaluable. Words cannot fully convey the depth of my gratitude or the immense significance she holds in my life. I extend my heartfelt appreciation for the boundless love and affection she has showered upon me. I hope that attaining my doctorate will bring her pride and immeasurable happiness.

To my beloved wife, Meryem, who fills my life with joy and has been a steadfast companion on my professional journey from its inception, I offer my special thanks. Her unwavering encouragement has been the driving force behind my

successful completion of this thesis. She has been my unwavering anchor, and I will forever cherish her role as the vital pillar of this project. Thank you for standing by me through uncertainties, healing wounds, and sharing moments of joy. This thesis belongs to you as much as it does to me.

I extend my sincere appreciation to my sisters Imane, Hanaa, Sara, and my brothers from different mothers, Amine, Reda, and Ali. Your presence, love, and unwavering moral support have been an immeasurable source of strength. I am deeply thankful for our unbreakable family bonds and the way we support each other in times of need.

My gratitude also goes out to my colleagues in the office, Ilias Bouchkira, Moussa Ziggaf, and Abdelouahed Ouardghi. Their warm welcome and countless enriching discussions have been invaluable. I offer heartfelt thanks to Amine Hamadi and Mustapha Bahari for the wonderful moments we've shared. I also acknowledge my friends and former classmates, Salah Benchra and Zaqaria Laaraich, for their unwavering support and encouragement across geographical distances. I am especially grateful to Mohamed Alaoui, whose unwavering support during my time in France has been indispensable. His consistent assistance on all fronts has been truly invaluable.

Finally, I wish to express my heartfelt gratitude to all those who have contributed to making my recent years enjoyable. May they find the sincere blessings and appreciation they deserve within these words.

Contents

List of Figures

List of Tables

Glossary of terms, Abbreviations, Acronyms and Symbols

Acronyms

ANN Artificial Neural Networks

ANOVA Analysis Of Variance

ASM Algebraic Slip Model

CFD Computational Fluid Dynamics

DEM Discrete Element Method

GSA Global Sensitivity Analysis

GUI Graphical User Interface

HDPE High Density Polyethylene

KTGF Kinetic Theory of Granular Flow

LAR Least Angle Regression

LDV Laser Doppler Velocimetry

LES Large Eddy Simulation

LMA Levenberg–Marquardt Algorithm

LOO Leave-One-Out

MAPE Mean Absolute Percentage Error

MC Monte Carlo

OCP Office Chérifien des Phosphates

PCA Principal Component Analysis

PCE Polynomial Chaos Expansion

PGD Proper Generalized Decomposition

PMS Pressure Monitoring Station

POD polynomial Orthogonal Decomposition

QOI Quantity of Interest

RANS Reynolds Average Navier Stockes

RNG Re-Normalisation Group

ROM Reduced Order Model

RSM Response Surface Methodologies

SA Sensitivity Analysis

SC Specularity Coefficient

SCADA Supervisory Control And Data Acquisition

SST Shear Stress Transport

TFM Two Fluid Model

UQ Uncertainty Quantification

VOF Volume of Fluid

VSD Vertical Sump Duty

Mathematical symbols

δ Angle of internal friction of the particle

λ_s Bulk viscosity

$\mathrm{k_{ls}}$ Conductivity of fluctuating energy

$\mu_{s,\mathrm{col}}$ Collisional shear viscosity

L_y Chord length

S_{coll} Collisional stokes number

$\mathcal{C}_d$ Drag coefficient

$\mathrm{C_{vd}}$ Delivered concentration

ε Dissipation rate

ϱ Density

l Distance

u_{dl} Deposition limit velocity

y^+ Dimensionless distance

μ_f Fluid viscosity

$\mu_{s,fr}$ Frictional shear viscosity

ϕ_f Fluid volume fraction

ϱ_f Fluid density

u_τ Friction velocity

u_f Fluid velocity

u_m Flow mixture velocity

f	Friction coefficient
Θ	Granular temperature
g	Gravitational acceleration
M_k^d	Generelized drag force
i_m	Hydraulic gradient
y_p	Height to center of the cell
ℓ	Inlet turbulence's length scale
cvi	In situ concentration
θ	Inclination
S_Λ	Integral scale Stokes number
M_p^d	Interfacial force
$\mu_{s,\mathrm{kin}}$	Kinetic shear viscosity
$\mathcal{C}_L$	Lift coefficient
M^{L}	Lift force
ϕ_{max}	Maximum packing fraction
$\tilde{\mu}_j$	Mass absorption
f_m	Mixture friction coefficient
S_λ	Micro-scale Stokes number
κ	Mean curvature of the interface
I_p	Moment of inertia of a particle
N_p	Number of particles
F_p	Net force on a particle
T_p	Net torque on a particle
Re_p	Particle Reynolds number
D	Pipe diameter
P	Porosity
p	Pressure
$\boldsymbol{\omega}_p$	Particle angular velocity
$\mathbf{u}_p$	Particle velocity
τ_p	Particle relaxation time
d_p	Particle diameter
m_p	Particle Mass
x_p	Particle location

$\frac{e}{D}$	Relative roughness
g_0	Radial distribution function
R^{eff}	Reynolds stress tensor
$\mathcal{P}$	Relative density
I	Radiation intensity
Re	Reynolds number
s_p	Relative density
e	Restitution coefficient
$\dot{M}_S$	Solid mass flow
$\mathcal{SC}$	Specularity coefficient
M^D	Standard drag force
μ_s	Solid/Shear viscosity
ϕ_s	Solid volume fraction/ Volume concentration
τ	Shear stress
ϱ_s	Solid density
u_s	Solid velocity
ω	Specific Dissipation Rate
σ	Surface tension
St	Stockes number
k	turbulent kinetic energy
ν_f^{eff}	Turbulent kinematic viscosity
t	Time
$\mathcal{C}_{vm}$	Virtual mass coefficient
u	Velocity
M^{VM}	Virtual mass force
V	Volume
c_w	Weight concentration

1 Introduction

Objectives:

In this opening chapter, we delve into the motivations, the scopes, and the methodologies utilized in this thesis. The chapter has been divided into three distinct sections. Section 1.1 is dedicated to exploring the engineering motivations behind the research and offering a comprehensive understanding of the work's overall context. Section 1.2 specifies the scientific goals that this thesis aims to achieve. Section 1.3 outlines the overall scope of the study as well as the organization of the thesis.

Contents

1.1 General context

The transportation of turbulent two-phase mixtures through pipelines is crucial to several modern industries. For example, pipe systems play a vital role in the chemical industry, where they transport energy products like petroleum and natural gas. In mining, pipelines (as shown in Fig. 1.1) are commonly used to transport mineral concentrates to processing plants. This study focuses specifically on the transportation of phosphate slurry within the phosphate mining industry and its value chain. Understanding the transport of this mixture is essential for optimizing the overall efficiency and profitability of the industry.

(a)

(b)

Figure 1.1: OCP phosphate slurry pipeline. (Photo credit: OCP, 21/01/2021)

In the context of the increasingly urgent need to reduce carbon emissions, pipelines are highly desirable for handling slurries in mining operations. Compared to railway transportation, pipelines are more efficient and environmentally friendly, with 77% fewer greenhouse gas emissions [Nimana et al., 2016]. Additionally, the enclosed nature of pipelines offers advantages for handling costly or even hazardous materials as they are less susceptible to theft or environmental depletion.

Slurry transport systems are becoming more and more popular in many industries due to their low maintenance cost, reliability, and round-the-clock availability of solid powder materials for both in-plant and long-distance transportation. Slurries are mixtures of solid particles in a carrier fluid, which can be either a

Newtonian or non-Newtonian liquid or a mixture of water and small particles that may behave like a non-Newtonian fluid. Water is typically the carrying liquid, but the carried solids can vary in size and weight. The interaction between the two phases (liquid and solid) significantly affects the behavior of the mixture flow in a conduit, making slurry transport in pipelines more complex than water transport. The particles have to be maintained in suspension, necessitating turbulent flow in the pipe. The physical properties of the slurry mixture depend on their composition. When the particle concentration of solids within the liquid is less than 10% by volume, the slurry can be considered a Newtonian fluid. However, when the solid concentration exceeds 10% of the liquid volume, it is generally considered a non-Newtonian fluid. Moreover, settling slurries tend to stratify in pipelines, resulting in solid sedimentation or even pipe clogging [Lahiri and Ghanta, 2010b]. Both pipeline resistance and transport safety are impacted by the degree of stratification. Therefore, to ensure a continuous and optimal flow and avoid such situations, the velocity of the liquid-solid mixture in the pipeline is kept much higher than the critical deposition velocity. However, there is always a trade-off between the slurry velocity and pressure drop in the system.

Accurate identification of slurry flow regimes and pressure drop prediction remains a challenge and must be controlled [Swamy et al., 2015]. Furthermore, in order to assess and measure the production and efficiency of the slurry transport system, it is crucial to consider other important factors such as the properties of the slurry and the characteristics of its flow. These aspects are discussed in detail in section 2.2. Compared to single-phase flows, slurry flows come with additional physical phenomena that make precise modeling challenging. Examples include the settling of slurry particles, which is difficult to describe and can cause unstable flow patterns, and the non-Newtonian viscous behavior of the carrier fluid if a large concentration of small slurry particles is dispersed. Therefore, a detailed understanding of the specific physical features of slurry transport is essential for designing proper slurry transport pipelines, and means of predicting the physics of the slurry flow are paramount for controlling the pipeline process.

1.2 Objectives

Slurry transport through pipelines has been extensively utilized in the mining and mineral processing industries for several decades. Numerous studies have been conducted since the 1960s to investigate various aspects of slurry transport. Researchers (e.g. [Pullum et al., 1992, Schaan et al., 2000b, Wilson et al., 2006]) in this field are interested in predicting pressure drop, determining the minimum velocity required for safe transport, and examining the influence of factors such as solids concentration, particle shape, and rheology on the pressure gradient. Also, there have been several studies to determine the power consumption required and sizing the slurry pumps to use, via experimental data [Schaan et al., 2000b], and

to optimize the pipeline design parameters (e.g. pipe diameter, percentage of fine particles), in order to minimize the capital cost and energy consumption. In slurry transport, maintaining a steady and optimal flow is crucial to prevent problems such as sedimentation of the solid phase and pipe clogging, which can affect the efficiency of the suspension transport. This requires effective pressure drop control, which is a key parameter in ensuring continuous and efficient transport of the slurry. Another important purpose of appropriate pressure drop management is to optimize the energy consumption of the pumps, which also translates to efficient slurry conveyance.

The energy efficiency of slurry flow in pipelines pertains to the capacity to transport slurry materials while minimizing energy consumption. This is particularly crucial in industries like mining and mineral processing, where slurry transportation can consume a considerable amount of energy. Numerous factors can influence the energy efficiency of slurry flows in pipelines, such as:

- Rheology: the rheological properties of the slurry, such as the viscosity and yield stress, can have a significant impact on the energy consumption of the flow.
- Particle size and concentration: the size and concentration of the solid particles in the slurry can affect the energy required to transport the slurry through the pipeline.
- Pipe geometry and roughness: the geometry of the pipeline and the roughness of the internal surface can affect the resistance to flow and the energy required to pump the slurry.
- Flow regime: the flow regime, such as laminar or turbulent, can affect the energy consumption of the flow.
- Flow rate: the flow rate of the slurry can affect the energy consumption of the flow.

There are several methods that can be used to improve the energy efficiency of slurry flows in pipelines. These include:

- Optimizing the slurry properties: The rheological properties of the slurry can be adjusted by changing the solids loading, particle size distribution, and adding additives such as polymers or surfactants. This can reduce the energy required for pumping and improve the overall efficiency of the system.
- Pipeline design: The diameter and length of the pipeline can have a significant impact on the energy required for pumping. By optimizing the pipeline design, such as reducing the number of bends and using larger diameter pipes, the energy consumption can be reduced.

- Pump selection: The choice of pump can also affect the energy efficiency of the slurry flow. Centrifugal pumps are commonly used, but positive displacement pumps may be more efficient in certain situations.
- Operating conditions: Adjusting the flow rate, pipeline pressure, and pump speed can also improve the energy efficiency of slurry flows in pipelines.
- Advanced control systems: Advanced control systems, such as model predictive control and simulation tools, can be used to optimize the operation of the slurry pipeline and reduce energy consumption.

It should be emphasized that the energy efficiency of slurry flows in pipelines is subject to significant variability based on the particular application. As for our thesis study, we are not able to make any modifications to the existing transport process, such as changing the pipe geometry, adding additives to the slurry, or altering the pumps. Therefore, the main emphasis of the research is placed on examining the physical properties of the slurry mixture and exploring how the hydrodynamic parameters influence slurry transport and energy efficiency utilizing simulation tools. Our goal is to identify the most effective means of optimizing these parameters, thereby enhancing the overall energy efficiency of the system.

The measure of the energy needed for transporting a slurry batch over a particular distance is known as specific energy consumption (SEC) and is an appropriate metric for quantifying transport efficiency. It exhibits a direct proportional relationship with the hydraulic gradient, which represents, in dimensionless form, the decrease in static pressure caused by friction in the slurry flow over a unit length of the pipe. The determination of power requirements for slurry flows is similar to that for water, but with additional consideration for the friction generated by the solids. Furthermore, non-Newtonian flow may occur if there is a high concentration of fine particles in the slurry. The specific energy consumption (SEC) for slurry flows is determined by considering the ratio of i_m and ϕ_s for solids of a certain relative density S_p. This ratio takes into account the density of the solid particles ϱ_s and the density of the carrier liquid, which in this case is water with a density of ϱ_w. The SEC is used as a measure of the energy required to move the slurry over a given distance and is affected by various factors such as the rheological properties of the slurry and the pipe geometry. The energy required to transport solids mass per unit length of pipe is given by [Wu et al., 2010] (in SI unit) (J/kg.m):

$$SEC = \frac{\mathcal{P}}{\dot{\mathcal{M}}_s \mathrm{L}} = \frac{\Delta p/L}{\phi_s \varrho_s}, \tag{1.1}$$

$\mathcal{P}$ is the power consumption (W), $\dot{M}_S$ is the solids mass flow (kg/s) and L is the pipe length (m), $\Delta P/\Delta L$ is the pressure gradient (kPa/m), ϕ_s is the volumetric solids concentration (v/v), and ϱ_s is the solids density (kg/m^3). The energy efficiency of a slurry pipeline is determined based on the properties of

the solid particles being transported since the primary purpose of the pipeline is to convey these solids, with the liquid phase serving only as a medium for their transportation. It is important to mention that in Eq. (1.1), ϕ_s represents the volumetric concentration of solids at the exit of the pipeline. It should be noted that this value may differ from the inline concentration of solids in the pipeline. It is clear that the energy efficiency of pipeline transport increases as the specific energy consumption (SEC) decreases. From the definition of SEC, it can be inferred that in order to achieve minimum energy consumption, the basic requirements include maintaining an optimal value for ϕ_s, along with operating the pipeline at a velocity near the deposition limit (u_{dl}). The optimal minimum for energy consumption can be determined by examining the pipe characteristic curve that displays the relationship between the flow velocity u_m and i_m at a constant slurry concentration (see Fig. 5.3c). Based on a compilation of 20 publications, Pullum et al. [1992] found that non-Newtonian viscous carrier fluids containing a high concentration of coarse particles, such as fly ash, require an increase in specific energy consumption (SEC). However, when the solids concentration is over 40% by volume, these fluids can be conveyed hydraulically at low velocities, with SECs comparable to or even lower than those required for conventional dilute solids phase systems. The results suggest that it is feasible to operate at substantially lower velocities compared to low viscosity Newtonian settling slurry systems, which require higher velocities to ensure that there is a safe margin above the deposition velocity.

Therefore, It is essential to conduct a thorough analysis of how the SEC is impacted by the slurry's characteristics to enhance efficiency and ensure operational safety. Moreover, having means to predict the physics of the slurry flow is paramount for the control of the transport process. This bring us to the primary challenges of the research to be conducted in the context of this thesis:

1. To explore various scenarios for minimizing energy consumption during slurry transport using a sensitivity analysis. The analysis will be carried out using stochastic spectral techniques based on Generalized Polynomial Chaos (gPC). This method will enable the identification of the different qualities and parameters that have a significant impact on pressure drop, and deducing the best combinations that lead to optimal energy efficiency.

2. Another challenge is to establish the groundwork for intelligent control of pressure drop in the transport process using computational fluid dynamics (CFD) simulation models. This system will enable optimal process operation, predict the evolution of critical parameters, and support operational decision-making. In fact, modern modeling strategies for industrial processes often utilize three-dimensional simulation techniques incorporating CFD and/or discrete element methods (DEM). These three-dimensional models are then integrated as surrogate models that can be utilized in operational simulation and monitoring tools, such as Decision Support Systems.

Response surface methodologies (RSM) are typically applied to construct polynomial surrogate models Rabhi et al. [2018]. However, recent works have shown that machine learning techniques, such as artificial neural networks (ANN), can also be employed Seong et al. [2020]. The current modeling approach involves developing a three-dimensional multi-phase CFD model for different types of pipe elements (horizontal, inclined), which are then used to construct surrogates that model pressure drop within each element. Such models can be utilized in dynamical models to monitor slurry pipe systems and conduct sizing studies to cover variations in operation conditions, such as inlet pressure and flow rate. This approach will first be applied to a single fluid flow to validate the approach of constructing a surrogate pressure drop model through three-dimensional numerical simulation, and then to slurry flows with solid volume fraction and particle diameters corresponding to the applications that are aimed to cover.

1.3 Dissertation outlines

The manuscript of this thesis is organized around the following chapters:

- In Chapter 1, the study's focus is introduced, the objectives and motivations are outlined, the logical organization of the dissertation is explained.
- Chapter 2 describe the problem addressed in this thesis, and provide the fundamental concepts and terminology of two-phase flows.
- In Chapter 3, we delve into the research approaches utilized to tackle the engineering problem and provide a detailed account of the key aspects of the Eulerian two-phase flow theory as applied to solid-fluid systems. The chapter provides an in-depth analysis and discussion of the application of this theory to the specific context of solid-fluid systems.
- Chapter 4 is dedicated to presenting the numerical simulation of solid-liquid flows through pipeline systems. The chapter includes details on the numerical methods employed, the model implementation process, and the validation of the model through comparison with experimental or empirical data.
- Chapter 5 illustrates the use of Polynomial Chaos Expansions (PCE) as a methodology to estimate the inherent uncertainty in the desired slurry flow. This chapter focuses on utilizing PCE to quantify and analyze the uncertainties associated with slurry flow, and specifically conducts a sensitivity analysis of flow energy efficiency. The chapter details the implementation of PCE and its application to the flow energy efficiency analysis, providing insights into the impact of uncertainties on the system performance.

- In Chapter 6, the utilization of the model to construct a CFD-based surrogate model for predicting pressure drop is demonstrated. The surrogate model's accuracy is evaluated through comparisons with experimental data from literature. Additionally, the same approach is employed to develop a surrogate model for predicting pressure drops of phosphate slurry in a real pipe-scale system. Experimental data from industry sensors is utilized to assess the performance of the newly developed model.

- Chapter 7 serves as the conclusion of the manuscript, providing a general summary of the work conducted and offering suggestions for future studies. Overall, it provides valuable insights and recommendations for further research in this field.

1
Introduction

Objectifs:

Ce chapitre d'introduction présente les motivations, la portée et les méthodologies de la thèse en cours. Le chapitre est divisé en trois sections. La section 1.1 met l'accent sur les motivations techniques et le contexte général du travail. La section 1.2 spécifie les objectifs scientifiques que cette thèse vise à atteindre. La section 1.3 décrit la portée globale de l'étude ainsi que l'organisation de la thèse.

1.1 Contexte général

Le transport de mélanges turbulents à deux phases, tels que la boue de phosphate, à travers des pipelines revêt une importance cruciale pour diverses industries. Cela inclut l'industrie chimique, où les pipelines sont utilisés pour transporter des produits énergétiques tels que le pétrole et le gaz naturel, ainsi que l'industrie minière, où les pipelines sont couramment utilisés pour transporter des concentrés minéraux vers les usines de traitement (comme illustré dans la Figure 1.1). Comprendre le transport de ce mélange est essentiel pour optimiser l'efficacité globale et la rentabilité de l'industrie.

(a) (b)

Figure 1.1: OCP phosphate slurry pipeline. Crédit photo : OCP, 21/01/2021

Dans le contexte de la nécessité croissante et urgente de réduire les émissions de carbone, les pipelines sont très souhaitables pour le transport de boues dans les opérations minières. Comparé au transport ferroviaire, les pipelines sont plus efficaces et respectueux de l'environnement, avec 77% d'émissions de gaz à effet de serre en moins [Nimana et al., 2016]. De plus, la nature fermée des pipelines offre des avantages pour la manipulation de matériaux coûteux ou même dangereux, car ils sont moins susceptibles de vol ou de dégradation environnementale.

Les systèmes de transport de boues deviennent de plus en plus populaires dans de nombreuses industries en raison de leur faible coût d'entretien, de leur fiabilité et de la disponibilité 24 heures sur 24 de matériaux solides en poudre pour le transport en usine et sur de longues distances. Les boues sont des mélanges de particules solides dans un liquide porteur, qui peut être soit un liquide newtonien ou non newtonien, ou un mélange d'eau et de petites particules qui peuvent se comporter comme un fluide non newtonien. L'eau est généralement le liquide porteur, mais les solides transportés peuvent varier en taille et en poids. L'interaction entre les deux phases (liquide et solide) affecte significativement le comportement de l'écoulement du mélange dans un conduit, rendant le transport de boues dans les pipelines plus complexe que le transport d'eau. Les particules doivent être maintenues en suspension, nécessitant un écoulement turbulent dans le tuyau.

Les propriétés physiques du mélange de boues dépendent de leur composition.

Lorsque la concentration en particules solides dans le liquide est inférieure à 10% en volume, la boue peut être considérée comme un fluide newtonien. Cependant, lorsque la concentration en solides dépasse 10% du volume du liquide, elle est généralement considérée comme un fluide non newtonien. De plus, les boues qui se déposent ont tendance à se stratifier dans les pipelines, ce qui entraîne la sédimentation des solides ou même l'obstruction du tuyau [Lahiri and Ghanta, 2010b]. Le degré de stratification affecte à la fois la résistance du pipeline et la sécurité du transport. Par conséquent, pour garantir un écoulement continu et optimal et éviter de telles situations, la vitesse du mélange liquide-solide dans le pipeline est maintenue beaucoup plus élevée que la vitesse critique de dépôt. Cependant, il y a toujours un compromis entre la vitesse de la boue et la perte de charge dans le système.

L'identification précise des régimes d'écoulement des boues et la prédiction de la perte de charge restent un défi et doivent être maîtrisées [Swamy et al., 2015]. De plus, d'autres quantités essentielles nécessaires pour évaluer et quantifier la production et l'efficacité du système de transport de boues incluent les propriétés de la boue et de l'écoulement de boue, qui sont présentées dans la section 2.2. Comparé aux écoulements monophasiques, les écoulements de boues présentent des phénomènes physiques supplémentaires qui rendent la modélisation précise difficile. Cela inclut le dépôt des particules de boue, qui est difficile à décrire et peut provoquer des schémas d'écoulement instables, ainsi que le comportement visqueux non newtonien du liquide porteur si une grande concentration de petites particules de boue est dispersée. Par conséquent, une compréhension détaillée des caractéristiques physiques spécifiques du transport de boues est essentielle pour concevoir des pipelines de transport de boues appropriés, et les moyens de prédire la physique de l'écoulement de boues sont primordiaux pour maîtriser le processus de pipeline.

1.2 Objectifs

Le transport de boues à travers les pipelines est largement utilisé dans les industries minières et de traitement des minéraux depuis plusieurs décennies. De nombreuses études ont été menées depuis les années 1960 pour étudier divers aspects du transport de boues. Les chercheurs (par exemple [Pullum et al., 1992, Schaan et al., 2000b, Wilson et al., 2006]) dans ce domaine s'intéressent à la prédiction de la perte de charge, à la détermination de la vitesse minimale requise pour un transport sûr, et à l'examen de l'influence de facteurs tels que la concentration en solides, la forme des particules et la rhéologie sur le gradient de pression. Il y a également eu plusieurs études pour déterminer la consommation d'énergie requise et dimensionner les pompes à boues à utiliser, via des données expérimentales [Schaan et al., 2000b], et pour optimiser les paramètres de conception du pipeline (comme le diamètre du tuyau, le pourcentage de fines particules), afin

de minimiser les coûts en capital et la consommation d'énergie. Dans le transport de boues, maintenir un écoulement régulier et optimal est crucial pour éviter des problèmes tels que la sédimentation de la phase solide et l'obstruction du tuyau, qui peuvent affecter l'efficacité du transport en suspension. Cela nécessite une gestion efficace de la perte de charge, qui est un paramètre clé pour garantir un transport continu et efficace des boues. Un autre objectif important de la gestion appropriée de la perte de charge est d'optimiser la consommation d'énergie des pompes, ce qui se traduit également par un transport efficace des boues.

L'efficacité énergétique de l'écoulement des boues dans les pipelines concerne la capacité à transporter des matériaux en minimisant la consommation d'énergie. Ceci est particulièrement crucial dans des industries comme l'exploitation minière et le traitement des minéraux, où le transport de boues peut consommer une quantité importante d'énergie. De nombreux facteurs peuvent influencer l'efficacité énergétique des écoulements de boues dans les pipelines, tels que :

- Rhéologie : les propriétés rhéologiques de la boue, telles que la viscosité et la contrainte seuil, peuvent avoir un impact significatif sur la consommation d'énergie de l'écoulement.
- Taille et concentration des particules : la taille et la concentration des particules solides dans la boue peuvent affecter l'énergie nécessaire pour transporter la boue à travers le pipeline.
- Géométrie et rugosité du tuyau : la géométrie du pipeline et la rugosité de la surface interne peuvent affecter la résistance à l'écoulement et l'énergie requise pour pomper la boue.
- Régime d'écoulement : le régime d'écoulement, qu'il soit laminaire ou turbulent, peut affecter la consommation d'énergie de l'écoulement.
- Débit d'écoulement : le débit d'écoulement de la boue peut affecter la consommation d'énergie de l'écoulement.

Il existe plusieurs méthodes qui peuvent être utilisées pour améliorer l'efficacité énergétique des écoulements de boues dans les pipelines. Celles-ci comprennent :

- Optimisation des propriétés de la boue : Les propriétés rhéologiques de la boue peuvent être ajustées en modifiant la charge en solides, la distribution de la taille des particules, et en ajoutant des additifs tels que des polymères ou des tensioactifs. Cela peut réduire l'énergie nécessaire pour la pompe et améliorer l'efficacité globale du système.
- Conception du pipeline : Le diamètre et la longueur du pipeline peuvent avoir un impact significatif sur l'énergie requise pour la pompe. En optimisant la conception du pipeline, comme en réduisant le nombre de coudes et en utilisant des tuyaux de plus grand diamètre, la consommation d'énergie peut être réduite.

- Sélection de la pompe : Le choix de la pompe peut également affecter l'efficacité énergétique de l'écoulement de boue. Les pompes centrifuges sont couramment utilisées, mais les pompes à déplacement positif peuvent être plus efficaces dans certaines situations.

- Conditions de fonctionnement : L'ajustement du débit d'écoulement, de la pression du pipeline et de la vitesse de la pompe peut également améliorer l'efficacité énergétique des écoulements de boues dans les pipelines.

- Systèmes de contrôle avancés : Les systèmes de contrôle avancés, tels que la commande prédictive basée sur des modèles et les outils de simulation, peuvent être utilisés pour optimiser le fonctionnement du pipeline de boue et réduire la consommation d'énergie.

Il convient de souligner que l'efficacité énergétique des écoulements de boues dans les pipelines est soumise à une variabilité significative en fonction de l'application particulière. En ce qui concerne notre étude de thèse, nous ne sommes pas en mesure d'apporter des modifications au processus de transport existant, telles que la modification de la géométrie du tuyau, l'ajout d'additifs à la boue ou l'altération des pompes. Par conséquent, l'accent principal de la recherche est mis sur l'examen des propriétés physiques du mélange de boues et sur l'exploration de la manière dont les paramètres hydrodynamiques influencent le transport des boues et l'efficacité énergétique en utilisant des outils de simulation. Notre objectif est d'identifier les moyens les plus efficaces d'optimiser ces paramètres, afin d'améliorer l'efficacité énergétique globale du système.

La mesure de l'énergie nécessaire pour transporter un lot de boues sur une distance particulière est connue sous le nom de consommation d'énergie spécifique (*SEC*) et est une métrique appropriée pour quantifier l'efficacité du transport. Elle est directement proportionnelle au gradient hydraulique, qui représente sous une forme adimensionnelle la baisse de pression statique due à la friction dans l'écoulement des boues le long de la longueur unitaire du tuyau. La détermination des besoins en puissance pour les écoulements de boues est similaire à celle de l'eau, mais avec une considération supplémentaire pour la friction générée par les solides. De plus, un écoulement non-newtonien peut se produire s'il y a une concentration élevée de fines particules dans la boue. La consommation d'énergie spécifique (SEC) pour les écoulements de boues est déterminée en considérant le rapport entre i_m et ϕ_s pour les solides d'une certaine densité relative S_p. Ce rapport prend en compte la densité des particules solides ϱ_s et la densité du liquide porteur, qui dans ce cas est l'eau avec une densité de ϱ_w. La SEC est utilisée comme mesure de l'énergie nécessaire pour déplacer les boues sur une distance donnée et est influencée par divers facteurs tels que les propriétés rhéologiques de la boue et la géométrie du tuyau. L'énergie nécessaire pour transporter la masse de solides par unité de longueur de tuyau est donnée par [Wu et al., 2010] (en

unité SI) (J/kg.m) :

$$SEC = \frac{\mathcal{P}}{\dot{\mathcal{M}}_s \mathrm{L}} = \frac{\Delta p/L}{\phi_s \varrho_s}, \tag{1.1}$$

$\mathcal{P}$ représente la consommation de puissance (en W), $\dot{M}S$ est le débit de masse des solides (en kg/s) et L est la longueur du tuyau (en m), $\Delta P/\Delta L$ est le gradient de pression (en kPa/m), ϕ_s est la concentration volumétrique des solides (en v/v) et ϱs est la densité des solides (en kg/m^3).

Il est donc essentiel de mener une analyse approfondie de l'impact des caractéristiques de la boue sur la SEC afin d'améliorer l'efficacité et garantir la sécurité opérationnelle. De plus, disposer de moyens pour prédire la physique de l'écoulement de la boue est primordial pour le contrôle du processus de transport. Cela nous amène aux principaux défis de la recherche à mener dans le cadre de cette thèse :

i) Explorer différents scénarios pour minimiser la consommation d'énergie lors du transport de la boue en utilisant une analyse de sensibilité. L'analyse sera réalisée à l'aide de techniques spectrales stochastiques basées sur les expansions polynômials du chaos généralisées (gPC). Cette méthode permettra d'identifier les différentes propriétés et paramètres qui ont un impact significatif sur la perte de charge et de déduire les meilleures combinaisons qui conduisent à une efficacité énergétique optimale.

ii) Un autre défi consiste à poser les bases d'un contrôle intelligent de la perte de charge dans le processus de transport en utilisant des modèles de simulation de dynamique des fluides (CFD). Ce système permettra d'optimiser le fonctionnement du processus, de prédire l'évolution des paramètres critiques et de soutenir la prise de décision opérationnelle. En fait, les stratégies modernes de modélisation des processus industriels utilisent souvent des techniques de simulation tridimensionnelle incorporant la CFD et/ou les méthodes d'éléments discrets (DEM). Ces modèles tridimensionnels sont ensuite intégrés en tant que modèles de substitution pouvant être utilisés dans des outils de simulation et de surveillance opérationnels, tels que les systèmes d'aide à la décision. Les méthodologies de surface de réponse (RSM) sont généralement appliquées pour construire des modèles de substitution polynomiaux Rabhi et al. [2018]. Cependant, des travaux récents ont montré que des techniques d'apprentissage automatique, telles que les réseaux neuronaux artificiels (ANN), peuvent également être utilisées Seong et al. [2020]. L'approche de modélisation actuelle consiste à développer un modèle CFD multiphase tridimensionnel pour différents types d'éléments de tuyauterie (horizontal, incliné), qui sont ensuite utilisés pour construire des modèles de substitution qui modélisent la perte de charge dans chaque élément. De tels modèles peuvent être utilisés dans des modèles dynamiques pour surveiller les systèmes de tuyauterie de boue et réaliser des études de dimensionnement pour couvrir les variations des conditions de fonctionnement, telles que la pression d'entrée et le débit. Cette approche sera d'abord appliquée à un écoulement de fluide unique

pour valider l'approche de construction d'un modèle de substitution de perte de charge par simulation numérique tridimensionnelle, et ensuite aux écoulements de boue avec une concentration volumique en solides et des diamètres de particules correspondant aux applications visées.

1.3 Plan de thèse

Le manuscrit de cette thèse est organisé autour des chapitres suivants :

Dans le Chapitre 1, la focalisation de l'étude est introduite, les objectifs et motivations sont exposés, et l'organisation logique de la dissertation est expliquée.

Le Chapitre 2 décrit le problème abordé dans cette thèse, et présente les concepts fondamentaux et la terminologie des écoulements biphasiques.

Le Chapitre 3 expose les approches de recherche utilisées pour aborder le problème d'ingénierie, et les principales caractéristiques de la théorie des écoulements biphasiques eulériens appliquée aux systèmes solide-fluide sont rapportées en se basant sur une revue exhaustive de la littérature. Le chapitre fournit une analyse approfondie et une discussion de l'application de cette théorie au contexte spécifique des systèmes solide-fluide.

Dans le chapitre 4, la simulation numérique des écoulements solide-liquide à travers les systèmes de pipelines est présentée. Le chapitre inclut des détails sur les méthodes numériques utilisées, le processus d'implémentation du modèle, et la validation du modèle par comparaison avec des données expérimentales ou empiriques.

Le Chapitre 5 illustre l'utilisation des développements en chaos polynomial (PCE) comme méthodologie pour estimer l'incertitude inhérente à l'écoulement souhaité de la boue. Ce chapitre se concentre sur l'utilisation de PCE pour quantifier et analyser les incertitudes associées à l'écoulement de la boue, et réalise spécifiquement une analyse de sensibilité de l'efficacité énergétique de l'écoulement. Le chapitre détaille la mise en œuvre de PCE et son application à l'analyse de l'efficacité énergétique de l'écoulement, fournissant des informations sur l'impact des incertitudes sur les performances du système.

Dans le Chapitre 6, l'utilisation du modèle pour construire un modèle de substitution basé sur la CFD pour prédire la perte de charge est démontrée. L'exactitude du modèle de substitution est évaluée par comparaison avec des données expérimentales de la littérature. De plus, la même approche est utilisée pour développer un modèle de substitution pour prédire les pertes de charge

de la boue de phosphate dans un système à l'échelle réelle de tuyauterie. Les données expérimentales des capteurs industriels sont utilisées pour évaluer les performances du modèle nouvellement développé.

Le Chapitre 7 sert de conclusion du manuscrit, fournissant un résumé général du travail réalisé et offrant des suggestions pour les études futures. Dans l'ensemble, il fournit des informations précieuses et des recommandations pour de futures recherches dans ce domaine.

2

Problem description and key concepts

Objectifves

This chapter provides a thorough overview of the OCP phosphate slurry pipeline transport process system in section 2.1, and provides the basic definitions and terminology concerning dispersed two-phase flows in section 2.2

Contents

2.1 Industrial context

The focus of this project is on the transportation of phosphate ores within the framework of Industry 4.0. In April 2014, the Moroccan phosphate slurry pipeline, shown in Fig. 2.1[1], became operational and is now recognized as one of the biggest slurry pipelines in the world. As the pipeline is located underground, it does

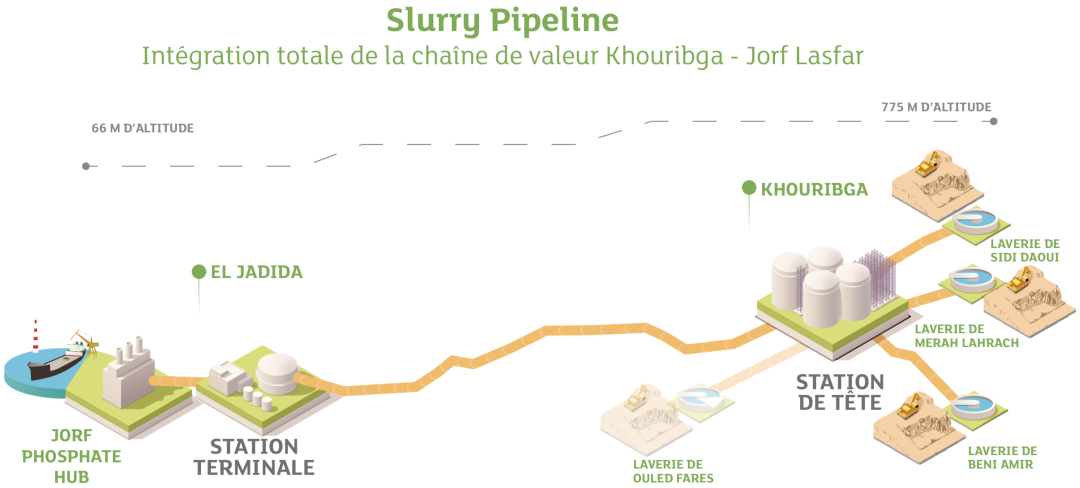

Figure 2.1: Transport process of phosphate slurry.

not have any negative impact on agriculture or transportation along the route connecting Khouribga and Jorf Lasfar. The system consists of multiple pipes, which altogether stretch over a distance of 227 kilometers.

2.1.1 Description of the transport system

To begin the process, the ore is first extracted from various locations and undergoes processing. This involves preparing different grades of phosphate at wash plants, which are then transformed into a pulp consisting of "Water + Phosphate" for transportation through a slurry pipeline. The pulp is subsequently pumped to the Main Slurry Pipeline Head Station in Khouribga and stored in agitated tanks.

The slurry pipeline receives phosphate ore of varying qualities from four different washing stations, resulting in the material having different flow properties such as viscosity, density, speed, pressure, and more.

The slurry is transported in batches of 187 km with water plugs in between to minimize intermingling of different product grades during the transportation process. This is done to deliver the phosphate ore to the industrial units for processing, as shown in Fig. 2.2.

[1] Adopted from https://amnistiegenerale.wordpress.com/2019/08/13/le-maroc-et-ses-phosphates/

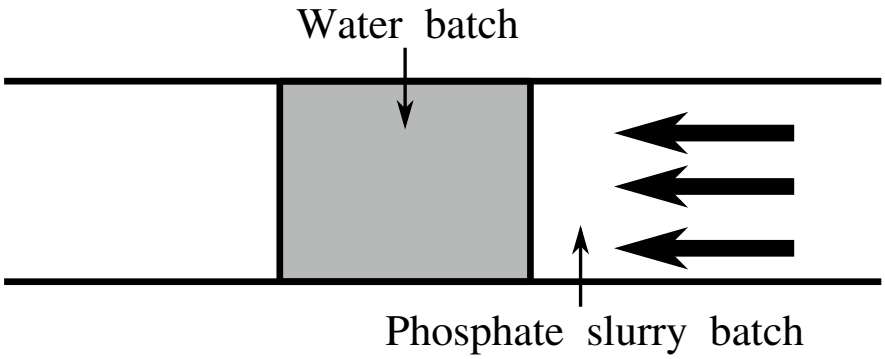

Figure 2.2: Phosphate slurry flow

The primary purpose of the pipeline is to transport slurry at a rate ranging from 26 to 38 million tons per annum. The system is fully automated and monitored from a central control room located at the Head Station. Operators receive notifications via alarms in the control system when the pipeline's operating conditions fall outside of the design range. Moreover, the system implements control measures to prevent equipment damage. The diagram in Fig. 2.4 illustrates the fundamental process components, beginning with the three processing plants:

1. Daoui: In this processing area, the phosphate ore undergoes processing, thickening, and is conveyed to the buffer tank with the single agitator located near to the pump station. Subsequently, the ore is pumped through a 22.2-kilometer pipeline to the storage tanks at the Head Station.

   Variable choke stations equipped with ceramic orifice plates are required at the Head Station due to the mostly downhill pipeline profile to prevent slack flow The choke station was intended to give the necessary choking range to cover all operational situations. However, if the pipeline is operating at maximum design throughput with high rheology slurries and is full of slurry, no choking is necessary as friction losses consume most of the available head Depending on the slurry qualities, different levels of choking may be required, which can be regulated from the control room. The pipeline, which has a capacity of approximately 1400 t/h, is made up of DN 450 steel pipes with a high density polyethylene (HDPE) liner. The pump station is outfitted with two trains of four centrifugal slurry pumps in series.

2. MEA: The MEA processing plant and the Head Station are located adjacent to each other. The low and high-grade ores are treated and thickened separately in their respective thickeners. The thickened ores are then transported through separate pipelines, which are 1.8 km long and powered by thickener underflow pumps, directly to the storage tanks at the MEA Head Station. The low-grade pipeline has a capacity of approximately 1400 t/h, while the high-grade pipeline has a capacity of around 700 t/h.

3. El Halassa: Low and high-grade ore are processed and thickened at the pump station before being transported to their respective buffer tanks.

   The ore is then pumped to the Head Station's storage tanks through a 14.9-kilometer pipeline. The pipeline has a capacity of around 1500 t/h, depending on the slurry qualities. The pump station is equipped with five pumps in sequence in each train of centrifugal slurry pumps, and each slurry pump is supplied with gland sealing water by a specialized plunger pump.

In the Head Station, slurry from the feeder pipelines is discharged into the station's four tanks, although only one tank is displayed in Fig. 2.4 for clarity Density transmitters are installed in each entering pipeline to detect batch interface. With the use of a piping manifold system, the necessary valves are activated to automatically direct slurry batches from the wash plants to specific groups of storage tanks. The leak detection systems in place use pressure transmitters installed on the feeder lines to gather real-time pressure data. The Head Station uses four agitated storage tanks to supply slurry to one of the two centrifugal main line pump trains, with each train consisting of six series pumps (as shown in Fig. 2.3). A plunger pump supplies gland sealing water to each slurry pump. The centrifugal main line pump trains consist of six pumps in series, with pumps

Figure 2.3: Head station slurry pump. Adopted from Rusconi et al. [2016]

1, 2, 5, and 6 equipped with 1850 kW motors and variable speed drives, while pumps 3 and 4 have fixed speed drives. The pumps have separate volute liners that are wear-resistant and can handle casing pressures of up to 6200 kPa. The VSD range and gearbox ratios allow the pumps to operate between 10m and 80m of head.

The Main Pipeline, which spans 187 kilometers from the Head Station to the Jorf terminal station, is constructed of DN 900 steel with an HDPE coating. The pipeline operates mostly downhill and can handle a capacity of approximately 4400 t/h, which varies based on the slurry properties. Flow monitoring, batch tracking, and leak detection are enabled by the installation of flow, density, and pressure transmitters at the head station of the pipeline. When the pipeline is shut down, a single intermediate valve station divides the static head to prevent over-pressurization of the mainline pipe below the valve station.

There are four pressure monitoring stations along the main pipeline, identified as PMS1, PMS2, PMS3, and PMS4 in Fig. 2.4. These stations monitor intermediate conditions in the pipeline and provide additional data to support decision-making by operators. The pipeline leak detection system relies on various data inputs, including pressure monitoring station data, pump station data, valve station data, and terminal data.

To ensure steady pipeline operation within the operational range, ceramic chokes are installed in the main line at the Terminal Station. However, most of the available head from the pump station to the terminal station is consumed by frictional losses in the pipeline. Therefore, relatively little choking is necessary. At the Terminal Station, a density transmitter is placed in the incoming pipeline, similar to the one at the beginning of the main pipeline. To enable the leak detection system, real-time flow and pressure data are required, which can be obtained by installing a flow meter and a pressure transmitter. Furthermore, the flow meter is also utilized for batch tracking. A piping manifold system is in place to allow the opening of necessary valves to route slurry batches of different grades from the head station to eight agitated storage tanks. Figure 2.4 shows only one tank for simplicity.

2.1.2 Main Pipeline Monitoring

The primary pipeline design should meet the transport demands of different batches and ensure proper distribution to downstream tanks. The system must be reliable and safe, accommodating various operating situations due to intermittent and varying flow characteristics of the batches. The control philosophy and ground profile, which mostly slope downhill with a brief uphill portion after the Head Station, must be considered in the design (cf. Fig. 2.5).

Due to the mostly downhill profile with an overall elevation change of approximately 580m, the terminal station must have a significant system of chokes. During operation, it is crucial to ensure that the following conditions are met:

- There must be no slack flow anywhere along the pipeline.
- The velocity must be maintained at a high enough level to prevent solid deposition.
- The slurry flow must stay turbulent instead of becoming laminar.

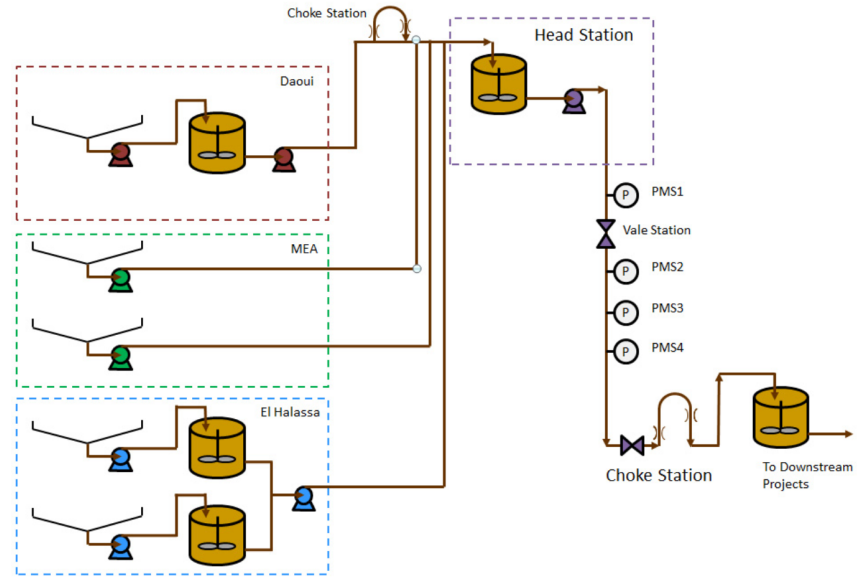

Figure 2.4: Main Pipeline Components. Adopted from Rusconi et al. [2016]

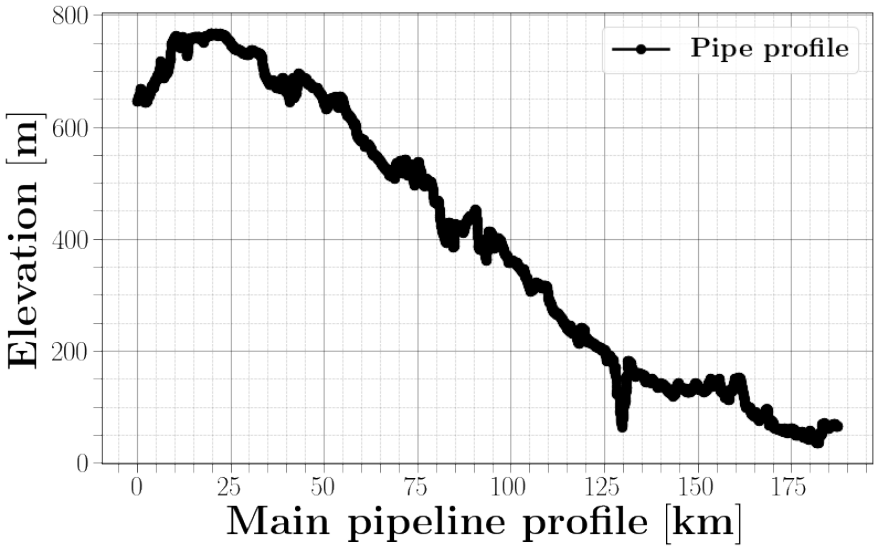

Figure 2.5: Main Pipeline profile.

- The flow rates must not exceed the maximum design limits.

The relationship between density, solids throughput, and flow conditions (laminar vs turbulent) for the pipeline can be observed in Fig. 2.6, which also displays the lowest allowable velocity and the transition point between laminar and turbulent flow. The chart depicts several concentrations expressed as percentages of mass, which can help establish a connection between solids and volumetric throughput.

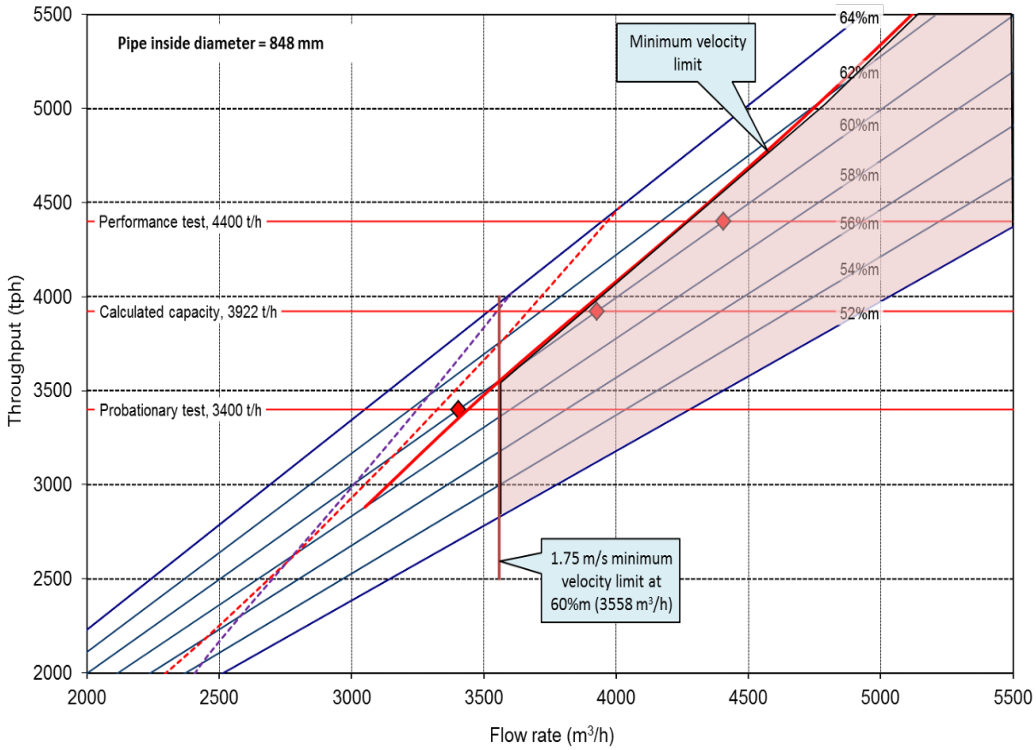

Figure 2.6: Operating Envelope. Adopted from Rusconi et al. [2016]

2.1.3 Phosphate ore properties

To transport OCP phosphate ore, it is important to consider the solid's density, which is typically $3.0t/m^3$. However, this value only accounts for the solid's dry density, and it is crucial to take into account that the solid particles are porous, as shown in Fig. 2.7. Porosity or void fraction is a measure of the void spaces in a material.

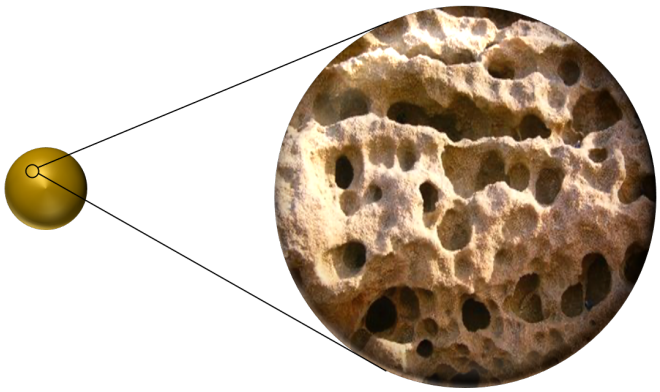

Figure 2.7: Particles properties

When dealing with porous solids, it is important to calculate the density of the solid excluding the open pores. In the case of OCP phosphate ore, the solid

particles are porous with pore sizes much smaller than $1\mu m$, but these pores make up a significant fraction of the total volume, typically 20%. As a result, the pores fill with water in the slurry, which affects the effective density of the particles ($\varrho_{s,effective}$).

$$\varrho_{s,effective} = (1 - P) \times \varrho_s + P \times \varrho_W \tag{2.1}$$

Therefore, at a porosity of 20 percent, the "effective" solids density for OCP slurry with a solids density of $3.0t/m^3$ is equivalent to $2.4t/m^3$. In addition, the phosphate pulp has a solid volume concentration that can reach up to 40 percent. The solid particles in the phosphate pulp have irregular shapes and a range of equivalent spherical diameters from 44 μ_{m} to 250 μ_{m}. For more details about phosphate slurry properties, please refer to Appendix A.

2.2 Basic concepts in solid-liquid flows

2.2.1 Introduction of key properties

At the outset, two broad categories of multiphase flow can be identified: dispersed flows and separated flows. Dispersed flows are characterized by the presence of a dispersed phase, which can be solid particles, liquid droplets, or gas bubbles, suspended in a continuous phase that can also be a gas, liquid, or solid. Examples of dispersed flows include gas-liquid flows in pipelines or bubble columns, oil-water flows in oil reservoirs, and solid-liquid flows in slurry pipelines. Separated flows, on the other hand, involve two or more distinct continuous phases that are separated by an interface. This interface can be sharp or diffuse and can be stationary or moving. Examples of separated flows include oil-gas flows in pipelines, gas-liquid flows in distillation columns, and air-water flows in rivers. The two-phase flows discussed in this thesis are categorized as dispersed, as they involve solid particles distributed in a continuous carrier phase of water. The following are fundamental principles and terminology of dispersed two-phase flows that are often used to provide a hydrodynamic characterization of solid-liquid mixtures containing dispersed particles.

As we shift from the flow of a pure liquid to that of a slurry, which is a mixture of solid particles in a carrier fluid, there is an immediate requirement for a more precise nomenclature system. As an illustration, in contrast to a simple liquid where only one density (ϱ) needs to be considered, the presence of solid particles in a carrier fluid necessitates the differentiation of several densities. These densities include the density of the carrier fluid (ϱ_f), the density of the solid particles (ϱ_s), and the density of the mixture (ϱ_m). In the case of a vast number of slurries, water serves as the carrier fluid with a density of approximately 1000 kg/m^3. The symbol ϱ_w is used to represent the density of water, while ϱ_f is reserved for fluids with densities different from that of water. The value of s_w (specific gravity of water) serves as the reference for expressing the relative density or specific gravity

of other materials. An example of such applications is when conveying solids with a density of approximately 2650 kg/m^3, a typical value for sand, and in this case, the relative density, ss or $\varrho s/\varrho_w$, is 2.65. The general formula for calculating the relative density, denoted as s_m (i.e., the mean specific gravity of the mixture), for a combination of solids and fluid is as follows:

$$s_m = s_f + (s_s - s_f)c_v \tag{2.2}$$

where c_v is the volumetric concentration, i.e. the fraction of the mixture volume which is occupied by the solids. In the case where the fluid in the mixture is water with standard density, s_f is equal to 1, then resulting in a simplified equation for Sm:

$$s_m = 1 + (s_s - 1)\, c_v \tag{2.3}$$

The particle concentration, also known as the volume fraction of particles, is one of the most crucial characteristics of a slurry mixture. It is determined by the ratio of the volume of particles in a specific area of the mixture to the total volume of the mixture. Another way to express the concentration of particles in a slurry is through the weight fraction. This is calculated by taking the ratio of the weight of the particles to the total weight of the mixture. It is also referred to as the solids concentration and is commonly expressed as a percentage. The volume concentration c_v of a slurry mixture can be calculated if the weight concentration c_w is known, using the following formula:

$$c_v = \frac{s_f c_w}{s_s - (s_s - s_f)\, c_w} \tag{2.4}$$

Conversely, the weight concentration c_w is determined by the following expression:

$$c_w = \frac{s_s c_v}{s_f + (s_s - s_f)\, c_v} \tag{2.5}$$

Since our goal is to present general approaches that can be applied to any slurry, including phosphate ore, we will use the volume concentration as the primary concentration parameter in our discussion. The volume concentration parameter offers a more accurate indication of slurry consistency, irrespective of the density of the solid phase, making it a suitable choice for our general approach that applies to any slurry, including phosphate ore. When specifying concentrations of slurries, it is important to distinguish between delivered and in situ values to ensure accuracy. The delivered concentration is the fraction of solid particles delivered or fed into the conveying system in relation to the total mass or volume of the mixture. When the slurry is collected in a tank after being discharged from the system, the volume fraction of solids for the mixture in the tank is referred to as the delivered volumetric concentration, which is denoted as c_{vd}. The in situ concentration, denoted as c_{vi}, represents the average concentration of the slurry within the system or in a specific part of it, such as a certain length

of pipe. Although it may seem that the two concentration measures should be equal, this is only true for non-settling slurries where there is no tendency for the solid and fluid components to separate. The values of cvd and cvi differ when the average velocity of the solids (u_s) is not the same as that of the fluid (u_f), and this is typically the case in stratified flows. While it is possible for the delivered concentration, cvd, and the in situ concentration, cvi, to differ without the presence of stationary solids in the pipe, an extreme example arises when a deposit of stationary solids occupies the lower half of the pipe. Water flows through the upper part of the pipe and moves only a few solid particles, which tend to roll along the top of the bed. As a result, the in situ concentration, cvi, is relatively high, but since most of the solids are not moving, the average velocity of the solids is much less than that of the water. Consequently, the delivered concentration, cvd, in this case is significantly smaller than the in situ concentration, $\mathrm{c_{vi}}$.

The volumetric flow rate of liquid, $\mathrm{Q_f}$, can be expressed as the product of its velocity and the cross-sectional area occupied by the fluid, i.e.:

$$\mathrm{Q_f} = u_s(1 - \mathrm{c_v})\pi \mathrm{D}^2/4 \tag{2.6}$$

Similarly, the volumetric flow rate of solids is $\mathrm{Q_s}$, i.e.:

$$\mathrm{Q_s} = u_s \mathrm{c_v} \pi \mathrm{D}^2/4 \tag{2.7}$$

The total flow rate of the mixture, $\mathrm{Q_m}$, is given by the sum of the fluid and solids flow rates, and is also equal to $\pi \mathrm{D}^2/4$ times the mean velocity of the mixture. Thus,

$$\frac{4Q_m}{\pi D^2} = u_m = u_s \mathrm{c_v} + u_f(1 - \mathrm{c_v}) \tag{2.8}$$

Going forward, it is important to recognize that the in-situ concentration of solids is denoted by the volume fraction of the solid phase, or solids concentration which is symbolized by ϕ_s.

In fact, the solid particles comprising the dispersed phase may vary in size. To analyze such slurries, a widely used method involves categorizing the particles into various size classes, as illustrated in Fig. 2.8. The solid concentration is then represented by:

$$\phi_s = \frac{\sum_i N_i V_{pi}}{V} \tag{2.9}$$

Here, V represents the total volume, and N_i denotes the number of particles with size i, each having a volume V_{p_i}. Typically, the volume of a particle with diameter d_{pi} is calculated using the formula $V_{pi} = \pi d_{pi}^3/6$, assuming spherical particles. For non-spherical particles, their equivalent diameter is used to calculate their volume as if they were spheres.

The previously mentioned equations are simplified if all particles have equal sizes. In such cases, the solid concentration can be expressed as $\phi_s = NV_p/V$,

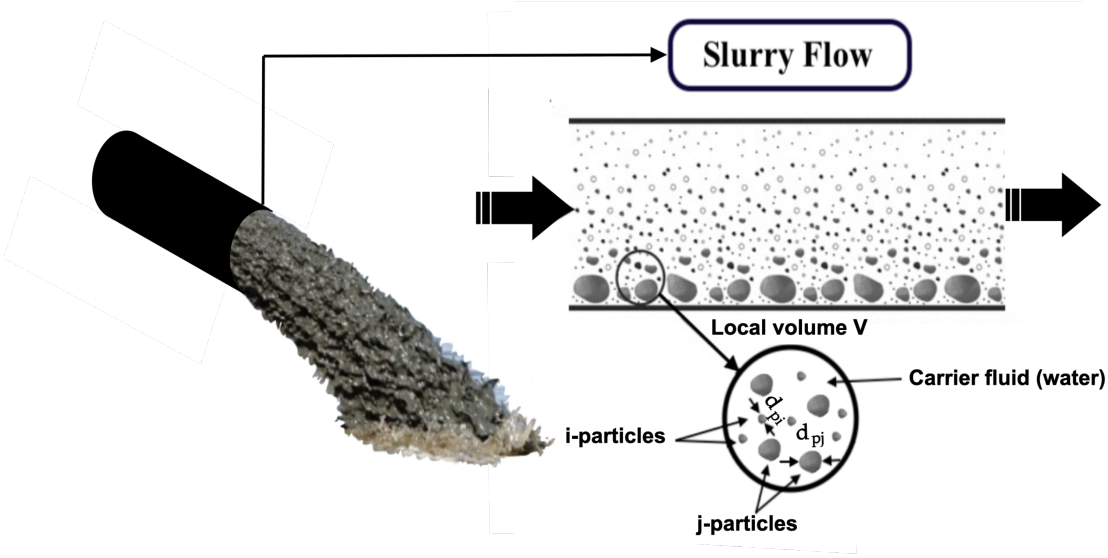

Figure 2.8: A qualitative illustration of dispersed two-phase flows

where N represents the total number of particles having volume V_p. It's also crucial to remember that the sum of the volume fractions of both the dispersed and carrier phases is equal to one. Therefore, the volume fraction of the carrier fluid, which is water in this particular case, can be calculated as follows:

$$\phi_w = 1 - \phi_s \tag{2.10}$$

The particle volume fraction, represented by ϕ_s, varies from 0 to a maximum value ϕ_{max}, which is commonly referred to as the maximum packing fraction. The maximum packing fraction or the maximum possible value of ϕ_s is primarily influenced by the shape and size distribution of the solid particles. For instance, for mono-dispersed particles, the closest packing can reach around 0.64 for spherical particles, while it can be as high as 1 for cubic particles. When dealing with a non-uniform particle size distribution, an increase in the maximum packing concentration can occur, as the smaller particles fill the spaces between the larger ones. Moreover, the maximum packing concentration may also be affected by other flow parameters [Peker et al., 2008]. Elevated shear rates have a tendency to bring the maximum packing concentration of spherical particles closer to the value of 0.64.

The shape of particles can have a slight impact on the behavior of slurry flow, but it is difficult to evaluate this property quantitatively. To characterize particle shape, various metrics have been introduced, with sphericity and roundness being the most significant. Traditionally, sphericity is defined as the ratio of the grain volume to that of the smallest circumscribing sphere, whereas roundness is the ratio of grain edge/corner curvature to the total grain curvature. Incorporating non-spherical particle shapes into predictive models is a challenging process. Al-

though there are various studies on non-spherical particles such as sand, iron ore, and slush nitrogen, little attention has been given to how particle shape affects the selection of drag models, determination of limiting solids concentrations, and establishment of specularity or rebound coefficients. Due to the complexity of considering particle shape, spherical particles are commonly assumed in many studies, including this thesis, for the sake of simplicity.

The boundary between a dilute and a dense slurry flow can be clearly defined by the volume fraction of the particles or the particle concentration. The motion of particles and their surroundings varies depending on the degree of slurry density. In each flow regime, there are specific interactions and couplings that exist between the particles and the fluid, as well as among the particles themselves. Fig. 2.9 shows a detailed classification between dispersed and dense two-phase flows, which is based on the type of coupling. This classification is reported by Loth [2010].

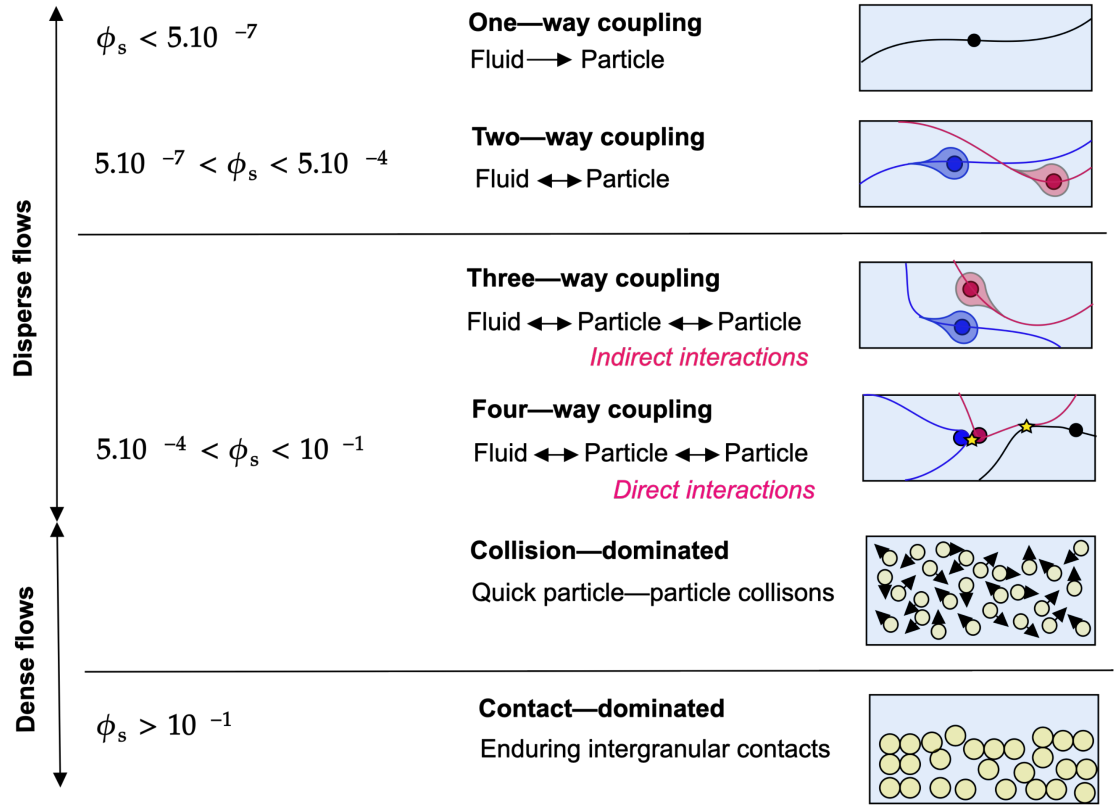

Figure 2.9: A categorization of particle-laden flows is established based on the coupling regime and the fundamental physical mechanisms governing the flow. Adapted from Messa et al. [2021]

The authors have proposed a classification of slurry flows based on the coupling sub-regimes, which can be approximately arranged in terms of increasing

particle concentration ϕ_s. The first is one-way coupling, where the fluid effects particle mobility but not vice versa. The second is two-way coupling, where particles affect the carrier fluid's velocity causing dissipation. As the solid concentration increases, the particle-particle interactions come into play, resulting in indirect interactions (three-way coupling) and direct collisions (four-way coupling). In both of these scenarios, dynamic collisions significantly affect particle motion. The collisional Stokes number S_{coll} is the non-dimensional parameter of effect. This quantity is the product of the particle relaxation time τ_p, which will be elaborated on in the subsequent discussion. Finally, If the solid concentration ϕ_s exceeds a value of 0.1, particle-particle contacts become dominant in the flow, leading to the collective motion of particles.

2.2.2 Slurry flow patterns in horizontal pipelines

In this section, we will provide a broad perspective on the classification of slurry flows into various flow regimes, including the (pseudo) homogeneous, heterogeneous, and deposition flow regimes. We will also discuss how the flow regime is dependent on flow velocity, solid concentration, and particle size. Furthermore, understanding the modeling aspects of different flow regimes is crucial for the development of hydraulic simulation tools, as well as the design and operation of slurry systems. This also requires a solid understanding of rheology and fluid flow. In slurry flows, settling is a typical phenomenon where solid particles interact with turbulent eddies of the flowing carrier, as well as with each other through inter-particle collisions or longer-lasting contacts. Interactions between the phases and surfaces of pipes can also occur [Matousek, 2002],[Spelay et al., 2017]. These interactions are heavily influenced by the physical properties of the slurry mixture such as flow velocity, particle concentration, and particle size distribution. The latter properties can result in different patterns and types of flow regimes. In summary, settling slurry flows can be categorized into four types, as shown in Fig. 2.10[2]: (a) homogeneous slurry, where particles are evenly distributed throughout the pipe with no concentration gradient from top to bottom; (b) heterogeneous slurry, where particles are not uniformly distributed and concentration gradients typically occur in the pipe cross-section; (c) moving bed slurry, where a bed of particles is formed and moves with the fluid flow, and particles can also move in this lower region of the pipe by saltation; and (d) stationary bed slurry, where the particle bed formed does not move with the fluid flow, which can result in scaling and blockages of fluid flow.

In fact, the discussed slurry flow patterns are strongly influenced by the frictions in the pipeline (see Fig. 5.3c), as these viscous frictions are responsible for flow energy losses that result in flow stratification within the pipeline. Understanding the flow patterns and their causes is essential because as the degree of stratification increases, the flow becomes more stationary, leading to increased

[2]Adapted from https://cfdflowengineering.com/slurry-flows-and-its-cfd-modelling/

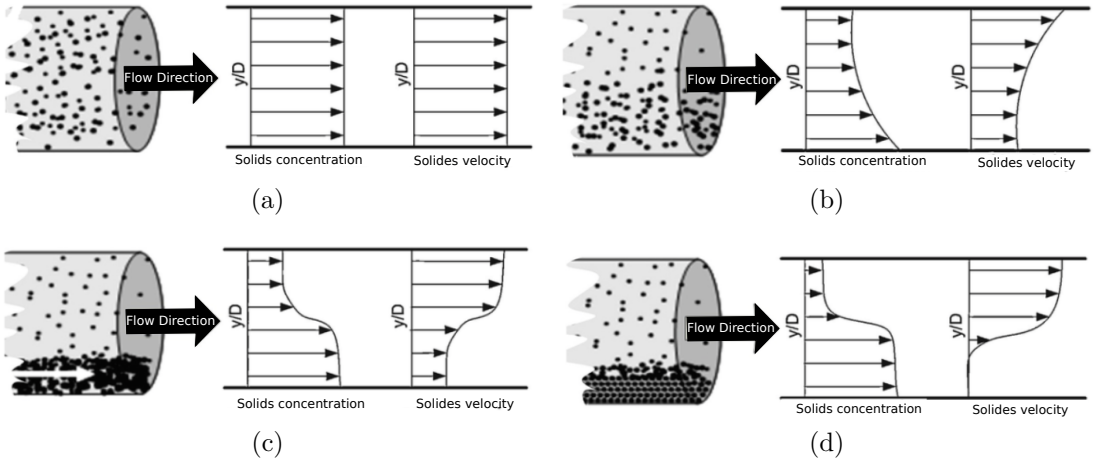

Figure 2.10: Typical settling slurry flows patterns.

pipeline resistance and reduced transport safety. The frictional pressure drop is an indicator of the resistance to flow caused by the frictional forces between the fluid and the pipe walls. This pressure drop can escalate due to the presence of solid particles in the slurry flow. On the other hand, the flow velocity is an important parameter for assessing the transport safety of the slurry flow, as high velocities can cause erosion and wear on the pipeline walls and lead to other operational issues. To prevent the risk of particle accumulation in the form of a deposit at the bottom of the pipe, the flow velocity must surpass the minimum safe velocity. Maintaining a flow velocity above this threshold ensures that the system operates safely and reduces the likelihood of pipe blockage, which could otherwise pose a safety hazard.The deposition-limit velocity (u_{dl}), which represents the velocity at which particles initiate the formation of deposits, is a crucial parameter in the design and operation of slurry transport systems. These systems commonly comprise a pipeline and a pump [Wilson, 1979],[Sanders et al., 2004]. The behavior of slurry flows discussed so far is complex and can be attributed to several mechanisms that govern the flow, including particle support and friction. To effectively control the energy losses and keep the particles in suspension, it is crucial to conduct a comprehensive analysis of the pressure drop in the slurry flow and the various factors that influence it.

2.2.3 Turbulence in slurry pipe flows

Turbulence plays a crucial role in slurry flows as it affects the suspension and mixing of solid particles in the flow, preventing them from settling or separating from the fluid. This is essential to ensure even transportation and mixing of solid particles in the flow and maintaining the stability of slurry flows, especially in pipelines, which can prevent the formation of instabilities that can lead to blockages or other flow problems. Actually, the turbulence behavior in slurry

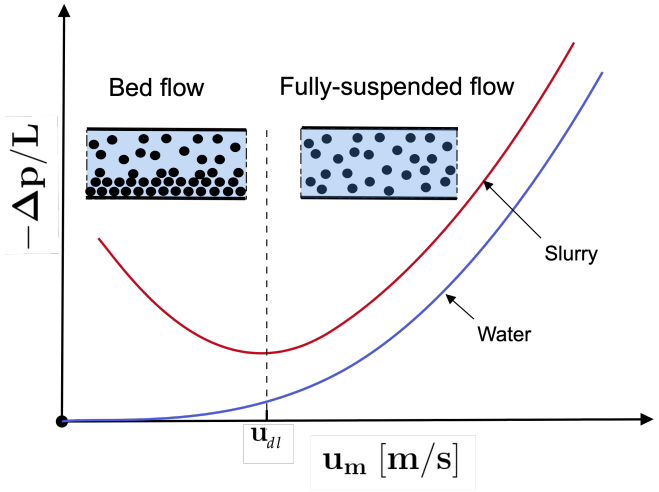

Figure 2.11: Effect of Pressure gradient on slurries flow patterns

flows is more closely related to the Reynolds number, which is a dimensionless quantity that describes the ratio of inertial forces to viscous forces in a fluid flow. The Reynolds number (Re) can help predict the onset of turbulence in a flow and is an important parameter for understanding the behavior of slurry flows. It is expressed by:

$$Re = \frac{\rho v D}{\mu} \tag{2.11}$$

On the other hand, the behavior of particles in the fluid is more related to the Stokes number. The Stokes number (St) is a dimensionless number that represents the ratio of the particle's response time (τ_p) to the characteristic time scale of the fluid flow. It describes the relative importance of inertial forces compared to viscous forces acting on particles. In slurry flows, the behavior of particles in the flow is strongly influenced by their Stokes number, it can be expressed as:

$$St = \frac{\tau_p(\varrho_s - \varrho_f)g}{u_f} \tag{2.12}$$

where: ϱ_s is the particle density, ϱ_f is the fluid density, u_f is the fluid velocity, g is the acceleration due to gravity. The Stokes number provides a measure of the relative importance of inertial and viscous forces in a fluid. When the Stokes number is below 1, the flow is usually laminar and is governed mainly by viscous forces. Under these conditions, the solid particles and fluid move smoothly and in a predictable way. If the Stokes number exceeds 1, the flow is primarily governed by inertial forces and usually becomes turbulent, resulting in the irregular and chaotic movement of both fluid and solid particles, promoting the mixing and transport of solid particles. The particle relaxation time refers to the time it takes for a particle to adjust to changes in the flow. The particle relaxation time

(τ_p) can be calculated as follows:

$$\tau_p = \frac{\varrho_s d_p^2}{(18\mu_f)} \tag{2.13}$$

where ϱ_s is the particle density, d_p is the particle diameter, μ_f is the fluid viscosity. This expression takes into account the force of drag acting on the particle, which is directly proportional to its diameter and inversely proportional to the viscosity of the fluid. The particle relaxation time is a measure of the time required for a particle to reach its terminal velocity in a fluid and depends on various factors such as the particle size, density, and fluid properties like viscosity. It plays an important role in the behavior of slurry flows and their ability to transport solid particles. Various Stokes numbers are defined based on the characteristic time scale τ with respect to which the particle relaxation time is normalized. The use of different Stokes numbers is necessary because turbulence is characterized by multiple time scales, as shown in Fig. 2.12. The integral scale Stokes number S_Λ and the micro-scale Stokes number S_λ are commonly used to account for these different time scales. The integral scale Stokes number S_Λ is defined in terms of

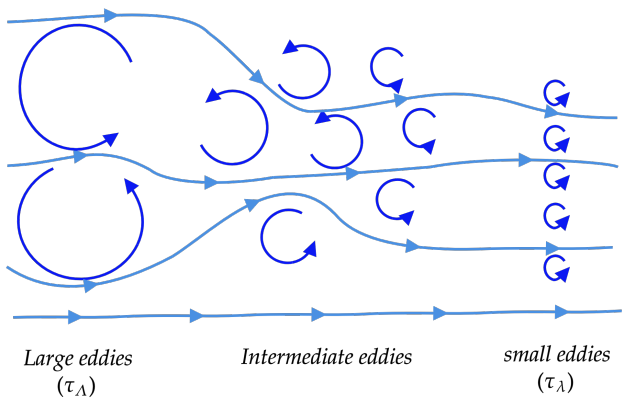

Figure 2.12: Scales of turbulence

the characteristic time of the largest and most energetic eddies τ_Λ, which have the most significant impact on the flow field. In the context of turbulence, the largest eddies continue to break down into smaller ones, which are characterized by a characteristic time scale of τ_λ. Eventually, these smaller eddies dissipate into thermal energy due to viscosity and disappear. When the value of $\mathrm{S}_\Lambda \ll 1$ is much smaller than 1, it indicates that the particles are in a state of local equilibrium with respect to the turbulent motion, and their behavior can be considered similar to that of a passive scalar. In contrast, when $\mathrm{S}_\lambda \gg 1$, as in the flow circumstances examined in this thesis, the particles are less influenced by small-scale turbulence. However, they might still experience the effects of integral-scale turbulence. Lastly, particles with $\mathrm{S}_\Lambda \approx 1$ will not achieve a state

of local equilibrium and will be significantly influenced by micro-scales. The movement of particles in a fluid is influenced by various forces that are determined by the fluid velocity and physical characteristics of the particles, such as size, shape, and density. These forces are commonly referred to as transfer laws, as they describe the interactions occurring at the interface between the phases. The generalized drag $\mathbf{M}_k^d$ represents the total force per unit volume acting on a suspension of particles. If the dispersed phase consists of spherical particles with a mean diameter d_p, $\mathbf{M}_p^d$ is typically modeled as [Enwald et al., 1996, Ishii and Mishima, 1984].

$$\mathbf{M}_p^d = n_p \left(\mathbf{M}^{\mathrm{D}} + \mathbf{M}^{\mathrm{L}} + \mathbf{M}^{\mathrm{VM}}\right) \tag{2.14}$$

where $\mathbf{M}^{\mathrm{D}}$, $\mathbf{M}^{\mathrm{L}}$, and $\mathbf{M}^{\mathrm{VM}}$ represent the forces acting on a particle in the suspension, which will be described below, and n_p is the number of particles per unit volume, given by

$$n_p = \frac{6\alpha_p}{\pi d_p^3}$$

. The forces in Eq. (2.14) are the followings:

1. The standard drag force $\mathbf{M}^{\mathrm{D}}$. This force comprises both friction and form drag. For a single solid sphere in a liquid, it is usually represented as:

$$\mathbf{M}^{\mathrm{D}} = \frac{1}{2}\left(\pi\frac{d_p^2}{4}\right)\mathcal{C}_d\rho_c\left|u_s - u_f\right|\left(u_s - u_f\right) \tag{2.15}$$

   where $\mathcal{C}_d$ is the drag coefficient, is evaluated from the particle Reynolds number $\mathrm{Re}_p = \rho_c\left(u_s - u_f\right)d_p/\mu_f$ Depending on the particle Reynolds number range, the drag coefficient can be determined using any of the correlations provided in Appendix B for calculation. In this study the drag coefficient is obtained through the correlation bellow Wen and Yu [1966]:

$$\mathcal{C}_D = \begin{cases} \frac{24}{\mathrm{Re}_p}\left(1 + 0.15\,\mathrm{Re}_p^{0.687}\right)\left(1-\phi_s\right)^{-2.7} & \text{, if } \mathrm{Re}_p \leqslant 10^3, \\ 0.44\left(1-\phi_s\right)^{-2.7} & \text{, if } \mathrm{Re}_p \geqslant 10^3, \end{cases} \tag{2.16}$$

2. The lift force $\mathbf{M}^{\mathrm{L}}$. The lift force in slurry flows is a force exerted by the fluid on a particle in the vertical direction, perpendicular to the direction of flow. This force has the potential to cause particles to deviate from their straight path, become suspended, and separate from the rest of the slurry. This phenomenon can have significant effects on the flow characteristics in a pipeline or process. Different models have been proposed in the literature to describe the lift force in slurry flows [Yilmaz and Gundogdu, 2009]. A commonly used model for the lift force in slurry flows is derived analytically by [Drew and Lahey Jr, 1987] and is given by:

$$\mathbf{M}^{\mathrm{L}} = \mathcal{C}_L\rho_c d_p^3\left(\mathbf{u}_p - \mathbf{u}_c\right) \times \left(\nabla \times \mathbf{u}_c\right) \tag{2.17}$$

where $\mathcal{C}_L$ is a constant lift coefficient, typically taken as 0.5 for spherical particles according to previous studies [Auton et al., 1988, Basirat and Salehi Neyshabouri, 2017].

3. Virtual mass force $\mathbf{M}^{\mathrm{VM}}$. This force emerges as a result of the added mass of the liquid that needs to be accelerated when a particle accelerates. It can be determined using the following expression:

$$\mathbf{M}^{\mathrm{VM}} = \left(\frac{4}{3}\pi\frac{d_p^3}{8}\right)\mathcal{C}_{vm}\rho_c\left(\frac{\mathrm{d}\mathbf{u}_c}{\mathrm{d}t} - \frac{\mathrm{d}\mathbf{u}_p}{\mathrm{d}t}\right) \tag{2.18}$$

Here, $\mathcal{C}_{vm}$ is a virtual mass coefficient. According to the frame indifference principle, which was invoked by Drew and Lahey Jr [1987], the virtual mass coefficient $\mathcal{C}vm$ must be equal to the lift coefficient $\mathcal{C}L$. Therefore, in practice, $\mathcal{C}_{vm}$ is often assumed to be a constant value, typically taken as 0.5 for incompressible flows. Sometimes, the virtual mass coefficient $\mathcal{C}_{vm}$ is expressed as a function of the solid volume fraction ϕ_s [Drew, 1983, Enwald et al., 1996]. The virtual mass force becomes significant if the density of the particles is much smaller than that of the continuous phase. This is because the added mass effect is more pronounced when the particle is much lighter than the fluid it displaces. [Manninen et al., 1996, Yilmaz and Gundogdu, 2009].

Fig. 2.2.3 illustrates the various forces acting on a single particle in a suspension, including the drag force, lift force, and virtual mass force. The interaction be-

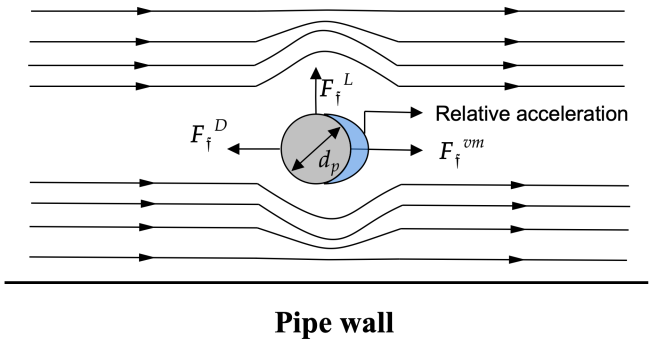

Figure 2.13: Mutual forces at the interface between the two phases.

tween the forces discussed determines the overall response of particles in the flow and significantly affects the transport of mass, heat, and solids. Including these forces in mathematical models for numerical simulations can improve the prediction of particle mobility, leading to a better understanding of slurry behavior in pipelines.

2

Description du problème et concepts clés

Objectifs:

Ce chapitre fournit une vue d'ensemble approfondie du système de transport de boue de phosphate OCP par pipeline dans la section 2.1, et fournit les définitions de base et la terminologie concernant les écoulements diphasiques dispersés dans la section 2.2.

2.1 Contexte Industriel

Le focus de ce projet est sur le transport de minerais de phosphate dans le cadre de l'Industrie 4.0. En avril 2014, le pipeline de boue de phosphate marocain, illustré à la Figure 2.1, est devenu opérationnel et est maintenant reconnu comme l'un des plus grands pipelines de boue au monde. Comme le pipeline est situé sous terre,

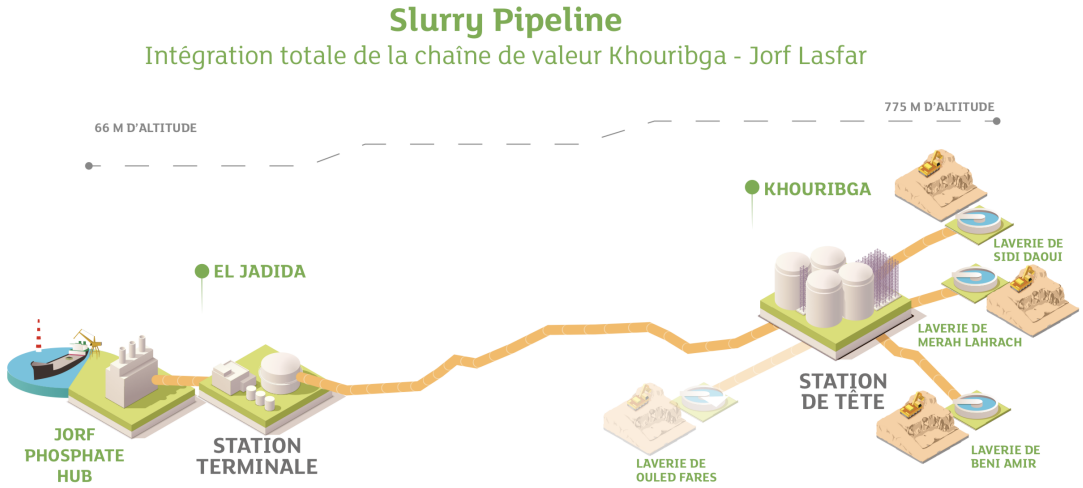

Figure 2.1: Transport process of phosphate slurry. Adopté depuis https://amnistiegenerale.wordpress.com/2019/08/13/le-maroc-et-ses-phosphates/

il n'a aucun impact négatif sur l'agriculture ou le transport le long de la route reliant Khouribga et Jorf Lasfar. Le système se compose de plusieurs conduites, qui s'étendent sur une distance totale de 227 kilomètres.

2.1.1 Description du système de transport

Le processus d'obtention de phosphate implique l'extraction du minerai de divers endroits et son traitement en différentes qualités de phosphate dans des usines de lavage. Le phosphate est ensuite transformé en une pulpe d'eau et de phosphate et transporté à travers un pipeline de boue. Le pipeline reçoit du minerai de phosphate de différentes qualités de quatre stations de lavage, ce qui donne différentes propriétés d'écoulement. La boue est transportée par lots avec des bouchons d'eau pour éviter le mélange des grades de produit. Le but ultime est de livrer le minerai de phosphate aux unités industrielles pour le traitement.

Le but principal du pipeline est de transporter de la boue annuellement à un débit de 26 à 38 millions de tonnes. Le système est entièrement automatisé et surveillé à partir d'une salle de contrôle centrale située à la station principale. Les opérateurs sont alertés par des alarmes dans le système de contrôle lorsque les conditions de fonctionnement du pipeline sortent de la plage de conception. De plus, le système dispose de mesures de contrôle pour éviter les dommages

aux équipements. Le diagramme de la Figure 2.2 illustre les composants fondamentaux du processus. Le pipeline principal est un pipeline de 187 kilomètres

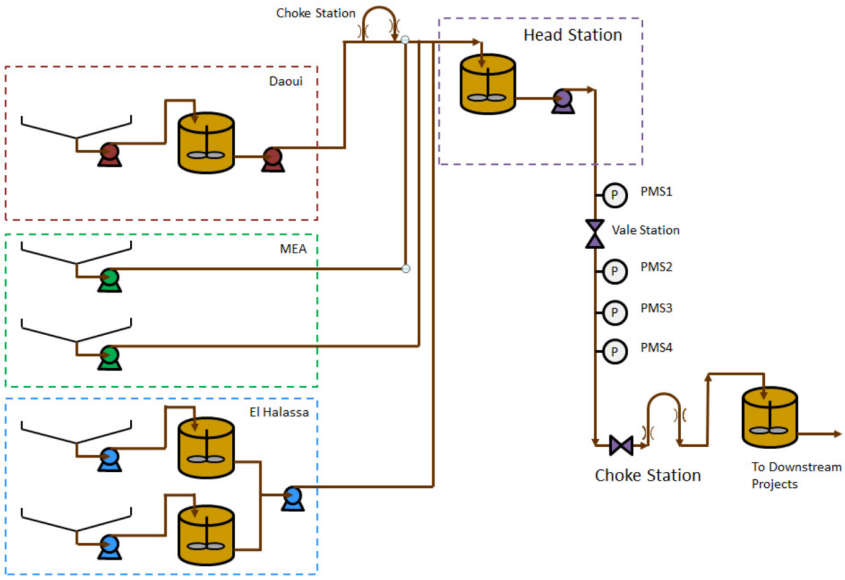

Figure 2.2: Main Pipeline Components. Adpaté depuis Rusconi et al. [2016]

qui transporte la boue de la station principale à la station terminale de Jorf. Il fonctionne principalement en descente et peut gérer une capacité d'environ 4400 t/h. Il y a quatre stations de surveillance de pression le long du pipeline principal et un transmetteur de densité est installé à la station terminale.

Pour transporter le minerai de phosphate d'OCP, il est important de prendre en compte la densité des solides, qui est généralement de $3,0t/m^3$. Cependant, à une porosité de 20 pour cent, la densité des solides "effective" pour la pulpe d'OCP avec une densité de solides de $3,0t/m^3$ est équivalente à $2,6t/m^3$. De plus, la pulpe de phosphate a une concentration de volume solide qui peut atteindre jusqu'à 40 pour cent. Les particules solides dans la pulpe de phosphate ont des formes irrégulières et des diamètres sphériques équivalents allant de 44 μ_{m} à 250 μ_{m}.

2.2 Concepts de base dans les écoulements solide-liquide

2.2.1 Introduction des propriétés clés

Les écoulements biphasiques dispersés se caractérisent par la présence d'une phase dispersée, qui peut être des particules solides, des gouttelettes liquides ou des bulles de gaz, en suspension dans une phase continue. Les principes fondamentaux et la terminologie des écoulements biphasiques dispersés sont utilisés pour

fournir une caractérisation hydrodynamique des mélanges solide-liquide contenant des particules dispersées. La densité du fluide porteur (ϱ_f), la densité des particules solides (ϱ_s) et la densité du mélange (ϱ_m). La valeur de s_w sert de référence pour exprimer la densité relative ou la gravité spécifique des autres matériaux. La formule pour calculer la densité relative, notée s_m (c'est-à-dire la gravité spécifique moyenne du mélange), pour une combinaison de solides et de liquide est la suivante :

$$s_m = 1 + (s_s - 1)\, c_v \tag{2.1}$$

où c_v est la concentration volumétrique, c'est-à-dire la fraction du volume de mélange occupée par les solides.

La concentration de particules d'une suspension est déterminée par le rapport entre le volume de particules dans une zone spécifique et le volume total du mélange. Elle est également exprimée en pourcentage de poids, qui est calculé en prenant le rapport entre le poids des particules et le poids total du mélange. La concentration en solides ou la fraction volumique de la phase solide, est symbolisée par ϕ_s.

Il est crucial de se rappeler que la somme des fractions de volume des phases dispersées et porteurs est égale à une. Par conséquent, la fraction de volume du liquide porteur, qui est de l'eau dans ce cas particulier, peut être calculée comme suit:

$$\phi_w = 1 - \phi_s \tag{2.2}$$

La fraction volumique de particules, représentée par ϕ_s, varie de 0 à une valeur maximale ϕ_{max}, communément appelée fraction d'empilement maximale.

2.2.2 Les régimes d'écoulement des suspensions dans les pipelines horizontaux.

Les écoulements de suspension sont généralement affectés par l'installation, où les particules solides interagissent avec les tourbillons turbulents du fluide porteur, ainsi qu'entre elles par des collisions inter-particules ou des contacts plus durables . Ces interactions sont fortement influencées par les propriétés physiques du mélange de suspension telles que la vitesse d'écoulement, la concentration de particules et la distribution de taille de particules. En résumé, les écoulements de suspension en installation peuvent être classés en quatre types comme présenter dans la figure Fig. 2.3: suspension homogène, suspension hétérogène, suspension à lit mobile et suspension à lit fixe. La suspension homogène a des particules réparties uniformément dans toute la conduite sans gradient de concentration de haut en bas; la suspension hétérogène a des particules non uniformément réparties et des gradients de concentration se produisent généralement dans la section transversale de la conduite; la suspension à lit mobile a des particules formées et déplacées avec l'écoulement de fluide ; et la suspension à lit fixe a des particules qui se sont déposées au fond de la conduite, formant une couche

stagnant.

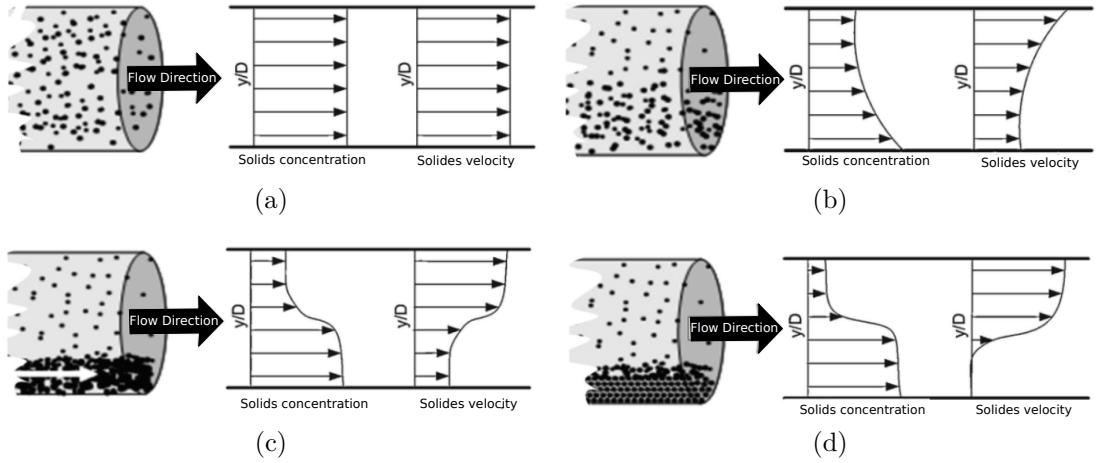

Figure 2.3: Typical settling slurry flows patterns. Adapté depuis https://cfdflowengineering.com/slurry-flows-and-its-cfd-modelling/

Les modèles d'écoulement des boues sont influencés par les frottements dans le pipeline, ce qui entraîne une résistance accrue et une sécurité de transport réduite. La perte de charge due aux frottements est un mesure de la résistance à l'écoulement causée par les forces de frottement entre le fluide et les parois de la conduite. La vitesse d'écoulement est un paramètre important pour évaluer la sécurité de transport de l'écoulement des boues, car des vitesses élevées peuvent causer l'érosion et l'usure sur les parois du pipeline. Pour contrôler efficacement les pertes d'énergie et maintenir les particules en suspension, il est essentiel de mener une analyse complète de la perte de charge et des facteurs qui l'influencent.

2.2.3 La turbulence dans les écoulements de boue

La turbulence joue un rôle crucial dans les écoulements de boues car elle affecte la suspension et le mélange des particules solides dans l'écoulement, les empêchant de se déposer ou de se séparer du fluide. Elle est étroitement liée au nombre de Reynolds, qui est une grandeur sans dimension décrivant le rapport des forces inertielles aux forces visqueuses dans un écoulement de fluide. Le nombre de Reynolds (Re) peut aider à prédire l'apparition de la turbulence dans un écoulement et est un paramètre important pour comprendre le comportement des écoulements de boues.

$$Re = \frac{\rho v D}{\mu} \tag{2.3}$$

D'autre part, le comportement des particules dans le fluide est plus lié au nombre de Stokes.

Le nombre de Stokes (St) est un nombre sans dimension qui représente le rapport du temps de réponse des particules (τ_p) à l'échelle de temps caractéristique

de l'écoulement du fluide.

Il décrit l'importance relative des forces inertielles par rapport aux forces visqueuses agissant sur les particules.

$$St = \frac{\tau_p(\varrho_s - \varrho_f)g}{u_f} \tag{2.4}$$

où : ϱ_s est la densité de la particule, ϱ_f est la densité du fluide, u_f est la vitesse du fluide, g est l'accélération due à la gravité. Le nombre de Stokes est une mesure de l'importance relative des forces inertielles et visqueuses dans un fluide. Lorsque le nombre de Stokes est inférieur à 1, l'écoulement est généralement laminaire et est principalement régi par les forces visqueuses. Lorsque le nombre de Stokes dépasse 1, l'écoulement est principalement régi par les forces inertielles et devient turbulent, ce qui entraîne un mouvement irrégulier et chaotique à la fois des particules fluides et solides. Le temps de relaxation des particules est le temps qu'il faut à une particule pour s'adapter aux changements de l'écoulement, il est calculé comme suit :

$$\tau_p = \frac{\varrho_s d_p^2}{(18\mu_f)} \tag{2.5}$$

où ϱ_s est la densité des particules, d_p est le diamètre des particules et μ_f est la viscosité du fluide.

Le mouvement des particules dans un fluide est influencé par diverses forces qui sont déterminées par la vitesse du fluide et les caractéristiques physiques de ces particules, telles que la taille, la forme et la densité. Ces forces sont communément appelées lois de transfert, car elles décrivent les interactions qui se produisent à l'interface entre les phases. La force de traînée généralisée $\mathbf{M}_k^d$, représente la force totale par unité de volume agissant sur une suspension de particules. Si la phase dispersée se compose de particules sphériques avec un diamètre moyen d_p, $\mathbf{M}_p^d$ est généralement modélisé comme [Enwald et al., 1996, Ishii and Mishima, 1984] :

$$\mathbf{M}_p^d = n_p \left(\mathbf{M}^{\mathrm{D}} + \mathbf{M}^{\mathrm{L}} + \mathbf{M}^{\mathrm{VM}}\right) \tag{2.6}$$

où $\mathbf{M}^{\mathrm{D}}$ est la force de traînée standard, $\mathbf{M}^{\mathrm{L}}$ la force de portance, $\mathbf{M}^{\mathrm{VM}}$ la force de masse virtuelle, sont les forces qui agissant sur une particule dans la suspension à savoir. n_p est le nombre de particules par unité de volume. L'interaction entre les forces discutées détermine la réponse globale des particules dans l'écoulement et affecte considérablement le transport de la masse, de la chaleur et des solides. L'inclusion de ces forces dans les modèles mathématiques pour les simulations numériques peut améliorer la prédiction de la mobilité des particules, ce qui conduit à une meilleure compréhension du comportement des suspensions dans les pipelines.

3

Research methodologies for exploring solid-liquid flows

Objectives:

The first section 3.1, outlines the feasible approaches that can be employed to study the flow of solids and liquids. The concise summary provided in the latter section is elaborated upon in the subsequent two sections. Section 3.2 details the various technologies that can be utilized to conduct measurements of solid-liquid flows, with a specific emphasis on their reliability and constraints. This helps to ensure that any comparisons made between numerical predictions and experimental data from existing literature are reliable and consistent. Section describes the different CFD methods and approaches for simulating two-phase flows. Section 3.4 provides a summary of past research efforts, categorizing the studies based on the approach that was employed. In Section 3.5, the focus is on the two-fluid model and it elaborates on the key characteristics of the Eulerian two-phase flow theory that is employed for solid-fluid systems. Finally, in section 3.5.3, the ways in which the two-fluid model addresses turbulence are explained, and the models that will be utilized later in this research are presented.

Contents

3.1 Research approaches

To accomplish the objective of this thesis, which aims to predict turbulent solid-liquid flows through horizontal and inclined pipelines, a comprehensive exploration of diverse research approaches must be conducted. As a starting point, just a basic summary of the possible approaches is first provided:

- **Experimental study:**
  Several researchers have conducted experimental investigations on the turbulent flow of solid-liquid suspensions in pipeline systems. It involves conducting physical experiments in a laboratory or in the field to gather data about a particular phenomenon or system. This approach typically involves measuring variables directly or indirectly related to the phenomenon, often using specialized equipment or instruments. The data collected from these experiments can then be analyzed to gain insights into the behavior of the system being studied. The primary benefit of this method is that the researcher is exposed to the actual flow, although on a smaller scale. However, experimental testing are prohibitively costly and need specialized equipment, and taking measurements presents considerable technical challenges, particularly for extremely concentrated mixtures. Experimental studies of dense solid-liquid flows are often restricted to horizontal pipelines, the experimenters then offer pressure drop, concentration distribution, and velocity distribution data. The experimental data can then be used to develop mathematical models that describe the behavior of the slurry. These models can be based on fundamental principles of physics, such as the conservation of mass, momentum, and energy, and/or on empirical relationships derived from experimental data. However, the experimental investigation for slurry flows is still complicated by a variety of restrictions coming mostly from the following three aspects of the issue:
  - The abundance of variables which influence the flow.
  - The broad range within which the majority of variables may fluctuate.
  - The inevitable restriction on the precision and reproducibility of data derived from heterogeneous settling slurries.
- **Computational fluid dynamics (CFD) approach:**
  This technique for solving the issue involves performing numerical simulations. Compared to experimental testing, this approach is relatively inexpensive and, most importantly, adaptable, since it permits the simulation of almost any system, regardless of its size. The complexity of solid-liquid flow, particularly in settling slurry, requires a detailed examination of flow behavior at a local level by studying the distributions of flow quantities across the flow domain. In recent times, Computational Fluid Dynamics (CFD) has proven to be a highly valuable and effective tool for modeling

and predicting different slurry flow scenarios. Furthermore, CFD allows researchers to access a wealth of fluid hydrodynamic information that is often challenging to obtain through conventional measuring instruments. Traditionally, the use of CFD simulations for engineering purposes has been limited to simpler one-phase flows due to constraints in computational power and CFD software capabilities. However, recent advancements in this field have led to a significant increase in research focused on numerically simulating slurry flows through pipelines within a relatively short time frame (as discussed in Section 3.4). This progress has opened up new possibilities for applying CFD in various engineering applications. The insights obtained from CFD simulations can be harnessed to enhance system performance, achieve higher reliability, confidently scale up operations, improve product consistency, and increase overall plant productivity [Bakker et al., 2001]. The advantages of CFD can be categorized as:

  - It provides a detailed understanding of flow distribution, mass and heat transfer, particulate separation, etc, especially for a settling slurry case. Consequently, all these will lead to a much better and deeper understanding of what is happening in a particular process or system.
  - It is able to reduce scale-up problems because the models are based on fundamental physics and are scale independent.
  - It is particularly useful in simulating conditions where it is not possible to take detailed measurements.

- **Physically-based reduced order models:**
  Engineers dealing with two-phase flows commonly make use of Reduced Order Models or surrogate models. These models can be partially or entirely based on empirical data but are grounded in physical principles and often involve simplifying assumptions about the flow's topology and empirical closures. In many instances, these models adopt a global formulation, encompassing integral equations for mass and momentum. This renders them a cost-effective and time-efficient solution for designers, providing satisfactory accuracy for most applications without the computational demands of CFD simulations. However, it is important to acknowledge the limitations of these models. Their global formulation makes them more suitable for estimating macroscopic factors, particularly head losses. Moreover, the need for simplifying assumptions restricts their applicability to specific flow scenarios. Furthermore, it should be noted that Reduced Order Models based on physical principles find their primary utility in horizontal pipe flows involving solid-liquid mixtures.

In fact, both the experimental and CFD approaches have their own strengths and limitations, and can be used together to gain a more comprehensive understanding

of fluid behavior in complex systems. Experimental data, as presented in section 6, play a pivotal role in the CFD simulation of slurry flows. They are essential for both calibrating and validating the CFD model. Calibrating a CFD model involves adjusting its empirical or challenging-to-evaluate parameters to match specific experimental measurements. On the other hand, validation ensures that the CFD model's predictions align well with experimental or numerical data. Following recommended practices in CFD, it is advisable to first calibrate the model's coefficients using a particular set of experimental data and then validate the model using a different set of experimental or numerical data. This two-step process ensures the model's accuracy and reliability when predicting real-world scenarios.

Once the calibration and validation steps have been completed, the CFD model becomes a valuable tool for obtaining information about challenging-to-measure aspects of the flow under the same testing conditions or for exploring different flow scenarios. If a CFD model is initially calibrated or validated against a specific set of experimental data and subsequently employed to gather information on other flow features under the same conditions, it is considered interpretative in nature. For instance, CFD models for slurry pipe flow are typically calibrated and validated based on parameters such as the hydraulic gradient or the vertical solid concentration profile, which are commonly recorded in experimental campaigns. With the same CFD model, researchers can then investigate other difficult-to-measure parameters or provide explanations for certain experimental observations. This interpretative approach enhances the model's versatility and utility in studying various aspects of the flow.

On the other hand, a CFD model can also be employed for flow conditions different from those used during the calibration and validation phases, which falls under the category of predictive purposes. Two pertinent examples of predictive CFD models for slurry pipe flows are models used to predict slurry flow in large-diameter pipes after calibration and validation on small-diameter pipes at the laboratory scale, and models used to predict slurry flows in pipe bends or other pipeline fittings after calibration based on straight pipe experiments. However, establishing a CFD model as predictive is a challenging task. To provide confidence in the model's predictions for conditions where no experimental data are available, it is essential to ensure that the model can accurately capture all relevant physical phenomena occurring in both the calibration/validation and the application scenarios. This entails rigorously validating the model's performance across a wide range of flow conditions to demonstrate its predictive capability.

In the following, the above research methodologies are further discussed with a practical point of view on slurry flows.

3.2 Experimental exploration of slurry flows

As mentioned in section 1.1, experimental analysis of solid-liquid flows poses considerable technical and cost challenges, especially when dealing with dense mixtures and intricate flow patterns. Among the most crucial fluid dynamic parameters, solids concentration, velocity, and pressure hold significant importance. Below is an overview of potential experimental methodologies for measuring each of these quantities.

3.2.1 Solids concentration

As was previously mentioned, either volume or mass can be used to express the concentration of the scattered phase. The changeover from one to the other seems to be a simple procedure. Volume fraction and concentration will now be referred to as the same thing. The concentration of solids can be specified using mean or local values when discussing solid-liquid fluxes. The mean solids concentration is the overall measurement that captures the concentration of solids as a whole.

A few studies on solids-liquids flows in horizontal pipes [Gillies et al., 2004, Schaan et al., 2000b] mention the in-situ concentration, which is determined by introducing a measured amount of solids into a water tank with a known volume. The mixture is then recirculated in the loop. Measuring the in-situ concentration is a simple process, but it may not accurately reflect the volume proportion of particles actually flowing into the circuit, which is known as the delivered concentration. This is due not only to the possibility of particles accumulating in certain areas within the equipment, but also to the fact that their velocity may differ from that of the surrounding fluid. As per [Gillies et al., 1991], the in-situ concentration corresponds to the delivered concentration only if the particles' relative velocity with respect to the fluid is zero. This condition typically arises when the particles have a small Stokes number. In order to overcome this problem, most researchers provide mean delivered concentration values. These values are determined either through the use of expensive counter flow meters [Matousek, 2000, 2002, Skudarnov et al., 2004], or are estimated from the locally acquired values obtained through the methods explained below. The measurement of concentration is accomplished through the absorption technique, which is dependent on the reduction in intensity of radiation (either X-rays or gamma rays). According to the Beer-Lambert law, a monochromatic radiation beam experiences a reduction in intensity as it travels through a substance.

$$I = I_0 e^{-\varrho \tilde{\mu}_j l} \tag{3.1}$$

Here, I represents the radiation intensity that is measured after the beam has passed through a distance of l within the substance, while I_0 denotes the initial intensity. Additionally, ϱ and $\tilde{\mu}_j$ refer to the density and mass absorption coefficient of the medium, respectively. If a beam passes through a mixture of

two components, such as solid particles and liquid, with their respective attenuation coefficients denoted as $\tilde{\mu}p$ and $\tilde{\mu}c$, and densities denoted as ρ_p and ρ_c, the corresponding relationship can be expressed as:

$$I = I_0 e^{-\rho_p \tilde{\mu}_p l_p - \rho_c \tilde{\mu}_c l_c} \tag{3.2}$$

The terms (l_p) and (l_c) refer to the distances that the radiation beam must travel through the particle and liquid components, respectively. By measuring two values of radiation intensity (as illustrated in Fig. 3.1), Equation 3.2 can be used to determine the chord-averaged concentration of solids. According to [Kumar et al., 1997], the absorption technique provides values for solids concentration that lie between local and mean values, rather than giving precise local values. Despite its expense, the absorption method remains the most commonly employed technique for studying the behavior of solid-liquid slurries in horizontal pipelines. The practice of using chord-averaged readings to reconstruct the distribution of solids concentration across a specific cross-section is known as tomography. To perform this technique, multiple measurements are taken at various angles of orientation, as illustrated in Fig. 3.2a. Since previous research has indicated that the concentration of particles in horizontal pipe flows is symmetric with respect to the vertical diameter [Kaushal et al., 2005, Roco and Shook, 1983b], a less expensive method known as densitometry is often utilized. In densitometry, the scanning beam is kept horizontal while traveling vertically. As depicted on the right-hand side of Fig. 3.2b, densitometry allows for the assessment of chord-averaged concentration at different vertical positions y. The average solids concentration can be calculated by weighting the data with the corresponding chord length L_y and taking the mean, as described by [Gillies, 1993]. A different technique for dynamically measuring the local solids concentration at the pipe wall is the wall conductivity probe, which was developed by [Klausner et al., 2000], as shown in Fig. 3.3. Unlike wall-sampling probes, this method is non-intrusive, utilizing a series of electrodes positioned outside the pipe, encompassing the entire wall. Conductance (or impedance) measurements between adjacent electrodes are utilized to estimate the local concentration of solids at the pipe wall. The

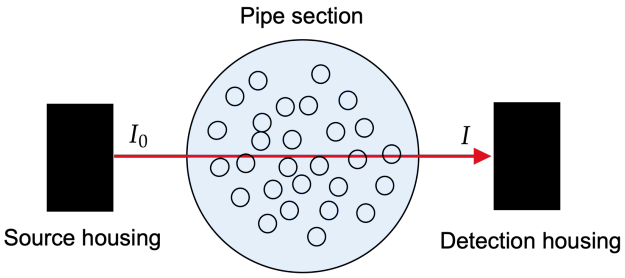

Figure 3.1: Principle of the absorption method

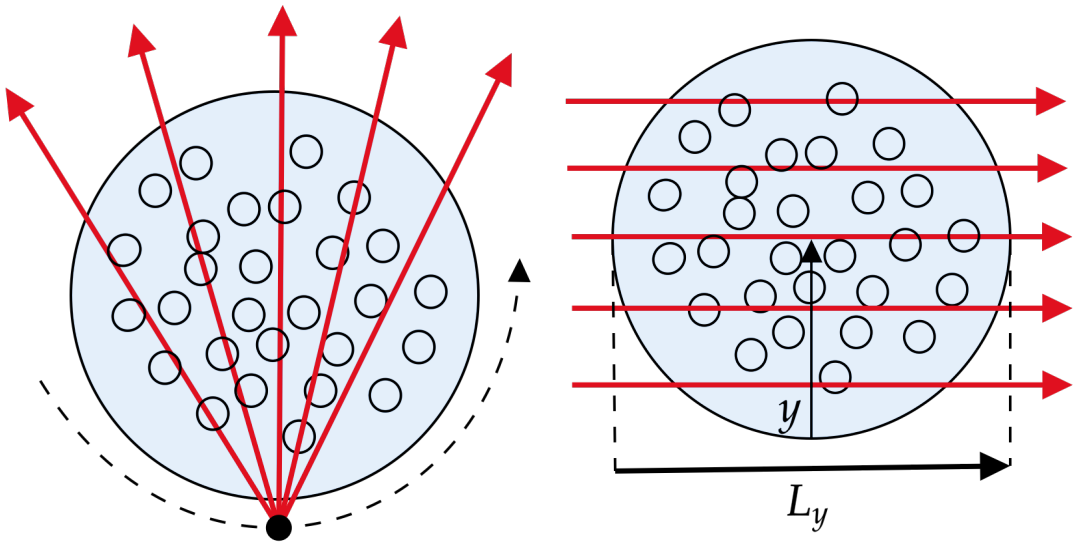

(a) tomography (b) Densimeter

Figure 3.2: The absorption method's scanning techniques: (a) Tomography, (b) Densimeter.

wall conductivity probe is commonly employed for slurries flowing through large-diameter horizontal pipelines. Under the assumption of horizontal uniformity in slurry concentration due to gravity stratification, the particles distribution and their mean concentration are calculated from the local values near the pipe wall.

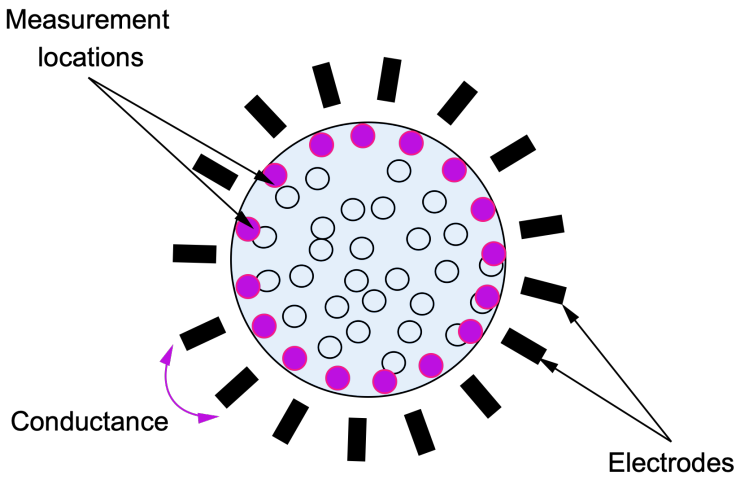

Figure 3.3: Wall conductivity probe

3.2.2 Velocity

The velocity fields of solid-liquid flows may be described using either mean or local parameters, similar to the solids concentration. To characterize the mixture, the volumetric flow rate is often monitored using electromagnetic flow meters, as in single-phase flows [Gillies, 1993, Kaushal and Tomita, 2007]. Laser Doppler Velocimetry (LDV) is a widely adopted technique for measuring the local velocities of both phases in the flow. In this method, two laser beams of equal intensity are directed to intersect at a precise point within the flow field. LDV has proven to be accurate and reliable for measuring flow velocities in single-phase flows, as depicted in Fig. 3.4. Tiny tracer particles are introduced into the fluid to trace

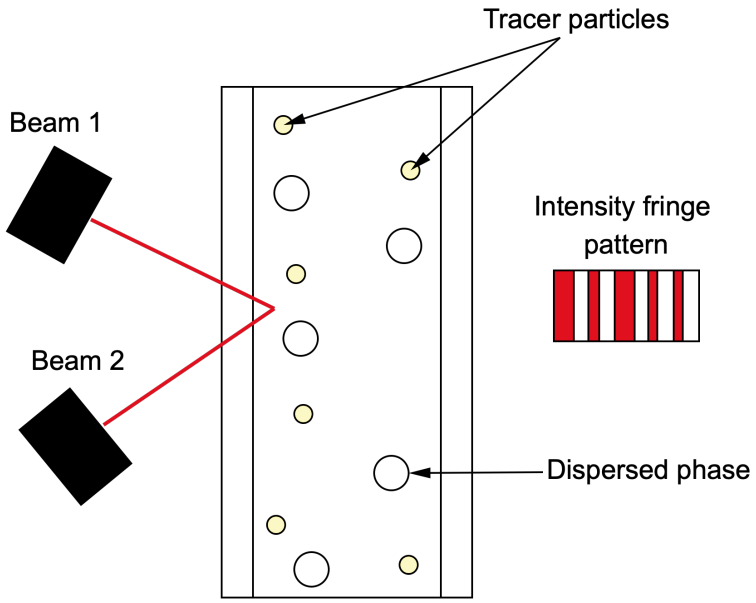

Figure 3.4: Laser Doppler Velocimetry principle

the fluid's movements in LDV. As a particle infused fluid passes through the measuring point, one of these particles will scatter and interfere with the light from all the beams. A detector detects the resulting variable intensity fringe patterns, which can be correlated to the velocity of the tracer particle, providing a reasonable estimate of the fluid velocity. The amount of light scattered as the dispersed phase particle passes through the beam varies depending on its size. Specific techniques have been developed to distinguish between the velocities of the two phases, enabling the LDV processor to avoid interpreting the light scattered by a dispersed phase particle as the velocity of the liquid phase. LDV is a widely used technique for measuring local velocities in solid-liquid flows, as evidenced by numerous studies reported in the literature [Chen, 1991]. However, this approach is considered unreliable for concentrated mixtures, where the mean solids concentration exceeds 15 to 20 percent, except for homogeneous flows with small

velocity differences between the phases, as stated by [Kumar et al., 1997].

3.2.3 Pressure

Pressure transducers are a widely used tool for monitoring the pressure of solid-liquid mixtures, as in single-phase flows. Separation chambers are often used to restrict access to the pressure transducers and their tubes to only the liquid phase, as reported in [Kaushal and Tomita, 2007].

3.3 Computational methods for dispersed two-phase flows

Numerical modeling and simulation offer the most effective means to investigate and conduct studies on such flows. Various models are available for predicting quantities in slurry flows. These models rely on different approaches, which come with varying levels of complexity and refinement. Simpler approaches are easier to use but yield less detailed outputs. The simplest modeling approach employs semi-empirical correlations, which focus solely on integral (cross-section averaged) quantities and provide predictions of key parameters under specific conditions. While these approaches offer valuable insights, they have limitations in capturing fine-grained flow characteristics. Typically, the models relate suitable dimensionless groups depending on the slurry type using empirical coefficients [Durand, 1953, Matoušek et al., 2020]. A more advanced modeling approach takes the internal flow structure into consideration, albeit in a simplified manner. This internal structure can be conceptualized as comprising layers with distinct properties and flow conditions. Layered models, such as the two-layer model proposed by [Matoušek et al., 2018], capture friction and support mechanisms by formulating force balances for each individual layer. In addition to the frictional hydraulic gradient (i_m), these models solve for the thicknesses and velocities of each layer. One of the notable predictions of the layered model is the deposition-limit velocity, which corresponds to the flow velocity at which the lowest layer, composed of particles in contact, ceases sliding over the pipe wall and transitions into the stationary bed layer. However, advancements in computational power have facilitated the widespread availability of commercial and open-source codes capable of simulating complex physics in realistic geometries. As a result, the engineering analysis of slurry flows can be enhanced by integrating traditional approaches with digital simulations. Among these digital simulation methods, Computational Fluid Dynamics (CFD) offers the most detailed solution for slurry flow. It is the primary focus of the present thesis and will be discussed in the following sections. CFD enables a comprehensive understanding of the flow behavior by considering the interactions of solid particles and the fluid in intricate flow scenarios.

All computational techniques for dispersed two-phase flows assume a continuous carrier fluid phase. Typically, the techniques are classified according to how the scattered phase is handled (see Fig. 2.9). The selection of the modeling approach for CFD simulations in solid-liquid flows is dictated by the flow regime and key flow mechanisms. Two main categories of CFD models are commonly used for such simulations: Eulerian-Lagrangian models and Eulerian-Eulerian models [Hiltunen et al., 2009]. In most cases, the carrier liquid is modeled in the Eulerian, cell-based framework by solving for a two-phase extension of the Navier-Stokes equations. On the other hand, the dispersed phase can be modeled using either the Lagrangian framework, by tracking computational particles' trajectories, or the Eulerian framework, by solving for the flow equations of a fictitious fluid representing the dynamic behavior of the ensemble of particles. To elaborate further, the two approaches are defined as follows [Crowe et al., 2011].

3.3.1 Methods based on kinetic (Eulerian–Lagrangian) approach

The liquid phase is modeled as a continuum and solved in an Eulerian cell-based framework, whereas the behavior of the solid phase is obtained by the Discrete Particle Method (DPM), in which the individual trajectories of computational particles are calculated and seeks to determine the properties of each particle [Benjelloun et al., 2012, Brennen and Brennen, 2005, El Hamra and Boukharfane, 2023a,b]. Particle tracking is accomplished by solving a set of differential equations that govern the particle's location $\mathbf{x}p$, velocity $\mathbf{u}p$, and angular velocity $\boldsymbol{\omega}_p$ [Laín and Sommerfeld, 2008]. These equations describe the trajectory and motion of individual particles as they interact with the fluid flow and other particles in the system. By solving these equations, the Lagrangian approach can accurately trace the movement and behavior of dispersed particles within the flow field.

$$\frac{\mathrm{d}\mathbf{x}_p}{\mathrm{d}t} = \mathbf{u}_p \tag{3.3}$$

$$m_p \frac{\mathrm{d}\mathbf{u}_p}{\mathrm{d}t} = \mathbf{F}_p \tag{3.4}$$

$$I_p \frac{\mathrm{d}\boldsymbol{\omega}_p}{\mathrm{d}t} = \mathbf{T}_p \tag{3.5}$$

In the set of differential equations for particle tracking, m_p represents the particle mass, I_p denotes the moment of inertia of a particle, while $\mathbf{F}_p$ and $\mathbf{T}_p$ represent the net force and the torque acting on a particle, respectively [Laín and Sommerfeld, 2008]. These equations encapsulate the motion and rotational behavior of individual particles as they interact with the fluid flow and other particles in the system. Section 2.2.3 discusses the analysis of various forces, such as drag, lift, and virtual mass forces, that contribute to the overall force acting on a particle. The classical Navier-Stokes equations are valid in all fluid domains, while

adhesive boundary conditions are imposed at the particle surface, as illustrated in Fig. 3.5. One commonly used approach for solving equations involving small

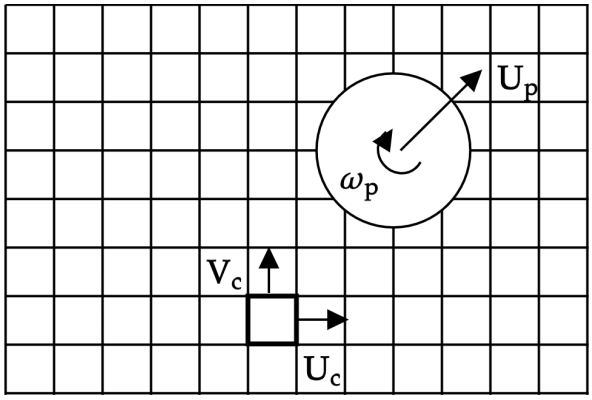

Figure 3.5: Tracking particles approach

particles is to represent them as zero-dimensional mass points. This is known as the point-particle approximation [Prosperetti and Tryggvason, 2009]. As a result, the fluid's equilibrium equations in local instant formulation are as follows:

$$\frac{\partial \rho_c}{\partial t} + \nabla \cdot (\rho_c \mathbf{u}_c) = 0 \tag{3.6}$$

$$\frac{\partial}{\partial t}(\rho_c \mathbf{u}_c) + \nabla \cdot (\rho_c \mathbf{u}_c \mathbf{u}_c) = \nabla \cdot \boldsymbol{T}_c + \rho_c \mathbf{g} + \sum_{n=1}^{N_p} \mathbf{F}^n \left(\mathbf{x}_p^n\right) \delta \left(\mathbf{x} - \mathbf{x}_p^n\right) \tag{3.7}$$

where ρ_c denotes the fluid density, $\mathbf{u}_c$ represents the local velocity field, $\boldsymbol{T}_c$ stands for the stress tensor, and $\mathbf{g}$ represents the gravitational acceleration.

The final term in Eq. (3.7) represents the force per unit volume exerted by the N_p particles on the fluid. This force is estimated by superimposing Dirac delta functions, centered at the location $\mathbf{x}_p^n$ of each particle. The conservation of angular momentum is expressed as $\boldsymbol{T}_c = \boldsymbol{T}_c+$, where the superscript '+' signifies the transposition of the dyadic. Equations 3.6 and 3.7 may be solved directly [Portela and Oliemans, 2003]. The grid size needs to be smaller than the Kolmogorov scales, similar to single-phase flow, because all scales of the phenomenon must be resolved. Moreover, the point-particle approximation necessitates that the particles are considerably smaller than the grid size. Unless the particles are relatively small, DNS of the equations in local instant formulation is not feasible. This is more commonly solved in an averaged form of Eqs. (3.6) and (3.7). In some cases, a Large Eddy Simulation (LES) method [Armenio et al., 1999, Portela and Oliemans, 2003, Yu et al., 2004] is employed to account for the influence of sub-grid scale stress tensors on resolved eddies, where the local

instantaneous equations are spatially filtered. The filtered pressure and velocity fields are acquired through this approach. Due to the high computational cost associated with Large Eddy Simulation (LES), an alternative approach is often employed, such as solving a Reynolds-averaged (RANS) formulation of the local instantaneous equations. This involves performing a Reynolds decomposition of the flow variables, followed by time averaging. The RANS approach provides a more computationally efficient way to model turbulence by capturing its statistical behavior, making it well-suited for practical engineering applications. The system of equations is closed by coupling an appropriate turbulence model, with the unknowns being the mean pressure and velocity fields.

3.3.2 Methods based on continuum (Eulerian–Eulerian) approach

In the continuum approach [Boukharfane et al., 2021, Brennen and Brennen, 2005], both phases are modeled as interpenetrating continua with moving boundaries (cf. Fig. 3.6), and two sets of conservation equations are solved jointly in the Eulerian framework. The following are the classic differential conservation

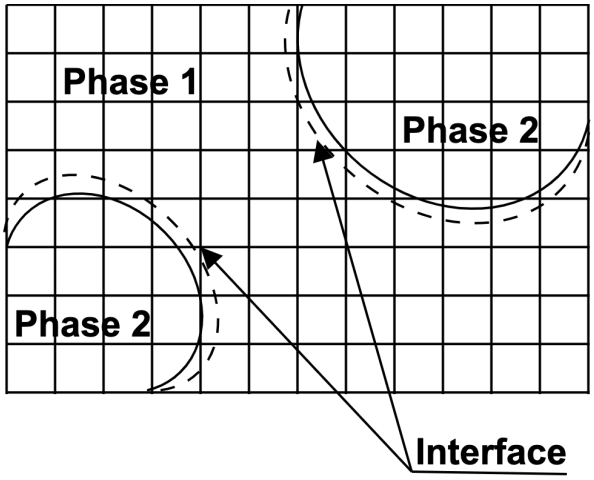

Figure 3.6: Continuum approach

equations of motion of phase k, which are valid in the interior of each phase:

$$\frac{\partial \rho_k}{\partial t} + \nabla \cdot (\rho_k \mathbf{u}_k) = 0 \tag{3.8}$$

$$\frac{\partial}{\partial t}(\rho_k \mathbf{u}_k) + \nabla \cdot (\rho_k \mathbf{u}_k \mathbf{u}_k) = \nabla \cdot \boldsymbol{T}_k + \rho_k \mathbf{g} \tag{3.9}$$

where: ρ_k is the density of pure phase k; $\mathbf{u}_k$ the local velocity field; and $\boldsymbol{T}_k$ the stress tensor. The symmetry of the dyadic $\boldsymbol{T}k$ is implied by conservation of

angular momentum for both phases, hence $\boldsymbol{T}k = \boldsymbol{T}_k^+$, as previously noted. The degree of coupling between the two phases varies based on the concentration of solids in the flow, ranging from one-way coupling in dilute slurries (where the particles have no effect on the liquid flow field) to four-way coupling in dense slurries, where particle-particle and particle-fluid interactions play a crucial role. More details are found in section 2.2. Matching conditions between the two phases are necessary to describe the exchange of mass and momentum across the interface. These conditions are based on a special form of the balancing equations applied at the interface and serve as a means of jumping from one phase to another. The local instantaneous leap requirements were derived in a detailed manner in [Ishii, 1975]. The final expressions presented in their work are as follows:

$$\sum_{k=1}^{2} \dot{m}_k = \sum_{k=1}^{2} \rho_k \mathbf{n}_k \left(\mathbf{u}_k - \mathbf{u}_i\right) = 0 \tag{3.10}$$

$$\sum_{k=1}^{2} \left(\dot{m}_k \mathbf{u}_k - \boldsymbol{T}_k \cdot \mathbf{n}_k\right) = \sigma \kappa \mathbf{n} \tag{3.11}$$

where: $\dot{m}_k$ is the mass transfer of phase k per unit area of interface and unit time; $\mathbf{u}_i$ the velocity of the interface; $\mathbf{n}_k$ the unit outward normal vector of phase k; σ the surface tension; κ the mean curvature of the interface; and $\mathbf{n}$ the unit interface curvature radius vector. The pressure and velocity of each phase, as well as the location of the interface, are the unknowns that can be directly solved by the conservation equations (Eqs. (3.8)-(3.9)) and the jump conditions (Eqs. (3.10)-(3.11)). Locating the interface where there is an abrupt change in density and viscosity is the most challenging aspect, in addition to the extensive computational time required to resolve all scales of the phenomenon up to the Kolmogorov scales. A common approach, known as the one-fluid technique [Prosperetti and Tryggvason, 2009], is frequently utilized. This method involves incorporating a marker function, H, which is set to 1 where a specific fluid exists and 0 elsewhere, and solving a transport equation for H. Various approaches, including Level Set, Shock Capturing, and Volume of Fluid (VOF), have been developed based on the concept of H. The sharpness of the H function in both directions may lead to an inaccurate determination of the interface location. Other methods, such as Front Tracking and Marker Particle are more accurate yet time-consuming. Solving the local instantaneous equations directly using the kinetic approach is typically limited to very basic flows that are only of academic interest. It is worth noting that the application of Eqs. (3.8)-(3.11) is not completely certain for solid-liquid flows, since solid particles are more likely to be characterized by solid continuum mechanics' balancing rules. However, since a group of solid particles can be considered as a type of "fluid", it is more commonly accepted to use an averaged version of the equations mentioned above. In the vast majority of numerical studies involving solid-liquid flows, this strategy, which has the added benefit of decreasing the simulations' computing cost, is commonly used. The

two-fluid model, which will be detailed in the following (section 3.5), and the algebraic slip model (ASM), commonly known as the mixture model, are methods that depend on an averaged version of Eqs. (3.8)-(3.11). The former approach involves solving the complete set of averaged equations for both phases. In the latter approach, the averaged equations are combined to obtain the balance equations for the mixture, which are solved along with the continuity equation for the dispersed phase and an estimated algebraic equation to consider the velocity difference between the phases. The ASM is based on the assumption that a local inter-phase equilibrium is established at small spatial length scales, meaning that the dispersed phase reaches its terminal velocity quickly. Therefore, its validity is limited to very low Stokes numbers and moderate concentrations [Kaushal et al., 2012]. Table 3.1 offers a brief comparison of the previously suggested models.

Table 3.1: Comparison between Euler-Euler models

VOF	Mixture Model	Two Fluid Model (TFM)
Modelling non-miscible fluid	Model used if there is a wide distribution of dispersed phases	Interphase laws available.
A single set of motion equations	Interphase laws not available	More precise.
Examples: free surface flow [Jing et al., 2016], large bubbles in a liquid [Al-Yaari and Abu-Sharkh, 2011], stratified flow [Akhtar et al., 2007]	Examples: particle-laden flow* with low load [Dufek and Bergantz, 2007], bubble flow, sludge flow [Chen et al., 2009a]	Examples: sludge flow [Ofei and Ismail, 2016], sedimentation [Gopaliya and Kaushal, 2016], fluidized beds [Ofei et al., 2014].

[1] The next literature review (cf section3.4) will explore more the model's applications as well as their performance.

3.4 Literature Review

In the past 25 years of publications, a vast majority of the studies relate to horizontal pipeline flows (e.g., [Chen et al., 2009b, Hashemi et al., 2016b, Kaushal et al., 2012], with only a few on vertical pipeline flows [Hadinoto, 2010, Krampa, 2009] and bends/fittings [Kaushal et al., 2013, Singh et al., 2020a]. Pipe diameters of 10–500 mm, flow velocities between 1-9 m/s, bulk solids volume concentrations up to 0.5, density ratios of 1.18 (slush nitrogen [Jiang and Zhang, 2012]) to 4.35 (iron ore slurry [Kumar et al., 2019]), and particle sizes of $0.004 - 2.4$ mm have been studied. A summary of the most relevant numerical studies on slurry flows in horizontal pipes published so far are reported, alongside with the adopted

[1]Particle-laden flow = Particle charge flows refer to a two-phase flow in which one of the phases is continuously connected and the other phase consists of small immiscible particles and typically diluted.

modeling approach, to provide some context regarding the application of each one.

3.4.1 Studies Using Eulerian–Lagrangian Models

First of all it should be outlined that it is not surprising to see that only a few studies dealt with the hydraulic pipe conveying of slurries using the Euler–Lagrange approach. The high values of solid concentration typical in slurry pipelines make it unreasonable to neglect particle–particle interactions, and, therefore, a high computational cost is probably the main reason behind the small number of published articles. This approach was employed for this kind of applications for sand-water slurry by Capecelatro and Desjardins [2013],where the Large Eddy Simulation (LES) method Versteeg and Malalasekera [2007] has been used to simulate the turbulent flow of the liquid phase, while the solid phase was treated by DPM. Comparison of experimental and numerical data showed a very good agreement for particle velocity profiles along the vertical axes. A slight over prediction of particle concentration close to the pipe bottom was observed. The computed pressure drop was about 20 % lower compared to the experimental data. In this study, the Eulerian–Lagrangian model was used to gather information on features of the flow that are hard, if not impossible, to measure experimentally. Arolla and Desjardins [2015] used the same numerical setup to characterize a sand-water flow pattern for increasing values of liquid superficial velocity. At low liquid flow rates, the sand will drop out of the carrier liquid and form a stable, stationary bed. When the liquid flow rate increases above a specific value, sand starts getting transported in a thin layer above the bed. As the flow rate increases further, the sand bed breaks into a series of slow-moving dunes which eventually form a moving bed along the bottom of the pipe. At even higher flow rates, the sand particles get fully suspended in the carrier liquid. This approach was also employed with different characteristics such as transportation of coarse NaCl particles in brine by Uzi and Levy [2017], where the liquid phase is handled by a computationally cheaper Reynolds-Average Navier-Stokes (RANS) technique, to examine the effects of the operating conditions on the flow (conveying velocity, particle concentration, particle size and pipe diameter) on flow pattern. Recently, this approach was used to present a numerical study of the horizontal hydraulic transport of coarse sand particles in water by Zhou et al. [2020]. They suggested that a RANS-based CFD-DEM can be used to predict the transition between slurry flow regimes and to simulate pressure drops. However, an extensive validation study is needed to give strength to this claim. In summary, it is clear that the CFD-DEM model has the potential to provide a great deal of insight into the pipe transport of solids in the form of slurry. However, up to now, the high computational cost has been a limiting factor to the use of this approach.

3.4.2 Studies Using Eulerian–Eulerian Models

In fact, highly concentrated slurry flows are typically modeled using the Eulerian–Eulerian framework where the suspending liquid and dispersed particulate phase are viewed as interpenetrating continua (i.e., "two-fluid" approach). This modelling approach requires one to describe the constitutive "solid-phase" properties (e.g., solid pressure and solids viscosity coefficients, see Section3.5.2). Slurry flows that are of practical interest generally have solid volume concentrations that exceed 10%, and are more commonly found in the range of $30-40\%$. Therefore particle collisions will play a significant role in determining friction losses (hydraulic gradients), solids dispersion (vertical solids concentration profile) and relative phase velocities. In such cases, the Kinetic Theory of Granular Flow (KTGF), is widely used. This approach was developed based on the kinetic theory of gases to account for inelastic particle collisions and provides the parameters needed to model the solid phase. In multiphase flow simulations, the KTGF was initially applied to gas–solids fluidized beds [Gidaspow, 1994, Gidaspow et al., 1991]. For slurry flow CFD simulations, the Eulerian–Eulerian KTGF approach is by far the most widely used. In numerous cases, the KTGF model are "tuned" for each simulation, to match different sets of experimental results. The study carried out by Krampa [2009] revealed that the implementation protocols for KTGF were still incomplete. In a recent study conducted by Piminchumo Marinos et al. [2020], new formulations were proposed for the solid viscosity and granular temperature, taking into account the effects of interstitial fluid. As a result, there was an improvement in predicting the solids volume concentration in the near-wall region. However, it also uncovered new issues related to turbulence modulation and the wake effects in the fluid around a particle. According to Jamshidi et al. [2019], the effective stress closure problem remains a significant challenge in implementing KTGF. This is because there is an underestimation of particle migration due to the neglect of the dominant source for particle fluctuations. Furthermore, they demonstrated that the assumption of Newtonian behavior holds true only for dilute suspensions, and there is a pressing need for experimentally validated closures to enhance the accuracy of the models. Turbulence is a common feature of slurry flows, and typically, turbulence modeling involves solving for the mean flow or the largest scales of turbulence using the RANS modeling approach.

In this Eulerarian framework, two models are discussed, namely mixture model and two-fluid model. The mixture model can be seen as a simplified version of the multi-fluid model, which is only valid under certain assumptions about the flow. [Manninen et al., 1996] is credited with offering the most comprehensive summary of the mixture model, having derived the fundamental equations from the Eulerian double-averaged conservation equations of mass and momentum for each phase. The exploration of the mixture model began with Ling et al. [2003], who conducted CFD simulations for the flow of sand-water slurry through horizontal pipes. In this study, a simplified 3D algebraic slip mixture

(ASM) model was introduced, and the RNG k-ε turbulent model was utilized to achieve an accurate numerical solution for fully developed turbulent flow. They compared CFD results of mean pressure gradients with experimental results, and found a big discrepancy between them takes place when the mean velocities of slurry flows are lower than corresponding critical deposition velocities. Lin and Ebadian [2008] numerically investigated sand–water slurry flows in the entrance region of horizontal pipe, again using ASM model, and have focused mainly on illustrating and comparing the developing processes of various flow parameters. Silva et al. [2016] performed simulations for Saline Water-Glass beads slurry using Mixture Model coupled with a High Reynolds k–ε turbulence model, results were validated with data attained with an Electrical tomography apparatus. The model produced accurate representations for the highest flow rates, while showing some deviations for the lower flow rate. Reyes and Ihle [2018] recently used this same modeling approach to simulate a fine-coarse sea water slurry pipeline. They have studied the ionic exchange that happens while transport which can result in a change in the chemical composition of the liquid phase. They reported that when a fine fraction is present in slurry pipelines, coarse particle organization has a significant effect on cation exchange processes. These findings imply that, in comparison to homogeneous slurry flows, particle flow heterogeneity may either facilitate or impede adsorption-desorption processes. The researchers in Wan et al. [2023] conducted a simulation to analyze the hydrodynamic characteristics and flow patterns of large particles in hydraulic lifting pipes situated in deep-sea environments. The same approach was used by Guo et al. [2023], the study aimed to improve the understanding of the flow characteristics of the slurry shield pipeline system, with the goal of optimizing the transportation of muck during slurry shield tunneling in sandy pebble stratum.

Nevertheless, the majority of the earlier CFD investigations of slurry pipe flows within the Eulerian approach were performed using Two Fluid Model (TFM). The most relevant and recent studies that worked on slurries, the study of Hernandez et al. [2008] for sand-water slurry, where homogeneous and heterogeneous flow regimes without bed were considered along with predictions of pressure gradients at the fully developed zone. Ekambara et al. [2009] investigated the effect of in situ solids volume concentration, particle size, mixture velocity, and pipe diameter, on local time-averaged solids concentration profiles, particle and liquid velocity profiles, and frictional pressure loss. Excellent agreement between the predicted and the experimental was obtained. Chen et al. [2009b] used the same numerical configuration to simulate a flow of Coal-Water Slurries (CWS) in horizontal pipelines, with bi-modal distribution for coal particles. They found out that the simulation results of the binary solid phase model are closer to experimental data, as compared to the results of the single solid phase model. Bossio et al. [2009] focused on modeling of non-Newtonian Laterite-Sand slurry where the mean pressure gradients were compared with experimental data. Antaya et al. [2012] performed simulations for concentrated mixtures of sand-water slurry with

mono-sized and bi-modal particle sizes. Shear stress model (SST) was tested in addition to the k-ε model to treat the turbulence of the continuous phase. Success has been achieved in the use of the k-ε model, with the SST model being superior, especially in the near-wall region. In addition, Kaushal et al. [2012], assessed both the Mixture and two-phase model to simulate mono-dispersed fine particles at high concentration of glass beads mixed with water. They proved again the failure of the mixture model predictions at high velocities and high solid concentrations compared to TFM. [Jiang and Zhang, 2012] worked on an unusual type of slurry flows which is slush nitrogen flow using the 2D Eulerian–Eulerian multiphase approach. The per-phase k–ε turbulence model is used in the study to model the turbulent two-phase flow. The effects of the flow velocity and the mean solid volume fraction on the flow characteristics of slush nitrogen are investigated numerically in this study. The same team the very next year Jiang and Zhang [2013] investigated the same slush and nitrogen flow. Based on the experimental and numerical results they distinguished three flow patterns, which for each one they had studied the variation of pressure drop. They obtained the general correlation of the friction factor with the slush Reynolds number of slush nitrogen with various solid volume fractions. Wang et al. [2013] applied the two fluid models to describe an ice slurry flow without considering ice melting. After the validation of the model with experimental data, it was used to investigate the distributions of ice slurry flow, ice particle concentration and pressure drop in horizontal, vertical and 90 elbow pipes respectively. They found that for pressure drop, the numerical model is found being able to provide results in good agreement with the experimental data where the relative errors are limited to 20%. Messa et al. [2013] developed a new two-fluid model for the simulation of Sand and Glass beads Water slurry. Contrary to previous works with TFM models, they did not integrate the kinetic theory of granular flows to determine solid viscosity. They studied the effect of the wall boundary condition for the solid phase on the pressure gradient, where they found that the best match between measurements and computations is obtained when the equilibrium logarithmic law of Launder and Spalding for smooth walls is applied to the solid phase. The novelty of the proposed model and its better performance compared to similar ones reside in the method of accounting for some key physical mechanisms governing these flows, namely turbulent dispersion, interphase friction, and viscous and mechanical contributions to friction. Hashemi et al. [2016a] performed experiments in a 265 mm diameter pipe loop with sand-in-water slurries, then selected experimental conditions were numerically simulated using a commercial CFD package, ANSYS CFX. They noticed that the agreement between the numerical results and the experimental data is concentration dependent, with relatively closer agreement at lower concentrations. Kumar et al. [2019] presented experimental data of iron-ore slurry flow cases through a $105mm$ pipe, the obtained results are validated using the TFM-KTGF model. A good resemblance was found between measured and predicted pressure drops, solid concentrations and velocity profiles. Singh

et al. [2020b] investigated the flow characteristics of coal water slurry having high solid concentrations in slurry pipeline. They have noticed that the coal-water slurry shows Newtonian behavior at 30% solid concentration (by-weight) and beyond this it depicts non Newtonian pseudo plastic behavior. In this study also SST k-ω turbulence model was found a better predictor over other models namely Standard k-ε, RNG k-ε, Realizable k-ε and Standard k-ω models. A three-dimensional multiphase hydrodynamic model, which is based on the kinetic theory of granular flow, was developed by Li et al. [2018] for simulating multi-sized glass beads-water slurry. The simulation results of different-sized particle behaviors in multi-sized slurry are of great importance. It was concluded by the researchers that the increase in speed of resistance in a graded slurry is less abrupt compared to a single-sized slurry with the same conditions as the solid concentration increases. They also observed that the wall shear stress of coarse particles significantly decreases with increasing flow rate and solid concentration, due to the presence of fine particles. Finally, the researchers confirmed that the existence of fine particles leads to a significant reduction in the collision intensity of coarse particles and velocity fluctuations in the multi-sized slurry. Recently, Dixit et al. [2022] utilized the same arrangement to carry out a computational analysis of sand-water slurry flow in a pipe bend, focusing on the assessment of head loss in this particular geometric setup. Sadeghi et al. [2022] explores the transport of monodisperse and bimodal particles in a turbulent non-Newtonian carrier using the same approach. The study investigates the effects of various parameters such as the particle diameter, solids concentration, mixture velocity, and carrier fluid density on flow behavior and specific energy consumption. Sontti et al. [2023] examined a four-phase slurry utilized in the processing of oil sand ore. They explored how the presence of secondary phases, such as bitumen droplets and bubbles, affects the flow characteristics in an oil sand tailings pipeline They examined how different factors, such as feed concentration, initial mixture velocity, and particle gradation, affected the behavior of the particles and the overall flow pattern. Another recent development in the utilization of CFD methodology in the domain of slurry flows involves the research of Zhou et al. [2023]. The objective of their study was to examine the transport behavior of proppants within limited spaces, such as hydraulic fractures and enhanced geothermal systems. To improve the accuracy of their numerical simulations, the researchers implemented a bimodal size distribution for the particles. This approach enabled a more detailed and extensive analysis of the proppants' behavior in the given systems. We also have the study conducted by Joshi et al. [2023], which focused on exploring the settling patterns of solid particles in a slurry pipeline. More specifically, the research aimed to examine how various Prandtl numbers influenced the flow behavior of the slurry through a horizontal pipe.

Based on the literature review provided, we have decided to employ the Euler-Euler approach (specifically, the Two Fluid Model) for our CFD modeling. This model is widely utilized in addressing transport problems related to suspensions

and is considered to be the most comprehensive and reliable option available. It has been demonstrated to produce generally satisfactory results and is highly accurate. On the other hand, the mixture model has been observed to yield incorrect predictions for pressure drops, with an increasing degree of error as the slurry concentration increases [Kaushal et al., 2012]. The key findings from the literature review are summarized in Table 3.2. The description of the TFM model is given in section 3.5.

3.5 The Two Fluid Model (TFM)

In the two-fluid Eulerian-Eulerian approach, each phase is described by a set of averaged conservation equations. The following Section covers the model's fundamental characteristics. In particular, the derivation of the averaged and the rules required to close the system of equations are shown in the sub-section 3.5.1. The closures for the KTGF to compute the solid phase viscosity are discussed in sub-section 3.5.2,

3.5.1 Averaged equations

In order to obtain the averaged equations, an average operator is applied to the balance equations and jump conditions in local instant formulations (see Eqs. (3.8)-(3.11)). Typical averages of the property $\phi(\mathbf{x}, t)$ are:

- **TIME AVERAGE:**

$$< \phi(\mathbf{x}, t) >= \frac{1}{T} \int_{t-T/2}^{t+T/2} \phi(\mathbf{x}, t) dt \tag{3.12}$$

The selected time period T for averaging must be such that the time scale of turbulent fluctuations is $\ll$ T, which is $\ll$ than the time scale of mean flow fluctuations.

- **VOLUME AVERAGE:**

$$< \phi(\mathbf{x}, t) >= \frac{1}{V} \int_{V} \phi(\mathbf{x}, t) dV \tag{3.13}$$

It is necessary to choose the volume V for averaging in such a manner that the characteristic dimension of phases is $\ll V$, and hence smaller than the characteristic dimension of the physical system.

- **ENSEMBLE AVERAGE:**

$$< \phi(\mathbf{x}, t) >= \int_{\Omega} \phi(\mathbf{x}, t; \omega) d\mu(\omega) \tag{3.14}$$

Where $\phi(\mathbf{x}, t; \omega)$ is a realization of the quantity ϕ across a range of potential "equivalent" realizations Ω.

Table 3.2: Summary on models classification

DPM (Eulerian-Lagrangian)	**Advantages** • Lot of information at the particle and sub-particle scales which guarantee a deep physical insight. **Disadvantages** • The discrete phase must be present at a fairly low volume fraction, usually less than 10-12%. • High computational cost
Mixture Model	**Advantages** • Low computational cost • Multiple solid phases allowed **Disadvantages** • There is a big discrepancy between CFD results with experimental, especially at lower flow rates. • Impose strict assumptions on the flow
TFM Model	**Advantages** • Accurate and give generally good results compared to the mixture model. • Results are better and closer to the experimental data in the case of bimodal particle sizes or at higher velocities. • Affordable computational cost **Disadvantages** • Several difficulties about setting coefficients, sub-models, and parameters persist. • Impose strict assumptions on the flow

In fact, the Eulerian Two-Fluid model's final formulation is formally the same regardless of the kind of average taken into account. In order to derive the averaged equations, a phase indicator function must be introduced first. Therefore, the model is formulated in term of volumetric fractions ϕ_p, material densities ϱ_p, and phase-averaged velocities u_p, where the subscript p refers either to fluid (f) or to solid (s) with $\phi_f + \phi_s = 1$. The mass and momentum equations read

$$\frac{\partial \left(\phi_p \varrho_p\right)}{\partial t} + \nabla \cdot \left(\phi_p \varrho_p \boldsymbol{u}_p\right) = 0, \tag{3.15}$$

and

$$\frac{\partial \left(\phi_p \varrho_p \boldsymbol{u}_p\right)}{\partial t} + \nabla \cdot \left(\phi_p \varrho_p \boldsymbol{u}_s \boldsymbol{u}_p\right) = -\phi_p \nabla p_p + \nabla \cdot \left(\phi_p \left[\boldsymbol{\tau}_p + \mathbf{R}^{\text{eff}}\right]\right) + \phi_p \varrho_p \boldsymbol{g} + \mathbf{M}_p^d, \tag{3.16}$$

where p denotes the pressure, $\boldsymbol{g}$ represents the gravitational constants and $\boldsymbol{\tau}_s$ is the laminar viscous stress tensor, $\mathbf{R}^{\text{eff}}$ is the Reynolds stress tensor, and $\mathbf{M}_p^d$ is the interfacial force per unit volume. Using the Newtonian fluid's assumption, the fluid shear stress tensor reads

$$\boldsymbol{\tau}_f = \mu_f \left[\nabla \boldsymbol{u}_f + \nabla \boldsymbol{u}_f^{\intercal} - \frac{2}{3} \nabla \boldsymbol{u} \mathbb{I}\right], \tag{3.17}$$

where μ_f and $\mathbb{I}$ are the viscosity and unit tensor respectively. For the solid phase

$$\boldsymbol{\tau}_s = \mu_s \left[\nabla \boldsymbol{u}_f + \nabla \boldsymbol{u}_f^{\intercal}\right] + \left(\lambda_s - \frac{2}{3}\mu_s\right) \left(\nabla \boldsymbol{u}_s\right) \mathbb{I}, \tag{3.18}$$

where μ_s and λ_s stand for the viscosity and bulk viscosity of the solid phase, respectively.

In the present study, the phases are coupled through the drag force $\mathbf{M}^{\text{D}}$, and non-drag efforts that includes the lift force $\mathbf{M}^{\text{L}}$, and the virtual mass force $\mathbf{M}^{\text{VM}}$ as in equation 2.14. For slurry systems, all these terms are of significant importance since they promote the agitation and detaching of particles. In the present study, the models employed to estimate the coupling terms are presented in section 2.2.3. Note that the resulting coupling term is essentially equal in magnitude in both phases but opposite in direction between solid and fluid phases so that Newton's third law of motion is not violated.

The momentum equation (cf. Eq. (3.16)) needs to be closed by modeling the terms $\mathbf{R}^{\text{eff}}$, which is formulated within Boussinesq's framework as:

$$\mathbf{R}^{\text{eff}} = \varrho_f \nu_f^{\text{eff}} \left[\nabla \boldsymbol{u}_f + \nabla \boldsymbol{u}_f^{\intercal} - \frac{2}{3} \nabla \cdot \boldsymbol{u}\right] - \frac{2}{3} \varrho_f \mathrm{k}_f \mathbb{I}, \tag{3.19}$$

where ν_f^{eff} is the turbulent kinematic viscosity of the fluid phase and k is the turbulent kinetic energy.

3.5.2 Solid-phase viscosity

In the representation of the solid phase with fluid-like characteristics (cf. Eq. (3.16)), hydrodynamic pressure p_s, shear viscosity μ_s, and bulk viscosity λ_s need to be reformulated similarly to the fluid phase. However, acquiring equivalent values for these parameters presents a significant challenge due to the inherently particulate nature of the solid phase. To address this, closures must be employed to express the behavior of the solid phase, such as contact pressure and velocity collisions, in terms of continuous pressure and viscosity. This ensures a state of continuous and chaotic agitation within the fluid. The approach adopted in this study is the Kinetic Theory of Granular Flow (KTGF), which generalizes the kinetic theory of gases to account for collisions of inelastic particles. Indeed, the Kinetic Theory of Granular Flow (KTGF) is a well-established approach for solid-gas flow, and it is frequently applied to solid-liquid flows as well. The KTGF is a highly intricate theory that relies on a strong physical foundation to replicate all the mechanisms governing the behavior of the mixture. It establishes a correlation between the total kinetic energy of a collection of particles randomly moving within the carrier fluid and their fluctuating velocity, achieved through the use of the granular temperature. In the context of solid-liquid flows, the KTGF allows for the definition of a granular temperature Θ in the solid phase, which directly affects the phase stress tensor [Mendygarin et al., 2017]. Analogous to the thermodynamic temperature for gases, the granular temperature Θ measures the energy of the fluctuating velocity of the particles. The introduction of the granular temperature introduces an additional partial differential equation (PDE) to the system of equations. The equation of conservation of solids fluctuating energy can be expressed as [Wang et al., 2013]:

$$\begin{aligned} \frac{3}{2}\left[\partial_t\left(\phi_s\varrho_s\Theta_{s,i}\right)+\partial_i\left(\phi_s\varrho_s u_{s,i}\Theta_s\right)\right] = \\ \underbrace{\partial_i\left(-p_s u_{s,i}+u_{s,i}\tau_{s,ij}\right)}_{\mathcal{T}_1}+\underbrace{\partial_i\left(\kappa_\Theta\partial_i\Theta_i\right)}_{\mathcal{T}_2}-\underbrace{\gamma_{\Theta_s}}_{\mathcal{T}_3}+\underbrace{\Phi_{\mathrm{ls}}}_{\mathcal{T}_4}, \end{aligned} \tag{3.20}$$

where the term $\mathcal{T}_1$ stands for the production term due to shear stress, $\mathcal{T}_2$ for diffusion, $\mathcal{T}_3$ for dissipation due to inelastic collisions, and $\mathcal{T}_4$ represents the flux of fluctuating energy dissipated due to the interaction with the carrier fluid. Rather than solving the complete granular energy balance given in Eq. (3.20), Ekambara et al. [2009] assume the granular energy is in a steady state and dissipated locally and neglect convection and diffusion. Retaining only the generation and the dissipation terms, Eq. (3.20) simplifies to an algebraic expression for the granular temperature:

$$\partial_i\left(-p_s u_{s,i}+u_{s,i}\tau_{s,ij}\right)-\gamma_{\Theta_s}+\Phi_{\mathrm{ls}}=0 \tag{3.21}$$

Expression for all the terms can be derived [Gidaspow, 1994]:

$$\begin{cases} \gamma_{\Theta_s} = \frac{12\left(1-e^2\right)g_0}{d_s\sqrt{\pi}}\varrho_s\phi_s^2\Theta_s^{3/2} \\ \Phi_{\mathrm{ls}} = -3\mathrm{k}_{\mathrm{ls}}\Theta_s \\ p_s = \phi_s\varrho_s\Theta_s + 2\varrho_s\left(1+e\right)\phi_s^2 g_0\Theta_s, \end{cases} \tag{3.22}$$

where e is the coefficient of restitution for particle collisions that quantifies the elasticity of particle collisions. (g_0) is the radial distribution function that can also be seen as a probability for interaction between particles, and k_{ls} represents the conductivity of fluctuating energy. The bulk viscosity λ_s that accounts for the solid particle resistance to expansion and compression is modeled using Lun's formulation [Lun et al., 1984]. It can be calculated by the following form:

$$\lambda_{\mathrm{S}} = \frac{4}{3}\phi_{\mathrm{s}}\varrho_{\mathrm{s}}d_{\mathrm{s}}g_0\left(1+e\right)\left(\frac{\Theta_{\mathrm{s}}}{\pi}\right)^{\frac{1}{2}}, \tag{3.23}$$

Then, the viscosity coefficients which include the combination of the following components:

$$\mu_s = \mu_{s,\mathrm{col}} + \mu_{s,kin}, \tag{3.24}$$

Where $\mu_{s,\mathrm{col}}$ and $\mu_{s,\mathrm{kin}}$, correspond to the collisional and kinetic components of the total solid phase viscosity [Syamlal et al., 1993b]. Table 3.3 displays various KTGF correlations for the calculation of μ_s and the radial function g_0.

	Granular viscosity μ_s
[Lun et al., 1984]	$\frac{4}{5}\phi_s^2\varrho_s d_s g_0(1+e)\sqrt{\frac{\Theta}{\pi}} + \frac{1}{15}\sqrt{\Theta\pi}\frac{\varrho_s d_s g_0(1+e)\left(\frac{3}{2}e-\frac{1}{2}\right)\phi_s^2}{\frac{3}{2}-\frac{1}{2}e} + \frac{1}{6}\sqrt{\Theta\pi}\frac{\varrho_s d_s\phi_s\left(\frac{s}{2}e+\frac{1}{4}\right)}{\frac{3}{2}-\frac{e}{2}} + \frac{10}{96}\sqrt{\Theta\pi}\frac{\varrho_s d_s}{(1+e)\left(\frac{3}{2}-\frac{1}{2}e\right)g_0}$
Syamlal et al. [1993a]	$\frac{4}{5}\phi_s^2\varrho_s d_s g_0(1+e)\sqrt{\frac{\Theta}{\pi}} + \frac{1}{15}\sqrt{\Theta\pi}\varrho_s d_s g_0\frac{(1+e)\left(\frac{3}{2}e-\frac{1}{2}\right)}{\frac{3}{2}-\frac{e}{2}}\phi_s^2 + \frac{1}{12}\frac{\phi_s d_s\varrho_s\sqrt{\pi\Theta}}{\frac{3}{2}-\frac{e}{2}}$
Gidaspow [1994]	$\frac{4}{5}\phi_s^2\varrho_s d_s g_0(1+e)\sqrt{\frac{\Theta}{\pi}} + \frac{1}{15}\sqrt{\Theta\pi}\varrho_s d_s g_0(1+e)\phi_s^2 + \frac{1}{6}\sqrt{\Theta\pi}\varrho_s d_s\phi_s + \frac{10}{96}\sqrt{\Theta\pi}\frac{\varrho_s d_s}{(1+e)g_0}$
Hrenya and Sinclair [1997]	$\frac{4}{5}\varepsilon_s^2\varrho_s d_s g_0(1+e)\sqrt{\frac{\Theta}{\pi}} + \frac{1}{15}\sqrt{\Theta\pi}\frac{\varrho_s d_s g_0(1+e)\left(\frac{3}{2}e-\frac{1}{2}\right)\varepsilon_s^2}{\left(\frac{3}{2}-\frac{e}{2}\right)} + \frac{1}{6}\sqrt{\Theta\pi}\frac{\varrho_s d_s\varepsilon_s\left(\frac{1}{2}\left(1+\frac{\lambda_m f_p}{R}\right)+\frac{3}{4}e-\frac{1}{4}\right)}{\left(\frac{3}{2}-\frac{1}{2}e\right)\left(1+\frac{\lambda_{m(p)}}{R}\right)} + \frac{10}{96}\sqrt{\Theta\pi}\frac{\varrho_s d_s}{(1+e)\left(\frac{3}{2}-\frac{1}{2}e\right)g_0\left(1+\frac{\lambda_m f_p}{R}\right)}$
	Radial Function g_0
Carnahan and Starling [1969]	$\frac{1}{1-\varepsilon_s} + \frac{3\varepsilon_s}{2(1-\varepsilon_s)^2} + \frac{\varepsilon_s^2}{2(1-\varepsilon_s)^3}$
Lun and Savage [1986]	$\left(1-\frac{\phi_s}{\phi_{s,\max}}\right)^{-2.65\phi_{s,\max}}$
Sinclair and Jackson [1989]	$\left[1-\left(\frac{\phi_s}{\phi_{s,\max}}\right)^{\frac{1}{3}}\right]^{-1}$
Gidaspow [1994]	$\frac{3}{5}\left[1-\left(\frac{\phi_s}{\phi_{s,\max}}\right)^{\frac{1}{3}}\right]^{-1}$

Table 3.3: KTGF correlations

Considering the granular viscosity correlations the following remarks were made:

- Gidaspow [1994] follows Lun et al. [1984], however, the kinetic component of the total stress in granular materials does not take into consideration the inelastic properties of particles.

- Hrenya and Sinclair [1997] adopt the approach proposed by Lun et al. [1984] for modeling the dynamics of non-spherical particles but introduce a constraint on the mean free path of the particle, using a dimension that is representative of the physical system being studied. This differs from Lun et al. [1984]'s theory, which allows the mean free path to approach infinity.

- Lun et al. [1984]'s theory also predicts that the solids viscosities tend towards a finite value as the solids volume fraction approaches zero.

- By introducing a constraint on the mean free path, the Hrenya and Sinclair [1997] expression for shear viscosity correctly predicts a limit of zero as the solids volume fraction approaches zero.

- The solids shear viscosity expression proposed by Syamlal et al. [1993a] also approaches zero as the solids volume fraction approaches zero. However, this limit is achieved by neglecting the kinetic contribution to the solids viscosity.

On the other hand, with respect to the radial function:

- Carnahan and Starling [1969] expression does not approach the correct limit at closest solids packing because the radial distribution function at contact tends towards infinity in this situation.

- To address this limitation, alternative expressions to the Carnahan and Starling [1969] expression have been proposed by Gidaspow [1994], Lun and Savage [1986], Sinclair and Jackson [1989], which are capable of approaching the correct limit at closest packing of the particles.

In summary, after analyzing the various components of the solid viscosity as derived from the KTGF theory, the Syamlal et al. [1993a]'s correlation for the granular viscosity and the Lun and Savage [1986]'s correlation for calculating the radial function were selected.

When the solid phase fraction is high in a particular zone of the domain, lots of contacts among particles occur and a frictional stress derives from them that must be accounted for in the mathematical model. In this state the collisions among particles could not be considered instantaneous as previously done in the kinetic theory and the frictional stress is accounted for adding a term in the granular viscosity. Hence, the solid shear viscosity μ_s is expressed by:

$$\mu_s = \mu_{s,\text{col}} + \mu_{s,\text{kin}} + \mu_{s,\text{fric}}, \tag{3.25}$$

The frictional shear viscosity on the other hand is calculated as:

$$\mu_{s,fr} = Fr\frac{(\phi_s - \min(\phi_s))^n}{(\phi_{s,\max} - \phi_s)^p}\sin(\delta), \tag{3.26}$$

where $Fr = 0.05$, $n = 2$ and $p = 5$ are empirical constants, and δ the angle of internal friction of the particle.
NB: The frictional stress is added to the stress predicted by the kinetic theory when the solids volume fraction exceeds a critical value. This value is normally set to 0.5 when the flow is three-dimensional and the maximum packing limit is about 0.63.

3.5.3 Turbulence in the two-fluid model

To guarantee the pseudo-homogeneity of the mixture and subsequently prevent total sedimentation of the solid phase, a turbulent flow regime is maintained inside the slurry pipe. Therefore, ν_f^{eff} in Eq. (3.19) is modeled using a turbulence model. Here, the turbulence is treated with two known models, namely $\mathrm{k}-\varepsilon$ [Launder and Spalding, 1983] and SST $\mathrm{k}-\omega$ model [Wilcox, 1988]. The $\mathrm{k}-\varepsilon$ turbulence model is derived from a combination of empirical observations and theoretical considerations. It is a two-equations ((3.27), (3.28)) model that predicts the turbulence characteristics of a fluid by solving for the turbulent kinetic energy k and the dissipation rate of turbulence kinetic energy ε within a fluid flow. The left hand side of the following equations is the Lagrangian derivative: $D/Dt := \partial/\partial t + u_i\partial/\partial x_i$.

$$\frac{D\varepsilon}{Dt} = \frac{1}{\rho}\frac{\partial}{\partial x_k}\left[\frac{\mu_t}{\sigma_\varepsilon}\frac{\partial\varepsilon}{\partial x_k}\right] + \frac{C_1\mu_t}{\rho}\frac{\varepsilon}{k}\left(\frac{\partial u_i}{\partial x_k} + \frac{\partial u_k}{\partial x_i}\right)\frac{\partial u_i}{\partial x_k} - C_2\frac{\varepsilon^2}{k}, \tag{3.27}$$

$$\frac{Dk}{Dt} = \frac{1}{\rho}\frac{\partial}{\partial x_k}\left[\frac{\mu_t}{\sigma_k}\frac{\partial k}{\partial x_k}\right] + \frac{\mu_t}{\rho}\left(\frac{\partial U_i}{\partial x_k} + \frac{\partial u_k}{\partial x_i}\right)\frac{\partial u_i}{\partial x_k} - \varepsilon. \tag{3.28}$$

The constants appearing in the above equations are given in table below: The SST

Table 3.4: The values of the constants in the $\mathrm{k}-\varepsilon$ model

C_μ	C_1	C_2	σ_k	σ_ε
0.09	1.44	1.92	1.0	1.3

$\mathrm{k}-\omega$ turbulence model in the other hand, is a two-equation eddy-viscosity model that has gained wide popularity due to its versatile formulation. This model combines the strengths of two approaches, using the wilcox $\mathrm{k}-\omega$ formulation in the inner parts of the boundary layer, allowing for direct application to the viscous sub-layer without extra damping functions, while switching to a $\mathrm{k}-\varepsilon$ behavior

in the free-stream, thereby reducing sensitivity to inlet free-stream turbulence properties. In order to achieve this, the $k-\varepsilon$ can be converted into a $k-\omega$ formulation. The difference between this formulation and the original $k-\omega$ model differs from the original version in that an extra cross-diffusion term is included in ω-equation and the modeling constants are adjusted accordingly. The original model is then multiplied by a function F_1 while the transformed model by a function $(1-F_1)$ and both are combined. The function F_1 is constructed to be one near the wall surface, thereby activating the original model, and zero elsewhere. The blending will take place in the wake region of the boundary-layer. The equations (3.29) and (3.30)) present the variables for the SST $k-\omega$ model, the turbulence Kinetic Energy k and the specific Dissipation Rate ω respectively.

$$\frac{D\varrho k}{Dt} = \tau_{ij}\frac{\partial u_i}{\partial x_j} - \beta^*\varrho\omega k + \frac{\partial}{\partial x_j}\left[\left(\mu + \sigma_k\mu_t\right)\frac{\partial k}{\partial x_j}\right], \tag{3.29}$$

$$\frac{D\varrho\omega}{Dt} = \frac{\gamma}{\nu_t}\tau_{ij}\frac{\partial u_i}{\partial x_j} - \beta\varrho\omega^2 + \frac{\partial}{\partial x_j}\left[\left(\mu + \sigma_\omega\mu_t\right)\frac{\partial \omega}{\partial x_j}\right] + 2\rho\left(1-F_1\right)\sigma_{\omega 2}\frac{1}{\omega}\frac{\partial k}{\partial x_j}\frac{\partial \omega}{\partial x_j}. \tag{3.30}$$

The constants for the SST model are: The $k-\omega$ SST is well-regarded for its

Table 3.5: The values of the constants in the SST $k-\omega$ model

σ_{k1}	$\sigma_{\omega 1}$	β_1	β^*	κ	γ_1
0.85	0.5	0.0750	0.09	0.41	$\beta_1/\beta^* - \sigma_{\omega 1}\kappa^2/\sqrt{\beta^*}$

ability to handle adverse pressure gradients and separating flows. However, it tends to overestimate turbulence levels in regions with large normal strain, such as stagnation regions and areas with strong acceleration, although to a lesser extent than a typical $k-\varepsilon$ model. In section 4.2.3, both turbulence models are tested and compared to assess their ability to give accurate results.

Near-wall treatment

The present study utilizes the turbulence models in conjunction with an enhanced wall function treatment. Wall functions are used to treat the boundary-layer development up to the wall. An important issue in the accurate prediction of industrial turbulent flows, is the formulation and the numerical treatment of the equations in regions close to the walls. The near-wall formulation in pipelines determines the accuracy of the wall shear stress predictions and has an important influence on the development of boundary layers, including the onset flow separation. Typically the wall-function method is used to model the flow in the near-wall region. In the wall-function approach, the viscosity affected sublayer region is bridged by employing empirical formulas to provide near-wall boundary

conditions for the mean flow and turbulence transport equations. These formulas connect the wall conditions (e.g. the wall shear stress) to the dependent variables at the near-wall grid node, which is presumed to lie in the fully-turbulent region of the boundary layer. One of the major drawbacks of the wall-function approach is that the predictions depend on the location of the point nearest to the wall and are sensitive to the near-wall meshing. To know in which condition wall functions approach can be used correctly, the near-wall region should be introduced. Some parameters which be used to introduce the near wall region Versteeg and Malalasekera [2007]:

$$u_\tau = \sqrt{\frac{\tau}{\rho}}, \tag{3.31}$$

$$y^+ = \frac{y \times u_\tau}{\nu}, \tag{3.32}$$

where u_τ is the friction velocity, which can be used to define dimensionless velocity later. τ is the wall shear stress, y is the distance to the wall to the first grid point and is often expressed in terms of the dimensionless y^+ parameter. The y^+ parameter is an indication of the distance of the grid point from the wall in terms of the size of the near-wall turbulent structures. The near-wall region can be divided into 3 parties: the viscous sub-layer, the buffer layer and the logarithmic region. Fig. 3.7 shows these sublayers.

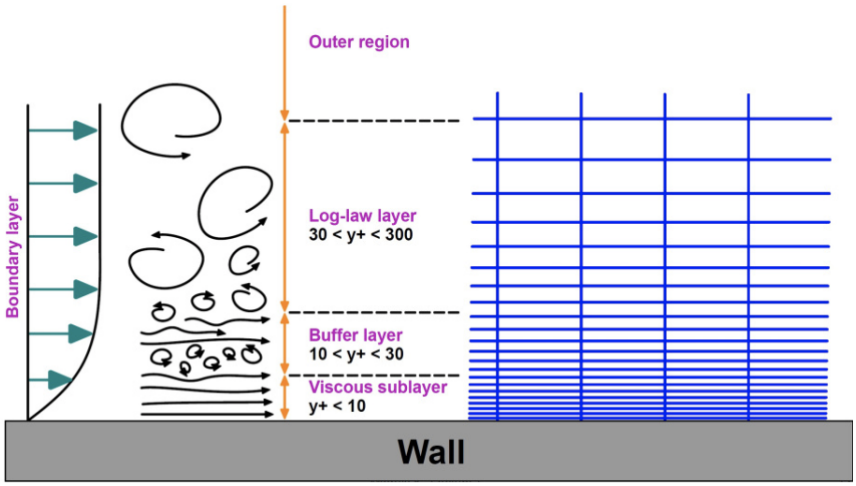

Figure 3.7: Near-wall boundary layers. Adopted from https://tariqkhamlaj.com/flow-over-a-flat-plate/page/4/

1. The viscous sublayer ($y^+ < 10$): in the viscous layer the fluid is dominated by the viscous affect so it can be assumed that the shear stress of fluid is equal to the wall shear stress τ.

2. The Buffer layer ($10 < y^+ < 30$): viscous and turbulent stresses are of

similar magnitude. In OpenFOAM® buffer layer is divided 2 parties, one is using the liner relation as that in viscous sublayer, the other is to use logarithmic function as that in logarithmic region.

3. The logarithmic area ($30 < y^+ < 300$): in the logarithmic layer turbulence stress dominate the flow and velocity profile varies very slowly with a logarithmic function along the distance y.

In order for the wall functions to be accurate, the y^+ parameter should fall within a certain range that depends on the specific wall function being used. For instance, for the commonly used "standard wall function", the y^+ value should be between 30 and 300. Therefore, the mesh resolution should be adjusted such that the first grid point away from the wall is located at a distance from the wall that gives a y^+ value within the recommended range for the specific wall function being used. The wall functions consist of wall boundary conditions that impose values for the kinetic energy k_p and the dissipation rate ε_p or for the turbulence specific dissipation rate ω_P depending on which model is used, in the center of the cells near the wall as shown by Eq. (3.33) and Eq. (3.34), to bridge turbulent quantities on the wall.

$$\mathrm{k}_p = \frac{\sqrt{fu^2}}{\sqrt{2C\mu}} \tag{3.33}$$

$$\varepsilon_p = \frac{C_\mu^{3/4}\, \mathrm{k}_p^{3/2}}{\mathrm{k} y_p} \tag{3.34}$$

$C_\mu = 0.09$ is a model coefficient and $k = 0.41$ is Von Karman constant. y_p is the height to the center of the cell adjacent to the wall and it can be calculated from y^+ according to the Eq. (3.35).

$$y_p = \frac{y^+ \mu}{\varrho \sqrt{fu}} \tag{3.35}$$

3.6 Conclusion

A comprehensive evaluation of past numerical studies of slurry flows in horizontal pipes has been conducted to identify appropriate modeling methodologies and mathematical models. Based on this state-of-the-art analysis, the two-fluid Eulerian model is chosen as it strikes an optimal balance between computational cost and the ability to represent the physical behaviors governing slurry pipe flow. To effectively model particle-particle and particle-wall interactions, the KTGF model is employed to describe the dynamics of the solid phase. It is worth noting that some drawbacks persist when using k-ε based turbulence models, particularly the overestimation of the eddy viscosity in the near-wall region and early onset flow separation [Antaya et al., 2012]. These limitations should be carefully considered when implementing turbulence models for simulating slurry flows in pipes.

3

Les méthodologies de recherche pour explorer les écoulements solide-liquide

Objectifs:

La première section 3.1 expose les approches réalisables pouvant être utilisées pour étudier les écoulements de solides et de liquides. La section 3.2 décrit les différentes méthodes et approches de CFD pour simuler les écoulements diphasiques. La section 3.3 fournit un résumé des efforts de recherche passés, en classant les études en fonction de l'approche utilisée. Dans la section 3.4, l'accent est mis sur le modèle à deux fluides et elle développe les caractéristiques clés de la théorie d'écoulement diphasique eulérienne qui est utilisée pour les systèmes solide-fluides. Enfin, dans la section 3.4.2, les façons dont le modèle à deux fluides aborde la turbulence sont expliquées, et les modèles qui seront utilisés ultérieurement dans cette recherche sont présentés.

3.1 Approches de recherche

Pour atteindre l'objectif de cette thèse, qui est d'anticiper les écoulements solide-liquide turbulents via des pipelines horizontaux et inclinés, il est nécessaire d'examiner différentes approches de recherche. Pour commencer, un résumé basique des approches possibles est d'abord fourni:

- **Étude expérimentale**
  L'étude expérimentale de la recherche sur les écoulements turbulents de mélanges solide-liquide dans les systèmes de pipelines implique la réalisation d'expériences physiques en laboratoire ou sur le terrain pour recueillir des données sur un phénomène ou un système particulier. Cette approche implique généralement la mesure de variables directement ou indirectement liées au phénomène, souvent à l'aide d'équipements ou d'instruments spécialisés. Les données collectées à partir de ces expériences peuvent ensuite être analysées pour obtenir des informations sur le comportement du système étudié. Cependant, les essais expérimentaux sont coûteux et nécessitent des équipements spécialisés, et la prise de mesures présente des défis techniques considérables. Les études expérimentales des écoulements solide-liquide denses sont souvent limitées aux pipelines horizontaux, et les données expérimentales peuvent être utilisées pour développer des modèles mathématiques décrivant le comportement de la suspension. Cependant, l'investigation expérimentale des écoulements de suspension reste compliquée.

- **Approche de la dynamique des fluides numérique (CFD)**
  Cette technique de résolution du problème implique la réalisation de simulations numériques. Elle est relativement peu coûteuse et adaptable, car elle permet la simulation de presque n'importe quel système, quelle que soit sa taille. La dynamique des fluides numérique (CFD) s'est révélée être un outil utile et puissant pour modéliser et prédire des scénarios d'écoulement de suspensions inconnus ou particuliers, en fournissant une série d'informations hydrodynamiques sur le fluide. Traditionnellement, les simulations CFD à des fins d'ingénierie ont été limitées à des écoulements plus simples à une phase en raison des limitations de la puissance informatique et de la capacité des codes CFD. Cependant, les avancées actuelles dans ce domaine ont permis d'augmenter de manière exponentielle la quantité de travaux de recherche sur la simulation numérique des écoulements de suspensions en pipeline en quelques années, ouvrant la voie à l'utilisation de cette approche pour des applications d'ingénierie. Les résultats de la CFD peuvent être utilisés pour améliorer les performances, obtenir une meilleure fiabilité et une mise à l'échelle plus confiante, améliorer la cohérence des produits et augmenter la productivité de l'usine.

- **Les modèles réduits à base physique**
  Les modèles d'ordre réduit ou modèles substituts sont largement utilisés par les ingénieurs travaillant avec des écoulements diphasiques. Ils sont peu coûteux, ne nécessitent pas autant de temps de calcul que la CFD et sont suffisamment précis pour la plupart des applications. Cependant, leur formulation globale limite leur utilisation à l'estimation de facteurs macroscopiques, tels que les pertes de charge, et leur applicabilité est limitée aux écoulements en ligne droite pour les mélanges solide-liquide.

Les approches expérimentale et de CFD ont chacune leurs propres avantages et limites et peuvent être utilisées ensemble pour obtenir une compréhension plus complète du comportement des fluides dans les systèmes complexes. Les données expérimentales sont nécessaires pour l'étalonnage et la validation du modèle de CFD, ce qui implique l'ajustement de ses paramètres empiriques ou difficiles à évaluer pour correspondre à une certaine mesure expérimentale. Les meilleures pratiques en CFD recommandent de calibrer d'abord les coefficients du modèle sur la base d'un certain ensemble de données expérimentales, puis de valider le modèle en utilisant un ensemble différent de données expérimentales ou numériques.

3.2 Méthodes numériques pour les écoulements diphasiques dispersés

La modélisation numérique et la simulation sont le meilleur moyen d'étudier les écoulements de boues. Il existe plusieurs modèles disponibles pour prédire les quantités d'écoulement de boues, avec l'approche la plus simple exploitant des corrélations semi-empiriques. Une approche de modélisation plus sophistiquée prend en compte une structure interne de l'écoulement, composée de couches de différentes propriétés et conditions d'écoulement. Les mécanismes de friction et de support sont capturés par des modèles en couches, qui formulent des bilans de forces pour chaque couche individuelle et résolvent les épaisseurs et les vitesses des couches individuelles. Il prédit la vitesse limite de dépôt comme la vitesse d'écoulement à laquelle la couche la plus basse, composée de particules en contact, cesse de glisser sur une paroi de la conduite et devient la couche de lit stationnaire.

L'augmentation rapide de la puissance de calcul a permis de distribuer largement des codes commerciaux et open source capables de modéliser des phénomènes physiques complexes dans des géométries réalistes. Cela a ouvert la voie à l'amélioration de la gestion d'ingénierie des écoulements de boues en complément des approches traditionnelles par des simulations numériques. Les approches CFD sont classées en deux catégories principales de modèles CFD pour les écoulements solide-liquide, à savoir les modèles Euler-Lagrange et les modèles Euler-Euler. Le liquide porteur est toujours modélisé dans le cadre eulerien en résolvant pour une extension à deux phases des équations de Navier-Stokes, tandis que la phase

dispersée peut être modélisée soit dans le cadre lagrangien en suivant les trajectoires de particules, soit dans le cadre eulerien en résolvant pour les équations d'écoulement d'un fluide fictif représentant le comportement dynamique du groupe de particules.

Méthodes basées sur l'approche cinétique (Euler-Lagrange) La phase liquide est modélisée comme un continuum et résolue dans un cadre cellulaire Eulerien, tandis que le comportement de la phase solide est obtenu par la méthode des particules discrètes (DPM), dans laquelle les trajectoires individuelles des particules sont calculées et cherchent à déterminer les propriétés de chaque particule [Brennen and Brennen, 2005].

Les méthodes basées sur l'approche du continuum (Eulerien-Eulerien)

Dans l'approche continue [Brennen and Brennen, 2005], les deux phases sont modélisées comme des milieux continus se pénétrant mutuellement avec des frontières mobiles (cf. Fig. 3.6), et deux ensembles d'équations de conservation sont résolus conjointement dans le cadre eulérien. Cependant, trois modèles sont disponibles dans cette approche. La Table 3.1 propose une brève comparaison de ces modèles. [1]

Table 3.1: Comparaison entre les modèles Euler-Euler

VOF	Modèle de mélange	Modèle à deux fluides(TFM)
Modélisation de fluides non miscibles	Modèle utilisé s'il y a une large distribution de phases dispersées	Lois interphasiques disponibles.
Une seule série d'équations de mouvement	Lois interphasiques non disponibles	Plus précis.
Exemples : écoulement de surface libre [Jing et al., 2016], grosses bulles dans un liquide [Al-Yaari and Abu-Sharkh, 2011], écoulement stratifié [Akhtar et al., 2007]	Exemples : écoulement chargé de particules* avec faible charge [Dufek and Bergantz, 2007], écoulement de bulles, écoulement de boues [Chen et al., 2009a]	Exemples : écoulement de boues [Ofei and Ismail, 2016], sédimentation [Gopaliya and Kaushal, 2016], lits fluidisés [Ofei et al., 2014].

3.3 La revue de littérature

Au cours des 25 dernières années de publications, la grande majorité des études se rapportent à des écoulements en conduites horizontales (par exemple [Chen et al., 2009b, Hashemi et al., 2016b, Kaushal et al., 2012]), avec seulement quelques études sur les écoulements en conduites verticales [Hadinoto, 2010, Krampa, 2009] et dans les coudes/raccords [Kaushal et al., 2013, Singh et al., 2020a]. Les diamètres de conduites étudiés varient entre 10 et 500 mm, les vitesses d'écoulement

[1] écoulement de particules chargées: désigne un écoulement diphasique dans lequel l'une des phases est en continuité et l'autre phase est constituée de petites particules immiscibles et généralement diluées.

entre 1 et 9 m/s, les concentrations volumiques de solides en vrac allant jusqu'à 0,5, les rapports de densité allant de 1, 18 (azote en suspension [Jiang and Zhang, 2012]) à 4, 35 (boue de minerai de fer [Kumar et al., 2019]), et les tailles de particules étudiées varient entre 0, 004 et 2, 4 mm. Un résumé des études numériques les plus pertinentes sur les écoulements de suspension dans des conduites horizontales publiées jusqu'à présent à était réalisée avec l'approche de modélisation adoptée, afin de fournir un contexte pour l'application de chaque approche.

Sur la base de la revue de la littérature fourni, nous avons décidé d'utiliser l'approche Euler-Euler (plus précisément, le modèle à deux fluides) pour notre modélisation CFD. Ce modèle est largement utilisé pour résoudre les problèmes de transport liés aux suspensions et est considéré comme l'option la plus complète et fiable disponible. Il a été démontré qu'il produit généralement des résultats satisfaisants et est très précis. En revanche, il a été observé que le modèle de mélange donne des prédictions incorrectes pour les chutes de pression, avec un degré croissant d'erreur à mesure que la concentration de la suspension augmente [Kaushal et al., 2012]. Les principales conclusions de l'examen de la littérature sont résumées dans le Tableau 3.2. La description du modèle à deux fluides est donnée dans la section 3.4.

3.4 Le modèle à deux fluides (TFM)

Dans l'approche eulerienne-eulerienne à deux fluides, chaque phase est décrite par un ensemble d'équations de conservation moyennées. Afin de dériver les équations moyennées, une fonction indicatrice de phase doit être introduite en premier lieu. Par conséquent, le modèle est formulé en termes de fractions volumiques ϕ_p, de densités de matériau ϱ_p, et de vitesses moyennes de phase u_p, où l'indice p se réfère soit au fluide (f) soit au solide (s) avec $\phi_f + \phi_s = 1$. Les équations de masse et de quantité de mouvement sont les suivantes :

$$\frac{\partial\left(\phi_p \varrho_p\right)}{\partial t} + \nabla \cdot \left(\phi_p \varrho_p \boldsymbol{u}_p\right) = 0, \tag{3.1}$$

and

$$\frac{\partial\left(\phi_p \varrho_p \boldsymbol{u}_p\right)}{\partial t} + \nabla \cdot \left(\phi_p \varrho_p \boldsymbol{u}_s \boldsymbol{u}_p\right) = -\phi_p \nabla p_p + \nabla \cdot \left(\phi_p \left[\boldsymbol{\tau}_p + \mathbf{R}^{\text{eff}}\right]\right) + \phi_p \varrho_p \boldsymbol{g} + \mathbf{M}_p^d, \tag{3.2}$$

où p représente la pression, $\boldsymbol{g}$ représente la constante gravitationnelle et $\boldsymbol{\tau} s$ est le tenseur de contrainte visqueuse laminaire, $\mathbf{R}^{\text{eff}}$ est le tenseur de contrainte de Reynolds, et $\mathbf{M} p^d$ est la force interfaciale par unité de volume. En utilisant l'hypothèse du fluide newtonien, le tenseur de contrainte de cisaillement du fluide est donné par :

$$\boldsymbol{\tau}_f = \mu_f \left[\nabla \boldsymbol{u}_f + \nabla \boldsymbol{u}_f^{\intercal} - \frac{2}{3} \nabla \boldsymbol{u} \mathbb{I}\right], \tag{3.3}$$

où μ_f et $\mathbb{I}$ sont respectivement la viscosité et le tenseur unité. Pour la phase solide:

$$\boldsymbol{\tau}_s = \mu_s \left[\nabla \boldsymbol{u}_f + \nabla \boldsymbol{u}_f^{\intercal}\right] + \left(\lambda_s - \frac{2}{3}\mu_s\right)(\nabla \boldsymbol{u}_s)\,\mathbb{I}, \tag{3.4}$$

où μ_s et λ_s représentent respectivement la viscosité et la viscosité volumique de la phase solide. Dans la présente étude, les phases sont couplées à travers la force de traînée $\mathbf{M}^{\mathrm{D}}$, ainsi que des forces non-liées à la traînée qui comprennent la force de soulèvement $\mathbf{M}^{\mathrm{L}}$, et la force de masse virtuelle $\mathbf{M}^{\mathrm{VM}}$ comme dans l'équation 2.6. Pour les systèmes de boues, tous ces termes sont d'une importance significative car ils favorisent l'agitation et le détachement des particules. Dans la présente étude, les modèles utilisés pour estimer les termes de couplage sont présentés dans la section 2.2.3. Il convient de noter que le terme de couplage obtenu est essentiellement de même magnitude dans les deux phases, mais de direction opposée entre les phases solide et fluide de sorte que la troisième loi de Newton sur le mouvement n'est pas violée.

L'équation de la quantité de mouvement (cf. Eq. (3.16)) doit être fermée en modélisant les termes $\mathbf{R}^{\mathrm{eff}}$, qui est formulé dans le cadre de Boussinesq comme suit :

$$\mathbf{R}^{\mathrm{eff}} = \varrho_f \nu_f^{\mathrm{eff}} \left[\nabla \boldsymbol{u}_f + \nabla \boldsymbol{u}_f^{\intercal} - \frac{2}{3}\nabla \cdot \boldsymbol{u}\right] - \frac{2}{3}\varrho_f \mathrm{k}_f \mathbb{I}, \tag{3.5}$$

où ν_f^{eff} est la viscosité cinématique turbulente de la phase fluide et k est l'énergie cinétique turbulente.

3.4.1 Viscosité de la phase solide

Comme la phase solide a une représentation semblable à un fluide (cf. Eq. (3.2)), la pression hydrodynamique p_s, la viscosité de cisaillement μ_s, et la viscosité en volume λ_s doivent être reformulées de manière similaire à la phase fluide. Cependant, l'acquisition de valeurs équivalentes pose un défi considérable en raison de la nature particulaire inhérente de la phase solide. Par conséquent, des fermetures doivent être utilisées pour exprimer le comportement de la phase solide, tel que la pression de contact et les collisions de vitesse, en termes de pression et de viscosité continus pour maintenir un état d'agitation continue et chaotique dans le fluide. L'approche adoptée dans cette étude est la théorie cinétique des écoulements granulaires (KTGF), qui est basée sur la théorie cinétique des gaz de manière généralisée pour prendre en compte les collisions de particules inélastiques. La viscosité de la phase solide incluent les composantes suivantes :

$$\mu_s = \mu_{s,\mathrm{col}} + \mu_{s,\mathrm{kin}} + \mu_{s,\mathrm{fric}}, \tag{3.6}$$

Où $\mu_{s,\mathrm{col}}$, $\mu_{s,\mathrm{kin}}$ et $\mu_{s,\mathrm{fric}}$ correspondent respectivement aux composantes collisionnelle, cinétique et de frottement de la viscosité totale de la phase solide [Syamlal et al., 1993b].

3.4.2 La turbulence dans le modèle à deux fluides

Pour garantir la pseudo-homogénéité du mélange et prévenir la sédimentation totale de la phase solide, un régime d'écoulement turbulent est maintenu à l'intérieur de la conduite de la boue. Par conséquent, ν_f^{eff} dans l'équation (3.5) est modélisée en utilisant un modèle de turbulence. Ici, la turbulence est traitée avec deux modèles connus, à savoir le modèle $\mathrm{k}-\varepsilon$ [Launder and Spalding, 1983] et le modèle SST $\mathrm{k}-\omega$ [Wilcox, 1988]. Le modèle de turbulence $\mathrm{k}-\varepsilon$ est dérivé d'une combinaison d'observations empiriques et de considérations théoriques. C'est un modèle à deux équations ((3.7), (3.8)) qui prédit les caractéristiques de turbulence d'un fluide en résolvant l'équation pour l'énergie cinétique turbulente k et le taux de dissipation de l'énergie cinétique turbulente ε dans un écoulement de fluide. Le côté gauche des équations suivantes est la dérivée lagrangienne: $D/Dt := \partial/\partial t + u_i \partial/\partial x_i$.

$$\frac{D\varepsilon}{Dt} = \frac{1}{\rho}\frac{\partial}{\partial x_k}\left[\frac{\mu_t}{\sigma_\varepsilon}\frac{\partial \varepsilon}{\partial x_k}\right] + \frac{C_1 \mu_t}{\rho}\frac{\varepsilon}{k}\left(\frac{\partial u_i}{\partial x_k} + \frac{\partial u_k}{\partial x_i}\right)\frac{\partial u_i}{\partial x_k} - C_2\frac{\varepsilon^2}{k}, \tag{3.7}$$

$$\frac{Dk}{Dt} = \frac{1}{\rho}\frac{\partial}{\partial x_k}\left[\frac{\mu_t}{\sigma_k}\frac{\partial k}{\partial x_k}\right] + \frac{\mu_t}{\rho}\left(\frac{\partial U_i}{\partial x_k} + \frac{\partial u_k}{\partial x_i}\right)\frac{\partial u_i}{\partial x_k} - \varepsilon. \tag{3.8}$$

C_μ, C_1, C_2, σ_k, σ_ε sont des constantes.

Le modèle de turbulence SST $\mathrm{k}-\omega$ est un modèle de viscosité turbulente à deux équations qui a gagné une grande popularité grâce à sa formulation polyvalente. Ce modèle combine les forces de deux approches, en utilisant la formulation de wilcox $\mathrm{k}-\omega$ dans les parties intérieures de la couche limite, permettant une application directe à la sous-couche visqueuse sans fonctions d'amortissement supplémentaires, tout en basculant vers un comportement $\mathrm{k}-\varepsilon$ en écoulement libre, réduisant ainsi la sensibilité aux propriétés de turbulence d'entrée en écoulement libre. Les équations (3.29) et (3.30)) présentent les variables pour le modèle SST $\mathrm{k}-\omega$, l'énergie cinétique turbulente k et le taux de dissipation spécifique ω respectivement.

$$\frac{D\varrho k}{Dt} = \tau_{ij}\frac{\partial u_i}{\partial x_j} - \beta^* \varrho \omega k + \frac{\partial}{\partial x_j}\left[\left(\mu + \sigma_k \mu_t\right)\frac{\partial k}{\partial x_j}\right], \tag{3.9}$$

$$\frac{D\varrho\omega}{Dt} = \frac{\gamma}{\nu_t}\tau_{ij}\frac{\partial u_i}{\partial x_j} - \beta\varrho\omega^2 + \frac{\partial}{\partial x_j}\left[\left(\mu + \sigma_\omega \mu_t\right)\frac{\partial \omega}{\partial x_j}\right] + 2\rho\left(1 - F_1\right)\sigma_{\omega 2}\frac{1}{\omega}\frac{\partial k}{\partial x_j}\frac{\partial \omega}{\partial x_j}. \quad , \tag{3.10}$$

avec σ_{k1}, $\sigma_{\omega 1}$, β_1, β^*, κ des constantes. Dans la section 4.2.2, les deux modèles de turbulence sont testés et comparés pour évaluer leur capacité à fournir des résultats précis.

Traitement près de la paroi

La présente étude utilise les modèles de turbulence en conjonction avec un traitement de fonction de paroi amélioré. Les fonctions de paroi sont utilisées pour traiter le développement de la couche limite jusqu'au mur. Une question importante dans la prédiction précise des écoulements turbulents industriels est la formulation et le traitement numérique des équations dans les régions proches des parois. La formulation de la zone proche de la paroi dans les conduites détermine la précision des prédictions de contrainte de cisaillement sur la paroi et a une influence importante sur le développement des couches limites, y compris le début de la séparation de l'écoulement. Typiquement, la méthode de fonction de paroi est utilisée pour modéliser l'écoulement dans la région proche de la paroi. Ces formules relient les conditions de paroi (par exemple, la contrainte de cisaillement sur la paroi) aux variables dépendantes au nœud de la grille proche de la paroi, qui est supposé se situer dans la région entièrement turbulente de la couche limite.

3.5 Conclusion

Afin de déterminer les méthodologies de modélisation appropriées et les modèles mathématiques pour les écoulements de boues dans les conduites horizontaux, une analyse approfondie des études numériques précédentes a été réalisée. Finalement, le modèle eulérien à deux fluides a été choisi en raison de sa capacité à représenter avec précision les comportements physiques de l'écoulement des boues dans les conduites tout en maintenant un niveau raisonnable de coût computationnel. Pour prendre en compte les interactions particule-particule et particule-paroi, le modèle KTGF a été utilisé pour modéliser la dynamique de la phase solide. Afin de traiter la turbulence de la phase liquide, deux modèles de turbulence sont présentés et seront testés au cours de la validation numérique à savoir SST $k-\omega$ SST et $k-\varepsilon$.

Table 3.2: Conclusions sur la classification des modèles

DPM (Eulérien-Lagrangien)	**Avantages** • Beaucoup d'informations sur les échelles de particules et de sous-particules qui garantissent une compréhension physique approfondie. **Inconvénients** • La phase discrète doit être présente à un volume fractionnaire assez faible, généralement inférieur à 10-12%. • Coût de calcul élevé.
Modèle de Mélange	**Avantages** • Faible coût de calcul • Permet plusieurs phases solides **Inconvénients** • Il existe une grande différence entre les résultats CFD et expérimentaux, surtout à des débits plus faibles. • Impose des hypothèses strictes sur l'écoulement
Modèle TFM	**Avantages** • Précis et donne généralement de bons résultats par rapport au modèle de mélange. • Les résultats sont meilleurs et plus proches des données expérimentales dans le cas de tailles de particules bimodales ou à des vitesses plus élevées. • Coût de calcul abordable. **Inconvénients** • Plusieurs difficultés persistent concernant le réglage des coefficients, des sous-modèles et des paramètres. • Impose des hypothèses strictes sur l'écoulement.

4

CFD modeling and numerical validation

Objectives

The present chapter is dedicated to the numerical simulation of solid-liquid flows within pipeline systems. In section 6, a summary of prior experimental investigations is provided. Section 4.2 delves into the details of the numerical simulation process and the incorporation of relevant modeling features to ensure an effective simulation of slurry flow. To establish specific parameters, such as the turbulence model, treatment of near-wall turbulence, and discretization scheme for the convective fluxes, a preliminary comparison between computations and measurements in the single-phase flow case was employed. Subsequently, two-phase flow simulations were carried out using the two-fluid model (TFM). The performance of the model is thoroughly assessed by comparing its results with experimental data from the literature. The results demonstrate that the model is well-suited for accurately simulating slurry flows across a wide range of operating conditions, as discussed in section 4.2.3.

Contents

4.1 Experimental database for validation

Numerous experimental investigations have been carried out by different authors to investigate the hydrodynamics of slurry flows in pipe One of the primary drawbacks of experimental tests is their substantial cost, as they often necessitate specialized equipment and resources. Additionally, performing measurements, particularly for highly concentrated mixtures, can be challenging due to significant technical difficulties. Almost all of the experiences concern the case of horizontal pipes, the dispersed phase is usually sand [Gillies et al., 2004, Gillies and Shook, 2000, Matousek, 2002, Roco and Shook, 1983a, Schaan et al., 2000a], and spherical glass beads [Kaushal and Tomita, 2007, Kaushal et al., 2005], ash [Kumar et al., 2003], and solid nitrogen particles [Jiang and Zhang, 2013] have also been considered. Only few studies were focused on vertical pipes for coarse sand and Polystyrene particles [Shook and Bartosik, 1994], and bends [Kaushal et al., 2013]. The experimental data presented here were judged suitable among those available in the literature to provide a quantitative assessment of the models capability. The proposed data is obtained for various pipe diameters, particle sizes, velocities and concentrations to guarantee a general validity as well as the reliability of the numerical model within a wide range of applications. Table 4.1 shows a summary of the selected Experimental DATA.

4.2 Numerical validation

4.2.1 Methodology

Following the choice of mathematical models for simulating the two-phase flow, the next step involves their implementation within the CFD tool. We use the open-source continuum mechanics suite OpenFOAM® [Weller et al., 1998], to investigate numerically the two phase slurry pipe flow. The solver TwoPhaseEulerFoam is used to conduct the CFD simulations. Table 4.2 shows OpenFOAM® software advantages compared to commercial softwares. The simulation process commences with pre-processing, where the generation of geometry and mesh takes place. Subsequently, an appropriate solver is chosen to accurately represent the model, followed by post-processing to visualize the simulation results. The `twoPhaseEulerFoam` solver has been adapted to an isothermal flow solver since there is no heat exchange between the phases. The different forces acting on the flow are defined based on assumptions made, and interphase momentum exchange models are established. The implementation of the KTGF model is performed, taking into account the restitution coefficients, while giving special consideration to defining boundary conditions that require a deep understanding of the physical phenomenon. The simulations are performed using an implicit-Euler scheme for time discretization, employing a cell-limited linear Gauss scheme for gradient terms. The second-order corrected linear Gauss scheme is utilized for Laplacian terms, and linear interpolation scheme is employed. A corrected scheme is used

Table 4.1: Summary of the selected Experimental DATA

Source	Fluid	Solid phase	$Pipe_{\text{Diameter}}$ $[mm]$	$Particle_{\text{size}}$ $[\mu_m]$	ϕ_s [%]	ϱ_s $[kg/m^3]$	u_m $[m/s]$
Roco and Shook [1983a]	Water	Sand	[50.7-51.5-263-495]	[165-480-520-1300]	[6-35]	2650	[1.5-4.5]
Schaan et al. [2000a]	Water	Sand	[50-150]	[85-90-100]	[15-45]	2650	[0.8-5.0]
Gillies and Shook [2000]	Water	Sand	[105-264-495]	420	[26-47]	2650	[1.8-5.8]
Gillies et al. [2004]	Water	Sand	103	[90-270]	[10-45]	2650	[2.0-8.0]
Kaushal et al. [2013]	Water	Glass beads	54.9	[125-440]	[0.05-0.5]	2470	[1.0-5.0]
Kaushal and Tomita [2007]	Water	Glass beads	54.9	[125-440]	[0.2-0.5]	2470	[1.0-5.0]
Matousek [2002]	Water	Sand	[50-150]	[85-90-100]	[0.11–0.35]	2650	[1.41-6.0]
Matoušek et al. [2013]	Water	Glass beads	100	180	[0.10–0.36]	2450	[1.48-4]
Kumar et al. [2019]	Water	Ash	150	[300-2 850-15]	[1-0.04] (by w)	[2080-2110]	[1.8-5.8]
Ohira et al. [2015]	Liquid nitrogen	Solid nitrogen	15	[500-2000]	[10-28]	2650	7
Shook and Bartosik [1994]	Water	Polystyrene	[26-40]	[12.5-44.5]	[0.10-0.67]	[2650-1045]	[2.4-6.4]

Table 4.2: Comparison between OpenFOAM® and commercial software like ANSYS, STAR-CCM+, etc

	OpenFOAM®	commercial Softwares
Cost effectiveness	✓	✗
Parallel computing	✓	✓
Source code	✓	✗
Redistribution of code	✓	✗
Collaboration development	✓	✗
Documentation	✗	✓
GUI / user friendliness	✗	✓

for the surface-normal gradient scheme, while a mesh-wave is used for wall distance computation. Table 4.3 provides a summary of the primary solvers utilized in creating the current database.

Table 4.3: Solver scheme used in the simulations

Term	TwoPhaseEulerFoam
Convection & Momentum transport	Gauss Van Leer
Turbulence & Artificial compression	Gauss upwind

4.2.2 Single phase flow

In the first stage, we simulate single-phase flow simulations to validate our modeling approach. This step is crucial to ensure accurate implementation of turbulence models, near-wall treatment parameters, and other essential parameters required for subsequent multiphase simulations. During this phase, pressure drop data is recorded for different water flow rates in various pipe configurations, including horizontal pipes, inclined pipes, and pipes with elbows. The CFD code results are then compared with predicted values from theoretical correlations obtained from published literature. Table 4.4 provides an overview of the different correlations utilized to calculate the pressure drop for each configuration.

Table 4.4: Pressure drop correlations

Correlations	Pipe Set up
$\Delta P_f = -f\frac{\varrho_w L}{D}\frac{{u_w}^2}{2}$	Horizontal Pipe
$\Delta P = -\Delta P_f - \varrho_w g L sin(\theta)$	Inclined Pipe
$\Delta P = -\Delta P_f - \varrho_w g L_{inclined} sin(\theta) - K_L\frac{\varrho u_w^2}{2}$	Pipe with Bend

The implicit relation proposed by Colebrook, Eq. (4.1), is used to calculate the friction factor f for turbulent flows in rough pipes.

$$\frac{1}{\sqrt{f}} = -2\log\left(\frac{e}{3.71D} + \frac{2.51}{\mathrm{Re}\sqrt{f}}\right), \tag{4.1}$$

where $\frac{e}{D}$ is the relative roughness, and is related to the pipe material properties. These predicted values of the theoretical correlations are used to judge the CFD results.

The different boundary conditions used in these single phase flows cases, are summarized in the Table 4.5 below: This section only considers the $\mathrm{k}-\varepsilon$ model

Table 4.5: Summary of the selected boundary conditions

Field	Inlet	Outlet	Solid walls
ε	fixedValue	zeroGradient	wall function
k	fixedValue	zeroGradient	wall function
v_t	zeroGradient	zeroGradient	wallFunction
p	zeroGradient	atmospheric pressure	zeroGradient
u	fixedValue	zeroGradient	noSlip

for treating turbulence, as the flow consists solely of water. The inlet turbulent kinetic energy "*fixedValue*" (k_{in}) is based on the turbulence intensity ($I = 0.05$) and the fluid inlet velocity (u) (Messa and Matoušek [2020]), which calculates:

$$\mathrm{k}_{in} = \frac{3}{2}u^2I^2 \tag{4.2}$$

Following that, the inlet turbulence's length scale (ℓ) should be given. For internal pipe flow, this is typically $\sim 7\%$ of the pipe diameter. As a result, the turbulent dissipation rate (ε_{in}) is derived as follows:

$$\varepsilon_{in} = C_\mu \frac{k_{in}^{3/2}}{\ell} \tag{4.3}$$

where the adjustable constant C_μ is set to 0.09 [Ashgriz and Mostaghimi, 2002].

Horizontal pipe

The geometry consists of a $40m$ horizontal pipe, with an internal diameter of $0.9m$. OpenFOAM's meshing utility blockMesh was used to generate the mesh which takes into account the near-wall refinement by calculating the height of the first cell on the wall, with a precise magnification ratio which is linked to y^+ while approaching the center of the pipe. However, a coarse grid is suitable and enough to conduct simulations for flows that involve only one phase, such

as water. Figs. 4.1a and 4.1b display a 2D slice and a 3D meshed structure, respectively. The flow density is $\varrho = 1000$ kg/m^3, with inlet velocities that range

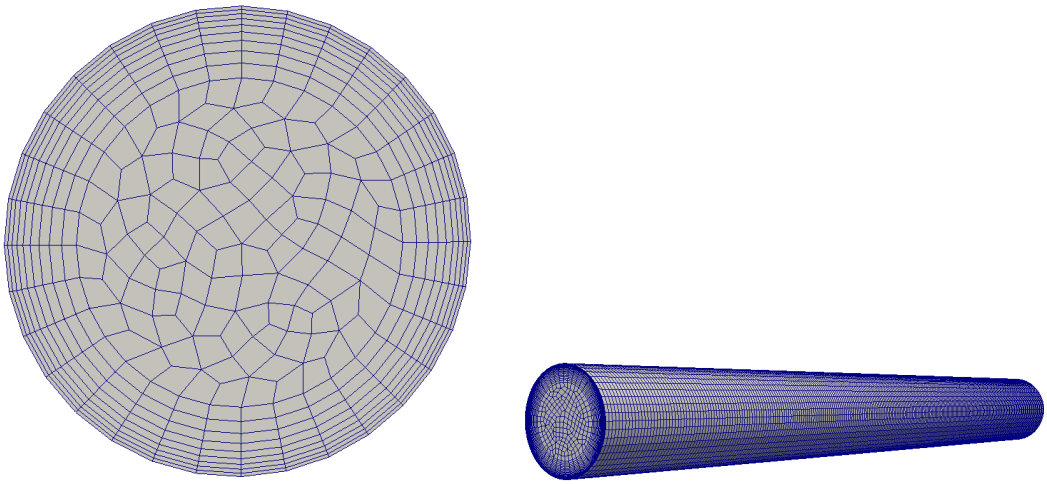

(a) (b)

Figure 4.1: Horizontal pipe geometry: (a) Cross-section mesh, (b) Profile mesh

from 1 to $3m/s$. The wall roughness is set at $0.045mm$, and the outlet pressure is fixed as atmospheric one. These initial conditions are the same for the next simulations of inclined and bended pipe. For a horizontal pipe, we have regular pressure drops, which are generated by the friction of the fluid on the internal wall of the pipe throughout its passage. They depend on the length of the pipe, the relative roughness of the pipe, and the inlet velocity (u_{in} m/s). Results are presented in Fig. 4.2, they were also compared in this case to experimental data were found for water flow in [Gillies et al., 2004]. In fact, as expected the pressure

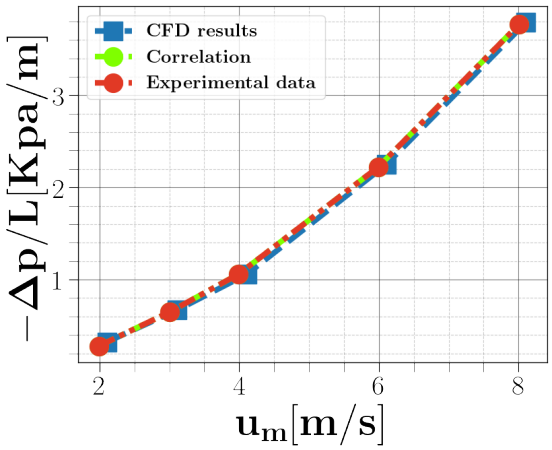

Figure 4.2: CFD simulations versus empirical formula in Table 4.4 and experimental measurements.

losses are increasing relatively with inlet velocities and good agreement was found

between CFD results and both the theoretical correlation and the experimental measurements.

Inclined pipe

The geometry is the same here as for the horizontal pipe, but with a negative slope. Concerning this pipe setup, it is characterized by a changing elevation. As a result, when the fluid reaches the end of the sloping pipe, the entire weight of the fluid applies pressure at that point, causing an increase in pressure. The total pressure difference can be calculated by adding the hydrostatic pressure to the friction component as in Table 4.4. Fig. 4.3 shows the pressure gradient as a function of inlet velocities. As noticed the pressure gain decreases while increasing the velocity, and this comes back to the augmentation of friction losses.

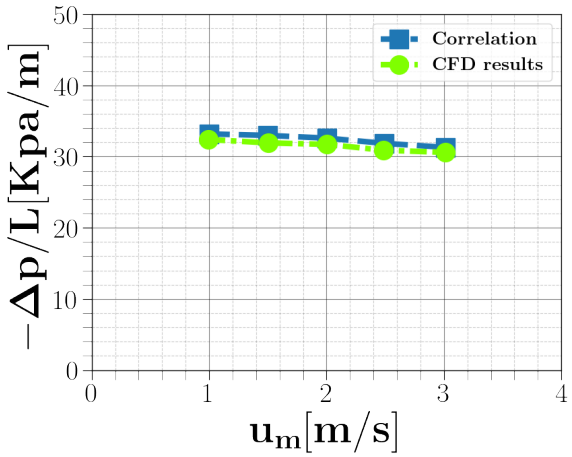

Figure 4.3: Pressure drop in inclined pipe

Bended pipe

For this setup, the geometry consists of a 45 degree bended pipe, of 6 m equivalent length with 0.9 m diameter. Figs. 4.4a and 4.4b show the cross-section and profile mesh.

This pipe setup is more complex, since in addition to the previously discussed components of the kinetic losses, another component is added namely the singular pressure drop as in Table 4.4. The singular pressure drops are mainly due to the geometric modification of the pipe, such as changes of direction like bends. Fig. 4.5 shows that the pressure loss is increased in such geometries. It can be also seen that the CFD simulations underestimates the pressure drop versus the empirical formula slightly.

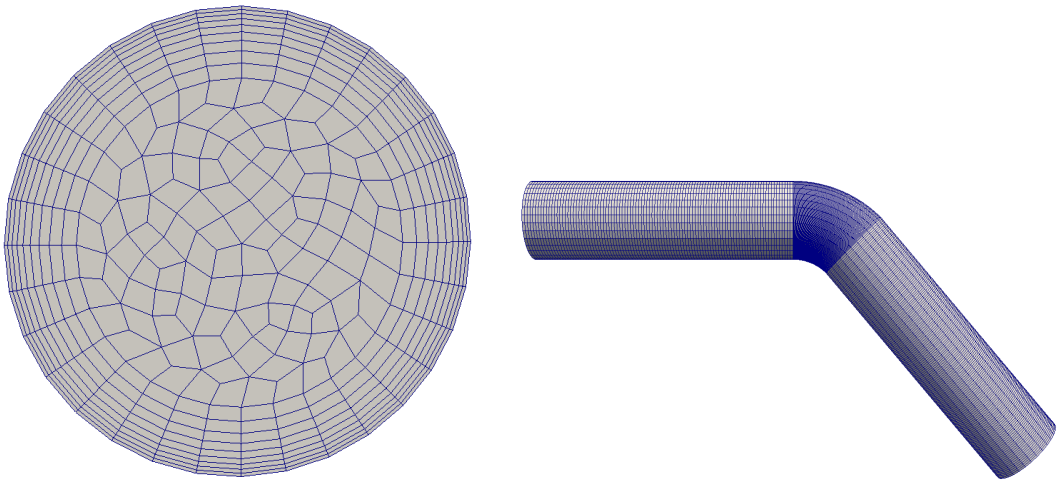

(a) (b)

Figure 4.4: Bended pipe geometry: (a) Cross-section mesh, (b) Profile mesh

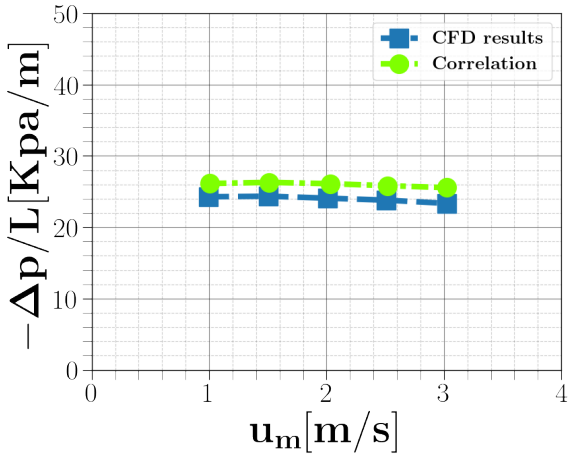

Figure 4.5: Pressure drop in bended pipe.

From the previous analysis we see that CFD reproduces very well the pressure drop measurement and the empirical models fit the CFD results for the classical geometrical configurations. These pressure drop formulae can constitute surrogate models for pressure calculations in piping systems with Newtonian fluids such as water. Hence, one can consider for example computing other pressure drop models for Newtonian fluids but for much more complex geometries, where experiments may be complex or time consuming to conduct. In the next section we will consider a two-phase flow, where the complexity is introduced in the fluid itself.

4.2.3 Two phase flow

Laminar flow modeling

Two phase simulations were presented by authors in (Elkarii et al. [2020]), where a slurry of mono-dispersed spherical polystyrene beads with rhodosil silicone oil were simulated in a laminar flow. Fig. 4.6 shows the evolution of the solid concentration profile of the mixture over time.

The previous study [Elkarii et al., 2020], validates the model for its capability

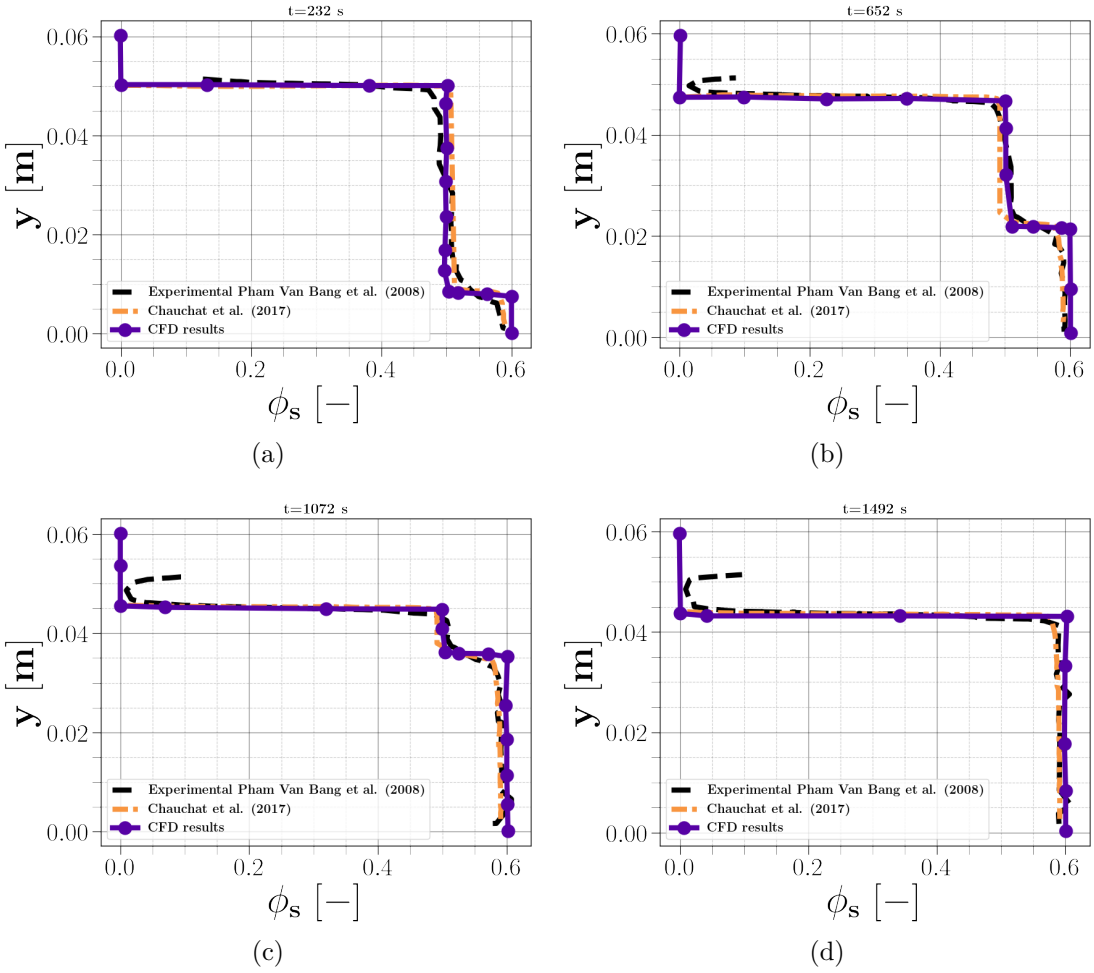

Figure 4.6: Sediment concentration profiles over time (a) At t = 232 s, (b) t = 652 s (c) t = 1072 s (d) t = 1492 s

to reproduce and predict high volume concentration profiles up to 60 %. The validation case consists of a sedimentation of non-cohesive particles by Chauchat et al. [2017], based on experimental data from Pham Van Bang et al. [2008]. The sedimentary phase was also modeled as continuous and consecutive laws were adopted to take sedimentary constraints into account.

However, to approach the simulation of a real slurry flow, the turbulence

aspect must be added to prevent sedimentation problems. Therefore, in this next part, CFD simulations were performed to fit the experimental results of a turbulent flow of water-sand slurry under isothermal conditions, reported by Gillies et al. [2004]. But first, to ensure reliable predictions especially for turbulent flows, the mesh convergence is firstly re-checked.

Turbulence modeling

To maintain the pseudo-homogeneity of the mixture and prevent total sedimentation of the solid phase, a turbulent flow regime is maintained within the slurry pipe. In our CFD modeling, we conducted an analysis of turbulence modeling, comparing two turbulence models: the standard k-ε model and the k-ω SST model, to assess their accuracy in providing results. Due to the presence of significant pressure gradients (though favorable) and mean streamline curvature in inclined pipes, the k-ω family of turbulence models is expected to outperform the k-ε models in predicting axial pressure. The k-ε models are known to face challenges in modeling such flow behavior [Wilcox, 1998]. Both turbulence models are employed with an enhanced wall function treatment, blending laminar and turbulent laws-of-the-wall to yield continuous and asymptotically correct values for all y^+. To ensure accuracy in the near-wall regions, a mesh refinement is performed. A priori estimates of shear stresses are used to determine the wall-adjacent mesh cell heights required to achieve $x_2 = y^+ \approx 1$ (see Fig. 4.8b), where $y^+ = u^* y/\nu$ is a function of the friction velocity $u^* = \sqrt{\tau_{\text{wall}}/\rho}$. The wall shear stress τ_{wall} is estimated using the friction factor approximation by Swamee and Jain [1976] in conjunction with the root-mean-squared value of the axial and circumferential Reynolds numbers, zero wall roughness, and the average axial velocity. To effectively capture the viscous sublayer, y^+ is kept less than 1. The mesh growth rate is set at 1.1 until it reaches the log-law layer, equivalent to $x_2^+ = 60$. Different meshes are refined in terms of the number and distributions of subdivisions along the azimuthal, radial, and axial directions. To verify the number of cells, a grid-dependency analysis of the predicted hydraulic pressure gradient is conducted. As shown in Fig. 4.7, the hydraulic gradient predictions practically match the experimental results of Matoušek et al. [2013] for the medium and fine meshes. Considering i) the total number of runs, ii) the rationalization of computational resources use, and iii) the computational time for the solution convergence, the medium mesh grid featuring 512×10^3 cells seems to be the suitable choice for predicting accurately the slurry flow dynamics. The grid meshes used to discretize the whole three-dimensional computational domain, is illustrated in Fig. 4.8a. To compare the two turbulence models, we utilize experimental data from Gillies et al. [2004], which presents a water-sand slurry under isothermal conditions. The experimental data includes pressure drops along the pipe, particle concentration profiles, and particle velocity profiles at the pipe outlet. The simulation domain consists of a 140 pipe diameter (D) long pipe to ensure fully developed

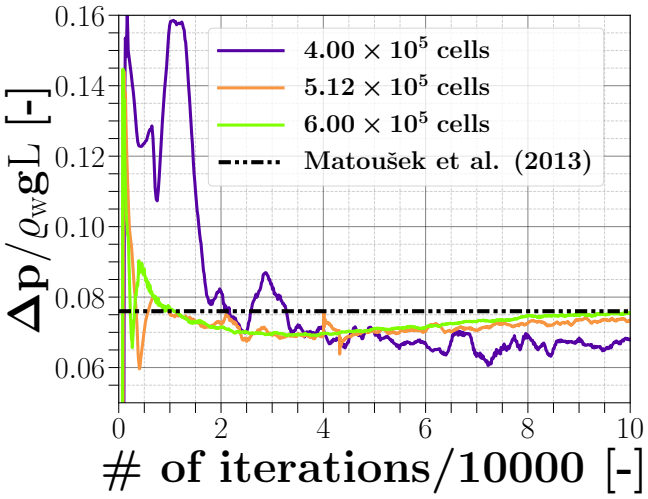

Figure 4.7: Grid independency test of the hydraulic pressure gradient.

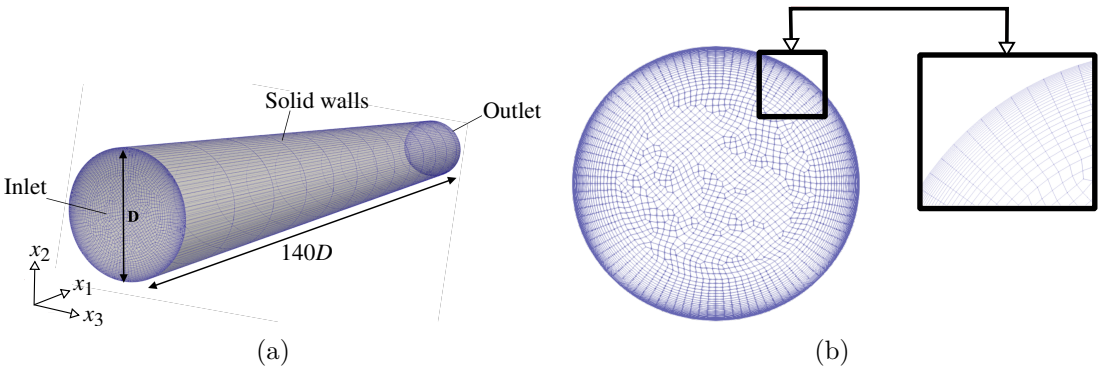

Figure 4.8: (a) Three dimensional view of the computational domain and boundary conditions, (b) detail of the discretization of the pipe section and local magnification of the mesh close to the near-wall cells.

flow. Depending on the desired flow regime, a specified value for the velocity is set as "fixedValue" at the inlet and "zeroGradient" at the outlet, implying zero velocity normal to the flow outlet. The velocity at the pipe wall is set to zero as "fixedValue" to enforce a non-slip boundary condition for the carrier fluid phase, similar to single-phase flow cases. However, for the solid phase in the two-fluid models based on the KTGF theory, a different treatment is applied to the wall solid phase velocity. The conventional no-slip wall boundary condition, used for the fluid phase to satisfy the adhesion condition, is not appropriate for the solid phase as the tangential velocity of particles is nonzero. Instead, the partial slip condition specified in Johnson and Jackson [1987] is imposed. In slurry flows, the Johnson-Jackson boundary conditions are employed to account for particle-wall collisions and the associated friction, which significantly affects particle movement. These boundary conditions incorporate friction by assuming that some

particles collide, while the rest slide heuristically. The momentum and energy transfer caused by colliding particles are quantified using a specularity coefficient $\mathcal{SC}$, and the momentum transfer caused by sliding particles is quantified using Coulomb friction. The specularity coefficient ($\mathcal{SC}$) ranges from zero for collisions without any loss of kinetic energy to a value of 1 for collisions leading to a total loss of particles' kinetic energy. The specific value of the specularity coefficient must be specified to characterize the tangential momentum transfer due to collisions. Recent studies on the effect of this coefficient on slurry flow behavior can be found in Liu et al. [2021]. In order to select the appropriate value for $\mathcal{SC}$, an assessment is conducted to determine its impact on the predicted pressure drop. The outcomes depicted in Fig. 4.9 are utilized to efficiently calibrate the specularity coefficient by comparing it with the experimental data from [Gillies et al., 2004] (cf. Table 4.1). The findings demonstrate that the use of the "*noSlip*"

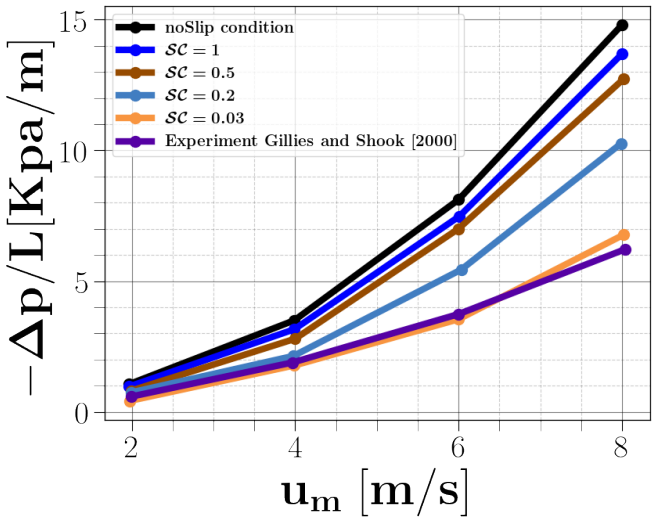

Figure 4.9: Effect of specularity coefficient on the pressure gradient

wall condition is indeed unsuitable for this type of flows. Recall that the specularity coefficient is a representation of particles kinetic energy losses after a wall collision. Therefore, the higher the value of the latter, the greater the losses of kinetic energy of the particles. This means more particle deposits and therefore a higher wall friction which leads to a superior pressure drop. In this work, the retained specularity coefficient is equal to $\mathcal{SC} = 0.03$. The flow is characterized by high inlet velocities ranging up to 8 m/s. Two diameters of particles are considered along with different solid concentrations. The physical parameters used are sand density $\varrho_s = 2650$ kg/m^3, water density $\varrho_w = 1000$ kg/m^3, and water viscosity $\mu_w = 10^{-3}$ Pa·s. The radial distributions of sand particles are presented in Fig. 4.10, for three inlet solid concentrations $\phi_s = 0.19$, $\phi_s = 0.33$, and $\phi_s = 0.4$. Numerical results of Bordet et al. [2018] are also plotted for $\phi_s = 0.19$. The solid concentration profile exhibits slight variations along the diameter of the pipe, with values ranging from 0.19 to 0.24. The simulation results for both

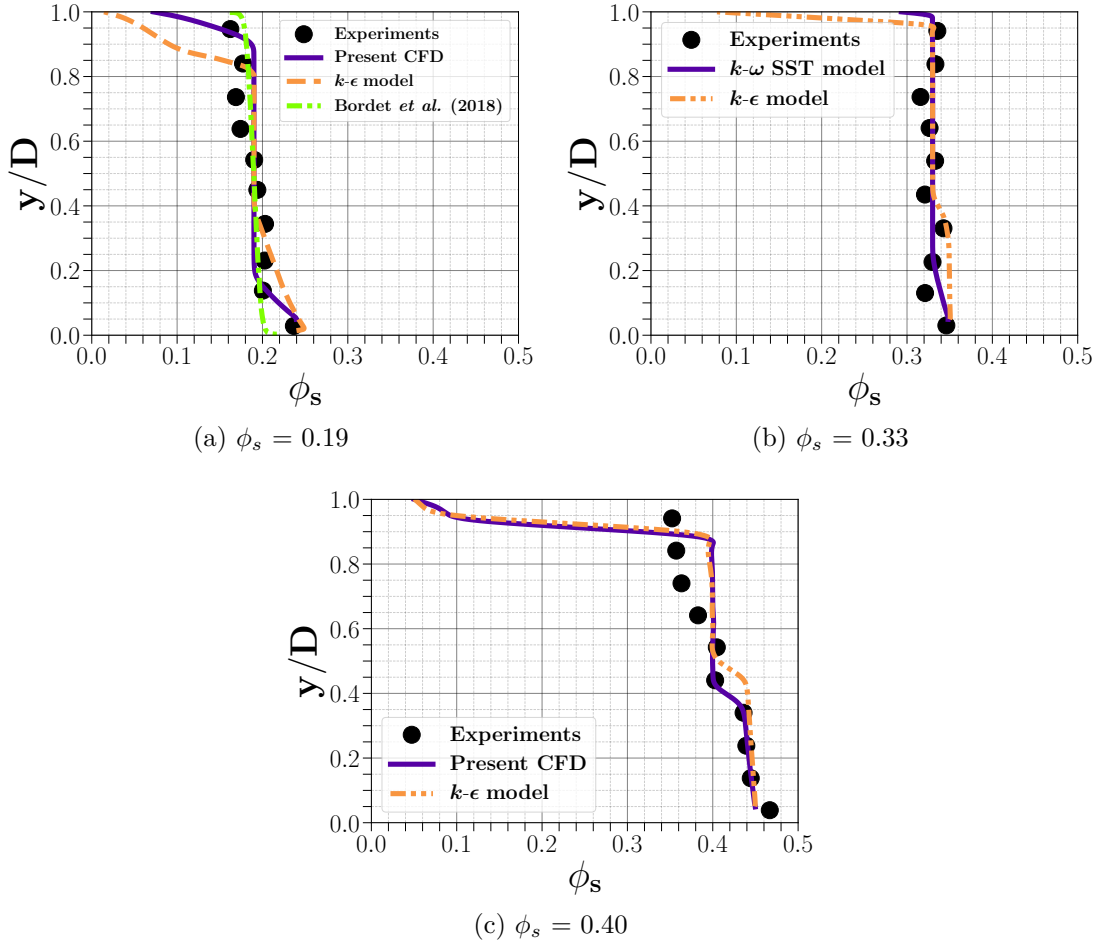

(a) $\phi_s = 0.19$ (b) $\phi_s = 0.33$

(c) $\phi_s = 0.40$

Figure 4.10: Comparison of radial distributions of the volume fraction of sand particles ϕ_s: (a,b) $d_p = 0.09$ mm and $u_m = 3$ m/s, (c) $d_p = 0.27$ mm and $u_m = 5.4$ m/s.

turbulence models agree reasonably well with the experimental data in the bulk flow region ($0.2 < y/D < 0.9$), as shown in Fig. 4.10a. However, the k-ε model underestimates the experimental solid concentration values near the upper wall ($y/D > 0.9$) and overestimates them along the lower wall ($y/D < 0.2$). This discrepancy in the k-ε model's performance may be attributed to its limited control over the turbulent viscosity term, leading to the phenomenon of sedimentation in a non-homogeneous concentration profile. As the solid concentration is increased to 33% (cf. Fig. 4.10b) and 40% (cf. Fig. 4.10c), the same observations are made along the lower wall, indicating a pseudo-homogeneous flow with the formation of a small bed of particles. To further investigate the influence of turbulence modeling concerning the inlet velocity (u_m), the particle velocity profiles are assessed for $u_m = 2$ m/s and $u_m = 3$ m/s, as shown in Fig. 4.11a and Fig. 4.11b, respectively. In contrast to the concentration distribution, both turbulence models predict the correct velocity profiles. It is noteworthy that the axial average

velocity distributions are slightly asymmetrical, and they closely follow a classic turbulent logarithmic profile.

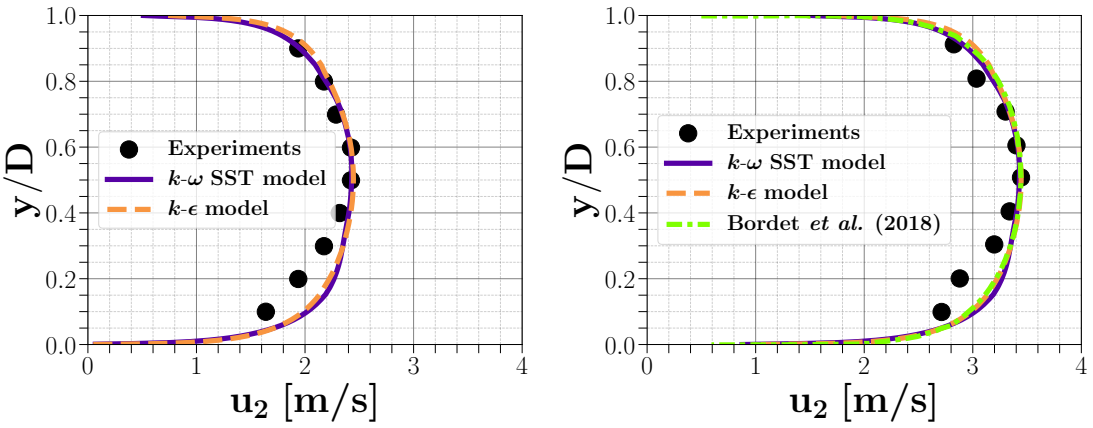

(a) $u_m = 2$ m/s (b) $u_m = 3$ m/s

Figure 4.11: Radial distributions of the mean axial velocity of sand particles at the outlet of the pipe for $\phi_s = 0.19$ and $d_p = 0.09$ mm.

Fig. 4.12 illustrates the variations of the pressure drop per unit length $\Delta p/L$ with respect to the inlet velocity of the mixture u_m. The simulations are conducted for two different particle diameters, $d_p = 0.09$ mm and $d_p = 0.27$ mm. In Figs. 4.12a and 4.12b, we present the solid concentrations $\phi_s = 0.19$ and $\phi_s = 0.20$, respectively, while Fig. 4.12c shows the solid concentration of $\phi_s = 0.40$. The experimental data from Gillies et al. [2004] is used for validation of the current simulations. The pressure drop increases almost linearly with the inlet velocity u_m. The numerical results agree well with the experimental data, but discrepancies are more significant at high velocities. The k-ω SST model slightly outperforms the k-ε model in predicting the pressure drop in all cases, even though the latter is used with wall functions to handle the boundary-layer development up to the wall. It is also noted that coarser particles have superior pressure drop at lower flow rates and an inferior one at higher flow rates. The reason behind this, is that the coarser particles at lower speeds deposit more, which comes down to the gravitational effect, and subsequently, the amount of particles in the bed increases which leads to more frictions. Hereafter, following the analysis in this section, the two-phase Eulerian model coupled to k-ω SST model is retained to predict the slurry flow hydrodynamics along the pipe.

4.3 conclusion

This chapter primarily focuses on the modeling of liquid-solid slurry pipe flows using CFD. The results obtained from the CFD simulations show a high level of agreement with the experimental data presented. The overall mean relative

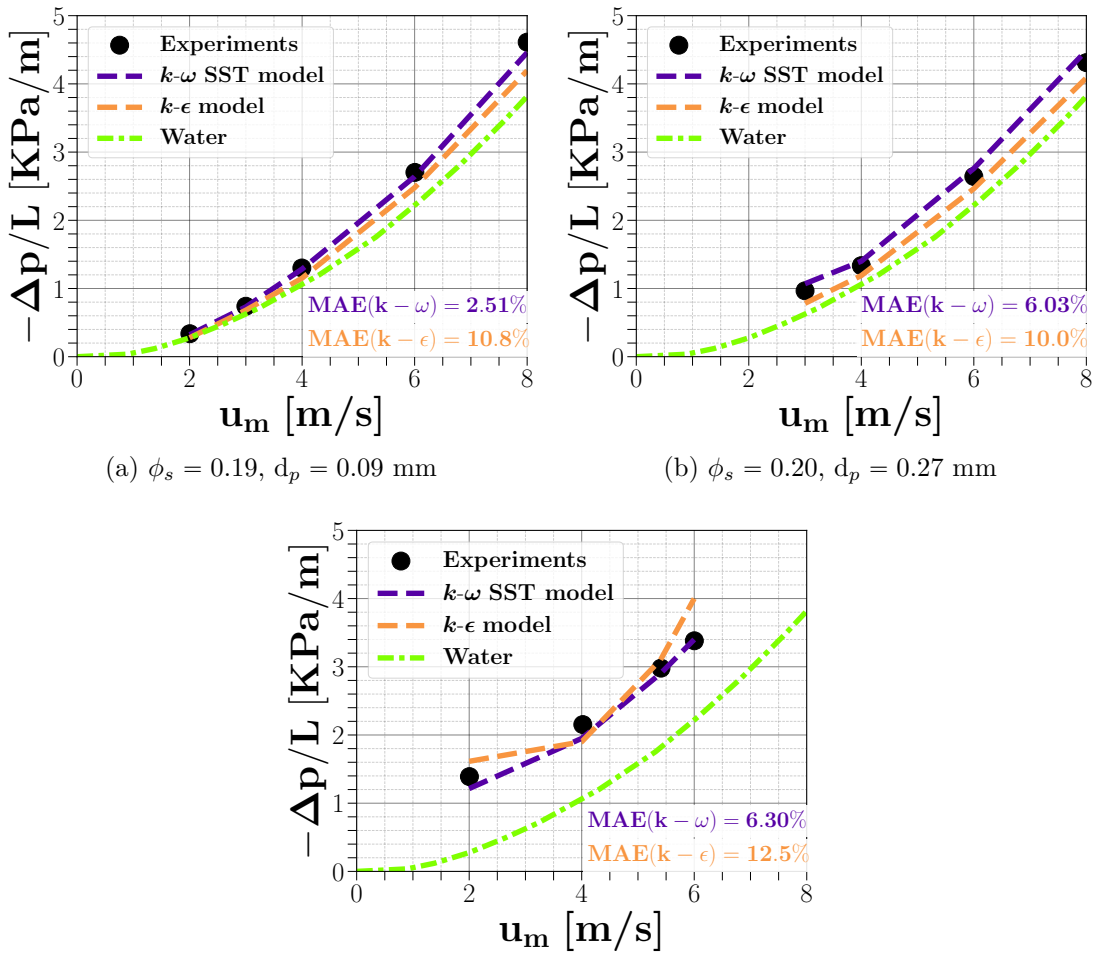

(a) $\phi_s = 0.19$, $d_p = 0.09$ mm

(b) $\phi_s = 0.20$, $d_p = 0.27$ mm

(c) $\phi_s = 0.40$, $d_p = 0.27$ mm

Figure 4.12: Pressure drop per unit of length $\Delta p/L$ versus slurry velocity computed with both turbulence models and from experimental data. Differences in relative errors between predictions and experiments are also displayed.

errors for the pressure drops are limited to 10%, which is considered acceptable and demonstrates the validity of the numerical model within the specified range of conditions. It should be noted that the CFD model used in this study is considered interpretive, as it is employed to acquire additional information about flow characteristics for the same testing conditions. The model is not used for predictive purposes to investigate flow scenarios beyond those of the calibration and validation stages. Instead, it is utilized to investigate situations with difficult-to-determine parameters and evaluate their impact on the desired outputs.

4

Modélisation CFD et validation numérique

Objectifs:

Le présent chapitre concerne la simulation numérique des écoulements solide-liquide à travers des systèmes de pipeline. Dans la section 6, un résumé des précédentes investigations expérimentales est présenté. La section 4.2 décrit le processus de simulation numérique et les caractéristiques de modélisation à prendre en compte pour une simulation efficace d'écoulement de suspension. La performance du modèle est étudiée en comparant les résultats contre des données expérimentales de la littérature dans la section 4.2.2.

4.1 Base de données expérimentale pour la validation

De nombreuses investigations expérimentales ont été menées par différents auteurs pour étudier l'hydrodynamique des écoulements de suspension dans les conduites. Le principal inconvénient des tests expérimentaux est qu'ils sont considérablement coûteux et nécessitent un équipement spécifique, et des difficultés techniques importantes se posent pour effectuer des mesures, surtout pour des mélanges fortement concentrés. Presque toutes les expériences concernent le cas de conduites horizontales, la phase dispersée est généralement du sable [Gillies et al., 2004, Gillies and Shook, 2000, Matousek, 2002, Roco and Shook, 1983a, Schaan et al., 2000a], et des billes de verre sphériques [Kaushal and Tomita, 2007, Kaushal et al., 2005], de la cendre [Kumar et al., 2003], et des particules solides d'azote [Jiang and Zhang, 2013] ont également été considérées. Seules quelques études se sont concentrées sur les conduites verticales pour le sable grossier et les particules de polystyrène [Shook and Bartosik, 1994], et les coudes [Kaushal et al., 2013]. Les données expérimentales présentées ici ont été jugées appropriées parmi celles disponibles dans la littérature pour fournir une évaluation quantitative de la capacité des modèles. Les données proposées sont obtenues pour divers diamètres de conduites, tailles de particules, vitesses et concentrations pour garantir une validité générale ainsi que la fiabilité du modèle numérique dans une large gamme d'applications.

4.2 Validation numérique

4.2.1 Méthodologie

Suite au choix des modèles mathématiques pour la simulation de l'écoulement diphasique, l'étape suivante consiste à les implémenter dans l'outil CFD. Nous utilisons le logiciel open source OpenFOAM® [Weller et al., 1998], pour étudier numériquement l'écoulement diphasique de boues dans une conduite. Le solveur TwoPhaseEulerFoam est utilisé pour mener les simulations CFD.

4.2.2 Ecoulement à deux fluides

Laminar flow modeling

Les auteurs de (Elkarii et al. [2020]) ont présenté des simulations à deux phases, où une suspension de billes sphériques de polystyrène mono-disperses avec de l'huile de silicone rhodosil a été simulée dans un écoulement laminaire. L'étude précédente a validé le modèle pour sa capacité à reproduire et à prédire des profils de concentration de volume élevé jusqu'à 60 %. Le cas de validation consiste en

une sédimentation de particules non cohésives réalisée par Chauchat et al. [2017], basée sur des données expérimentales de Pham Van Bang et al. [2008].

Cependant, pour approcher la simulation d'un véritable écoulement de suspension, l'aspect turbulence doit être ajouté pour éviter les problèmes de sédimentation. Par conséquent, dans cette prochaine partie, des simulations de CFD ont été effectuées pour adapter les résultats expérimentaux d'un écoulement turbulent de suspension eau-sable dans des conditions isothermes, rapporté par Gillies et al. [2004]. Mais d'abord, pour assurer des prédictions fiables, en particulier pour les écoulements turbulents, la convergence du maillage est d'abord vérifiée à nouveau.

Modélisation de la turbulence

Dans notre modélisation CFD, une analyse de la modélisation de la turbulence est effectuée. Deux modèles de turbulence, à savoir le modèle standard k-ε et le modèle k-ω SST, sont testés et leur capacité à donner des résultats précis est comparée. Notez que les deux moune conduitedèles de turbulence sont employés avec un traitement de fonction de paroi amélioré, qui mélange les lois de paroi laminaires et turbulentes pour fournir des valeurs continues et asymptotiquement correctes pour tous les y^+. Pour assurer l'exactitude dans les régions proches de la paroi, un raffinement de maillage est effectué. Un total de 512×10^3 maillages sont utilisés pour discrétiser l'ensemble du domaine de calcul tridimensionnel.

Pour comparer les deux modèles de turbulence, on utilise une suspension eau-sable rapportée expérimentalement sous des conditions isothermes par Gillies et al. [2004]. Le domaine de simulation consiste en une conduite de 140D de long pour assurer que l'écoulement est entièrement développé. Les conditions appliquées au mur pour la phase fluide sont similaires à celles des cas d'écoulement monophasique. Cependant, dans ces modèles à deux fluides basés sur la théorie KTGF, la vitesse de la phase solide en contact avec le mur est traitée différemment. La condition de paroi de non-glissement commune appliquée pour la phase fluide pour satisfaire la condition d'adhérence, n'est pas adaptée pour la phase solide car la vitesse tangentielle des particules est différente de zéro. La condition de glissement partiel spécifiée dans [Johnson and Jackson, 1987] est imposée.

L'écoulement est caractérisé par des vitesses d'entrée élevées allant jusqu'à 8 m/s. Deux diamètres de particules sont considérés ainsi que différentes concentrations solides. Les paramètres physiques utilisés sont la densité du sable $\varrho_s = 2650$ kg/m^3, la densité de l'eau $\varrho_w = 1000$ kg/m^3, et la viscosité de l'eau $\mu_w = 10^{-3}$ Pa·s. Les distributions radiales de particules de sable sont présentées dans la Fig. 4.1, pour trois concentrations solides d'entrée $\phi_s = 0,19$, $\phi_s = 0,33$ et $\phi_s = 0,4$. Les résultats numériques de Bordet et al. [2018] sont également tracés pour $\phi_s = 0,19$. Le profil de concentration solide varie légèrement le long du diamètre de la conduite ($0,19 < \phi_s < 0,24$). La présente simulation concorde assez bien avec les expériences dans l'écoulement en vrac ($0,2 < y/\mathrm{D} < 0,9$) pour les

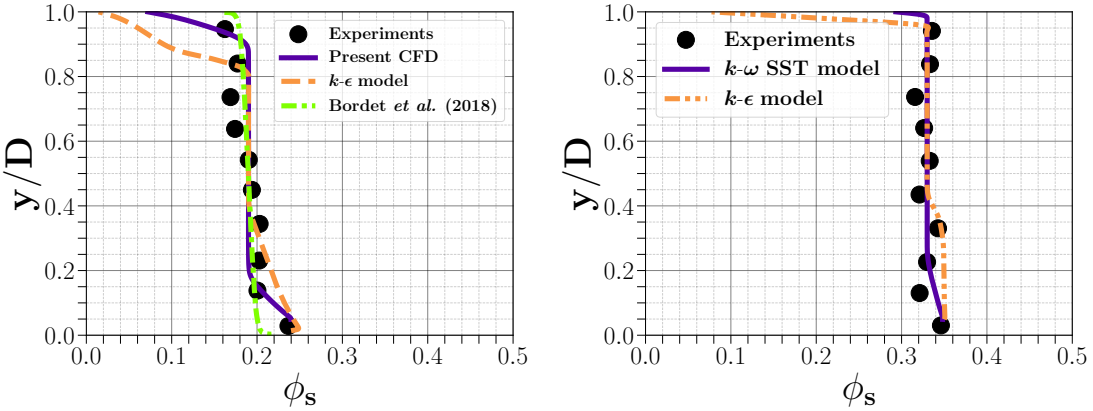

(a) $\phi_s = 0.19$ (b) $\phi_s = 0.33$

(c) $\phi_s = 0.40$

Figure 4.1: Comparison of radial distributions of the volume fraction of sand particles ϕ_s: (a,b) $d_p = 0.09$ mm and $u_m = 3$ m/s, (c) $d_p = 0.27$ mm and $u_m = 5.4$ m/s.

deux modèles de turbulence, comme le montre la figure 4.1a, tandis que le modèle k-ε sous-estime les valeurs expérimentales de ϕ_s près de la paroi supérieure ($y/D > 0,9$) et les surestime le long de la paroi inférieure ($y/D < 0,2$). La performance insuffisante du modèle k-ε pourrait être attribuée au manque de contrôle total de la viscosité turbulente, ce qui favorise le phénomène de sédimentation dans un profil de concentration non homogène. Lorsque la concentration solide est augmentée jusqu'à 33% (cf. Fig.4.1b) et jusqu'à 40% (cf. Fig.4.1c), les mêmes constatations sont observées le long de la paroi inférieure, ce qui correspond à un écoulement pseudo-homogène avec formation d'un petit lit de particules.

Pour étudier plus en profondeur l'influence de la modélisation de la turbulence par rapport à la vitesse d'entrée u_m, les profils de vitesse des particules sont évalués pour $u_m = 2$ m/s et $u_m = 3$ m/s, comme indiqué dans les figures Fig.4.2a et Fig.4.2b respectivement. Contrairement à la distribution de concentration, les deux modèles de turbulence prédisent le bon profil de vitesse. On remarque

que les distributions de vitesse moyenne axiale sont légèrement asymétriques, et qu'elles correspondent presque exactement à un profil logarithmique turbulent classique.

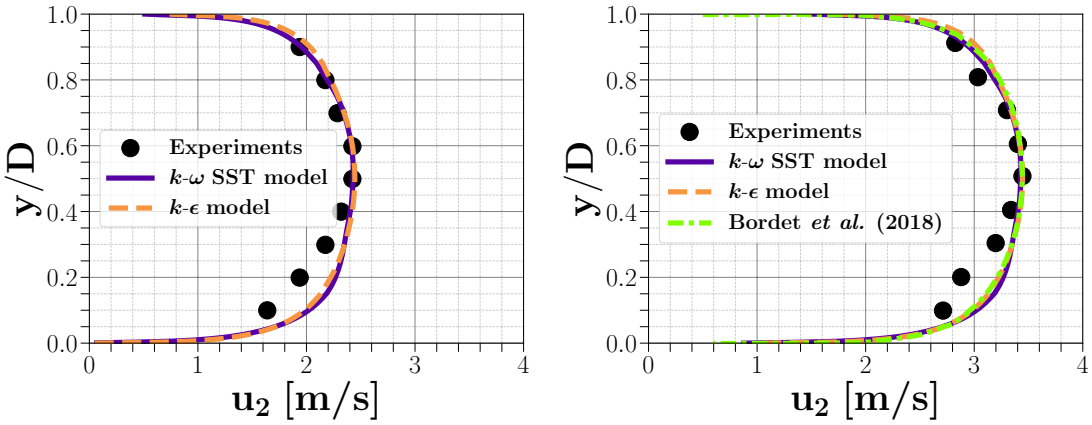

(a) $u_m = 2$ m/s (b) $u_m = 3$ m/s

Figure 4.2: Les distributions radiales de la vitesse axiale moyenne des particules de sable à la sortie de la conduite pour$\phi_s = 0.19$ and $d_p = 0.09$ mm.

Les variations de la perte de charge par unité de longueur $\Delta p/L$ par rapport à la vitesse d'entrée du mélange um sont représentées dans la Figure 4.3. Les simulations présentées sont obtenues pour deux diamètres de particules différents d$p = 0.09$ mm et d$p = 0.27$ mm. Dans les Figures 4.3a et 4.3b, nous représentons les concentrations de solides de $\phi s = 0.19$ et $\phi_s = 0.20$, respectivement, tandis que la concentration de solides de $\phi_s = 0.40$ est présentée dans la Figure 4.12c. Les données expérimentales de Gillies et al. [2004] sont utilisées pour valider les simulations actuelles. On note que la perte de charge augmente presque linéairement avec u_m. Comme on peut le remarquer, les résultats numériques actuels correspondent bien aux données expérimentales. Cependant, les écarts sont plus importants à des vitesses élevées. Le modèle k-ω SST est légèrement meilleur que le modèle k-ε pour prédire la perte de charge dans tous les cas, même si ce dernier a été utilisé avec des fonctions murales pour traiter le développement de la couche limite jusqu'au mur. Il est également remarqué que les particules plus grosses ont une perte de charge supérieure à des débits plus faibles et inférieure à des débits plus élevés. La raison derrière cela est que les particules plus grosses à des vitesses plus faibles se déposent davantage, ce qui est dû à l'effet gravitationnel, et par conséquent, la quantité de particules dans le lit augmente, ce qui entraîne plus de frictions. Par la suite, suivant l'analyse de cette section, le modèle diphasique d'Euler couplé au modèle k-ω SST est retenu pour prédire l'hydrodynamique de l'écoulement de la boue le long de la conduite.

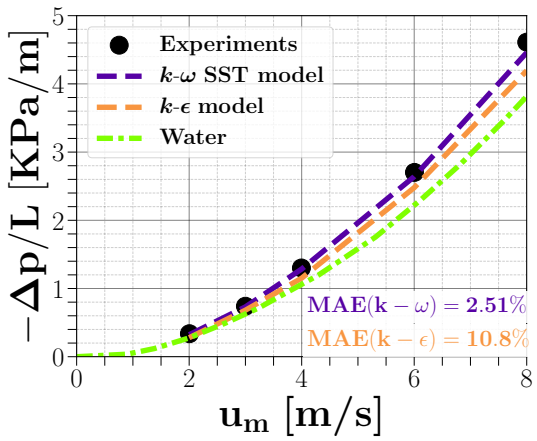

(a) $\phi_s = 0.19$, $d_p = 0.09$ mm

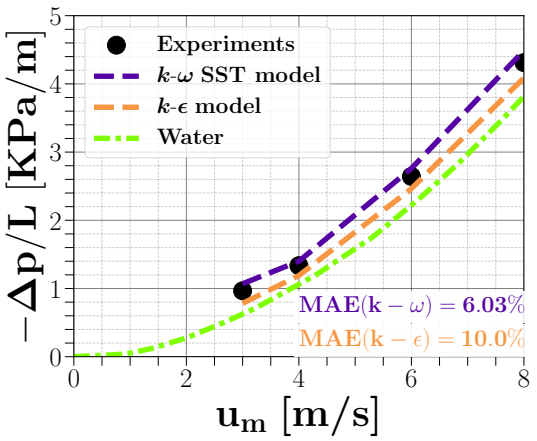

(b) $\phi_s = 0.20$, $d_p = 0.27$ mm

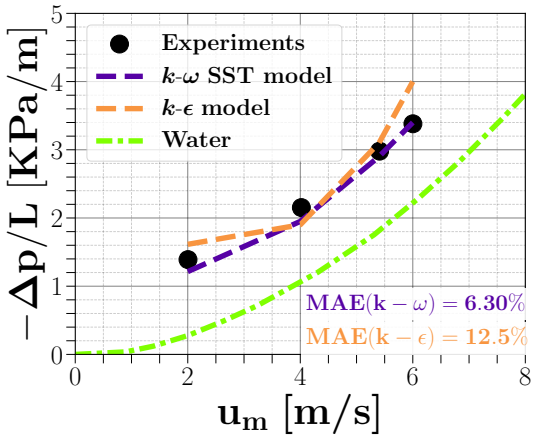

(c) $\phi_s = 0.40$, $d_p = 0.27$ mm

Figure 4.3: Perte de charge par unité de longueur $\Delta p/L$ en fonction de la vitesse du mélange calculée avec les deux modèles de turbulence et à partir de données expérimentales. Les différences dans les erreurs relatives entre les prévisions et les expériences sont également affichées..

4.3 Conclusion

Ce chapitre se concentre sur la modélisation des écoulements de boues liquide-solide dans des conduites. Les résultats de CFD ont montré une correspondance élevée avec les données expérimentales présentées. Les erreurs relatives moyennes globales des chutes de pression sont limitées à 10%. Cela est largement acceptable et démontre la validité du modèle numérique dans les conditions spécifiées. Nous rappelons ici qu'après avoir été calibré ou validé sur un ensemble de données expérimentales, un modèle CFD peut être considéré comme interprétatif s'il est utilisé pour acquérir des informations sur d'autres caractéristiques de l'écoulement pour les mêmes conditions de test. D'un autre côté, il peut être utilisé pour des conditions d'écoulement autres que celles des étapes de calibration et de

validation, et dans ce cas, on peut parler d'un objectif prédictif. Dans ce travail, le modèle CFD est utilisé essentiellement pour accomplir la première tâche, c'est-à-dire pour étudier des situations avec des paramètres difficiles à définir et évaluer leur impact sur les sorties d'intérêt.

5 Sensitivity Analysis

Objectives

The current chapter focuses on performing a global sensitivity analysis on phosphate slurry, utilizing the generalized polynomial chaos expansions (PCE) method. In order to investigate uncertainty quantification in the context of slurry flows and their uniform and 1-dimensional quantities of interest (QoIs), we utilized the PCE technique, which is described in section 5.1.2. Section 5.1.5 delves into the outcomes of the uncertainty quantification and sensitivity analysis for our QoIs. In Section 5.1.6, we provide concluding remarks for this initial part. Next, in section 5.2, we introduce the second part of our uncertainty quantification and global sensitivity analysis study, which focuses on 2-dimensional quantities of interest (QoIs). To reduce the cost of constructing the PCE model, we employ a reduced model called POD-PCE. The outcomes of the analysis using the POD-PCE technique are discussed in section 5.2.3.

Contents

5.1 GSA for Phosphate Slurry Flow in Pipelines using gPC

5.1.1 Introduction

In the present work, we consider the Eulerian-Eulerian CFD modeling approach to simulate the phosphate slurry flow and quantify the uncertainty of the numerical response. The use of two-phase flow models for sediment transport in pipelines is common, but due to the significant number of parameters needed for each simulation, considerable uncertainty is expected in the results. Therefore, a comprehensive analysis that addresses uncertainty quantification (UQ) and sensitivity analysis (SA) is necessary to improve prediction reliability. In this study, we consider the Eulerian-Eulerian CFD modeling approach to simulate phosphate slurry flow and quantify the uncertainty of the numerical response. The objective of UQ is to propagate the uncertainties of input parameters and quantify their impact on a Quantity of Interest (QoI) simulated through a physically based model. This allows associating every simulation result with a level of confidence since its accuracy depends significantly on the quantity and quality of input data. One major problem when tackling UQ with multiphase hydraulic computations is the curse of dimensionality. The most common method to address UQ is through Monte Carlo simulations, which have practical advantages, such as being non-intrusive and easy to implement, and theoretical advantages, such as being well-established. However, they require a considerable amount of simulations, which limits their utility for many applications, especially those with a significant computational cost.

Since simulation results describing the flow of the mixture depend on both space and time, the use of classical numerical methods based on stochastic simulations is often time-consuming. To alleviate this burden, surrogate models, also known as meta-models or response surfaces, are commonly used to mimic the behavior of the true model while being less time-consuming. In addition to UQ, SA is another major goal of many studies [Saltelli and Tarantola, 2002]. SA seeks to quantify the relative importance of each input parameter. Generally, SA can be carried out following one of two approaches: local SA, which focuses on the influence of input parameters on the model at a local level, or global SA, which attempts to measure the uncertainty of the output resulting from the uncertainty of the input parameters, either separately or in association with others. Global SA has retained much attention over the last decades due to its ability to consider large variations of input parameters, and Saltelli and Tarantola [2002] provides a solid state-of-the-art of the method.

In this study, we employ a variance-based method to conduct a global sensitivity analysis. Sobol' indices [Sobol, 1993, 2001] have been extensively used in this context due to their ability to efficiently handle highly nonlinear models [Saltelli et al., 2006].

We adopt the use of Generalized Polynomial Chaos expansions (PCE) for Uncertainty Quantification (UQ) and GSA [Blatman and Sudret, 2011a]. PCE has proven to be effective for a range of engineering problems such as hydraulic [Alghosoun et al., 2022], wave propagation [El Moçayd et al., 2020, El Mocayd et al., 2021], thermal problems [Le Maıtre et al., 2003], and the analysis of turbulent velocity fields [Simon et al., 2010]. Moreover, PCE has been used efficiently in the context of phosphate slurry flows, as evidenced by a data-driven approach based on experimental features of the suspension [El Moçayd and Seaid, 2021]. While sensitivity analysis has been successfully carried out in this study, it has not been fully addressed using numerical simulations.

The fundamental concept behind PCE is to project the model response onto a space spanned by orthonormal multivariate polynomials defined with respect to an appropriate probability measure [Ghanem and Spanos, 2003]. PCE enables the discovery of the relationship between input parameters and their effects on model outputs. Once a PCE representation is provided, UQ and sensitivity indices could be estimated with the PCE coefficients [Sudret, 2008]. We perform UQ on a numerical model that allows us to simulate the flow of slurry mixtures in pipelines. Given the different parameters that affect the rheological behavior of a fluid and hence the slurry motion, GSA is performed to rank these parameters based on their influence on the uncertainty of the *QoI*.

To perform UQ and GSA for the problem of slurry flows in pipelines, one should identify the various sources of uncertainty that will be considered as model inputs. The behavior of slurry flows is often described by the properties of the materials being transported. The inputs here consist of five variables, which are investigated and sampled within a physical range. Initially, we address the physical parameters defining the transport of the intended slurry, including the size distribution of solid particles, the initial solid concentration in the flow, and the inlet velocity of the flow mixture. In slurry transport, the inclination of the pipe, a geometry-related factor, is also taken into consideration as a crucial component. Lastly, we also analyze the specularity coefficient, a modeling parameter, a wall boundary parameter connected to the kinetic theory for granular flows [Zhong et al., 2015]. The range of variability of the above parameters is chosen based on the operating conditions of the intended phosphate slurry flow [Rusconi et al., 2016].

Finally, it should be noted that the general purpose of the current study is to evaluate the uncertainty of the energy efficiency in slurry flows.

5.1.2 Generalized Polynomial Chaos Expansion for Sensitivity Analysis

We consider a physical model that is represented by a deterministic mapping and is dependent on K-uncertain input parameters $\boldsymbol{y} = \mathcal{M}(\boldsymbol{x})$, where the input variables are considered independent random variables compiled into a random

vector denoted by $\boldsymbol{x} = (x_1, \ldots, x_K)^\top \in \mathbb{R}^K, K \geqslant 1$, which represents the required physical parameters (e.g. geometry, material properties, transport properties) for the simulation. The model's set of *QoIs* is represented by vector $\boldsymbol{y} = (y_1, \ldots, y_Q)^\top \in \mathbb{R}^Q, Q \geqslant 1$ (e.g. post-processed quantities such as pressure drop along the pipe, averaged chord values of solid concentration and outlet particles velocity), referred to in the following as the model response. $\boldsymbol{x}$, the input vector, is supposed to be uncertain; therefore, it is represented with a random vector $\mathbf{X}$ with a given probability density function (PDF) $f_{\mathbf{X}}(\boldsymbol{x})$. Consequently, the model response is likewise a random variable (or vector), indicated as $\mathcal{Y} = \mathcal{M}(\mathbf{X})$. From a mathematical point of view, the probability space $\left(\mathbb{R}^K, \mathcal{B}_K, \mathbb{P}_X\right)$ needs to be defined, where $\mathcal{B}^K$ is the Borel of $\mathbb{R}^K$ σ-algebra, and $\mathbb{P}_{\mathbf{X}}$ is the probability measure of $\mathbf{X}$, *i.e.*, $\mathbb{P}_{\mathbf{X}}(d\boldsymbol{x}) = f_{\mathbf{X}}(\boldsymbol{x})d\boldsymbol{x}$. For the sake of simplicity and without loss of generality, only a scalar response $\mathcal{Y}$, *i.e.*, $Q = 1$ is considered here. Note that the following derivations hold component-wise for a model response with vector values. On the other hand, it is supposed that $\mathcal{Y}$ has a finite variance, denoted by $\mathbb{V}[\mathcal{Y}] < \infty$. $\mathcal{Y}$ is assumed to be a $\mathbb{P}_X$-square integrable functional of $\mathbf{X}$ in the space $L^2 \equiv L^2\left(\mathbb{R}^K, \mathcal{B}_K, \mathbb{P}_X\right)$. Hence, it has a finite variance. Consequently, the subsequent inner product is well defined:

$$\langle g(\mathbf{X}), h(\mathbf{X})\rangle \equiv \mathbb{E}[g(\mathbf{X})h(\mathbf{X})] \quad = \int g(\mathbf{X})h(\mathbf{X})f_{\mathbf{X}}(\boldsymbol{x})d\boldsymbol{x}. \tag{5.1}$$

which induces the norm:

$$\|g(\mathbf{X})\| \equiv \sqrt{\langle g(\mathbf{X}), g(\mathbf{X})\rangle} \equiv \sqrt{\mathbb{E}[g(\mathbf{X})]} \tag{5.2}$$

L^2 equipped with the inner product $\langle \cdot, \cdot \rangle$ is well-known to be a Hilbert space.

5.1.3 Generalized Polynomial Chaos Expansion

Within the framework of uncertainty quantification, the PCE has seen extensive applications as a surrogate model, as its objective is to recreate the global behavior of a simulation through a polynomial decomposition. The latter are multivariate orthogonal polynomials and serve as the basis functions selected with respect to the joint probability distributions of the stochastic input variables following the so-called Askey scheme of polynomial [Xiu and Karniadakis, 2002]. In the present study, if our variables (shown in Table 5.1) are stored in the vector $\mathbf{X} \in \mathbb{R}^d$, and $\mathcal{Y}$ represents the model responses discussed earlier, then one may write, according to PCE:

$$\mathcal{Y} = \mathcal{M}(\mathbf{X}) = \sum_{\alpha \in \mathbb{N}^d} \boldsymbol{a}_\alpha \Psi_\alpha(\mathbf{X}), \tag{5.3}$$

where $\mathbb{N}^d$ denotes a multi-index $\boldsymbol{\alpha} = \{\boldsymbol{\alpha}_1, \ldots, \boldsymbol{\alpha}_d\}, \{\boldsymbol{a}_{\boldsymbol{\alpha}}, \boldsymbol{\alpha} \in \mathbb{N}\}$ representing the expansion coefficients that need to be estimated, $\{\Psi_{\boldsymbol{\alpha}}(\mathbf{X}), \boldsymbol{\alpha} \in \mathbb{N}\}$ are multivariate polynomials. Those are orthonormal with respect to the joint PDF $f_{\mathbf{X}}$ of

$\mathbf{X}$, *i.e*, $\mathbb{E}\left[\Psi_{\boldsymbol{\alpha}}(\mathbf{X})\Psi_{\beta}(\mathbf{X})\right] = 1$ if $\boldsymbol{\alpha} = \boldsymbol{\beta}$ and 0 otherwise. Based on the independence assumption between the input variables, the multivariate polynomials Ψ_{α} are constructed through the tensor product of their corresponding univariate polynomials $\Psi_{\alpha}(\mathbf{X}) = \prod_{i=1}^{d} \phi_{\alpha_i}^{(i)}(X_i)$, along with the joint PDF $\mathbf{X}$ that can also be casted as $f_{\mathbf{X}}(X) = \prod_{i=1}^{d} f_{\mathbf{X}_i}(X_i)$, where $\phi_{\alpha_i}^{(i)}$ is a polynomial in the i-th variable of degree α_i. The PCE in Eq. (5.3) must be truncated after p terms for computational purposes. Only the polynomials $\Psi_{\boldsymbol{\alpha}}$ with total degree up to p are maintained as:

$$\Psi_{\alpha}(\mathbf{X}) = \sum_{\alpha \in \mathcal{A}^{d,p} \subset \mathbb{N}^d} \boldsymbol{a}_{\alpha} \Psi_{\alpha}(\mathbf{X}). \tag{5.4}$$

The set $\mathcal{A}^{d,p}$ is defined here based on a total polynomial degree. This set is traditionally defined as

$$\mathcal{A}^{d,p} = \left\{\alpha \in \mathbb{N}^d : \quad |\alpha| \leqslant p\right\} \tag{5.5}$$

It is worth noting that when this method is used to define the set of multi-indices, $\mathcal{A}^{d,p}$ comprises $\begin{pmatrix} d+p \\ p \end{pmatrix}$ items that obey the binomial rule for a given value of the maximum polynomial degree p. Here the number of decomposition increases exponentially with the dimension d. This problem is known as the curse of dimensionality and makes the application of a meta-model based on the PCE rather complicated and expensive in applications where the number of input parameters is large. However, this issue could be alleviated through the use of hyperbolic truncation approach as introduced by Blatman and Sudret [2011a]. The next step is the computation of the PCE coefficients $\{\boldsymbol{a}_{\alpha}, \alpha \in \mathcal{A}\}$. The literature provides many numerical methods for the estimation of the spectral coefficient:

- Intrusive Polynomial Chaos

The intrusive PC expansion originally introduced in [Ghanem and Spanos, 2003] is based on a Galerkin-type projection formulation of the model equations. Dinescu et al. [2010] showed the first application of an intrusive PC to the 3D Navier-Stokes equations. It consists in introducing the calculation of the coefficients of the PC directly into the numerical model. For each unknown u is therefore replaced with its expansion coefficients u_i. The number of unknowns is therefore basically multiplied with a factor $P + 1$, which can be quite high for high stochastic dimensions and/or high polynomial order. This approach is very delicate to implement and poses difficulties for strongly nonlinear models [Berveiller, 2005]. It requires important changes to the CFD code, making it less attractive for industry who are relying on their own well validated codes, or for use with commercial softwares. As a result attention was focused on non-intrusive approaches requiring no change in the CFD code. When it comes to consider variable parameters for sensitivity and robustness analyses, non-intrusive meth-

ods for uncertainty quantification (UQ) are typically considered in CFD.

- Non-intrusive Polynomial Chaos

Regarding non-intrusive PC expansions, it does not require modifying the numerical model but considers it as a black box. The PC coefficients are determined after evaluating the numerical model at different points in the parameter space, which requires a design of experiments. Two approaches for computing the PC coefficients of the output quantities of interest have usually been considered: (i) the projection approach, in which they are computed by structured quadratures, i.e., Gauss quadratures, or unstructured quadratures, i.e., Monte Carlo or quasi Monte Carlo sampling; and (ii) the regression approach, minimizing some error measure or truncation tolerance of the PC expansion for some particular values of the inputs. In both cases, a series of deterministic simulations for different realizations of the uncertain parameters must be calculated. Practical application of these techniques to CFD problems is available in [Berveiller et al., 2006, Reagana et al., 2003].

The gPC application is herein used in its non-intrusive approach, i.e., the variables, and more precisely the error cost functions are directly projected over the orthogonal basis spanning the random space, without any modification of the deterministic solver of the forward model. This analysis focuses on regression techniques. The regression technique estimates the spectral coefficients $\boldsymbol{a}_\alpha$ by solving a least-square (LS) minimization problem [Berveiller et al., 2006] in ℓ_2-norm. To put this into application, first an error metric is defined ε_{PC} as the difference between the (exact) model evaluation ($\mathcal{Y}$) and the PCE surrogate estimations for a finite training set of randomly sampled input variables $\mathbf{X}$. A set of N_{ls} independent realizations of the input vector, $\mathbf{X} = \left(X^{(1)}, \ldots, X^{(N_{ls})}\right)$, is then performed, called Design of Experiment (DE). The generation of the DE is obtained in the present work using Latin Hypercube sampling approach, this help to reduce the computational cost of the classical Monte Carlo sampling, since it requires a large size sample to accurately estimate the PCE coefficients. Therefore, when the direct model is too expensive, which is the case here, using this latter approach is quasi impossible. The employed LS error used in this work reads:

$$\varepsilon_{PC} = \|\mathcal{Y} - \boldsymbol{a}^\top \Psi\|_{L_2}^2, \tag{5.6}$$

where $\mathcal{Y} = \left(\mathcal{Y}^{(1)}, \ldots, \mathcal{Y}^{(N_{ls})}\right)^\top$ is the vector of the training set's output parameters. $\boldsymbol{a} = \left(a_{\alpha_0}, \ldots, a_{\alpha_{N_{PC}-1}}\right)^\top$ is also introduced as the vector of the $N_{PC} = \text{Card}\left(\mathcal{A}^{d,p,q}\right)$ unknown coefficients (where Card (X) is the number of elements in the set X) and Ψ is the $N_{PC} \times N_{ls}-$ valued matrix assembling the values of all orthonormal polynomials at the ED nodes $\Psi_{ik} = \Psi_i\left(\zeta^{(k)}\right)$, with $i = 0, \ldots, N_{PC-1}$ and $k = 1, \ldots, N_{ls}$. Using the ordinary least-squares functional as in Eq. (5.6) to

estimate the set of coefficients $\boldsymbol{a}$ is equal to minimizing the following function:

$$\mathrm{LS}(\boldsymbol{a}) = \varepsilon_{PC}^{\top}\varepsilon_{PC} = \left(\mathcal{Y} - \boldsymbol{a}^{\top}\boldsymbol{\Psi}\right)^{\top}\left(\mathcal{Y} - \boldsymbol{a}^{\top}\boldsymbol{\Psi}\right) \tag{5.7}$$

and such that,

$$\frac{\partial \mathrm{LS}}{\partial \boldsymbol{a}} = -2\boldsymbol{\Psi}^{T}\mathcal{Y} + 2\boldsymbol{\Psi}^{T}\boldsymbol{\Psi}\boldsymbol{a} = 0. \tag{5.8}$$

Determining $(\boldsymbol{a})$ as the ordinary least-square solution of the minimization problem formulated in Eq. (5.8) is a classical problem in linear algebra. Which yields:

$$\boldsymbol{a} = \left(\boldsymbol{\Psi}^{\top}\boldsymbol{\Psi}\right)^{-1}\boldsymbol{\Psi}^{\top}\mathcal{Y}. \tag{5.9}$$

In case of high dimensional problem an attractive modification on the conventional least squares formulation could be adopted, that limits the sum of the absolute regression coefficients. In fact, the least-angle regression (LAR), offers a sparse PCE representation with fewer regressors than the traditional complete representation. Furthermore, the PCE allows better capture of the behavior of the model by excluding irrelevant variables from the set of regressors and therefore lowering the number of terms in Eq. (5.3). Here, we apply the LAR approach as suggested in [Blatman and Sudret, 2011a]. For further information on the LARS approach and its use in the context of adaptive sparse PCE (see [Blatman and Sudret, 2011a, Efron et al., 2004]). Finally, in order to evaluate the quality of the PCE, Leave-One-Out (LOO) error is often used as an excellent measure of accuracy since it enables error estimates without acquiring further forward evaluation of the numerical model [Blatman and Sudret, 2010]. The definition of the relative LOO error is as follows:

$$\varepsilon_{\mathrm{LOO}} = \frac{\sum_{i=1}^{N}\left(\frac{\mathcal{M}\left(\boldsymbol{x}^{(i)}\right)-\mathcal{M}^{PC}\left(\boldsymbol{x}^{(i)}\right)}{1-h_i}\right)^{2}}{\sum_{i=1}^{N}\left(\mathcal{M}\left(\boldsymbol{x}^{(i)}\right)-\hat{\mu}_Y\right)^{2}}, \tag{5.10}$$

where h_i is the i^{th} diagonal term of matrix $\boldsymbol{\Psi}\left(\boldsymbol{\Psi}^{T}\boldsymbol{\Psi}\right)^{-1}\boldsymbol{\Psi}^{T}$, where $\boldsymbol{\Psi} = \left\{\boldsymbol{\Psi}_{ij} = \Psi_j\left(\boldsymbol{X}^{i}\right)\right\}$ and $\hat{\mu}_Y = \frac{1}{N}\sum_{i=1}^{N}\mathcal{M}\left(\boldsymbol{x}^{(i)}\right)$ According to a research summarized by Molinaro et al. [2005], the leave-one-out method has a low estimate bias and a low mean-square error, and could be comparable with standard relative L_2 error in some cases [El Moçayd et al., 2018a].

5.1.4 Variance-Based Sobol' Sensitivity Indices

Consider a mathematical model whose random parameters are K-independent. $\mathbf{X} = \{X_1, \ldots, X_M\}$ that produces a random response $\mathcal{M}(\mathbf{X})$ at a specified space-time position. Sobol [1993] demonstrated that if $\mathcal{M}(\mathbf{X})$ is a member of the space

of square integrable functions, L^2, it may be extended as:

$$\mathcal{M}(\mathbf{X}) = \mathcal{M}_0 + \sum_{i=1}^{K} \mathcal{M}_i\left(X_i\right) + \sum_{1 \leqslant i < j \leqslant K} \mathcal{M}_{ij}\left(X_i, X_j\right) + \ldots + \mathcal{M}_{12\ldots K}(\mathbf{X}), \quad (5.11)$$

where $\mathcal{M}_0$ represents the predicted value of $\mathcal{M}(\mathbf{X})$, and $\mathcal{M}_{i_1 \ldots i_s}$ $(\{i_1, \ldots, i_s\} \subseteq \{1, \ldots, K\})$ denote a set of orthogonal functions. This is commonly referred to as the ANalysis Of VAriance (ANOVA) decomposition. In fact, the variance decomposition of $\mathcal{M}(\mathbf{X})$ may be found by squaring Eq. (5.11), followed by computing the expectation. Furthermore, due to the uniqueness of the decomposition, an orthogonality characteristics between different terms could be deducted, namely:

$$\mathbb{E}\left[\mathcal{M}_i\left(\mathbf{X}_i\right) \mathcal{M}_j\left(\mathbf{X}_j\right)\right] = 0. \quad (5.12)$$

Thus, the random response's total variance is straightforward decomposed into partial ones and is presented by:

$$V = \sum_{i=1}^{K} V_i + \sum_{j>1}^{K} V_{ij} + \cdots + V_{1,\ldots,K}, \quad (5.13)$$

where V stands for the total variance of $\mathcal{M}(\mathbf{X}), V_i$ is the partial variance attributable to the input X_i alone, and $V_{i_1,\ldots,i_s}$ is the partial variance brought on by the interactions of the inputs corresponding to the subset of the parameters known as $\{X_{i_1}, \ldots, X_{i_s}\}$, respectively. Sobol's variance-based sensitivity indices are therefore naturally calculated as

$$S_{i_1,\ldots,i_s} = \frac{V_{i_1,\ldots,i_s}}{V}. \quad (5.14)$$

The sensitivity indices quantify how much an input, alone or in combination with other inputs, contributes to the variance of the output. From Eq. (5.13), $2^K - 1$ sensitivity indices may be defined. The first-order sensitivity index (also known as the major impact of X_i) is stated as follows:

$$S_i = \frac{V_i}{V}, \quad (5.15)$$

The latter estimates the predicted amount by which the variance of $\mathcal{M}(\mathbf{X})$ is decreased when the real value of X_i is known and is correlated with the parameter's identifiability. In other words, if for example S_i tends toward a value of 1, it is possible to estimate X_i with accuracy. The total sensitivity indices thus provide the entire contribution of a parameter X_i to the response variance, inclusive of its interactions with other factors. They take into account the primary effects S_i

as well as any joint terms involving the parameter X_i, i.e.

$$S_i^T = \sum_i \frac{V_{\boldsymbol{i}}}{V}. \tag{5.16}$$

Generally, the total sensitivity index should be used to deduce the significance of the parameters [Saltelli and Tarantola, 2002]. The more significant a parameter for the model response X_i is, the greater the value of S_i^T. In contrast, if $S_i^T = 0$, X_i is considered "unimportant" (from the perspective of probabilistic modeling).

All of the sensitivity indices in this section are derived using the PCE approach with a non-intrusive sampling procedure. Therefore, once the PCE is built, the mean μ and the total variance D can be obtained using the value of the spectral coefficients such that

$$\mu = y_0, \text{ and } D = \sum_{\alpha \in \mathcal{A} \setminus 0} y_{\boldsymbol{\alpha}}^2 v. \tag{5.17}$$

As previously noted, the computation of Sobol' indices of any order is a straightforward process. The first order and total Sobol' indices can be expressed as follows:

$$S_i = \sum_{\boldsymbol{\alpha} \in \mathcal{A}_i} y_{\boldsymbol{\alpha}}^2 / D, \text{ with } \mathcal{A}_i = \{\boldsymbol{\alpha} \in \mathcal{A} : \alpha_i > 0, \alpha_{j \neq i} = 0\} \tag{5.18}$$

and

$$S_i^T = \sum_{\boldsymbol{\alpha} \in \mathcal{A}_i^T} y_{\boldsymbol{\alpha}}^2 / D, \text{ with } \mathcal{A}_i^T = \{\boldsymbol{\alpha} \in \mathcal{A} : \alpha_i > 0\} \tag{5.19}$$

5.1.5 Results and discussions

To perform UQ and GSA for the problem of slurry flows in pipelines, one should identify the various sources of uncertainty, which will be considered as model inputs. The slurry pipe flows behavior is often described by the properties of the materials transported, which leads us to define the model random input parameters as $\mathbf{X} = \{\phi_s, u_m, d_p, \theta, \mathcal{SC}\}$. These random variables are presented according to their respective pdf's and their range of variability in table 5.1. In view of

Table 5.1: Phosphate slurry flow: parameters of the model

Parameters	Type of PDF	Orthogonal polynomials	Range of variability
Inlet velocity u_m (m/s)	Uniform	Legendre	$[1.75, 5]$
Solid concentration ϕ_s[%]	Uniform	Legendre	$[20, 40]$
Particles size d_p (μm)	Uniform	Legendre	$[44, 250]$
Pipe inclination θ (°)	Gaussian Hermite $[0, 4]$		
Specularity coefficient $\mathcal{SC}$ (-)	Uniform	Legendre	$[0, 1]$

computing the PCEs of the model outputs, three design of experiments of sizes $N = \{200, 500, 1000\}$ are generated using a the latin hypercube sampling method

(LHS). Once the design of experiments are defined, the computational model is run for each sampling node in those sets to obtain the vector y of observations of the *QoI*.

GSA of the total head loss

The analysis is carried using the total head loss as the quantity of interest. The head loss is a measure of the energy reduction and could be estimated as the sum of elevation head, velocity head and frictions head of the fluid as it passes through a fluid system as

$$\Delta H_{\text{Total}} = \Delta H_{\text{Friction}} + \Delta H_{\text{Kinetic}} + \Delta H_{\text{Potential}} \tag{5.20}$$

The PCE methodology is employed to construct a metamodel using the Least Angle Regression (LARS) method. The head loss is selected as the target variable for UQ and GSA, in accordance with the methodology outlined in section 5.1.2. To evaluate the quality of the constructed metamodel, a validation set consisting of 1000 random model evaluations is employed to assess its robustness. Additionally, three independent DE sets, each comprising 200, 500, and 1000 samples, respectively, are randomly generated to build the PCE. The values of LOO error for the different PCEs constructed using the aforementioned DE sets are shown in Fig. 5.1. The error is presented as a function of the polynomial degree. As

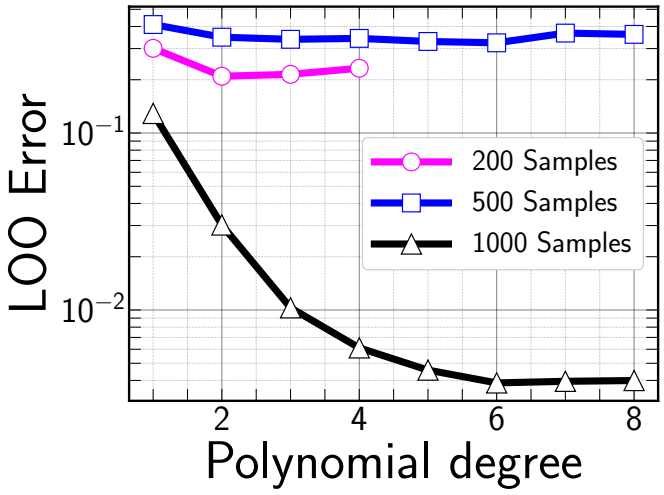

Figure 5.1: Convergence test of the PCE: Number of samples against LOO error along with the optimal PCE degree

expected, the error decreases as the degree of the polynomial increases. However, a polynomial degree of 6, computed using a DE of size 1000 samples, is sufficient to obtain a good approximation. Subsequently, the obtained metamodel is evaluated using the validation set. The results of this evaluation, depicted in Fig. 5.2, demonstrate that the metamodel behaves similarly to the CFD model. Consequently, the obtained PCE can be employed for UQ and GSA.

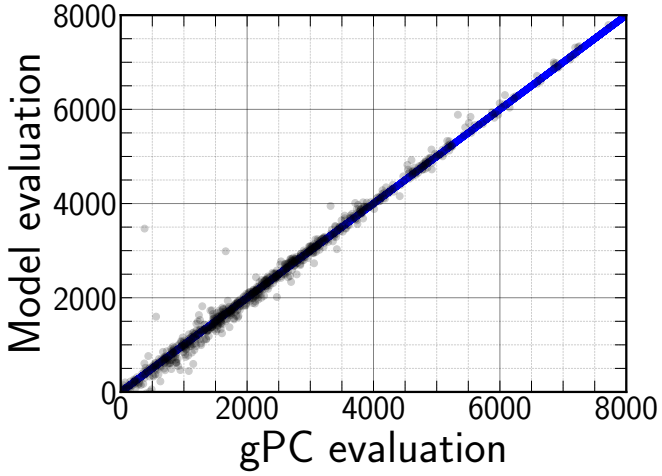

Figure 5.2: Comparison between PCE and the true model on 1000 validation runs for the model outputs using LAR method

First, the marginal effect of the uncertain parameters on the total head loss is analyzed. This effect refers to the variation of the model output with respect to a single parameter, while keeping the other parameters at their mean values. The marginal effect, also known as the univariate effect [Deman et al., 2016], provides a means to evaluate the range of variation in the model response due to changes in a specific parameter. It is defined as the sum of the mean values and first-order summands comprising only univariate polynomials, given as:

$$\mathbb{E}\left[\mathcal{M}(\boldsymbol{X}) \mid X_i = x_i\right] = \mathcal{M}_0 + \sum_{\alpha \in \mathcal{A}_i} y_\alpha \Psi_\alpha \left(\boldsymbol{x}_i\right). \tag{5.21}$$

The results of the marginal effect analysis of the parameters on ΔH_{Total} are presented in Fig. 5.3. It indicates the level of influence of each parameter, with differences in scale observed. Additionally, some non-linear behavior is evident, particularly with respect to u_m and $\mathcal{SC}$.

Fig. 5.3e demonstrates that the total enthalpy difference, ΔH_{Total}, increases with the positive slopes of θ, whereas it decreases with negative slopes. This is due to the longitudinal resultant force, which acts as an additional resisting force for the wall contact layer at positive slopes and tends to decrease its velocity compared to horizontal flow. Conversely, as the suspension travels down a pipe, the flow is accelerated due to the elevation effects, and the pressure levels increase downstream. This additional kinetic energy is used to overcome frictional effects. However, when exceeding a certain declination degree ($-15°$), as reported in [Matoušek et al., 2018], the flows display varying degrees of stratification, with a thicker sliding bed and a thinner shear layer on the top wall. The thicker sliding bed causes more friction, resulting in a greater pressure decrease.

Regarding the solids concentration and particle sizes, Figs. 5.3b and 5.3c indicate that ΔH_{Total} increases as both of these variables rise. This can be attributed

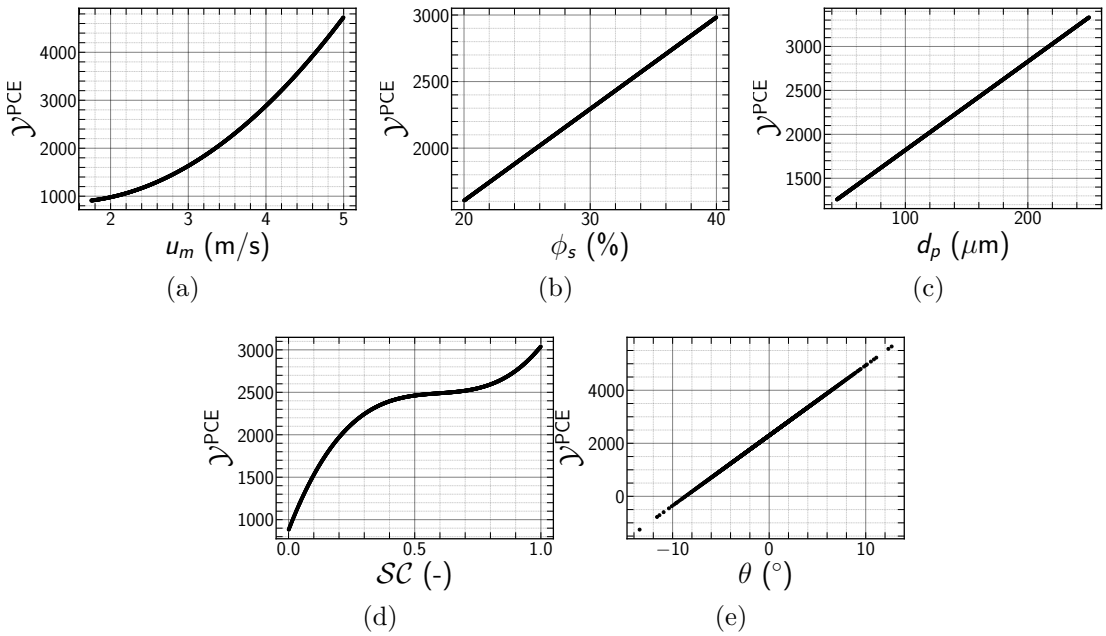

Figure 5.3: Univariate effects of the input parameters on ΔH_{Total}

to the formation of a moving bed of particles, which has a greater wall normal shear stress in the case of coarser particles. Finally, with respect to the specularity coefficient $\mathcal{SC}$, Fig. 5.3d shows that the pressure drop increases with increasing $\mathcal{SC}$. It is important to note that $\mathcal{SC}$ quantifies the momentum and energy transfer caused by colliding particles with the pipe wall. Therefore, a higher specularity coefficient indicates that a significant loss of the particles' kinetic energy occurs after colliding with the pipe wall, leading to an increase in the pressure drop. It can be concluded that a good calibration of this parameter in the numerical validation step is crucial to ensure reliable predictions of the pressure drop along the pipe. Subsequently, a GSA is conducted to identify the most influential parameters. The sensitivity of head loss to the variability of the random parameters, namely $\{\phi_s, u_m, d_p, \theta, \mathcal{SC}\}$, is evaluated using Sobol' indices. Fig. 5.4 displays bar plots of the computed first-order and total Sobol' indices, which provide valuable insight into the contribution of individual parameters and their interactions to the overall variance. The total Sobol' indices were utilized to rank the parameters based on their significance, enabling the identification of the most influential parameters. The analysis of the sensitivity indices indicated that the variability of the total head loss $\Delta p/L$ is predominantly attributed to the principal effects of u_m, followed by θ, and then d_p. The most influential parameter among the considered parameters is u_m, exhibiting a total Sobol' index of $S^T = 0.45$. Additionally, the results highlighted a non-negligible, albeit relatively small influence of ϕ_s and $\mathcal{SC}$. Moreover, the comparison between the first-order and total-order Sobol' indices revealed noticeable discrepancies, implying interactions between the random parameters. Overall, these findings provide valuable

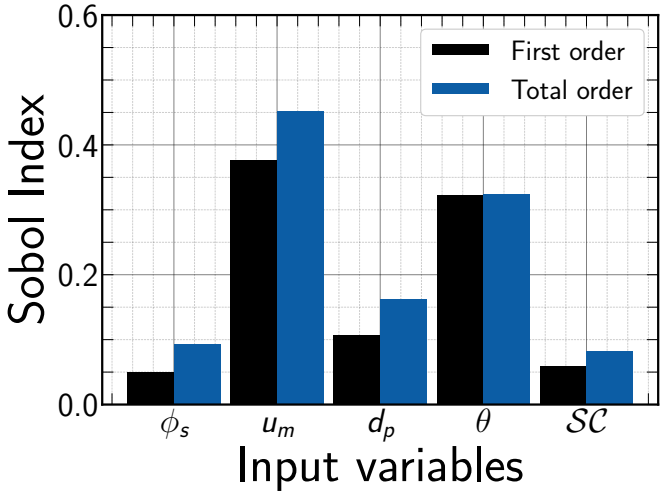

Figure 5.4: First and total Sobol' indices for total head loss

insight into the contribution of individual parameters and their interactions to the overall variance of the total head loss.

GSA of the pressure drop by frictions

Here, we only focus on the component of pressure drop by friction per unit length of the pipe $\Delta p_{\text{Friction}}/L$. The constructed PCE for $\Delta p_{\text{Friction}}/L$ is assessed in Figs. 5.5 and 5.6. The $1,000$ samples are obviously the suitable DE to construct

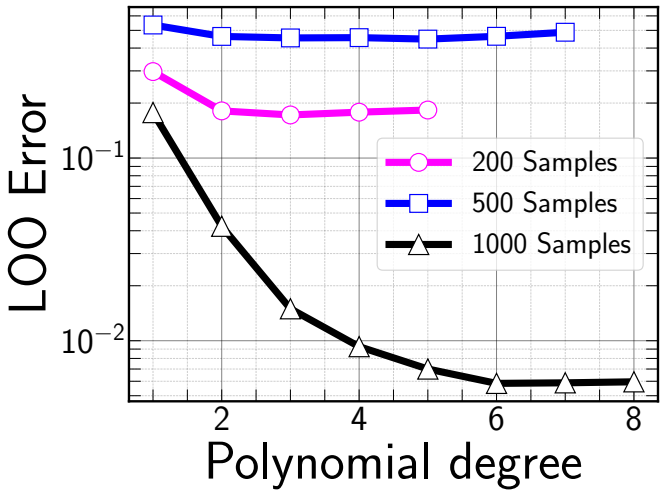

Figure 5.5: (Convergence test of the PCE: Number of samples against LOO error along with the optimal PCE degree

an accurate PCE. Here also, a polynomial of degree $p = 6$ is sufficient to carry on UQ and GSA using the surrogate model. Fig. 5.7, displays the calculated first and total Sobol' indices as bar graphs. Focusing on Fig. 5.4, we can observe that when dealing with pressure losses due to friction the pipe inclination has no influence

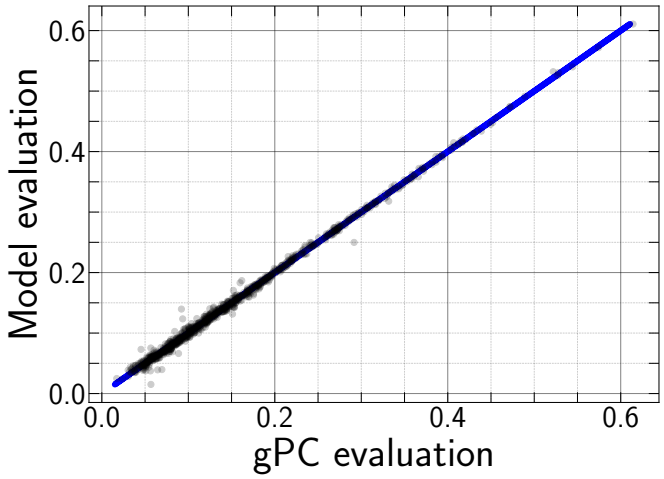

Figure 5.6: (Comparison between PCE and the true model on 1,000 validation runs for the model outputs using LAR method

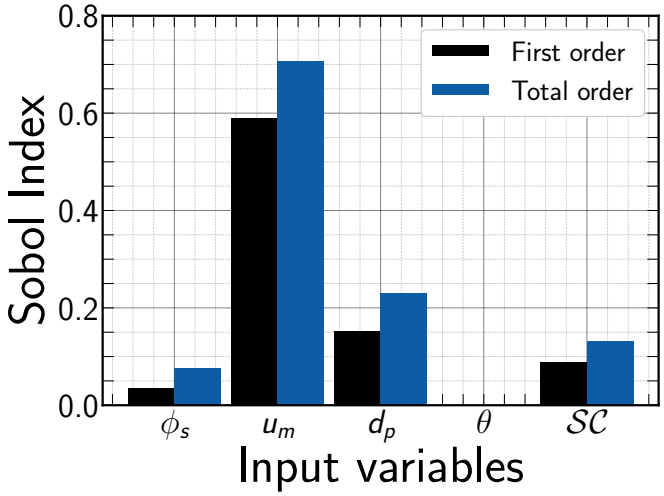

Figure 5.7: First and total Sobol' indices for the frictional contribution in pressure drop per unit length of the pipe

at all. On the other hand, it appears that the impact of other parameters is still the same. Here the variability of $\Delta p_{\text{Friction}}/L$ is mainly controlled by the mixture velocity u_m with $S^T = 0.60$, followed by the particles diameter. The friction loss is a measure of the amount of energy your piping system loses, when the slurry is meeting resistance, which is directly related to the viscosity of the slurry. These findings prove that the latter is only affected by the physical properties of the flow mixture.

GSA of 1-Dimensional solid concentration and velocity profiles

Numerical results are obtained for the chord-averaged solid concentration and velocity profiles across the diameter of a pipe, where the slurry flow has achieved

full development. The data was collected at the outlet of the pipe, precisely defined at a position that is 90% of the pipe length. PCE meta-models are constructed by applying the same procedure to the *QoI*s under consideration. In the case of multivariate output, such as for solid concentration and velocity profiles, a PCE is constructed for each component along the chord-averaged pipe diameter. The maximum degree p of the PCE has been varied from 1 to 10, and the optimal sparse PCE has been selected for each point along the chord-averaged profile using the corrected relative LOO error.

GSA of the solid concentration distribution

In this section, the solid concentration distribution is considered as the QoI in UQ and GSA. Since this parameter is a random vector, the analysis is performed along the pipe to capture the spatial variations. To construct the PCEs, three different DEs are tested. The performance of each DE, along with the number of samples required, is evaluated using the LOO error as shown in Fig. 5.8. The previous figure provides a visual representation of the accuracy of the PCEs for each DE. Furthermore, Fig. 5.9 shows the polynomial degree that provides the

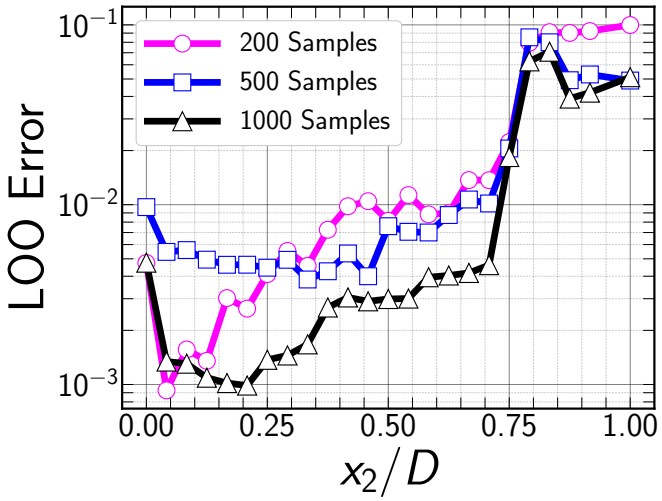

Figure 5.8: Convergence test of the PCE: Number of samples against LOO error

best accuracy for the PCEs. The optimal degree can be selected based on this figure to obtain the most accurate results. The results indicate that the lowest LOO error is obtained with a sample size of 1,000, as anticipated. However, it is observed that the accuracy of the PCE diminishes as it approaches the upper limit. The PCEs achieve optimal performance at $p = 10$ for most of the pipe sections. Validation of the PCE values is performed against the corresponding values obtained from the physical model, using a validation set consisting of 1,000 Monte Carlo (MC) simulations. To evaluate the accuracy of the PCE, check points are selected along the length of the pipe diameter, as illustrated in Fig. 5.10. In zones where the dimensionless distance from the wall, x_2/D, is

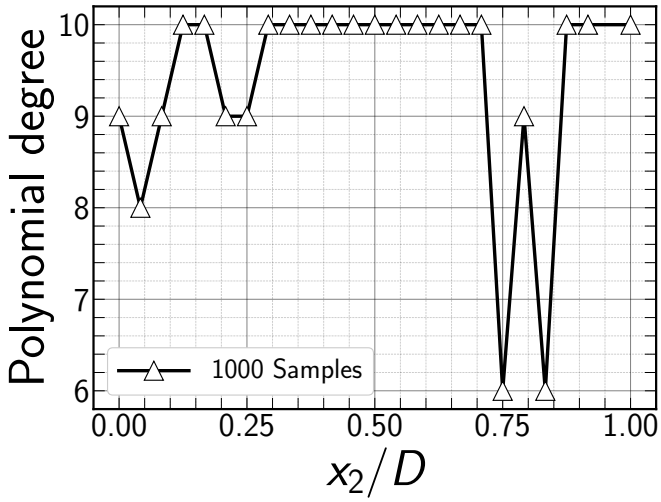

Figure 5.9: The optimal PCE degree along the chord average of the pipe diameter

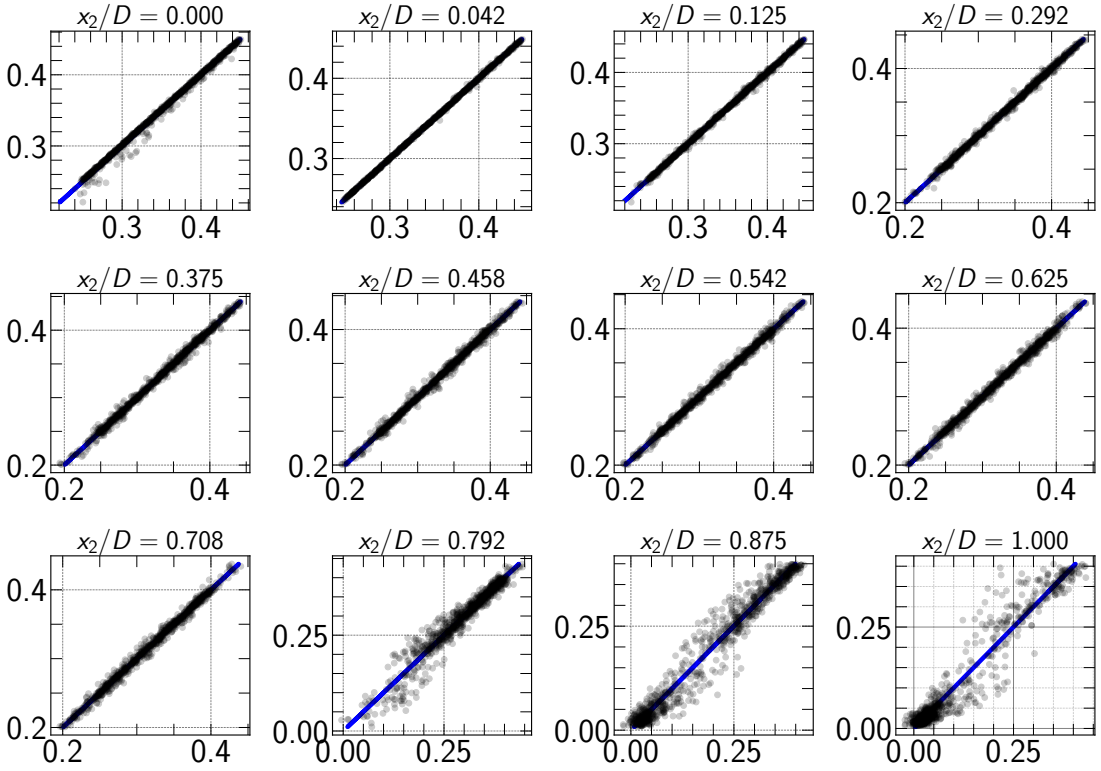

Figure 5.10: Comparison between PCE (black dots) and the true model (blue lines) on 1,000 validation runs for each checkpoint of the chord average

less than or equal to 0.7, the validation results for predicting solid concentration exhibit excellent agreement with the true model. This agreement is supported by a small LOO error of less than 0.001. However, in the upper zone of the pipe where $x_2/D \geqslant 0.7$, discrepancies between the predicted concentration estimate (PCE) and the true model are observed. This discrepancy may be attributed

to the dilution of the flow's top layer, resulting in chaotic movement of particles and significant non-linearities in the solid phase concentration. To further investigate these discrepancies, the variance may be calculated as illustrated in Fig. 5.11. Our observations indicate that the zone with the thickest layer exhibits

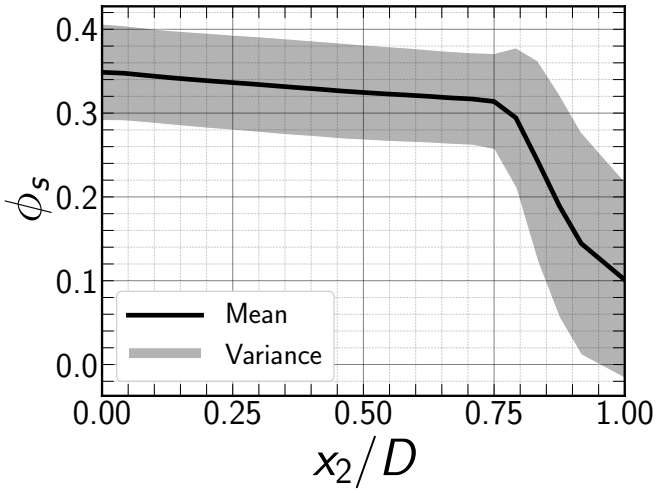

Figure 5.11: Mean and variance of the solid concentration distribution along the pipe diameter

the smallest variation, owing to the tightly packed particles and the consequent restriction of arbitrary particle motion and collisions. This high concentration region in the lower layers not only results in a reduced variation, but also facilitates the development of accurate PCEs. In contrast, the variation increases towards the thin layer near the top wall. Concentration fluctuations in fact alter the distribution of variance while maintaining a constant level of variability. To evaluate the sensitivity of the solid concentration profile across the pipe diameter to the variability of random parameters, spatial Sobol' indices can be utilized. The 1-dimensional spatial distribution of the total Sobol' index due to uncertainty in $\{\phi_s, u_m, d_p, \theta, \mathcal{SC}\}$ is portrayed in Fig. 5.12. The results indicate that the impact of solid concentration decreases towards the top wall and increases inversely towards the bottom wall, suggesting a stronger particle presence towards the bottom wall. This behavior of particles is induced by their size, as larger particles generally cause sedimentation, resulting in a significant change in the in situ solid concentration near the top wall. This interpretation is consistent with the zone of maximum solid concentration variance. The first and total Sobol' indices are estimated by averaging their value along the pipe, and the results are presented in bar plots in Fig. 5.13. The analysis of these indices shows that the variability of the solid concentration is mainly due to the principal effects of ϕ_s and d_p. Overall, these findings suggest that particle size and initial solid concentration are important factors to consider when studying the distribution of solids in a pipe. The differences between the first-order and total indices are negligible, indicating insignificant interactions between the parameters.

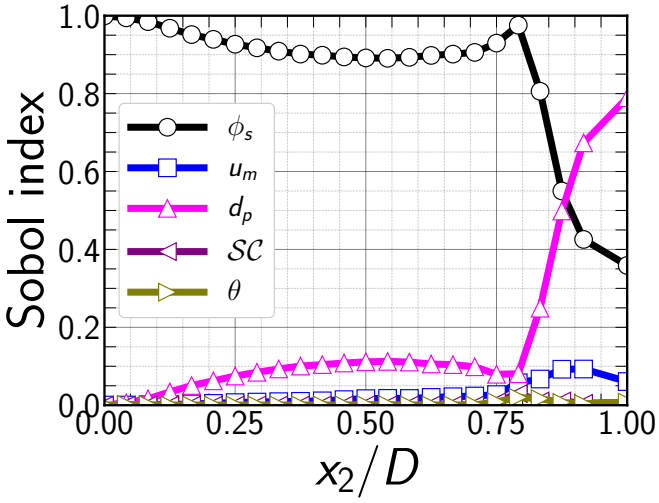

Figure 5.12: 1-dimensional spatial distribution of the total Sobol' indices for solid concentration

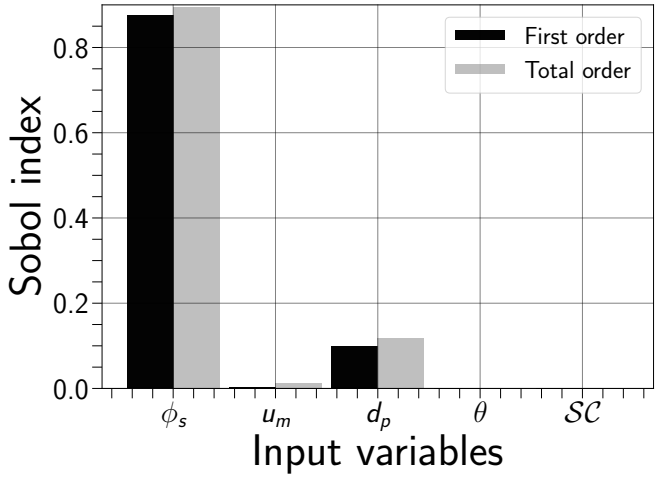

Figure 5.13: Aggregated first and total Sobol' indices for solid concentration

GSA of the solid velocity profile

The same procedure was repeated to study the sensitivity of the particle's velocity profile. As before, we begin first by constructing the PCEs for predicting the particle's velocity in each point of the pipe diameter chord average. LOO error, as shown in Fig. 5.14, is used to evaluate each PCE's performance in relation to the number of samples. The optimum degree of polynomials that provides the highest accuracy is shown in Fig. 5.15. The 1,000 set samples clearly produce the lowest LOO error. The PCE's accuracy here increases as we go closer to the top wall, in contrast to the solid concentration instance. In the majority of pipe section zones, best PCEs are achieved for degrees p between 8 and 7, increasing to $p = 9$ near the bottom wall. The PCE's accuracy is examined in Fig. 5.16. Except for $x_2/D = 0$, an excellent match is observed for all the points of the

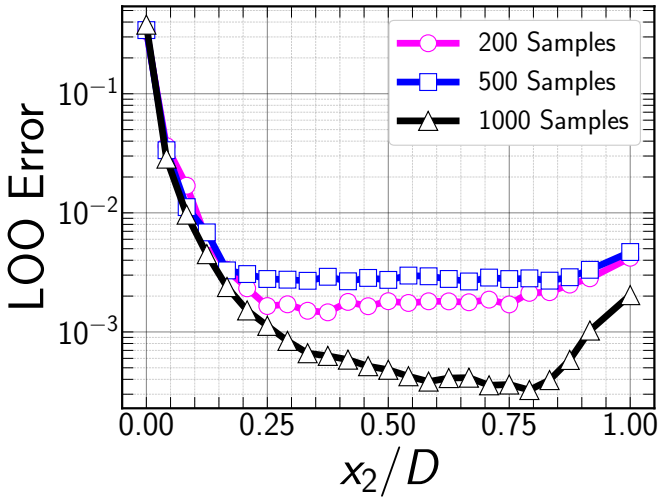

Figure 5.14: Convergence test of the PCE: Number of samples against LOO error

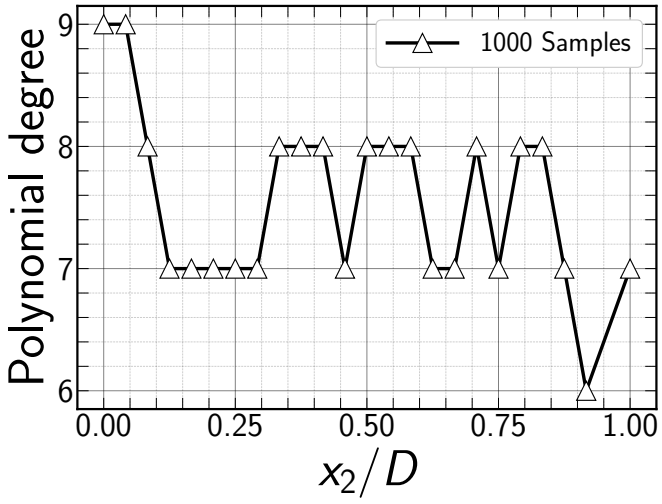

Figure 5.15: The optimal PCE degree along the chord average of the pipe diameter

section's chord average. In fact, the friction and collisions between particles and the bottom wall have a significant impact on the particle velocity in this area. A mean asymmetrical velocity profile along with a small variance of the solid velocity is indeed noticed at that same spot (cf. Fig. 5.17).

The 1-dimensional spatial distribution of the total Sobol' index of solids velocity profiles is represented in Fig. 5.18. When particles are located near the bottom wall, their velocity variability is influenced by all parameters except for the inclination angle θ. As previously discussed, this region exhibits a high solids concentration that is further amplified by an increase in particle diameter, thereby enhancing the impact of friction and collisions with the pipe wall. Consequently, these effects lead to a reduction in the particle velocity. The observed phenomena in this region demonstrate that the flow characteristics promote a stratified flow

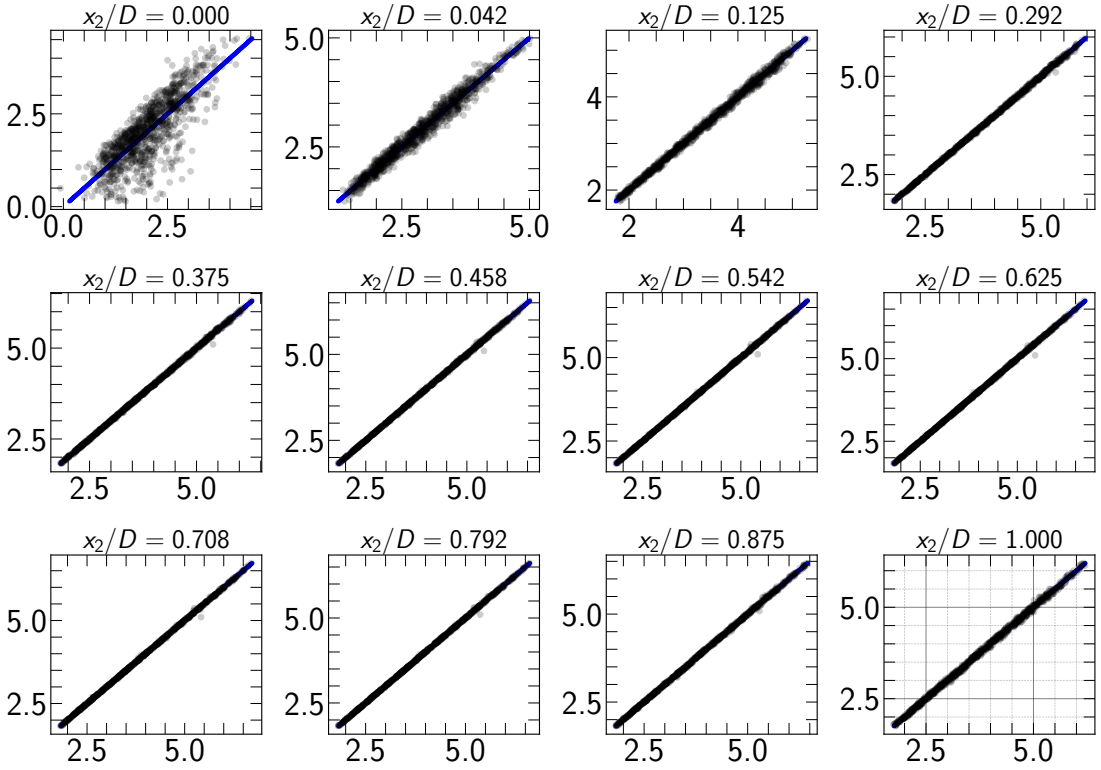

Figure 5.16: Comparison between PCE (black dots) and the true model (blue lines) on 1,000 validation runs for each checkpoint of the chord average

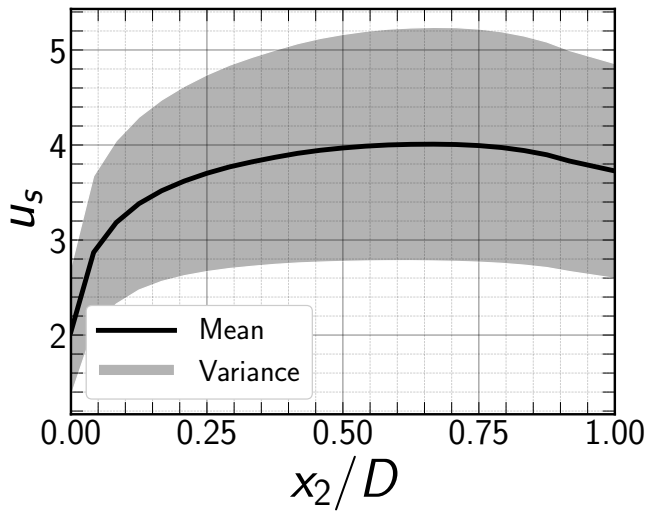

Figure 5.17: Mean and variance of the solid velocity profile along the pipe diameter

regime, commonly referred to as a two-layer flow. Based on bar plots of the first and total Sobol' indices in Fig. 5.19, the in-situ particle velocity in slurry flows is significantly influenced by the inlet mixture velocity u_m and particle size d_p. No significant interaction is observed between these parameters.

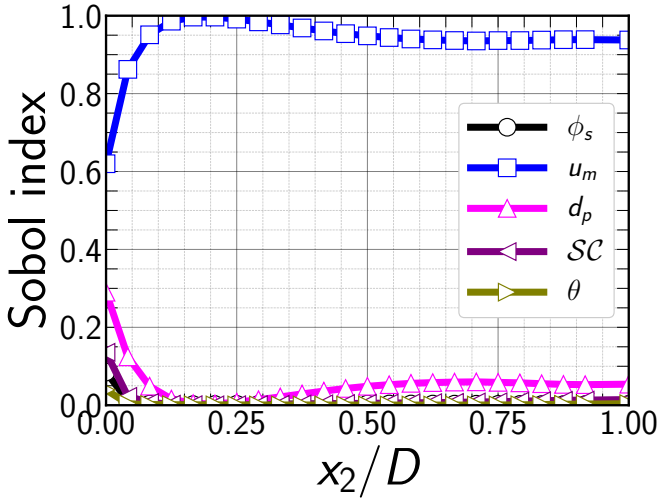

Figure 5.18: 1-dimensional spatial distribution of the total Sobol' indices for solid velocity profile

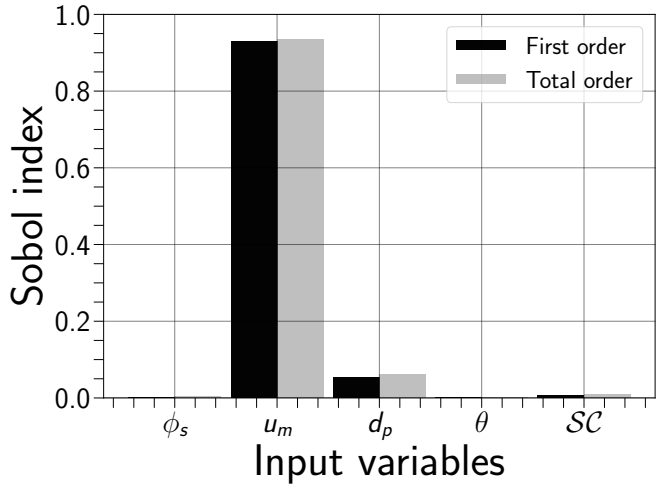

Figure 5.19: Aggregated first and total Sobol' indices for solid velocity

5.1.6 Conclusion

The results obtained from the study provide insights into the impact of system uncertainties on the energy consumption of slurry flow in pipelines, and highlight the importance of accounting for these uncertainties in order to optimize energy efficiency.

The Sobol' indices calculated for pressure drop demonstrate that the variability of pressure drop is heavily influenced by the effects of the mixture velocity, u_m, and particle diameter, d_p. Therefore, reducing the mixture velocity can help to alleviate wall friction caused by solids. However, to maintain solids in suspension, they must be transported by the liquid at a minimum velocity. The pressure losses are also affected by the particle size of the solids; larger particles require

higher velocities for transportation. When the particle density differs from that of the fluid, slurries with very large particles become highly stratified, causing an increase in pipeline friction due to a combination of fluid and Coulomb friction between the particles and the pipe wall. Thus, using velocities near the deposition condition and employing medium-fine particles is optimal for efficient pipeline slurry transport. Based on the marginal effect of mixture velocity u_m, a minimum conveying velocity of around $2m/s$ was determined. The solid concentration, ϕ_s, appears to have a minor influence on the flow pressure drop within the proposed variation range. The bivariate effect of the latter along with the mixture velocity on the pressure drop (c.f Fig. 5.20), confirm that when operating around u_{dl} low levels of pressure drop are ensured, even at the highest solid concentration 40%.

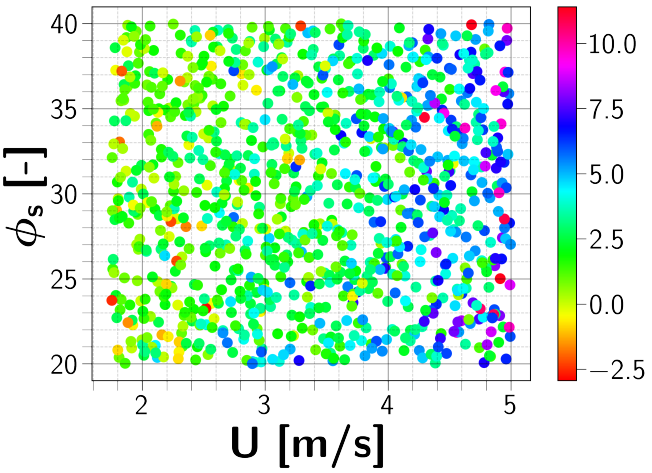

Figure 5.20: Bivariate effect of ϕ_s and u_m on the pressure drop

To further investigate, we examined the 1-dimensional solid distribution across the pipe section. The Sobol' indices of the solid concentration distribution allowed us to identify the spatial zone of influence of each parameter. Results indicate that the variability of the solid distribution over the pipe diameter is mainly controlled by the initial solid concentration, ϕ_s, and particle size, d_p. Based on the mean and variance of the solids profile, we conclude that the studied slurry falls within the "settling" category of slurries, where particle-wall contact is the prevailing mechanism. High solid concentrations increase friction, but depend upon the ratio of the solids concentration to the maximum settled concentration. The high solid concentration zone, promoted by an increase in particle diameter, favors the effects of friction and collisions with the pipe wall, encouraging a stratified flow, also known as a two-layer flow regime. To achieve efficient slurry transport, controlling the inlet velocity, u_m, and particle sizes, d_p, is crucial. The inlet velocity of the solid-liquid mixture should be decreased as low as possible while ensuring not to go below the velocity deposition limit to avoid the total sedimentation of particles. Particle sizes should also be within the optimal range of medium to

fine particles. Furthermore, this research serves as a prototype to demonstrate the value of GSA and UQ in understanding the behavior of complicated slurry flows. Such research is essential for the safe design and risk assessment of slurry transport systems.

5.2 Uncertainty Quantification and GSA for 2D slurry transport

In order to further investigate the behavior of slurry flow, we analyze the two-dimensional distributions of our quantities of interest (QoI). As discussed in the previous chapter, the literature presents various research that highlight the effectiveness of PCE in the context of UQ and sensitivity analysis, see for instance [Wang et al., 2019]. Various efforts have been made to tackle the challenges posed by complex numerical models by developing meta-models to reduce the computational cost in uncertainty quantification (UQ). This is primarily driven by the exponential increase in construction time required for polynomial chaos expansion (PCE) with the increase in the number of uncertain parameters. One of the solutions to tackle the problem of stochastic dimensions was to introduce the adaptive sparse PCE. The objective is to estimate the PCE using a regression approach using least angle regression, as specified in [Efron et al., 2004]. Another way to counter this curse of dimensionality was to combine Kriging with PCE to offer a novel meta-model [Yamazaki et al., 2018]. This method enables UQ's global and local behaviors to be considered. However, while the previously discussed methods enabled to alleviate the dimension in the model input parameters, they neglected the physical dimension of the output variables. Indeed, when applying an uncertainty quantification (UQ) algorithm to a numerical model and obtaining a physical field as the output solution, which is discretized on a mesh, the process requires polynomial chaos expansion (PCE) calculations at each node of the mesh, as demonstrated in [El Moçayd et al., 2018b]. In such cases, dealing with complex slurry flow characteristics necessitates the use of fine meshes, leading to significant computational costs. Furthermore, it is essential to emphasize that the physical outputs are stochastic processes with spatial and temporal correlations, not just stochastic variables. Consequently, the computation of outputs is required for each node in the computational mesh and at every time step within the time interval. This highlights the need to develop less computationally intensive methods for uncertainty quantification when the output is a stochastic process. Various approaches, such as the Principal Component Analysis (PCA) [Blatman and Sudret, 2011b], the Proper Generalized Decomposition (PGD) [Chevreuil and Nouy, 2012], and the Proper Orthogonal Decomposition (POD) [Raisee et al., 2015], might be used to address this problem. It should be highlighted that the main concept underlying these strategies is to represent uncertainty characteristics as responses of random vectors with only a few

non-physical factors. Using resampling of the new surrogate model, the statistical interests are derived. As a result of the complicated physical characteristics in the two-phase Navier-Stokes equations, which display steep gradients and localized structures in the slurry flow response, the POD is used in the present work. This chapter develops and applies a non-intrusive reduced-order approach to the two-dimensional transport of slurries. In fact, quantifying the impact of uncertainties on system performance is crucial to enhance the contribution and accuracy of computational slurry flows in the design process of industrial equipment.

Our main focus in the current section is on uncertainty associated with the initial and boundary conditions as well as solid properties to analyze how it affects the energy efficiency of the slurry pipe flows. Usually the slurry transport energy consumption is affected by random environmental factors, which will negatively affect the certainty of the measured results. Quantifying the effect of such uncertainties is important to validate the deterministic problem solution. The main focus is on the UQ in the pressure drop and delivered solid concentration of the intended slurry resulting from uncertain modeling and physical parameters. Along with the UQ study a global sensitivity analysis (GSA) is conducted [Saltelli and Tarantola, 2002]. Also in the present chapter, a variance-based method is used to conduct a global sensitivity analysis via computing sobol' indices. In summary, the main objective of this study is to conduct uncertainty quantification (UQ) in the simulation of slurry transport, considering uncertain slurry properties. To achieve this, we employ the proper orthogonal decomposition (POD) technique to reduce the dimensionality of the output responses. In order to assess the performance of our proposed methodology, we compare it with a class of massive Monte Carlo (MC) simulations in terms of mean and variance fields. The structure of this chapter is organized as follows. Section 5.2.1 presents the model reduction methodology, along with the Polynomial Chaos Expansion (PCE) and POD techniques. In Section 5.2.3, we present the results obtained from the UQ and sensitivity analysis for our quantities of interest ($QOIs$). Finally, Section 5.3 contains the concluding remarks.

5.2.1 Stochastic proper orthogonal decomposition

The POD method enables a high-dimensional system to be addressed by a low-dimensional one. This approach involves establishing a set of orthogonal eigenvalues that are representative of the simulated physics. Solving the integral of Fredholm yields the eigenvectors, while the kernel of this integral is derived from a series of simulations performed using an experimental design. Specifically, the eigenfunctions associated with the problem are optimal within the context of the dynamic representation (explained below), allowing them to be used to build a simplified representation of physics. In uncertainty quantification, the POD serves to decrease the size of a random vector produced by the model. As a result, the uncertainty is applied for each direction given by the eigenvectors λ_i. The

concept is based on the projection of the model's solution $\mathcal{M}\left(X^{(i)}\right)$ onto a finite and orthonormal basis $\{\phi_i, i \in \mathcal{I}_{POD}\}$, where $\mathcal{I}_{POD}$ is a discrete finite collection of indices. Thus, the procedure $\mathcal{M}\left(X^{(i)}\right)$ is decomposed as follows:

$$\mathcal{M}(X) = \sum_{i \in \mathcal{I}_{\mathrm{POD}}} \lambda_i(X)\phi_i, \tag{5.22}$$

where ϕ_i is estimated by decomposing the spatial covariance matrix constructed as:

$$\mathbf{C} = \frac{1}{\mathtt{N}}\mathcal{M}\mathcal{M}^{\intercal}. \tag{5.23}$$

In addition, we construct a POD-truncated error ε so that only the k most valuable eigenvectors are maintained as the solution following the estimate:

$$\frac{\sum_{i=0}^{k} \lambda_i}{\sum_{i=0}^{\mathtt{N}} \lambda_i} > 1 - \varepsilon, \tag{5.24}$$

where $\widehat{\lambda}_i$ is the mean value of $\lambda_i(X^{(i)})$. To summarize, the stochastic POD technique may be implemented as follows:

1. Define the covariance matrix $\mathbf{C}$ as in Eq. (5.23).

2. Using a Singular Value Decomposition (SVD) approach, expand the matrix $\mathbf{C}$ in order to find λ_i and ϕ_i.

3. Using the condition in Eq. (5.24), retain just the first k eigenvalues and eigenvectors in the expansion. Note here that the choice of convergence criteria ε is problem-dependent.

4. Reconstruct the stochastic solutions $\mathcal{M}\left(X^{(i)}\right)$ using Eq. (5.22).

5.2.2 POD-PCE meta-model

The eigenvalues are handled as random variables after rebuilding the stochastic POD. This suggests that we may preserve the spatial dependence suggested by the eigenvectors ϕ_i while generating a PCE for each eigenvalue in the manner described in the section on polynomial chaos expansions before.

$$\lambda_i(X) = \sum_{j=0}^{\mathtt{M}} \gamma_j \psi_j \left(X^{(i)}\right). \tag{5.25}$$

The equation (5.3) becomes,

$$\mathcal{M}(X) = \sum_{i \in \mathcal{I}_{POD}} \left(\sum_{j=0}^{\mathtt{M}} \gamma_j \psi_\alpha (X) \right) \phi_i. \tag{5.26}$$

A summary of both algorithms retained in the present study for quantification of uncertainties in stochastic slurry flows is depicted in Fig. 5.21. It should be noted

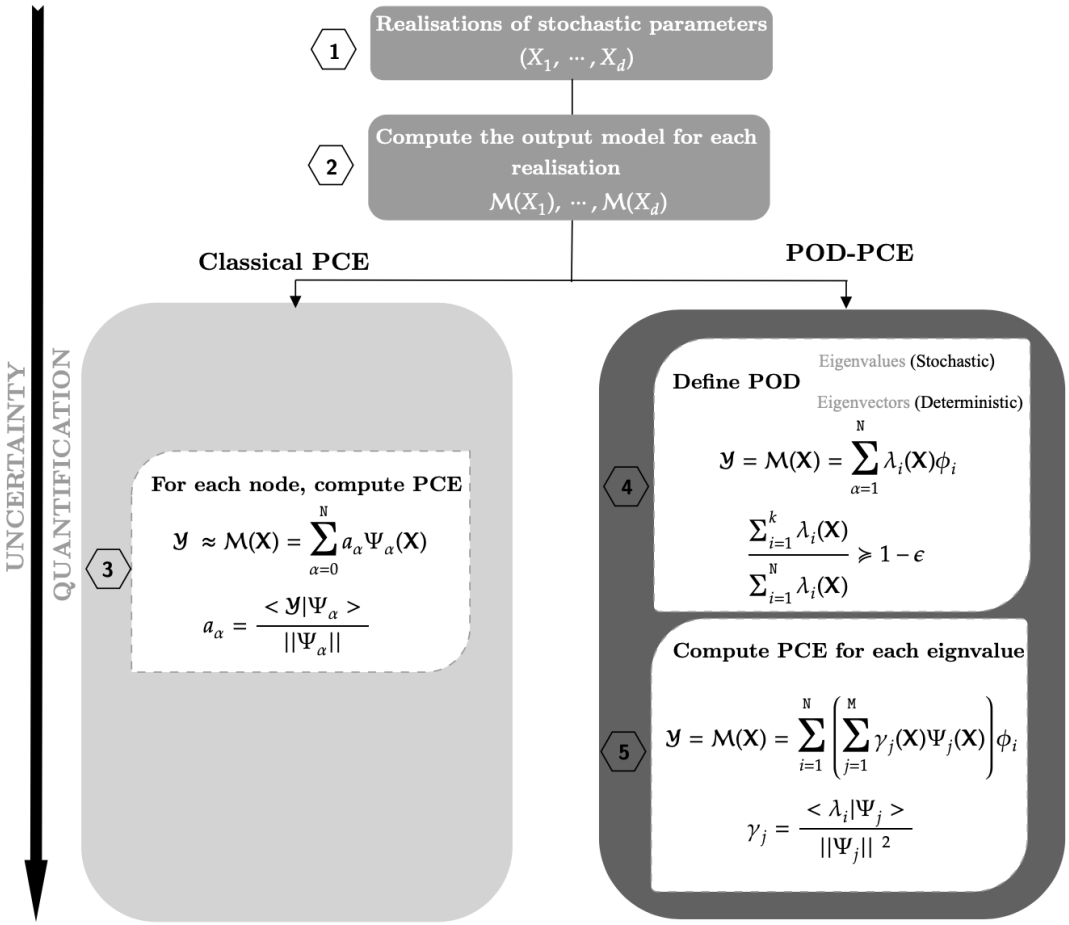

Figure 5.21: Diagram illustrating the distinction between the traditional PCE-based surrogate model and the POD-based surrogate model.

that the traditional method of dealing with an uncertainty quantification issue utilizing the PCE is conducted when a decomposition is completed for each node in the computational mesh. This procedure is shown in Fig. 5.21 flowchart by steps 1 through 3. However, as previously stated, one way to ease the spatial distribution is to do a first reduction using the POD. The stochasticity is assumed to be incorporated in the related eigenvalues, this latter will aid in distinguishing the spatial dependence from the stochastic dependency. Once the POD is performed, just a few eigenmodes are preserved, allowing for less PCE to be generated than its traditional equivalent. This procedure is shown in Fig. 5.21 flowchart as stages 1, 2, 4, and 5. The accuracy of the approaches under consideration is evaluated by comparing their findings to large MC simulations (with 1000 samples) for the quantities of interest in the mean and variance fields.

5.2.3 Numerical results

This section assesses the computational efficiency of the proposed POD approach for analyzing slurry flows. For each test case, we compare the results of the mean and variance of the potential solution using two methods: MC and POD with POD-PCE. The two-dimensional plan considered in the present study is the mid-plane of the pipe that is a squared domain $\Omega \equiv L_{x_1} \times L_{x_2} = [0, 140D] \times [-0.5D, 0.5D]$. Consequently, we extract the two-dimensional two-phase flow solution by employing the deterministic solution obtained from the three-dimensional two-phase Navier-Stokes equations. In this context, our objective is to evaluate the uncertainty associated with the QoIs, which include the solid concentration, velocity, and pressure distribution over the mid-plane pipe.

2-D solid concentration

To begin, we conducted 1000 three-dimensional CFD simulations following a design of experiment Subsequently, we obtained the solution on a structured mesh consisting of a total of 18894 nodes by extracting a mid-plane section. Next, surrogate models were constructed using POD-PCE methodology. It is important to highlight that, unlike the conventional PCE method applied to the complete model, the POD-PCE method solves a reduced model. The accuracy of the POD-PCE method for each eigenvalue is evaluated and presented in Table 5.2.

Table 5.2: Optimal polynomial degrees with LOO errors for the POD modes in the slurry particles concentration ϕ_s

Number of modes	LOO error	Polynomial degree
Mode #1	1.2758×10^{-5}	6
Mode #2	5.7266×10^{-4}	8
Mode #3	3.1746×10^{-3}	7
Mode #4	1.0955×10^{-2}	10
Mode #5	3.3131×10^{-2}	10
Mode #6	1.3435×10^{-1}	10
Mode #7	2.9421×10^{-1}	10
Mode #8	1.0350×10^{-1}	10
Mode #9	4.7471×10^{-1}	10
Mode #10	7.8437×10^{-2}	9
Mode #11	6.7515×10^{-1}	10
Mode #12	1.1624×10^{-1}	10

In this particular scenario, employing a truncation criterion of $\varepsilon = 10^{-4}$, the model selectively retains only the initial 12 eigenvalues, and the PCE process is carried out individually for each mode. As a result, the surrogate model significantly reduces computational requirements, necessitating only 12 decompositions instead of the original 18894 associated with the total number of nodes in the

two-dimensional numerical model. Table 5.2 showcases the optimal polynomial degrees employed to approximate each spectral mode using the POD technique, alongside an evaluation of the Leave-One-Out (LOO) error generated by the PCE method when estimating the numerical solution. Upon analyzing the outcomes, it is evident that the problem exhibits nonlinearity, as high polynomial degrees are required to effectively capture the uncertainty. Furthermore, the findings indicate satisfactory magnitudes for the LOO errors. Moving forward, in Fig. 5.22, we compare the mean solid concentration solutions obtained from the stochastic simulation with the deterministic exact solution, while also presenting the discrepancy between the two solutions for easy visual comparison. The results depicted

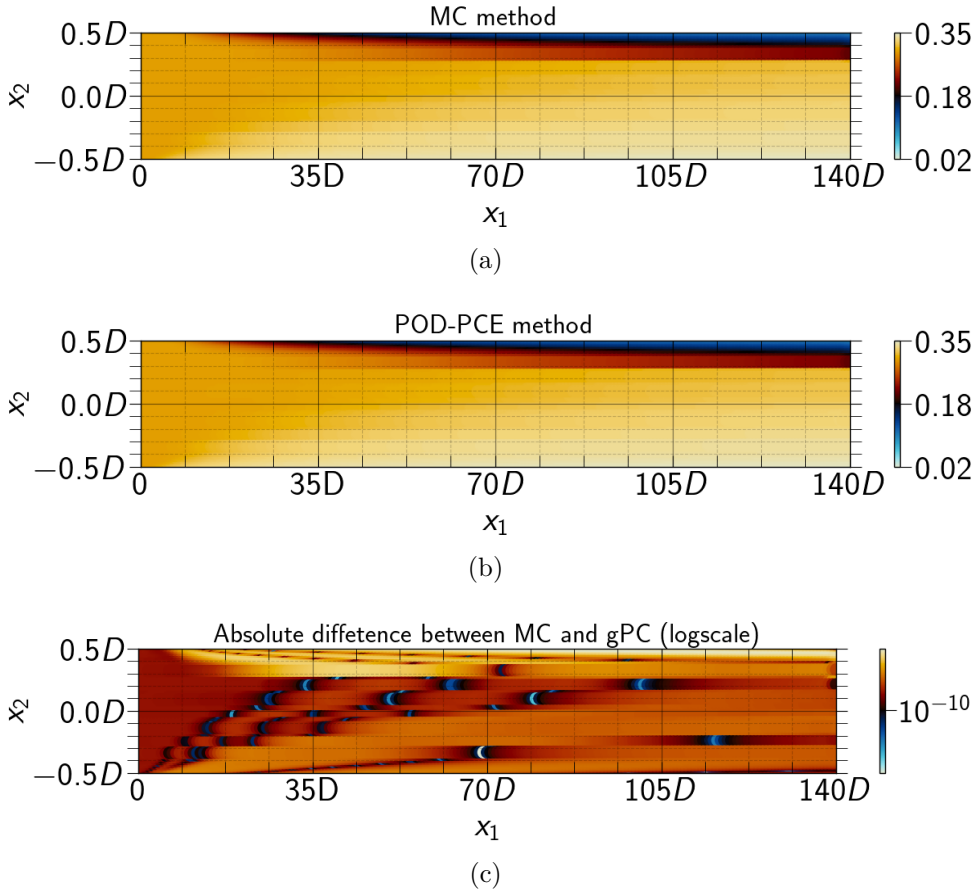

Figure 5.22: Mean solid concentration ϕ_s obtained for the stochastic simulation, (a) the deterministic exact solution (b) and the difference between the two solutions (c) obtained for a slurry flow problem.

in Fig. 5.22 illustrate that, considering the level of uncertainty examined in the problem, the mean solutions computed by both methods exhibit similar trends and patterns. The stochastic approach successfully addresses the distribution of solid concentration, producing numerical outcomes that are devoid of any non-physical oscillations. In general, these findings imply that the model reduction has minimal impact on the accuracy of UQ. Furthermore, Fig. 5.23 showcases

the obtained results for the variance. The results for mean and variance make it

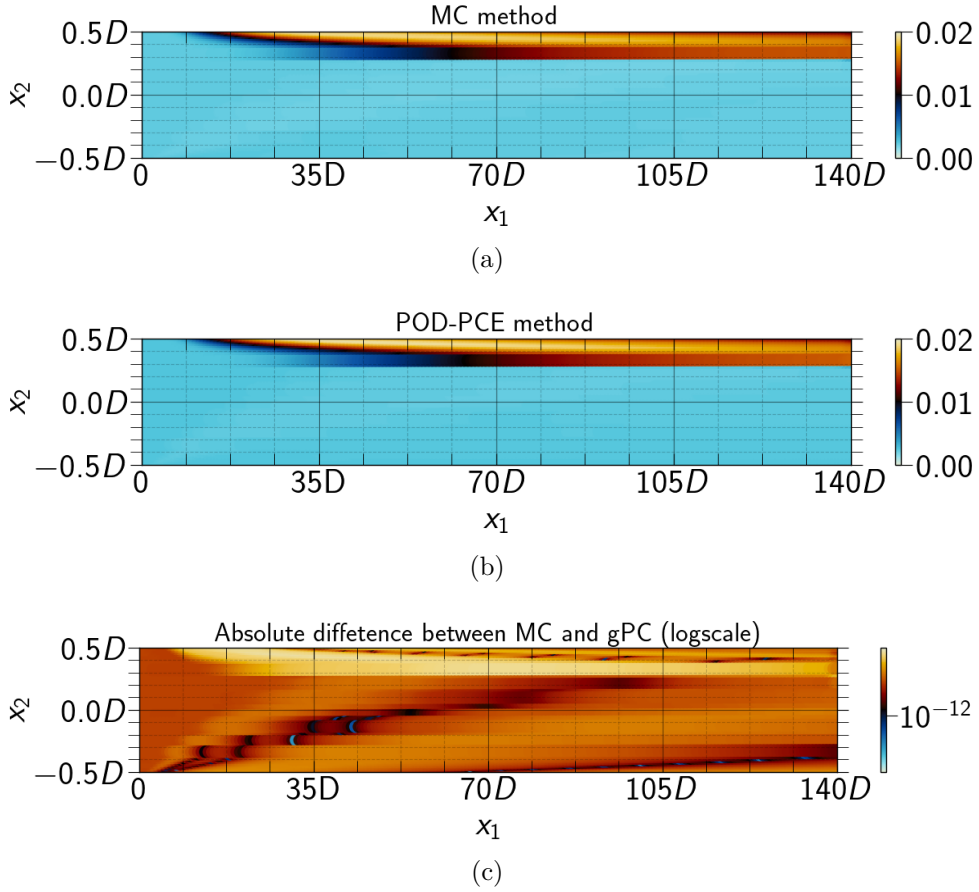

Figure 5.23: Same as Fig. 5.22 but for the variance.

evident that the two methods under consideration exhibit identical flow patterns and accurately capture the solid concentration over the two-dimensional pipe. To provide a more comprehensive understanding, Figs 5.13c and 5.23c illustrate the logarithmic ℓ_2-error in estimating the statistical moments considered. The remarkably low magnitude of the error ($< 10^{-10}$) clearly indicates that the surrogate models proficiently capture the uncertainty manifested over the physical domain for the slurry flow problem under consideration. An additional benefit is that the proposed POD-PCE method attains this high level of accuracy while incurring significantly lower computational costs in comparison to the MC and PCE methods. For a better insight, we display in Fig. 5.24 vertical cross-sections of the mean and variance at $x_1 = 126D$.

The distribution of the mean solid concentration reflects the general behavior of the flow in the case of phosphate slurry. The findings indicating that the average concentration of particles in the phosphate slurry flow is stratified into two distinct layers. This confirms that the slurry flow is of the settling type. In the core and lower wall of the pipe where particles move slowly, the solid concentration variance is insignificant. However, the top wall exhibits the highest

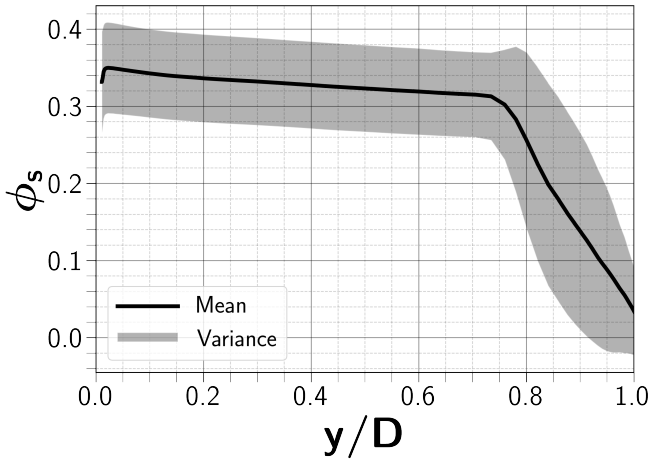

Figure 5.24: Cross-sections of the mean and variance solutions of the solid concentration distribution using PCE-POD

variance values due to the relatively sparse flow and increased particle movement and kinetic energy.

The ability of the surrogate model to estimate the whole Probability Density Function (PDF) of the solids concentration is also investigated. This comparison is shown in Fig. 5.25 where the estimation of the whole PDF using Monte-Carlo simulation are compared to those obtained using the PCE-POD surrogate model. PDF estimation is done here using a non-parametric estimation following a kernel smoothing methodology. It is clear that the results demonstrate that there is a

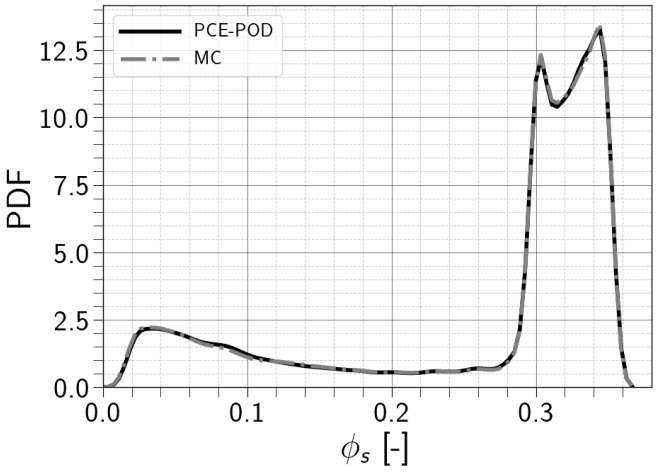

Figure 5.25: Visualization of solid concentration (ϕ_s) PDF through Kernel smoothing (KS) method, estimated using MC and PCE-POD techniques.

good estimation of the probability density function using the tools presented in this study. The results demonstrate a robust convergence in the decomposition, rendering them suitable for UQ in the distribution of solid concentration in slurry flows. The general shape of the PDF exhibits also the non-linearity effects, as

it is not suited to a Gaussian-like shape. One can also see the presence of two modes. This may be due to segregation effects. The slurry flow experiences segregation phenomena during transportation and the PDF of the slide concentration indicates the formation of two distinct modes in the concentration distribution.

The sensitivity of the solid concentration field to the variability of the random parameters $\{\phi_s, u_m, d_p, \theta, \mathcal{SC}\}$, can be assessed by means of bar-plots of the first order and total aggregated Sobol' indices (cf. Fig. 5.26). It is important to mention that a sensitivity analysis using only the PCE method has already been conducted for one-dimensional and scalar OoIs Elkarii et al. [2023b]. The corresponding Sobol' indices results will be presented alongside the outcomes obtained through the POD-PCE method, with the intention of facilitating a comprehensive comparison. The objective of this comparison is to assess whether increasing the dimensionality of our QoIs has any impact on the obtained results. The re-

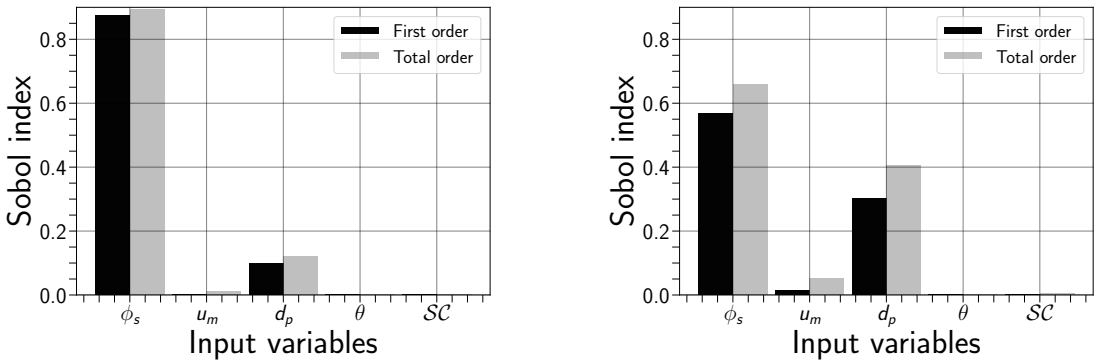

(a) (b)

Figure 5.26: Barplots of first and total Sobol' indices for solid concentration field calculated based on: (a) One-dimensional data, (b) Two-dimensional data

duced model generates a comparable ranking of the most influential parameters; however, there are variations in the magnitude of the Sobol' indices. The Sobol' indices analysis conducted indicates that the distribution of solid concentration along the vertical diameter of the pipe remains primarily influenced by the initial concentration introduced into the pipeline, followed by the particle sizes. Thus, these two parameters are responsible for regulating the behavior and pattern of the slurry flow. Indeed, the inlet concentration of a slurry directly impacts the mixture density, and it plays a significant role in the behavior of particles, including their collisions and friction, ultimately leading to their arrangement inside the pipeline. The behavior of particles is also induced by their size, as larger particles generally cause sedimentation, resulting in a significant change in the in situ solid concentration in the pipeline.

2-D solid velocity

Our second OoI consists of a two-dimensional velocity field of particles. Similar to the previous example, we have provided the optimal polynomial degree distribution for approximating each spectral mode using the POD technique (cf. Table 5.3). Additionally, we have included the Leave-One-Out (LOO) error associated with the PCE method for estimating the numerical solution for each mode. By

Table 5.3: Optimal polynomial degrees with LOO errors for the POD modes in the slurry particles velocity u_s

Number of modes	LOO error	Polynomial degree
Mode #1	4.4253×10^{-5}	7
Mode #2	2.0990×10^{-3}	9
Mode #3	1.1500×10^{-2}	6
Mode #4	2.0464×10^{-2}	7
Mode #5	3.9424×10^{-2}	8

using a set of 5 eigenmodes, the physical model can be significantly reduced. This means that the surrogate model for two-dimensional solid velocity can be represented by only the first 5 modes, rather than the 18894 required to represent the total number of nodes in the two-dimensional numerical model.

The ability of the proposed POD-PCE method for recovering the particle velocity of a plane pipe is examined. We showcase in Fig. 5.27 the results estimated using MC and the proposed surrogate model for the mean solid velocity, as well as , the difference between them. Under the considered conditions of the slurry flow, both methods show comparable trends in the velocity profiles of particles. Fig. 5.28 presents the comparative results obtained for the variance. The magnitude of logarithmic ℓ_2-error being less than ($< 10^{-6}$) indicates that both methods show comparable velocity profile trends for the solid phase. Once again, the results that have been presented demonstrate a strong convergence in the decomposition process, making them trustworthy for UQ purposes. This confirms that the proposed POD-PCE approach is effective in resolving the issue of the two-dimensional velocity distribution of particles. Fig. 5.29 depicts the vertical cross-sections of the mean and variance at $x_1 = 126D$.

The presence of an asymmetrical profile in the distribution of mean solid velocity is likely a contributing factor to the observed differences in solid concentration variance across the various walls of the pipe. Specifically, the skewness of the velocity profile towards the top wall indicates that the flow in that region is relatively more diluted, and the particles have a higher kinetic energy. This is consistent with the highest variance values observed in that area.

The surrogate model ability to estimate the whole Probability Density Function (PDF) of the solids velocity is also checked here. This comparison is shown in Fig. 5.30 where the estimation of the whole PDF using Monte-Carlo simula-

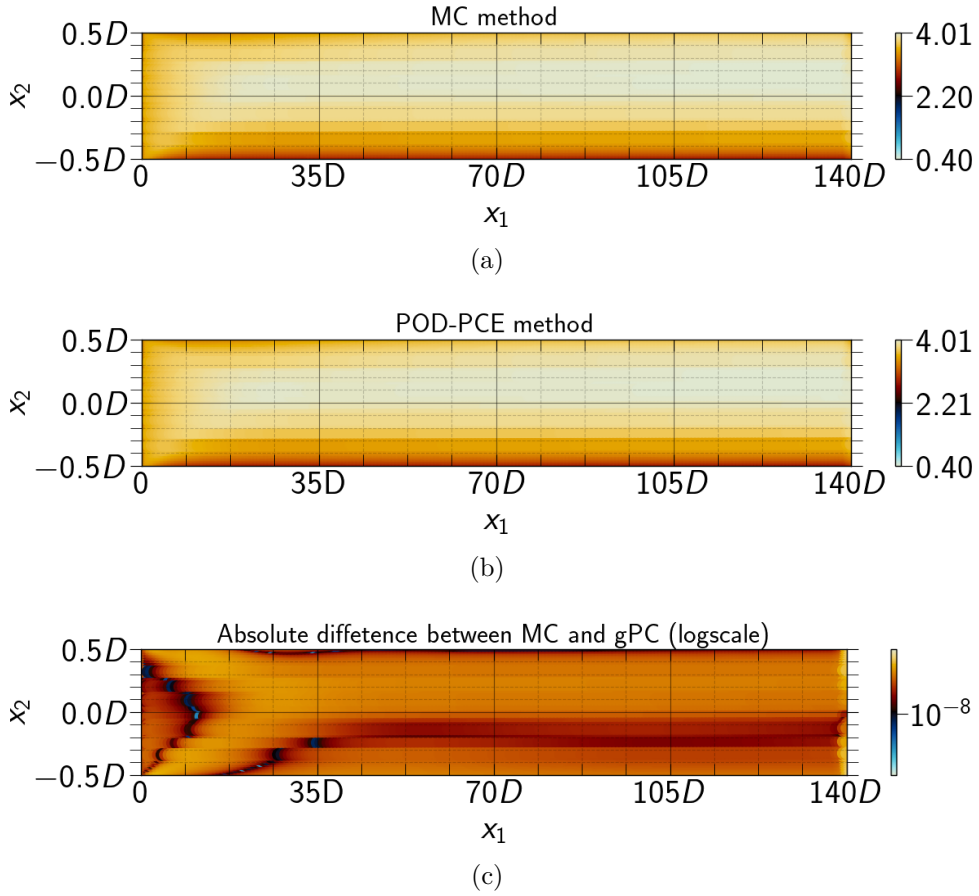

Figure 5.27: Mean solid velocity u_s obtained for the stochastic simulation (a), the deterministic exact solution (b) and the difference between the two solutions (c) obtained for a slurry flow problem.

tion are compared to those obtained using the PCE-POD surrogate model. Once again, the nonlinear behavior of the model and its impacts on the velocity distribution is emphasized. This considers a further assessment of the ability of the surrogate model to perform UQ correctly.

Similar to ϕ_s the sensitivity of the solid velocity field to the variability of our random parameters can also be evaluated through barplots of the first-order and total Sobol' indices. The velocity distribution of solids in the pipe, as depicted in Fig. 5.31, is primarily influenced by the inlet flow rate. On the other hand, the utilization of the POD-PCE technique reveals slightly dissimilar outcomes, indicating that the velocity distribution of particles is relatively more affected by their sizes and also slightly by the pipe inclination. Based on their values, the observed discrepancies could be attributed to the stochastic nature of the methodology. Normally, smaller particles have higher velocities than larger particles at the same temperature. This is because smaller particles have a higher surface area-to-volume ratio, which means they have more contact with the surrounding fluid, allowing them to exchange energy and momentum more efficiently. Addi-

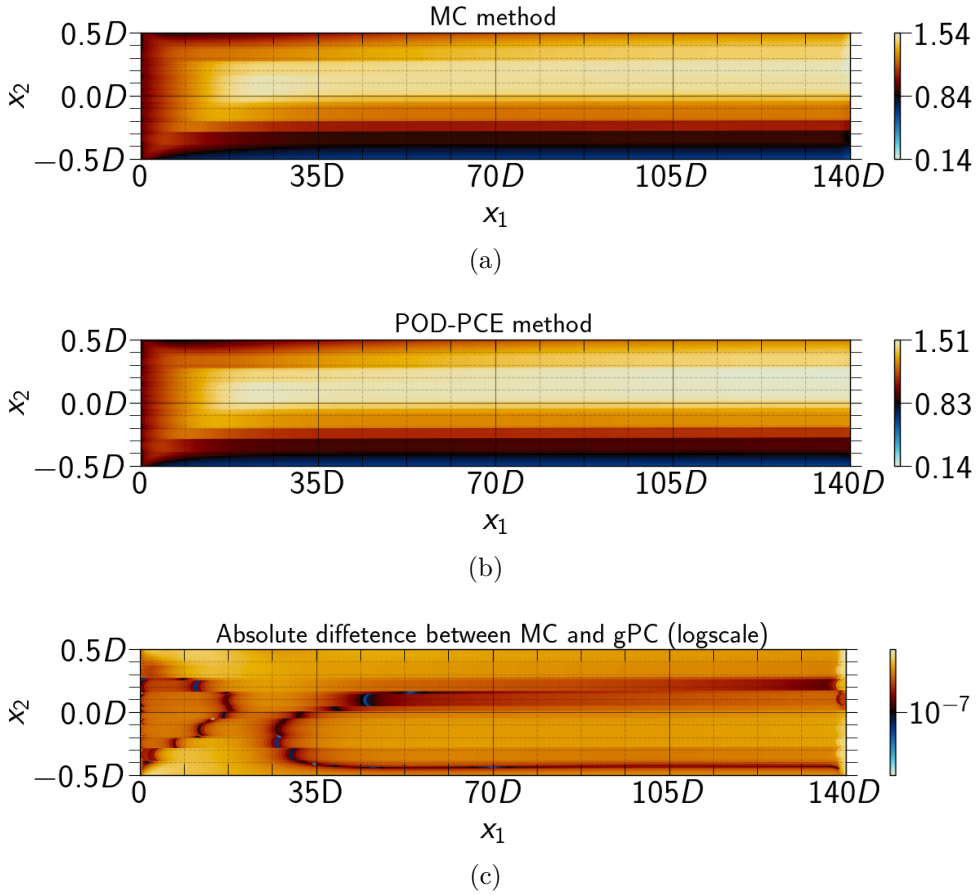

Figure 5.28: Same as Fig. 5.27 but for the variance.

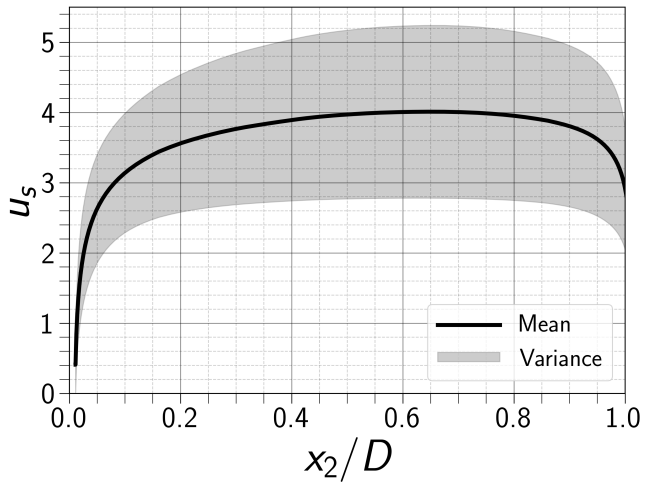

Figure 5.29: Cross-sections of the mean and variance solutions of the solid velocity distribution using PCE-POD

tionally, smaller particles experience less drag and resistance from the surrounding fluid, which can also contribute to their higher velocity.

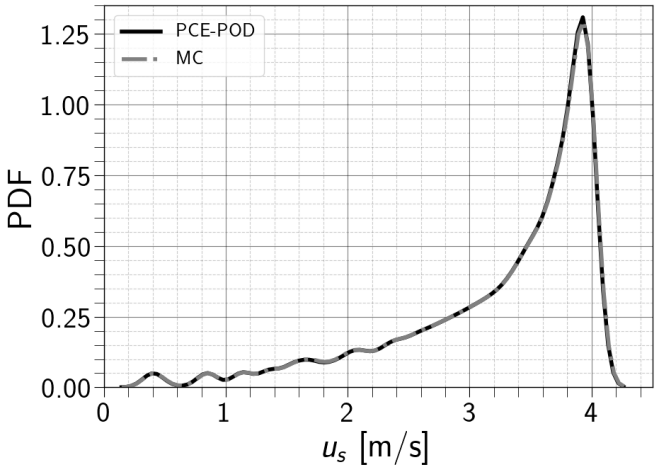

Figure 5.30: Visualization of solids velocity (u_s) PDF through Kernel smoothing (KS) method, estimated using MC and PCE-POD techniques.

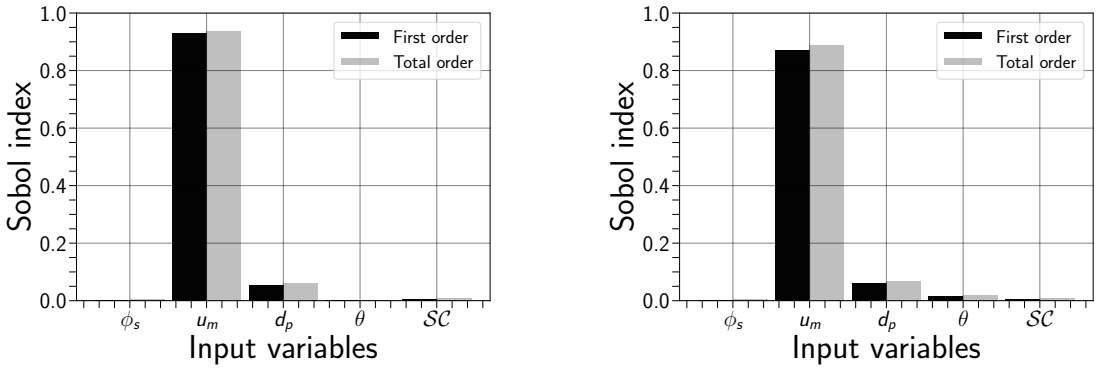

(a) (b)

Figure 5.31: Barplot of first and total Sobol' indices for solid velocity calculated based on: (a) One-dimensional data, (b) Two-dimensional data

Two-dimensional pressure distribution

The pressure distribution within the slurry flow is the third OoI that was addressed in this study. Table 5.4 summarizes the results obtained for PCE-POD modes. It can be observed that the model size has significantly decreased, as the

Table 5.4: Optimal polynomial degrees with LOO errors for the POD modes in the slurry flow pressure P

Number of modes	LOO error	Polynomial degree
Mode #1	6.0655×10^{-3}	6
Mode #2	3.1614×10^{-3}	6

pressure distribution of the slurry flow can be reconstructed using only two modes

instead of the 18894 that were required for obtaining the deterministic solution.

Similar to previous analyses, we compare the average pressure distribution obtained from both MC and POD-PCE methods to evaluate the capability of the proposed POD-PCE approach in reconstructing the pressure of the two-dimensional pipe flow. One should note that the results displayed here for the pressure are calculated in bar unit. The outcomes are depicted in Fig. 5.32. There

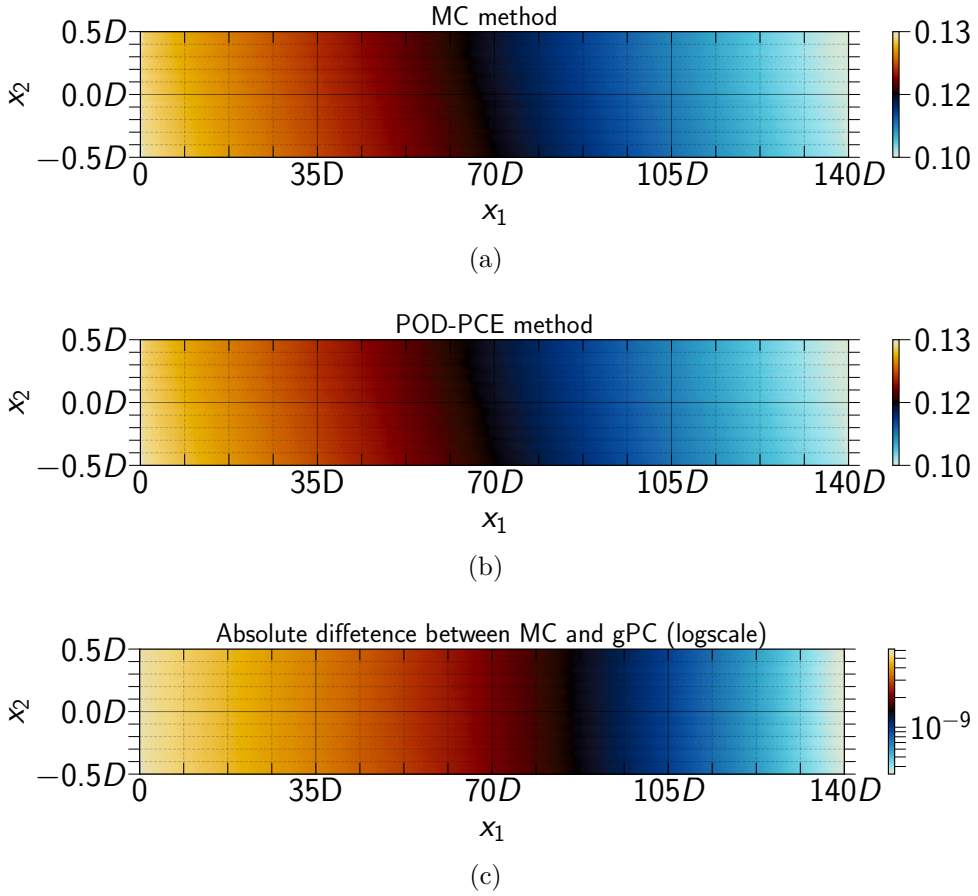

Figure 5.32: Mean flow pressure P obtained for the stochastic simulation (a), the deterministic exact solution (b) and the difference between the two solutions (c) obtained for a slurry flow problem.

are no significant changes between the two solutions, it is further confirmed by the logarithmic ℓ_2-error estimation. Since, the error's magnitude depicted here is less than 10^{-8}.

Fig. 5.33 presents the comparative results obtained for the variance. The surrogate models effectively capture the uncertainty observed across the physical domain in the slurry flow problem under consideration. Given the relatively low computational effort required to implement the PCE-POD method, it can be deemed an ideal algorithm for conducting uncertainty quantification in computational slurry flows involving stochastic inputs. By analyzing the distribution of the mean flow pressure, it can be deduced that the pressure of the slurry typically

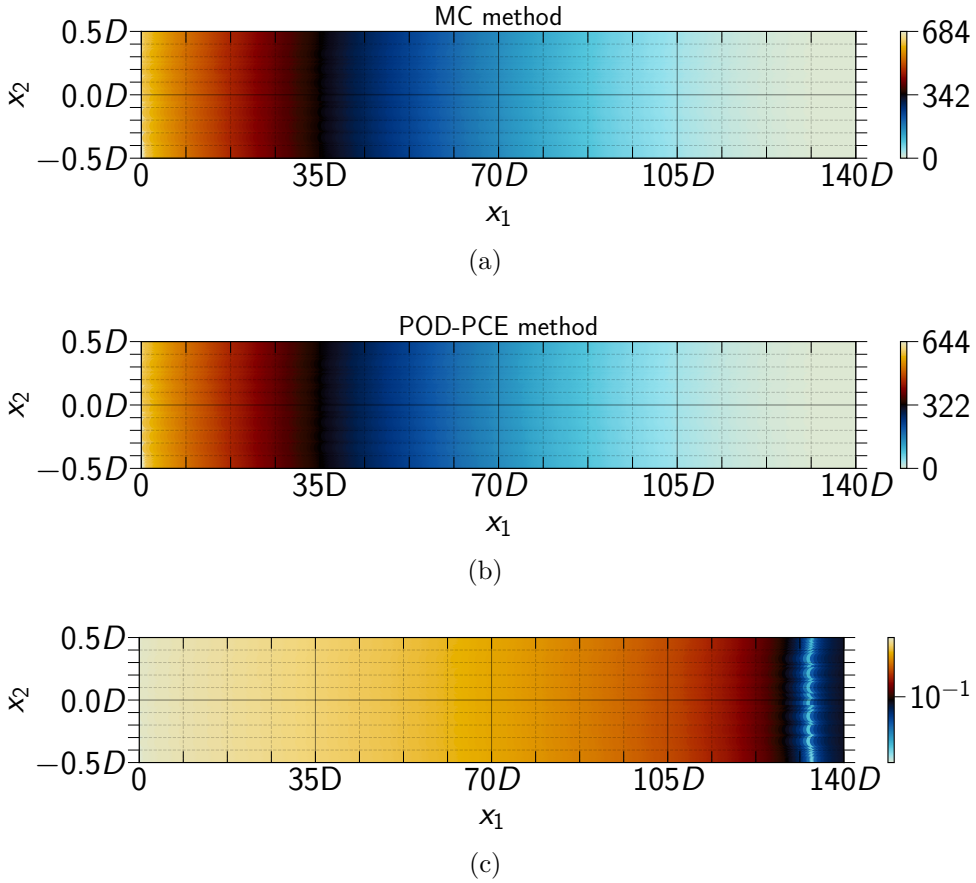

Figure 5.33: Same as Fig. 5.32 but for the variance.

decreases within the range of variability of the random inputs. This pressure evolution along the pipeline is evident from the stratified flow pattern discussed in subsection 5.2.3. Such slurry flows exhibit fluctuations in particle concentration and velocity, resulting in frictional resistance and subsequent pressure decrease. The highest variance values are observed at the inlet of the pipe because the pressure at the inlet varies in conjunction with the velocity.

The ability of the surrogate model to estimate the entire Probability Density Function (PDF) of the flow's pressure drop is examined. This comparison is depicted in Fig. 5.34, where the estimation of the complete PDF using Monte Carlo simulation is compared to that obtained using the PCE-POD surrogate model. Sobol' indices are utilized to evaluate the sensitivity of slurry flow pressure. The first and total aggregated Sobol' indices are shown in Fig. 5.35. The reduced model exhibits the same ranking of the most influential parameters as the full-order model. The results clearly indicate that the velocity and pipe inclination have the greatest impact on the pressure drop, followed by particle size, particle concentration, and the specularity coefficient. When considering the range of pipe inclination variations, it is concluded that it only affects the magnitude of the pressure drop and does not result in a pressure gain when the pipe is inclined

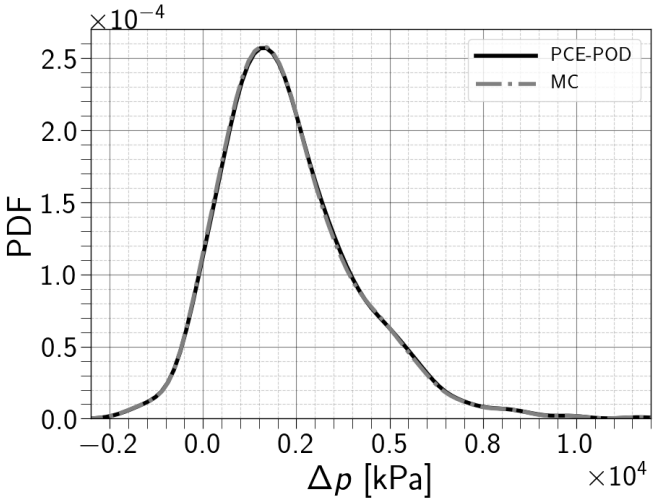

Figure 5.34: Visualization of the flow's pressure drop PDF through Kernel smoothing (KS) method, estimated using MC and PCE-POD techniques.

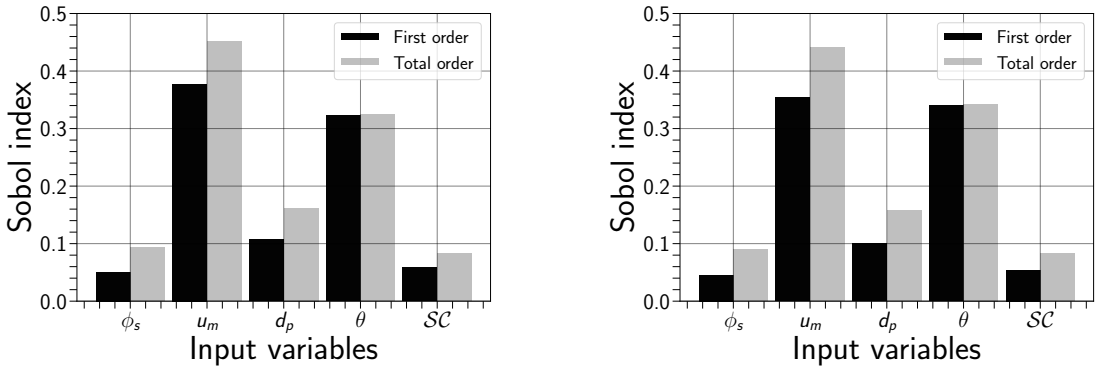

Figure 5.35: Barplots of first and total Sobol' indices for the flow's pressure drop calculated based on: (a) One-dimensional data, (b) Two-dimensional data

downward. The particle size influences the friction along the lower wall, and as the slurry flows through the pipeline, the different layers of particles interact with the component walls in varying ways. Moreover, the layer with the highest particle concentration experiences greater frictional resistance against the wall, leading to a larger pressure drop compared to the layer with lower particle concentration. Consequently, a pressure gradient forms across the slurry, where the pressure decreases as the particle concentration increases.

5.3 Conclusion

In the present chapter, an efficient analysis of uncertainty quantification for slurry flows problems is presented and discussed. The complexity and the high non-

linearity of slurry flows make such studies useful to provide physical insights into the involving process. In the first part, uncertainty quantification is performed using the full polynomial chaos expansion for scalar and 1-dimensional *QOIs*. We have analyzed the impact of the uncertain parameters on the output quantities of interest (QoIs) allowing assessment of the energy efficiency of the slurry transport. Conclusions of UQ and GSA study in this part are presented in subsection 5.1.6. The second part of this chapter was dedicated to study UQ and GSA in a two-dimensional case of phosphate slurry flow Reduced-order model is applied to the two-dimensional TFM equations. The numerical results show that the developed reduced-order model is able to produce acceptable results for such statistical quantities. Distributions of mean and variance obtained from the reduced-order model are compared to those computed using the deterministic simulations. Herein, we have also performed a comprehensive global sensitivity analysis and uncertainty quantification for our 2-dimensional *QOIs*. The variability of each *QOI* is well represented in this case and gives more informations about the distribution of the outputs. The phosphate slurry within these operating conditions is confirmed to be classified as two-layer (stratified) flow. The GSA (Global Sensitivity Analysis) results have enabled us to quantify the uncertainty in our inputs. As a result, it is important to prioritize the control of those parameters where their uncertainty has a greater impact on the overall uncertainty of the simulation. By focusing our efforts on these critical parameters, we can achieve greater control and optimization of the slurry flow, leading to more reliable and accurate simulations. The statistical approach utilized in this study is superior to the classical "one-at-a-time" sensitivity analyses, which involve freezing all parameters except one to study the effect of the remaining parameter. By using Global Sensitivity Analysis (GSA) and Uncertainty Quantification (UQ), we can better understand how the complex system of slurry flows in pipelines behaves. To sum up, this study serves as a prototype for highlighting the advantages of using Global Sensitivity Analysis (GSA) and Uncertainty Quantification (UQ) to gain a better understanding of the behavior of slurry flows in pipelines, which is a complex system. Through the use of GSA and UQ, we can identify critical parameters that impact the performance of the system and optimize the flow for improved efficiency and reliability. By demonstrating the effectiveness of these techniques, this study paves the way for future research in the field of slurry flow analysis and optimization.

5
Analyse de sensibilité

Le présent chapitre se concentre sur la réalisation d'une analyse de sensibilité globale sur une boue de phosphate, en utilisant la méthode d'expansion de chaos polynomial généralisée (PCE). Afin d'étudier la quantification de l'incertitude dans le contexte des écoulements de boues et de leurs quantités d'intérêt (QoIs) uniformes et unidimensionnelles, nous avons utilisé la technique PCE, qui est décrite dans la section 5.1.2. La section 5.1.3 se penche sur les résultats de la quantification de l'incertitude et de l'analyse de sensibilité pour nos QoIs. Dans la section 5.1.4, nous donnons des remarques conclusives pour cette première partie. Ensuite, dans la section 5.2, nous présentons la deuxième partie de notre étude de quantification de l'incertitude et d'analyse de sensibilité globale, qui se concentre sur des quantités d'intérêt bidimensionnelles (QoIs). Pour réduire le coût de construction du modèle PCE, nous utilisons un modèle réduit appelé POD-PCE. Les résultats de l'analyse en utilisant la technique POD-PCE sont discutés dans la section 5.2.1.

5.1 GSA pour l'écoulement de boues de phosphate dans les pipelines en utilisant gPC

5.1.1 Introduction

Dans cette étude, nous considérons l'approche de modélisation CFD Euler-Euler pour simuler l'écoulement de boues de phosphate et quantifier l'incertitude de la réponse numérique. L'utilisation de modèles d'écoulement diphasique pour le transport de sédiments dans les pipelines est courante, mais en raison du nombre important de paramètres nécessaires pour chaque simulation, une incertitude considérable est attendue dans les résultats. Par conséquent, une analyse complète qui aborde la quantification de l'incertitude (UQ) et l'analyse de sensibilité (SA) est nécessaire pour améliorer la fiabilité des prévisions. Dans cette étude, nous considérons l'approche de modélisation CFD Euler-Euler pour simuler l'écoulement de boues de phosphate et quantifier l'incertitude de la réponse numérique. L'objectif de l'UQ est de propager les incertitudes des paramètres d'entrée et quantifier leur impact sur une quantité d'intérêt (QoI) simulée à travers un modèle basé sur la physique. Cela permet d'associer chaque résultat de simulation à un niveau de confiance, car sa précision dépend significativement de la quantité et de la qualité des données d'entrée. Un problème majeur lors de l'approche de l'UQ avec des calculs hydrauliques multiphasiques est la malédiction de la dimensionnalité.

En plus de l'UQ, l'analyse de sensibilité (SA) est un autre objectif majeur de nombreuses études [Saltelli and Tarantola, 2002]. L'objectif de la SA est de quantifier l'importance relative de chaque paramètre d'entrée. Nous adoptons ici l'utilisation des expansions de chaos polynomial généralisé (PCE) pour la quantification de l'incertitude (UQ) et GSA [Blatman and Sudret, 2011a]. Pour effectuer l'UQ et la GSA pour le problème d'écoulement de boues dans les pipelines, il convient d'identifier les différentes sources d'incertitude qui seront considérées comme entrées du modèle. Le comportement des écoulements de boues est souvent décrit par les propriétés des matériaux transportés. Les entrées consistent en cinq variables, qui sont étudiées et échantillonnées dans une plage physique. Initialement, nous abordons les paramètres physiques définissant le transport de la boue recherchée, y compris la distribution granulométrique des particules solides, la concentration initiale de solides dans l'écoulement, et la vitesse d'entrée du mélange d'écoulement. Dans le transport de suspension, l'inclinaison de la conduite, un facteur lié à la géométrie, est également prise en compte comme un composant crucial. Enfin, nous analysons également le coefficient de spécularité, un paramètre de modélisation, un paramètre de la limite murale lié à la théorie cinétique des écoulements granulaires [Zhong et al., 2015]. La plage de variabilité des paramètres ci-dessus est choisie en fonction des conditions de fonctionnement du débit de suspension de phosphate prévu [Rusconi et al., 2016]. Enfin, il convient de noter que l'objectif général de l'étude actuelle est d'évaluer l'incertitude

de l'efficacité énergétique dans les écoulements de suspension.

5.1.2 Expansion du chaos polynomial généralisé pour l'analyse de sensibilité

L'expansion gPC vise à recréer le comportement global d'une simulation de manière cohérente avec une décomposition polynomiale. Ces derniers sont des polynômes orthogonaux multivariés et servent de fonctions de base qui sont sélectionnées en fonction des distributions de probabilité conjointes des variables d'entrée stochastiques suivant le schéma de polynômes Askey [Xiu and Karniadakis, 2002]. Dans la présente étude, si nos variables (indiquées dans le Tab. 5.1) sont stockées dans le vecteur $\mathbf{X} \in \mathbb{R}^d$, et que $\mathcal{Y}$ représente les réponses du modèle discutées précédemment, alors on peut écrire, selon l'expansion gPC:

$$\mathcal{Y} = \mathcal{M}(\mathbf{X}) = \sum_{\alpha \in \mathbb{N}^d} \boldsymbol{\pi}_\alpha \Psi_\alpha(\mathbf{X}), \tag{5.1}$$

Où $\mathbb{N}^d$ désigne un multi-indice $\boldsymbol{\alpha} = \{\boldsymbol{\alpha}_1, \ldots, \boldsymbol{\alpha}_d\}, \{\boldsymbol{\pi}_{\boldsymbol{\alpha}}, \boldsymbol{\alpha} \in \mathbb{N}^d\}$ ont les coefficients spectraux qui doivent être calculés. La technique de régression peut être utilisée pour estimer les coefficients spectraux $\boldsymbol{\pi}\alpha$. Cela peut être réalisé en résolvant un problème de minimisation des moindres carrés (LS) dans la norme ℓ_2 [Berveiller et al., 2006]. Nous définissons d'abord l'erreur métrique εPC comme la différence entre l'évaluation exacte du modèle ($\mathcal{Y}$) et les estimations de substitution gPC pour un ensemble fini d'entraînement de variables d'entrée échantillonnées aléatoirement $\mathbf{X}$. Un ensemble de N_{ls} réalisations du vecteur d'entrée, $\mathbf{X} = X(1), \cdots, X(N_{ls})$, est ensuite nécessaire, appelé plan d'expérience (ED). Le problème de régression est résolu à l'aide d'une approche de régression par les moindres angles (LAR), qui offre une représentation gPC clairsemée. Afin de surmonter la malédiction de la dimensionnalité. Ici, nous suivons la procédure suggérée dans Blatman and Sudret [2011a]. Évaluer sa qualité est d'un intérêt crucial, c'est pourquoi l'erreur Leave-One-Out (LOO) est utilisée car elle donne une excellente mesure de l'exactitude en permettant des estimations d'erreur à un traitement raisonnable.

Une fois que le PCE est construit, la moyenne μ et la variance totale D peuvent être obtenues en utilisant les valeurs des coefficients spectraux tels que $\mu = y_0$ et $D = \sum_{\alpha \in \mathcal{A} \setminus 0} y_{\boldsymbol{\alpha}}^2$ et par conséquent, les indices de Sobol de tout ordre peuvent être calculés de manière directe.

5.1.3 Résultats et discussions

Pour effectuer une UQ et une GSA pour le problème des écoulements de suspensions dans les pipelines, il convient d'identifier les différentes sources d'incertitude, qui seront considérées comme des entrées du modèle. Le comportement des écoulements de suspension dans les pipelines est souvent décrit par les propriétés

des matériaux transportés, ce qui nous amène à définir les paramètres d'entrée aléatoires du modèle comme $\mathbf{X} = \{\phi_s, u_m, d_p, \theta, \mathcal{SC}\}$. Ces variables aléatoires sont présentées selon leurs densités de probabilité respectives et leur plage de variabilité dans le tableau 5.1. En vue de calculer les PCE des sorties du modèle,

Table 5.1: Écoulement de suspension de phosphate : paramètres du modèle

Parameters	Type de PDF	Polynômes orthogonaux	Plage de variabilité
Vitesse d'entrée u_m (m/s)	Uniforme	Polynômes de Legendre	$[1.75, 5]$
Concentration solide ϕ_s[%]	Uniforme	Polynômes de Legendre	$[20, 40]$
Taille des particules d_p (μm)	Uniforme	Polynômes de Legendre	$[44, 250]$
Inclinaison du pipeline θ (°)	Gaussienne	Polynômes d'Hermite	$[0, 4]$
Coefficient de spécularité $\mathcal{SC}$ (-)	Uniforme	Polynômes de Legendre	$[0, 1]$

trois plans d'expériences de tailles $N = \{200, 500, 1000\}$ sont générés en utilisant la méthode d'échantillonnage latin hypercube (LHS). Une fois que les plans d'expériences sont définis, le modèle numérique est exécuté pour chaque nœud d'échantillonnage dans ces ensembles afin d'obtenir le vecteur y d'observations de la *quantité d'intérêt*.

GSA de la perte de charge totale

L'analyse est réalisée en utilisant la perte de charge totale comme quantité d'intérêt. La perte de charge est une mesure de la réduction d'énergie et peut être estimée comme la somme des pertes de charges dues à l'élévation, la cinétique et les frictions. De plus, trois ensembles de DE indépendants, comprenant chacun 200, 500 et 1000 échantillons, sont générés au hasard pour construire le PCE. Les valeurs d'erreur LOO pour les différents PCE construits à l'aide des ensembles DE susmentionnés sont présentées dans la figure 5.1. Comme prévu, l'erreur diminue

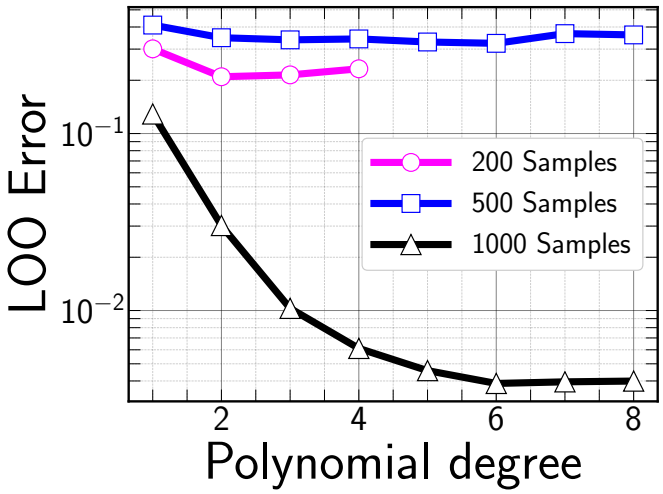

Figure 5.1: Test de convergence du PCE : Nombre d'échantillons par rapport à l'erreur LOO ainsi que le degré optimal du PCE.

lorsque le degré du polynôme augmente. Cependant, un degré de polynôme de 6, calculé à l'aide d'un DE de 1000 échantillons, est suffisant pour obtenir une bonne approximation. Par la suite, le méta-modèle obtenu est évalué à l'aide de l'ensemble de validation. Les résultats de cette évaluation, représentés dans la Fig. 5.2, démontrent que le méta-modèle se comporte de manière similaire au modèle CFD. Par conséquent, le PCE obtenu peut être utilisé pour l'UQ et le GSA. Une analyse de sensibilité globale est effectuée pour identifier les

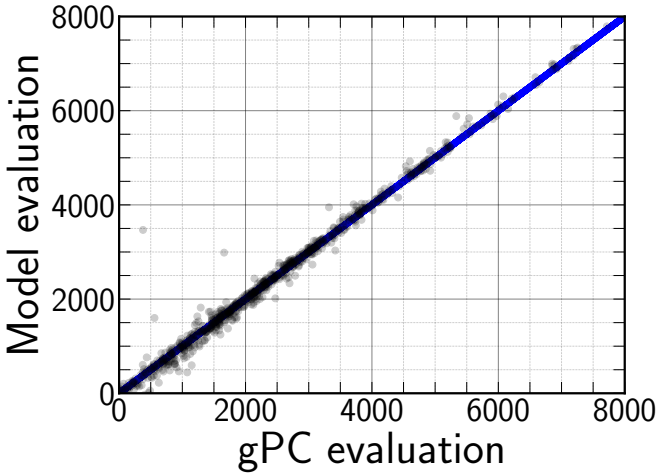

Figure 5.2: Comparison between PCE and the true model on 1000 validation runs for the model outputs using LAR method

paramètres les plus influents. La sensibilité de la perte de charge à la variabilité des paramètres aléatoires, à savoir $\{\phi_s, u_m, d_p, \theta, \mathcal{SC}\}$, est évaluée à l'aide des indices de Sobol'. La figure 5.4 présente des graphiques en barres des indices de Sobol' du premier ordre et totaux calculés, qui fournissent une information précieuse sur la contribution des paramètres individuels et de leurs interactions à la variance globale. Les indices de Sobol' totaux ont été utilisés pour classer les paramètres en fonction de leur importance, permettant ainsi l'identification des paramètres les plus influents. L'analyse des indices de sensibilité a montré que la variabilité de la perte totale de charge $\Delta p/L$ est principalement attribuée aux effets principaux de u_m, suivis de θ et ensuite de d_p. Le paramètre le plus influent parmi les paramètres considérés est u_m, présentant un indice de Sobol' total de $S^T = 0.45$. De plus, les résultats ont souligné une influence non négligeable mais relativement faible de ϕ_s et $\mathcal{SC}$. De plus, la comparaison entre les indices de Sobol' d'ordre 1 et d'ordre total a révélé des écarts significatifs, impliquant des interactions entre les paramètres aléatoires. Dans l'ensemble, ces résultats fournissent des informations précieuses sur la contribution des paramètres individuels et de leurs interactions à la variance globale de la perte totale de charge.

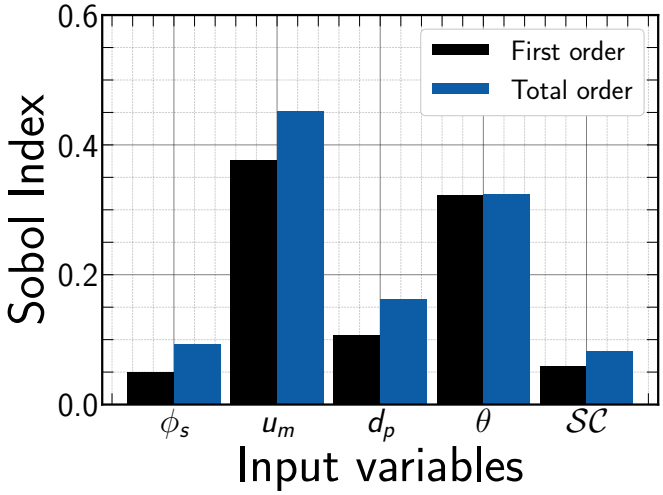

Figure 5.3: Les indices de Sobol' de premier ordre et total pour la perte de charge totale.

GSA de la perte de charge due aux frottements

Nous nous concentrons ici uniquement sur la composante de la perte de charge due à la friction par unité de longueur de la canalisation, $\Delta p\text{Friction}/L$. La figure 5.4 affiche les indices de Sobol du premier ordre et total calculés sous forme de graphiques à barres. En se concentrant sur la figure 5.4, on peut observer que

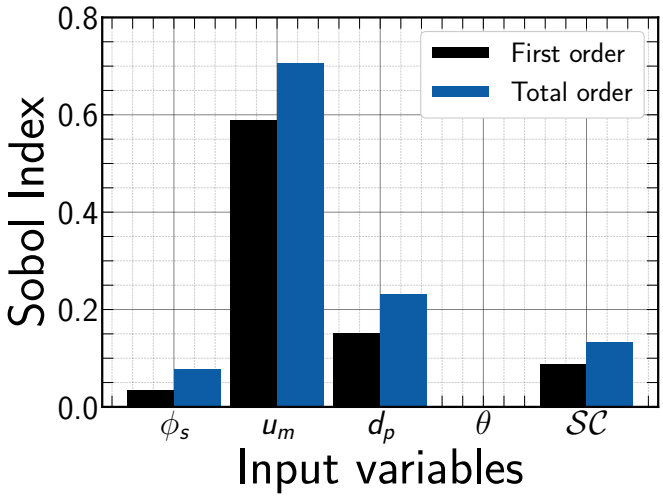

Figure 5.4: First and total Sobol' indices for the frictionnal contribution in pressure drop per unit length of the pipe

lorsqu'il s'agit de pertes de pression dues à la friction, l'inclinaison de la canalisation n'a aucune influence. D'un autre côté, il semble que l'impact des autres paramètres reste le même. Ici, la variabilité de $\Delta p_{\text{Friction}}/L$ est principalement contrôlée par la vitesse de mélange u_m, suivie du diamètre des particules. Les pertes de friction mesurent la quantité d'énergie que votre système de canalisa-

tion perd lorsque la suspension rencontre une résistance, ce qui est directement lié à la viscosité de la suspension. Ces résultats prouvent que cette dernière n'est affectée que par les propriétés physiques du mélange de fluide.

GSA des profils de concentration solide et de vitesse 1-D

Des résultats numériques sont obtenus pour les profils de concentration solide et de vitesse moyennés sur la corde à travers le diamètre d'une canalisation, où l'écoulement de la suspension a atteint un développement complet. Les données ont été collectées à la sortie de la canalisation, précisément définie à une position qui est à 90% de la longueur de la canalisation. Dans le cas de sorties multi-variées, telles que les profils de concentration solide et de vitesse, un PCE est construit pour chaque composante le long du diamètre moyenné sur la corde de la canalisation, comme illustré dans la figure 5.5.. Dans les zones où

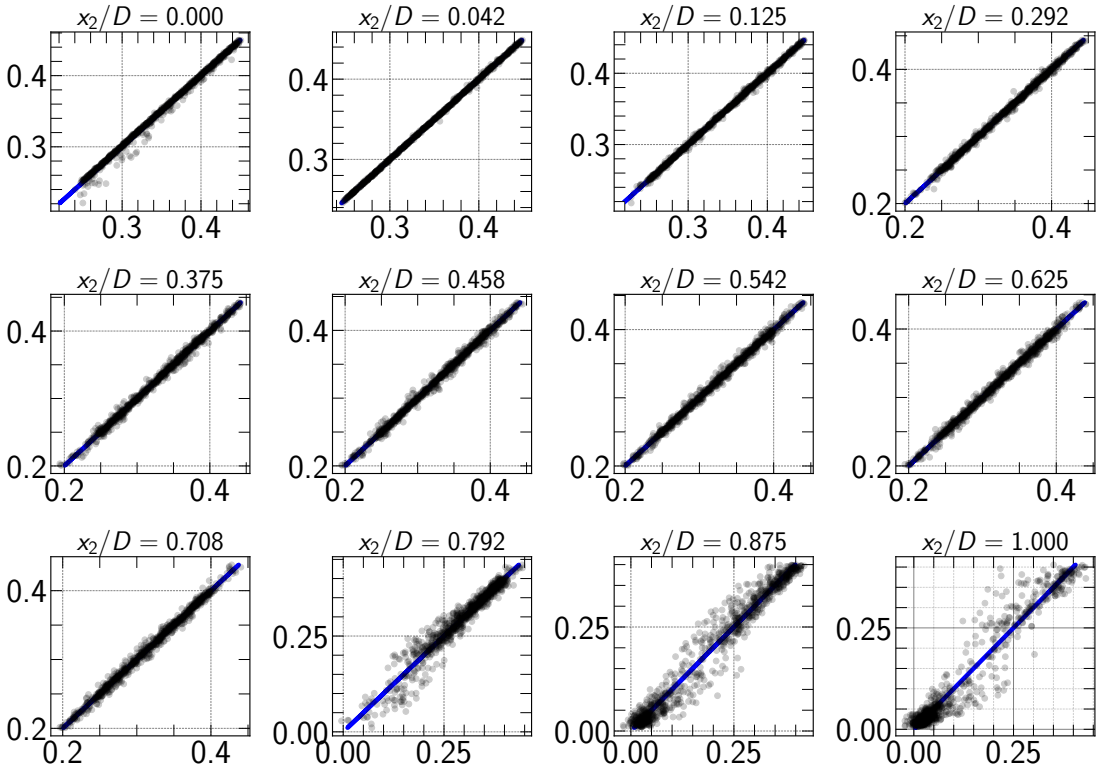

Figure 5.5: Comparaison entre le PCE (points noirs) et le modèle réel (courbes bleues) sur 1 000 exécutions de validation pour chaque point de contrôle de la moyenne de corde.

la distance sans dimension par rapport à la paroi, x_2/D, est inférieure ou égale à 0,7, les résultats de validation pour la prédiction de la concentration solide montrent une excellente concordance avec le vrai modèle. Cette concordance est étayée par une petite erreur de LOO inférieure à 0.001. Cependant, dans la zone supérieure de la conduite où $x_2/D \geqslant 0.7$, des différences entre l'estimation de

concentration prédite (PCE) et le vrai modèle sont observées. Ces différences peuvent être attribuées à la dilution de la couche supérieure de l'écoulement, ce qui entraîne un mouvement chaotique des particules et des non-linéarités importantes dans la concentration de la phase solide. Pour enquêter davantage sur ces différences, la variance peut être calculée comme illustré dans la Figure 5.11. Nos observations indiquent que la zone avec la couche la plus épaisse présente

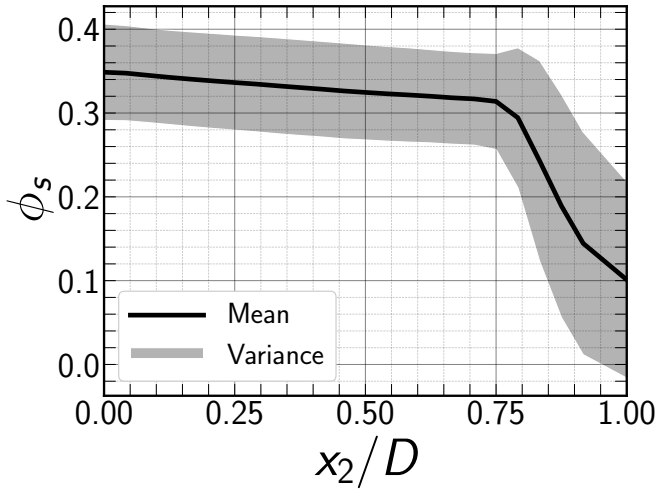

Figure 5.6: Moyenne et variance de la distribution de la concentration solide le long du diamètre de la conduite.

la plus petite variation, en raison des particules serrées et de la restriction conséquente du mouvement arbitraire des particules et des collisions. Cette région de haute concentration dans les couches inférieures ne permet pas seulement une variation réduite, mais facilite également le développement de PCE précises. En revanche, la variation augmente vers la couche mince près du mur supérieur. Les fluctuations de concentration modifient effectivement la distribution de la variance tout en maintenant un niveau constant de variabilité. Pour évaluer la sensibilité du profil de concentration solide à travers le diamètre de la conduite à la variabilité des paramètres aléatoires, les indices de Sobol spatiaux peuvent être utilisés. La distribution spatiale unidimensionnelle de l'indice de Sobol total due à l'incertitude dans $\{\phi_s, u_m, d_p, \theta, \mathcal{SC}\}$ est représentée dans la Fig. 5.12. Les résultats indiquent que l'impact de la concentration solide diminue vers la paroi supérieure et augmente inversement vers la paroi inférieure, suggérant une présence de particules plus forte vers la paroi inférieure. Ce comportement des particules est induit par leur taille, car les particules plus grandes provoquent généralement une sédimentation, ce qui entraîne un changement significatif de la concentration solide in situ près de la paroi supérieure. Cette interprétation est cohérente avec la zone de variance de concentration solide maximale. Les premiers et les indices Sobol' totaux sont estimés en moyennant leur valeur le long de la conduite , et les résultats sont présentés sous forme de graphiques à barres dans la figure 5.8. L'analyse de ces indices montre que la variabilité de

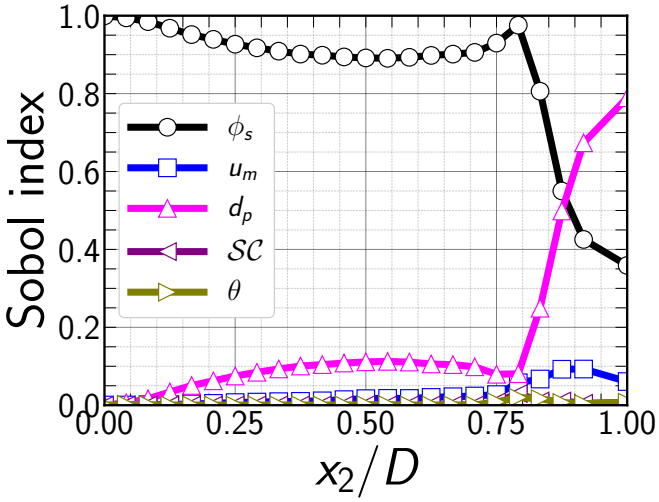

Figure 5.7: La distribution spatiale unidimensionnelle des indices de Sobol totaux pour la concentration solide

la concentration solide est principalement due aux effets principaux de ϕ_s et d_p. Dans l'ensemble, ces résultats suggèrent que la taille des particules et la concentration solide initiale sont des facteurs importants à considérer lors de l'étude de la distribution des solides dans une conduite

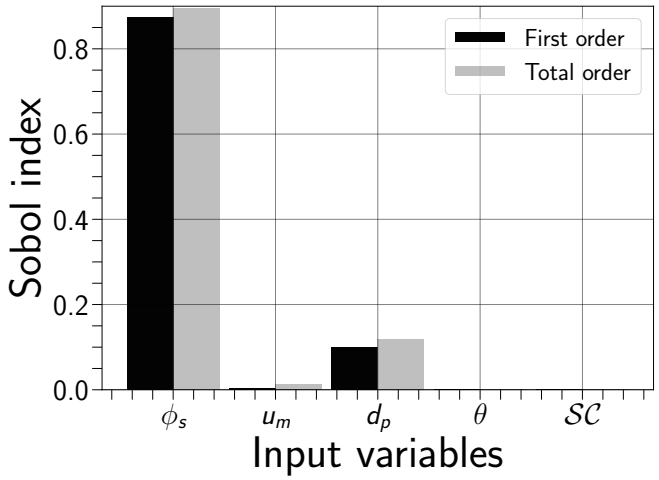

Figure 5.8: Les indices de Sobol' d'ordre 1 et totaux agrégés pour la concentration solide

GSA of the solid velocity profile

La même procédure a été répétée pour étudier la sensibilité du profil de vitesse des particules. Comme précédemment, nous commençons d'abord par construire les PCEs pour prédire la vitesse des particules en chaque point de la moyenne de la corde du diamètre de la conduite. À l'exception de $x_2/D = 0$, une correspon-

dance excellente a été observée pour tous les points de la moyenne de la corde de la section. En effet, la friction et les collisions entre les particules et le mur inférieur ont un impact significatif sur la vitesse des particules dans cette zone. Un profil de vitesse asymétrique moyen ainsi qu'une faible variance de la vitesse solide sont en effet remarqués au même endroit (cf. Figure 5.9). La distribution

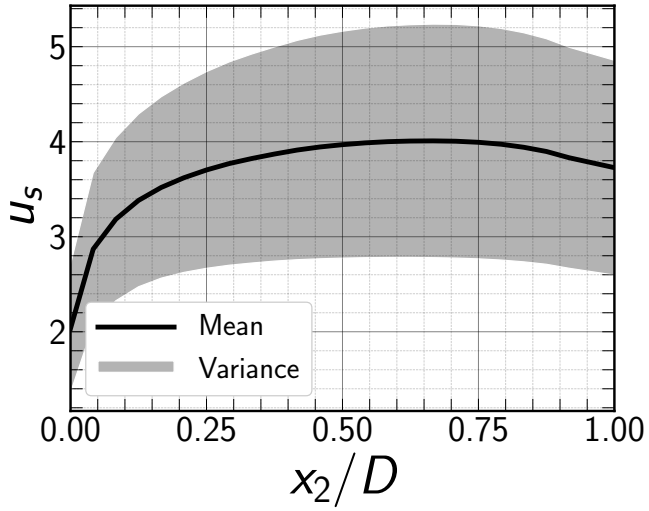

Figure 5.9: Moyenne et variance du profil de vitesse des solides le long du diamètre de la conduite

spatiale à une dimension de l'indice de Sobol total des profils de vitesse des solides est représentée dans la Figure 5.10. Lorsque les particules sont situées près du

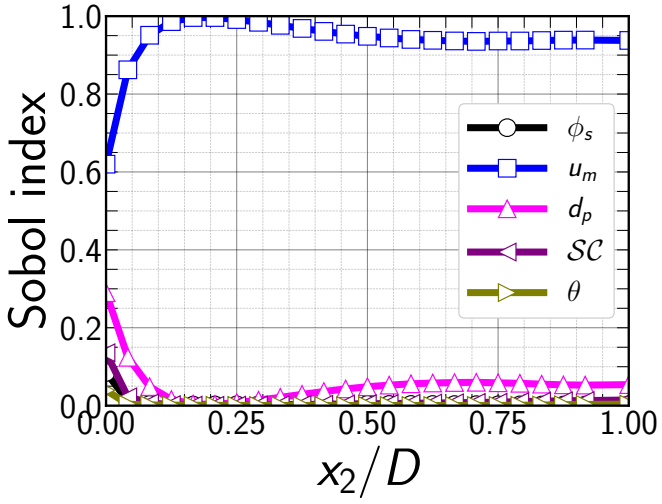

Figure 5.10: Distribution spatiale unidimensionnelle des indices de Sobol totaux pour le profil de vitesse des solides.

mur inférieur, leur variabilité de vitesse est influencée par tous les paramètres sauf l'angle d'inclinaison θ. Comme discuté précédemment, cette région présente

une concentration élevée de solides qui est amplifiée par une augmentation du diamètre des particules, renforçant ainsi l'impact de la friction et des collisions avec la paroi de la conduite. Par conséquent, ces effets entraînent une réduction de la vitesse des particules. Les phénomènes observés dans cette région démon-

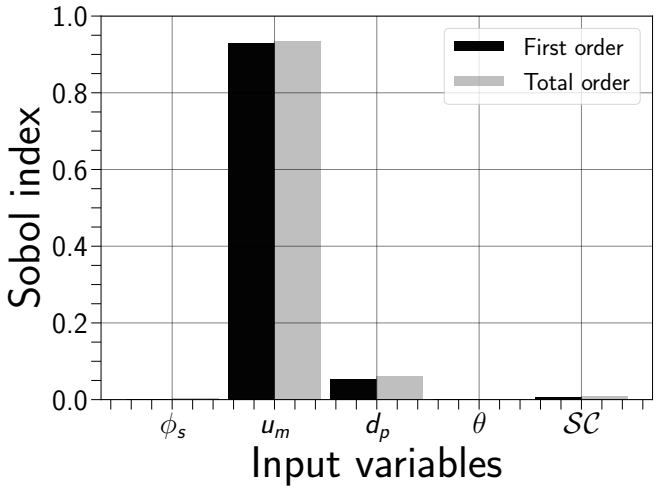

Figure 5.11: Indices de Sobol agrégés du premier ordre et totaux pour la vitesse des solides.

trent que les caractéristiques de l'écoulement favorisent un régime d'écoulement stratifié, communément appelé écoulement à deux couches. Selon les graphiques à barres des indices de Sobol de premier ordre et totaux dans la Figure 5.19, la vitesse des particules in situ dans les écoulements de suspension est significativement influencée par la vitesse du mélange d'entrée u_m et la taille des particules d_p. Aucune interaction significative n'est observée entre ces paramètres.

5.1.4 Conclusion

Les résultats obtenus à partir de l'étude fournissent des informations sur l'impact des incertitudes du système sur la consommation d'énergie des écoulements de suspension dans les pipelines, et mettent en évidence l'importance de prendre en compte ces incertitudes afin d'optimiser l'efficacité énergétique.

Les indices de Sobol calculés pour la perte de charge démontrent que la variabilité de la perte de charge est fortement influencée par les effets de la vitesse du mélange, u_m, et du diamètre des particules, d_p. Par conséquent, réduire la vitesse du mélange peut aider à atténuer la friction des parois causée par les solides. Cependant, pour maintenir les solides en suspension, ils doivent être transportés par le liquide à une vitesse minimale. Les pertes de pression sont également affectées par la taille des particules des solides; des particules plus grosses nécessitent des vitesses de transport plus élevées. Lorsque la densité des particules diffère de celle du fluide, les suspensions avec des particules très grandes deviennent fortement stratifiées, ce qui entraîne une augmentation de la friction dans le pipeline

en raison d'une combinaison de la friction du fluide et de la friction de Coulomb entre les particules et la paroi de la conduite. Ainsi, utiliser des vitesses proches de la condition de dépôt et employer des particules de taille moyenne-fine est optimal pour le transport efficace de suspensions dans les pipelines. Sur la base de l'effet marginal de la vitesse de mélange u_m, une vitesse de transport minimale d'environ $2m/s$ a été déterminée. La concentration de solides, ϕ_s, semble avoir une influence mineure sur la perte de charge d'écoulement dans la plage de variation proposée. L'effet bivarié de cette dernière avec la vitesse de mélange sur la perte de charge (voir Fig. 5.12) confirme que lorsque l'on opère autour de u_{dl}, des niveaux de perte de charge faibles sont assurés, même à la concentration de solides la plus élevée, soit 40%

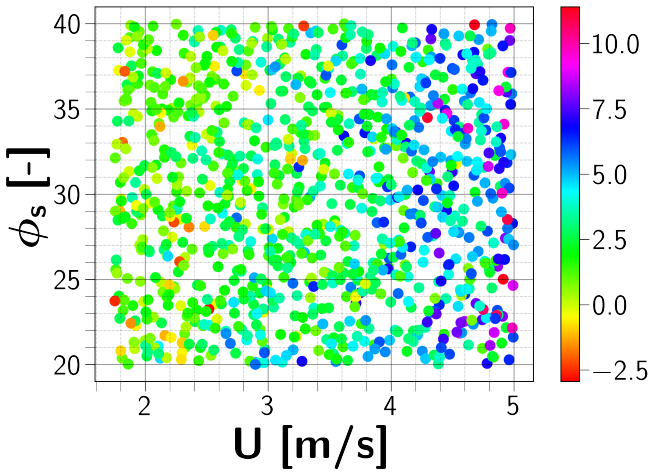

Figure 5.12: L'effet bivarié de la concentration solide ϕ_s et de la vitesse de mélange u_m

Pour approfondir l'étude, nous avons examiné la distribution unidimensionnelle des solides à travers la section de la conduite. Les indices de Sobol de la distribution de concentration de solides nous ont permis d'identifier la zone spatiale d'influence de chaque paramètre. Les résultats indiquent que la variabilité de la distribution des solides sur le diamètre de la conduite est principalement contrôlée par la concentration de solides initiale, ϕ_s, et la taille des particules, d_p. En nous basant sur la moyenne et la variance du profil de solides, nous concluons que la boue étudiée appartient à la catégorie des boues "en décantation", où le contact particule-paroi est le mécanisme prédominant. Les concentrations élevées de solides augmentent la friction, mais dépendent du rapport entre la concentration de solides et la concentration maximale de décantation. La zone de forte concentration de solides, favorisée par une augmentation de la taille des particules, favorise les effets de friction et de collisions avec la paroi de la conduite, encourageant un régime d'écoulement stratifié, également connu sous le nom de régime d'écoulement à deux couches. Pour assurer un transport efficace de la boue, il est crucial de contrôler la vitesse d'entrée, u_m, et la taille des particules,

d_p. La vitesse d'entrée du mélange solide-liquide doit être diminuée autant que possible tout en s'assurant de ne pas descendre en dessous de la limite de dépôt de vitesse pour éviter la sédimentation totale des particules. Les tailles de particules devraient également être dans la plage optimale de particules moyennes à fines. De plus, cette recherche sert de prototype pour démontrer la valeur de l'analyse globale de sensibilité (GSA) et de l'analyse d'incertitude (AI) pour comprendre le comportement des écoulements de boue complexes. De telles recherches sont essentielles pour la conception sûre et l'évaluation des risques des systèmes de transport de boues.

5.2 Quantification de l'incertitude et Analyse de sensibilité globale pour le transport de suspension en 2D

Pour approfondir notre étude sur l'écoulement de la boue, nous examinons les distributions bi-dimensionnelles de nos indicateurs de sortie (QoI). Cette partie développe et applique une approche d'ordre réduit non intrusive pour le transport bi-dimensionnel des suspensions. En raison des caractéristiques physiques compliquées des équations de Navier-Stokes biphasiques, qui présentent des gradients abrupts et des structures localisées dans la réponse de l'écoulement de boue, la méthode de Décomposition Orthogonale Propre (POD) [Raisee et al., 2015], est utilisée dans le présent travail. La méthode de décomposition orthogonale propre (POD) permet de traiter un système de grande dimension avec un système de basse dimension [Dubreuil et al., 2014]. Cette approche consiste à établir un ensemble de valeurs propres orthogonales qui sont représentatives de la physique simulée. Dans les quantifications d'incertitude, la POD permet de réduire la taille d'un vecteur aléatoire produit par le modèle. Ainsi, l'incertitude est appliquée pour chaque direction donnée par les vecteurs propres λ_i.

5.2.1 Résultats numériques

Cette section évalue l'efficacité computationnelle de l'approche de décomposition orthogonale propre suggérée pour l'analyse des écoulements de boues. Pour chaque cas de test, nous comparons les résultats de la moyenne et de la variance de la solution potentielle en utilisant deux méthodes, à savoir MC (Monte Carlo) et POD-PCE (Proper Orthogonal Decomposition - Polynomial Chaos Expansion). Nous considérons le problème de l'écoulement de boues dans un domaine carré $\Omega = [0, 14] \times [-0.05, 0.05]$. Ainsi, nous résolvons l'écoulement bi-dimensionnel à deux phases de telle sorte que sa solution déterministe soit obtenue à partir des équations de Navier-Stokes pour les écoulements diphasiques. Dans ce contexte, nous cherchons à évaluer l'incertitude associée aux quantités d'intérêt, qui comprennent la concentration en solides, la vitesse et la distribution de pression sur

la conduite plan.

Concentration en solides en 2D

Nous extrayons la solution sur une grille structurée comprenant un total de 18894 nœuds en coupant une section du plan médian. Ensuite, la construction des modèles de substitution POD-PCE est établie. Initialement, l'objectif principal est de démontrer l'efficacité numérique des méthodes susmentionnées pour quantifier les incertitudes dans les écoulements de boues. La figure 5.22 présente les solutions de concentration moyenne en solides obtenues à partir de la simulation stochastique, ainsi que la solution exacte déterministe. Pour faciliter la comparaison, nous avons inclus dans la figure l'écart entre les deux solutions.

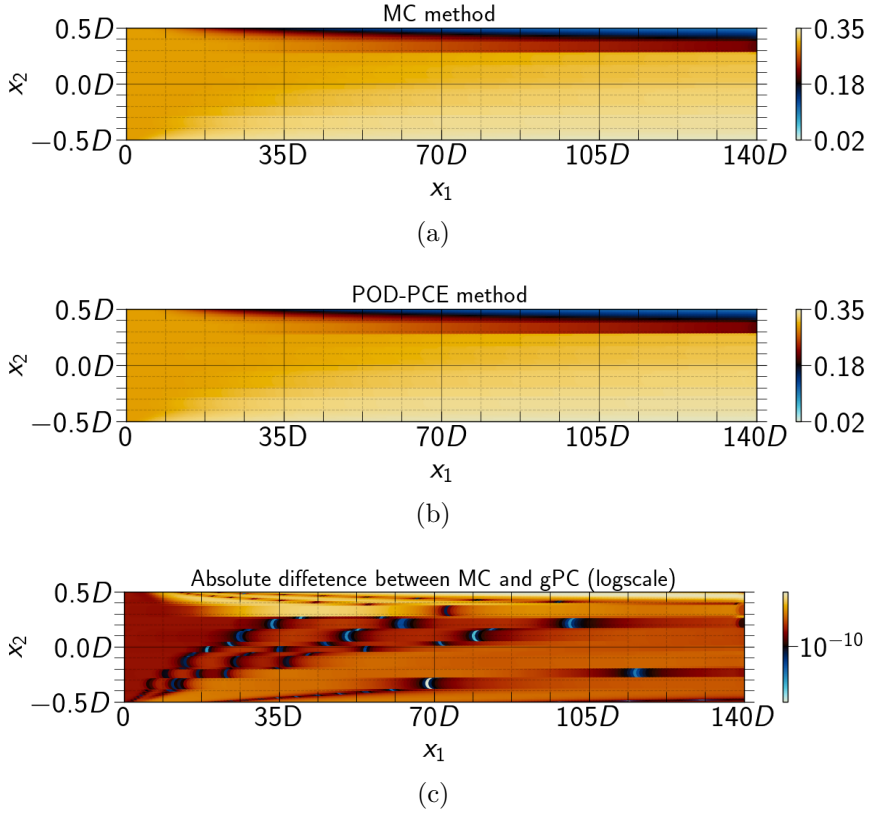

Figure 5.13: Concentration moyenne en solides ϕ_s obtenue pour la simulation stochastique (a), la solution exacte déterministe (b) et la différence entre les deux solutions (c) obtenues pour un problème d'écoulement de boue.

La méthode stochastique aborde efficacement la distribution de la concentration en solides, générant des résultats numériques exempts d'oscillations non-physiques. Le modèle de substitution nécessite uniquement 12 décompositions au lieu des 18894 décompositions représentant le nombre total de nœuds dans le modèle numérique 2D. Dans l'ensemble, les résultats suggèrent que la réduction n'a pas d'effet significatif sur la précision de l'UQ.

La Figure 5.14 illustre les résultats obtenus pour la variance. La distribution

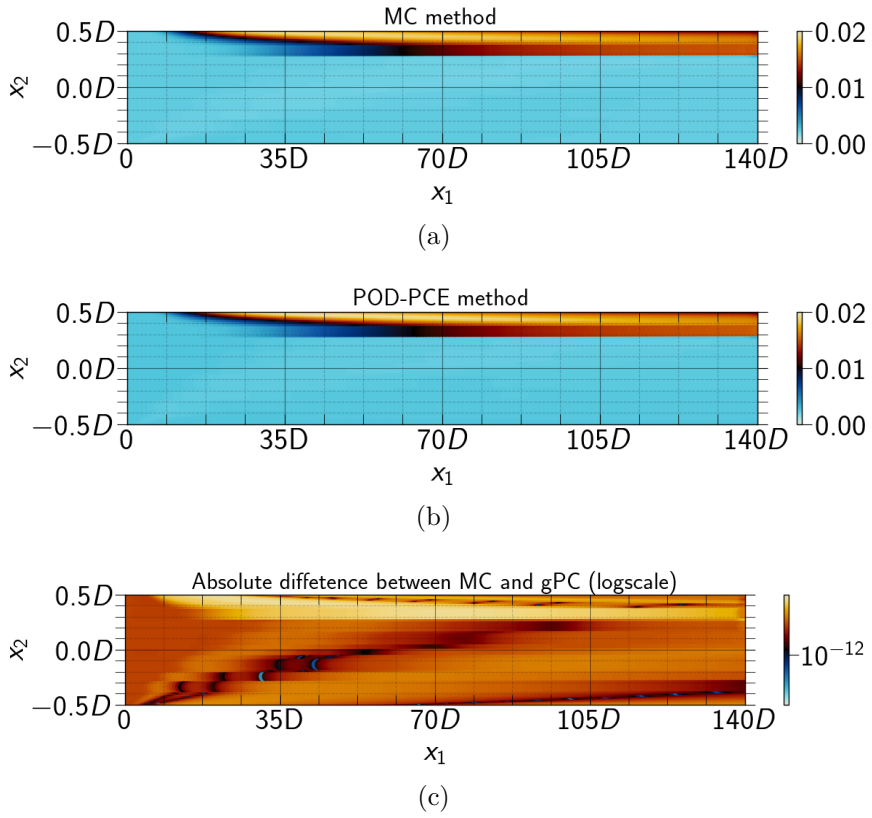

Figure 5.14: Même que la Figure 5.13, mais pour la variance.

de la concentration moyenne de particules solides reflète le comportement général de l'écoulement dans le cas de la boue de phosphate. Les résultats de l'analyse 2D confirment les résultats obtenus lors de l'étude initiale d'UQ, indiquant que la concentration moyenne des particules dans l'écoulement de boue de phosphate est stratifiée en deux couches distinctes. Cela confirme que l'écoulement de la boue est de type décantation. Dans le cœur et la paroi inférieure de la conduite où les particules se déplacent lentement, la variance de la concentration solide est insignifiante. Cependant, la paroi supérieure présente les valeurs de variance les plus élevées en raison de l'écoulement relativement clairsemé et de l'augmentation de la mobilité des particules et de leur énergie cinétique. La méthode PCE-POD donne des résultats équivalents au modèle d'ordre complet décrit dans la section 5.1.3, concernant les indices de Sobol d'ordre premier et total.

Vitesse de solide 2D

Notre deuxième *QOI* consiste en des distributions de vitesse bi-dimensionnelles de particules. La capacité de la méthode POD-PCE proposée à récupérer la vitesse des particules d'un pipe plan est examinée. Nous présentons dans la Figure 5.15

les résultats de la simulation stochastique et de l'approche déterministe pour la vélocité moyenne des particules, ainsi que la différence entre les deux.

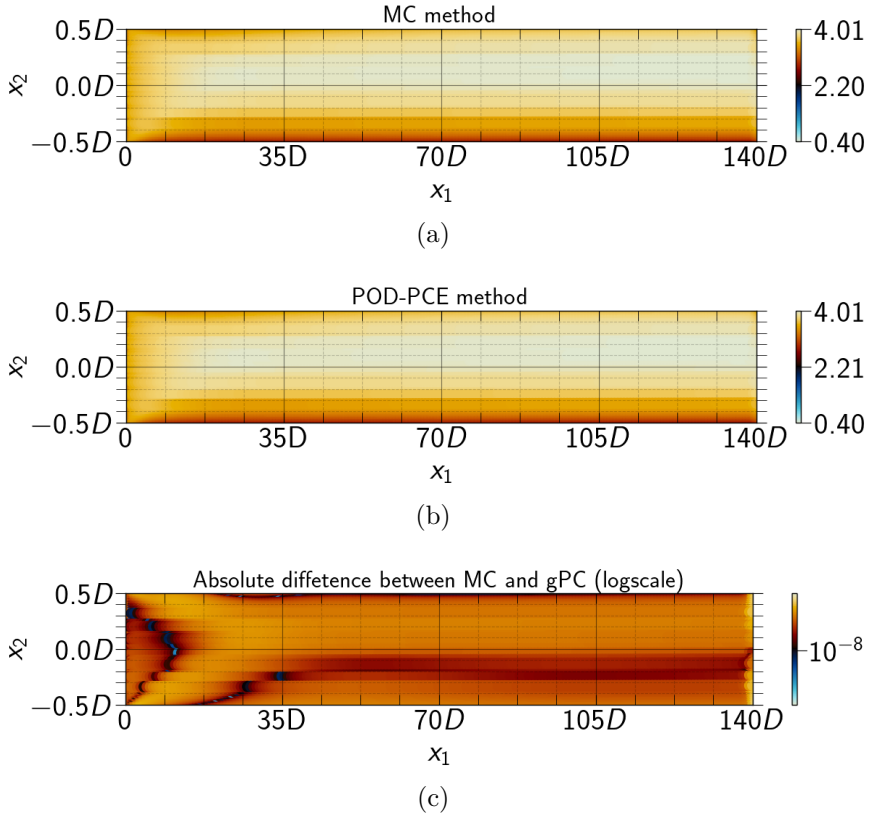

Figure 5.15: Vitesse solide moyenne u_s obtenue pour la simulation stochastique (a), la solution déterministe exacte (b) et la différence entre les deux solutions (c) obtenues pour un problème d'écoulement de suspension.

Sous les conditions considérées de l'écoulement de la suspension, les deux méthodes montrent des tendances comparables dans les profils de vélocité des particules. La Figure 5.16 présente les résultats comparatifs obtenus pour la variance.

La présence d'un profil asymétrique dans la distribution de la vélocité solide moyenne est probablement un facteur contributif aux différences observées dans la variance de la concentration solide à travers les différentes parois de la conduite. Plus précisément, l'asymétrie du profil de vélocité vers la paroi supérieure indique que l'écoulement dans cette région est relativement plus dilué et que les particules ont une énergie cinétique plus élevée. Cela est cohérent avec les valeurs de variance les plus élevées observées dans cette zone. La sensibilité du champ de vitesse solide à la variabilité de nos paramètres aléatoires donne presque les mêmes résultats comme illustré dans la Figure 5.11.

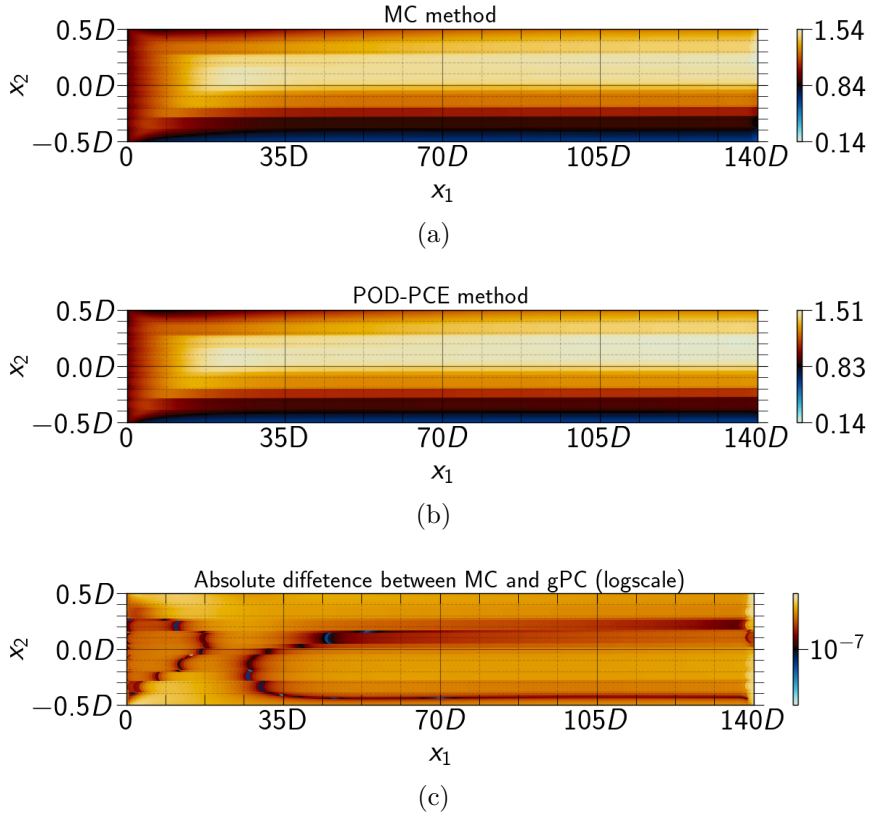

Figure 5.16: De même que pour la Figure 5.27, mais pour la variance.

Distribution de pression 2D

La distribution de pression à l'intérieur de l'écoulement de boue est le troisième objectif de qualité (QOI) abordé dans cette étude. Il convient de noter que les résultats présentés ici pour la pression sont exprimés en unité de bar. Les résultats sont représentés dans la Figure 5.32.

La Figure 5.18 présente les résultats comparatifs obtenus pour la variance de la pression. On peut conclure que les deux modèles de substitution capturent efficacement l'incertitude manifestée sur l'ensemble du domaine physique pour le problème d'écoulement de boue considéré. Compte tenu de l'effort de calcul relativement faible requis pour mettre en œuvre la méthode PCE-POD, elle peut être considérée comme un algorithme idéal pour effectuer la quantification de l'incertitude dans les écoulements de boue computationnels qui impliquent des entrées stochastiques.

En se basant sur la distribution de la pression moyenne de l'écoulement, on peut déduire que la pression de notre boue diminue généralement dans la plage de variabilité de nos entrées aléatoires. L'évolution de la pression le long du pipeline est évidente à partir du schéma d'écoulement stratifié illustré dans la sous-section 5.2.1. Ces types d'écoulements de boue produisent des fluctuations dans la concentration et la vitesse des particules, ce qui entraîne une résistance

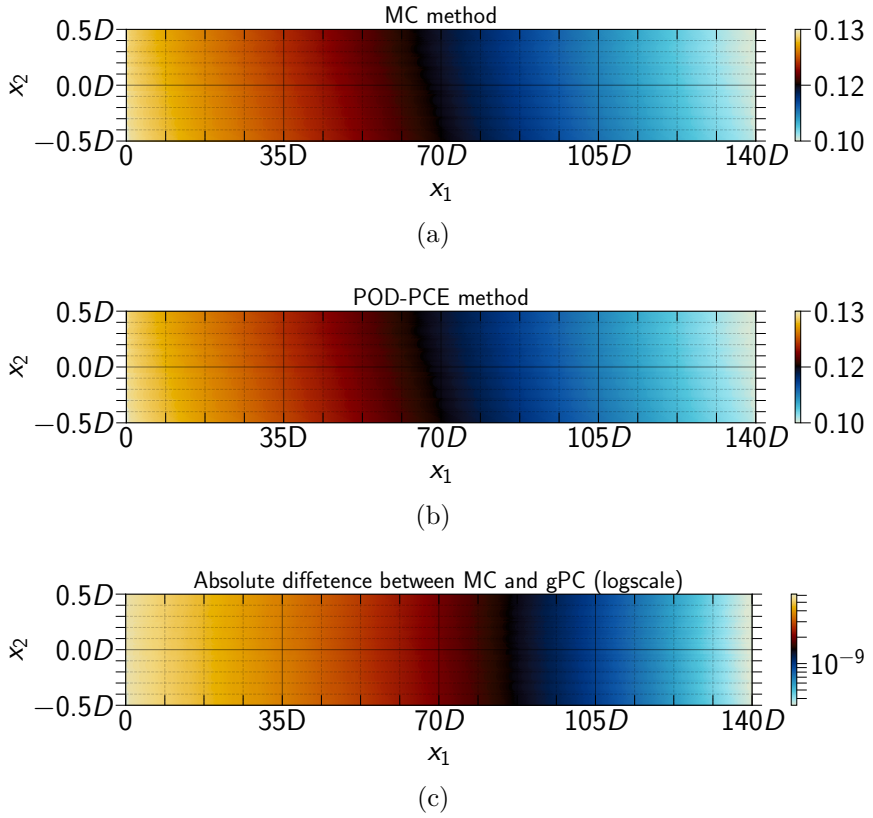

Figure 5.17: La pression moyenne de l'écoulement P obtenue pour la simulation stochastique (a), la solution déterministe exacte (b) et la différence entre les deux solutions (c) obtenues pour un problème d'écoulement de boue.

par frottement et une diminution de la pression. L'entrée de la conduite présente les valeurs de variance les plus élevées car la pression à l'entrée varie en fonction de la vitesse.

Le modèle réduit génère un classement comparable des paramètres les plus influents, cependant, il y a des variations dans l'amplitude des indices de Sobol.

5.3 Conclusion

Dans le présent chapitre, une analyse efficace de la quantification de l'incertitude pour les problèmes d'écoulement de boue est présentée et discutée. La complexité et la grande non-linéarité des écoulements de boue rendent de telles études utiles pour fournir des informations physiques sur le processus en question. Dans la première partie, la quantification de l'incertitude est réalisée en utilisant l'expansion du chaos polynomial complet pour les quantités d'intérêt (QoIs) scalaires et unidimensionnelles. Nous avons analysé l'impact des paramètres incertains sur les sorties d'intérêt, permettant ainsi d'évaluer l'efficacité énergétique du transport de boue. Les conclusions de l'étude de l'UQ et de la GSA dans cette partie sont

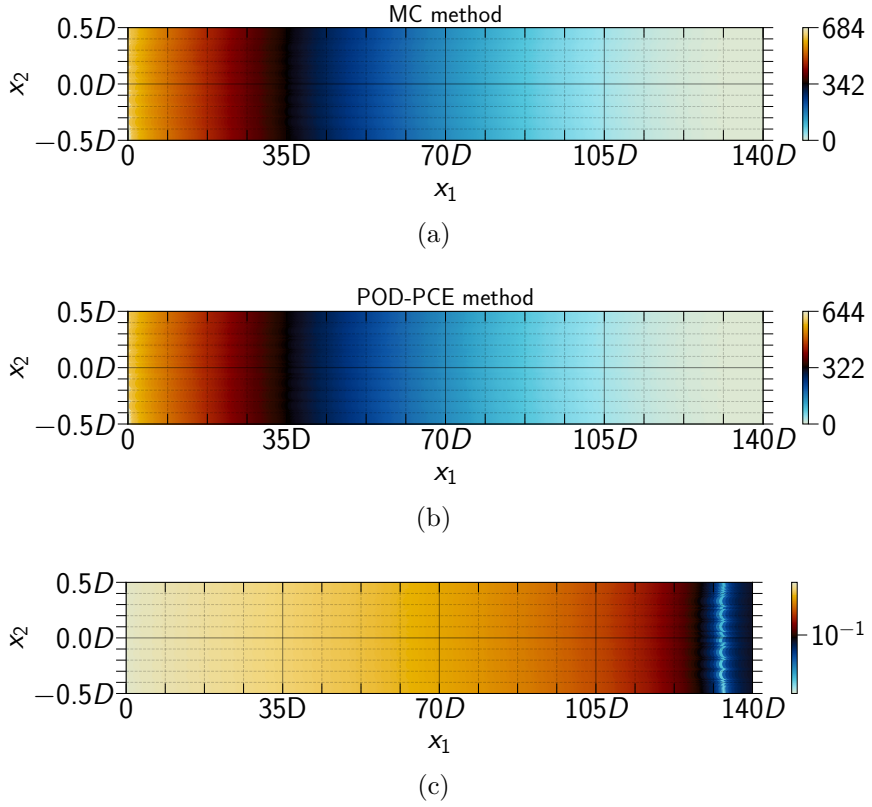

Figure 5.18: Same as Figure 5.17 but for the variance.

présentées dans la sous-section 5.1.4. La deuxième partie de ce chapitre était consacrée à l'étude de l'UQ et de la GSA dans un cas bi-dimensionnel d'écoulement de boue de phosphate. Un modèle d'ordre réduit est appliqué aux équations TFM bidimensionnelles. Les résultats numériques montrent que le modèle d'ordre réduit développé est capable de produire des résultats acceptables pour de telles quantités statistiques. Les distributions de moyenne et de variance obtenues à partir du modèle d'ordre réduit sont comparées à celles calculées à l'aide des simulations déterministes. Dans cette étude, nous avons également réalisé une analyse globale de sensibilité complète et une quantification de l'incertitude pour nos QoIs bidimensionnelles. La variabilité de chaque QoI est bien représentée dans ce cas et fournit plus d'informations sur la distribution des sorties. Il est confirmé que la boue de phosphate dans ces conditions de fonctionnement est classée comme un écoulement à deux couches (stratifié). Les résultats de la GSA ont permis de quantifier l'incertitude de nos entrées. Il est donc important de donner la priorité à la maîtrise de ces paramètres dont l'incertitude a un impact plus important sur l'incertitude globale de la simulation. En concentrant nos efforts sur ces paramètres critiques, nous pouvons obtenir un meilleur contrôle et une meilleure optimisation de l'écoulement de boue, ce qui conduit à des simulations plus fiables et précises. L'approche statistique utilisée dans cette étude est supérieure aux analyses de sensibilité classiques "un à la fois", qui consistent

à figer tous les paramètres sauf un pour étudier l'effet du paramètre restant. En utilisant l'analyse globale de sensibilité (GSA) et la quantification de l'incertitude (UQ), nous pouvons mieux comprendre le comportement du système complexe des écoulements de boue dans les pipelines. En résumé, cette étude sert de prototype pour mettre en évidence les avantages de l'utilisation de l'analyse globale de sensibilité (GSA) et de la quantification de l'incertitude (UQ) pour mieux comprendre le comportement des écoulements de boue dans les pipelines, qui est un système complexe. En utilisant l'Analyse de Sensibilité Globale (GSA) et la Quantification de l'Incertitude (UQ), nous pouvons identifier les paramètres critiques qui influencent la performance du système et optimiser l'écoulement pour une meilleure efficacité et fiabilité. En démontrant l'efficacité de ces techniques, cette étude ouvre la voie à de futures recherches dans le domaine de l'analyse et de l'optimisation des écoulements de suspension.

6

Experimental validation through surrogate modeling

Objectives:

In this chapter, the experimental approach utilized to validate the two-phase CFD model formulated in chapter 4 is presented. However, the computational complexity associated with performing three-dimensional multiphase CFD simulations makes it extremely difficult to compare with experimental data from real industrial long pipelines. To overcome these computational challenges, surrogate models are utilized to execute experimental validation in this thesis. Section 6.1 is dedicated to the development of a novel CFD-based surrogate model that can accurately predict the pressure drop in slurry flows. The performance of this new model is then evaluated by comparing it to experimental data from the industrial plant's phosphate flow in section 6.2. In order to facilitate the utilization of this new model, a graphical user interface (GUI) was developed within the MSDA group and is presented in section 6.3.

Contents

6.1 Surrogate modeling

6.1.1 Introduction

Surrogate modeling is employed in various engineering and scientific disciplines where complex computer simulations or physical experiments are utilized Elkarii et al. [2023a,c]. In such scenarios, acquiring more data necessitates conducting additional experiments, leading to significant economic or material expenses, along with computationally demanding operations. It is comparatively simpler to obtain such information from a surrogate model as it incurs significantly lower computational costs. There are multiple approaches proposed in literature to obtain a surrogate such as polynomial regression, kriging, and neural networks. Surrogate model, also known as meta-model or a response surface model, has been widely applied in many different fields of science and engineering. Here is a brief review of some of the common applications of surrogate modeling:

- Chemical process optimization: Surrogate models can be used for process modeling [Meert and Rijckaert, 1998], for process design and optimization [Fernandes, 2006, Palmer and Realff, 2002], and process control [Bloch and Denoeux, 2003]. By building a surrogate model of the chemical process, engineers can quickly evaluate different control strategies and process conditions.

- Aerospace engineering: Surrogate models are used to optimize the design of aircraft components and systems [Balabanov et al., 1998, Giunta et al., 1997]. For example, a surrogate model can be used to predict the aerodynamic performance of a new aircraft design, or the structural performance of a new engine component.

- Environmental science: Surrogate models have been used to optimize environmental monitoring systems and to model the behavior of complex environmental systems. For example, a surrogate model can be used to predict the distribution of pollutants in a waterway or to optimize the placement of air quality sensors in a city [Kim and Hwangbo, 2018].

- Computational fluid dynamics (CFD): Surrogate models have been used to speed up the optimization of complex fluid dynamic simulations. For example, a surrogate model can be used to predict the performance of a new design in a wind tunnel, without the need for expensive wind tunnel tests.

Here, the surrogate model is used as a mathematical representation of a computational fluid dynamics (CFD) model that can be used to predict the output of the CFD model for a given set of inputs. This methods can be used to create a variety of different types of surrogate models, including global models that can

be used to predict the output of the CFD model for any set of inputs, and local models that are only accurate for a specific region of the input space. The objective is to reduce the computational cost of running a CFD simulation, as they can provide accurate predictions with a much smaller computational burden than the original CFD model. Several models have been developed to predict the behavior of slurry flow in pipelines. These models can be broadly categorized into two groups: empirical models and computational models. Empirical models are based on experimental data and are typically used to predict the flow behavior of a specific slurry system. Examples of empirical models include the Herschel-Bulkley model and the Power Law model. And the aim is to use the CFD approach to develop pressure drop models for complex fluids and to understand the physics behind . Moreover, once the simulations validated they can be used to develop response models (or surrogate models) for other physical quantities than pressure drops. For instance, in a slurry pipe flow a sedimentation model along pipe of different geometries can be useful for applications.

6.1.2 Pressure drop surrogate model

Surrogate models are increasingly being built for use in control and decision support in various industries. For a piping industry, prediction of the pressure drop of the flow along the pipe is of paramount importance. Especially for two-phase slurry flows, good pressure drop control is essential, as it allows on one hand to optimize the energy consumption of the pumps, and on the other hand to avoid problems resulting from the sedimentation of the solid phase and the clogging of the pipe. Currently, there are no theoretical methods for predicting the pressure drop when dealing with settling suspensions. Many empirical equations correlate data in certain situations, but none have yet been proposed to provide accurate predictions of pressure drops for general solid-liquid mixture. The most pertinent correlations for determining pressure drop will be reviewed briefly hereafter. To the best of our knowledge, Durand [1953] was one of the first to suggest a pressure loss correlation in dimensionless form, based on experimental data for sand and gravel slurries. Another way to approach the problem is by using dimensional analysis as performed by Turian and Yuan [1977]. They regarded spherical particles with a close size distribution moving through smooth pipes. In this study, two correlations are examined for their ability to fit the CFD results. The first one, proposed by Turian and Yuan [1977], is given by

$$\Delta p = \frac{2\varrho L\|u\|^2}{D}\left(f + a_1\phi_f^{a_2} f^{a_3}\mathcal{C}_d^{a_4}\left(\frac{\|u\|^2\sqrt{\mathcal{C}_d}}{gD(\mathcal{S}-1)}\right)^{a_5}\right), \tag{6.1}$$

where $a_1, \ldots, a_5$ are constants that depend only on the flow regime for which the pressure drop is to be calculated. Three flow regimes within this correlation are explored in this section: homogeneous flow, heterogeneous flow and stratified or two-layer flow. The constants $a_1, ..., a_5$ for homogeneous, heterogeneous flow and

for the two-layer flow are given below in table 6.1.

Table 6.1: Constants of Eq. (6.1) [Turian and Yuan, 1977]

Flow Pattern	Constants				
	a_1	a_2	a_3	a_4	a_5
Homogeneous Flow	0.8444	0.5024	1.428	0.1516	−0.3531
Heterogeneous Flow	0.5513	0.8687	1.200	−0.1677	−0.6938
Two-Layers Flow	0.9857	1.018	1.046	−0.4213	−1.354

The second correlation is due to Weber [1986], it is discussed in [Abd Al Aziz and Mohamed, 2013] and reads:

$$\Delta p = \left[\alpha^{1/m} \left(\frac{Dg}{\|u\|^2} \frac{\mathcal{S}-1}{\sqrt{\mathcal{C}_D}} \right)^{1.5/m^3} \phi_s + 1 \right] f \frac{\varrho_s}{2} \|u\|^2 \frac{L}{D}, \tag{6.2}$$

where $\alpha = 83$, $m = 2 - (d_{s,90}/d_{s,10})^{-0.04}$, in which $d_{s,90}$ is the grain size at 90% passing sieve and $d_{s,10}$ is grain size at 10% passing sieve.

Calculation of the optimal friction coefficient f for each particle diameter is used to perform the fitting process of both correlations as portrayed in Fig. 6.1. In the case of this solid-liquid flow, previous correlations demonstrate their limitations in accurately estimating the hydraulic gradient, with the exception of Turian and Yuan [1977]'s one, which is dedicated to homogeneous and heterogeneous flow, and which fitted the CFD data well. Furthermore, even though Turian and Yuan [1977]'s approach has yielded good results in fitting data, it has been demonstrated that it is not producing promising results and fails to correctly identify the regimes [Lahiri and Ghanta, 2010a]. On the other hand, the correlation proposed by Weber [1986] demonstrated a poor level of agreement.

To the author's knowledge, the pertinent correlations for calculating slurry flow pressure drops suggested in the literature are either totally empirical or semi-empirical. Surrogate models are classified into two types depending on their approximation strategy: (i) model driven or physics based approach ([Durlofsky, 2010]); (ii) data driven or black box approach [Kleijnen, 2015]. Reduced Order Models (ROMs) are model-driven techniques that approximate the original equations with lower order equations, hence lowering the computing cost. By contrast, data-driven techniques create the surrogate model using just the input data and output responses, while treating the CFD simulation as a blackbox. The purpose of this work is to establish the assessment of a model-driven surrogate model that can be used to estimate the pressure drop of a phosphate ore slurry flow. The suggested reduced order model, which is intended to approximate the phenomenological model, employs the empirical formula for pressure losses due

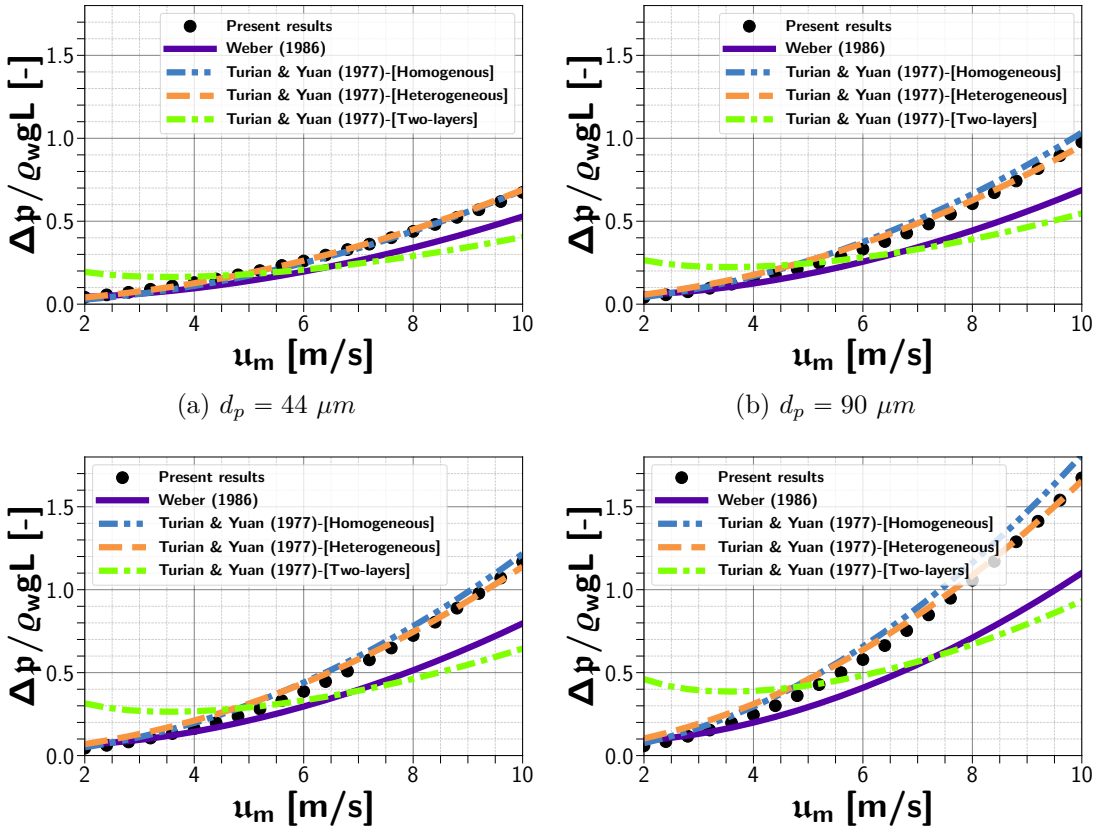

(a) $d_p = 44\ \mu m$ (b) $d_p = 90\ \mu m$

(c) $d_p = 125\ \mu m$ (d) $d_p = 250\ \mu m$

Figure 6.1: Fitting of pressure drop correlations to the CFD data for a flow containing 40% solids for different particle's diameter.

to friction in horizontal pipes, that reads

$$\Delta p_f = f_m \frac{\varrho_m L}{D} \frac{u_m^2}{2}, \tag{6.3}$$

where the density and velocity are those of the solid-liquid mixture. The surrogate model will be constructed for the estimation of the friction coefficient of the mixture f_m as function of particles' diameter and solid concentration.

The simulations will make use of the characteristics related to the phosphate slurry material and its transport operating parameters, including the particle size distribution, solid concentration, and velocity variations. The CFD database contains 525 functional points, with varied values of particles' size, solid concentration, and inlet velocities. A solid density of $\varrho_s = 2450$ kg/m^3, and a water density of $\varrho_w = 1000$ kg/m^3, are retained for the flow. The sizes of the particles range from $d_p = 44\ \mu$m to $d_p = 250\ \mu$m along with a solid concentration that goes from $\phi_s = 20\%$ to $\phi_s = 40\%$. The slurry is transported via a pipe with a diameter of $D = 100$ mm, and covering a velocity range from 2 m/s to 10 m/s. We seek to find the optimal friction factor of the slurry mixture f_m, which fits well with the

CFD results through a minimization process. The Levenberg–Marquardt algorithm (LMA) [Levenberg, 1944, Marquardt, 1963], which is a hybrid method that supports both the Gauss–Newton and steepest descent techniques to converge to an optimum solution, is utilized to carry out this optimization process. This algorithm is fast and suitable for problems that include relatively small sizes of data [Moré, 1978]. The primary step is to build an objective function that takes the values of the fitting variables, calculates the values that are to be minimized, and returns at the end the friction coefficient f_m. For such a problem, the chi-square (χ^2) statistic is often used :

$$\chi^2 = \sum_{i}^{N} \frac{\left[\mathcal{Y}_i^{\text{num}} - \mathcal{Y}_i^{\text{correlation}}(f_m)\right]^2}{\varepsilon_i^2}, \tag{6.4}$$

where $\mathcal{Y}_i^{\text{num}}$ is the set of CFD data points, $\mathcal{Y}_i^{\text{correlation}}$ (f_m) is the calculation of the pressure drop correlation and f_m is the variable in the correlation to be optimized in the fit, and ε_i is the estimated uncertainty in the data. The fitting results, at different particles' diameters and solid concentrations, are illustrated in Fig. 6.2.

A graphical surrogate model giving the fitted friction factor as a function of the particle diameter d_p and the concentration of solids ϕ_s is generated in Fig. 6.3. It is noticed that the f_m increases with both the concentration of solids and the diameter of the particles. This is due to the formation of a moving bed of particles, which has a greater wall normal shear stress in the case of coarser particles. Similar phenomena have been observed in [Gopaliya and Kaushal, 2015, 2016] and studied recently by Zhang et al. [2021] for single sized and multi-sized slurries.

At this stage, the surrogate model predictions are compared to experimental results published in the literature that employed the same physical and geometrical parameters as in this study to test its reliability. The degree of agreement between predicted and measured hydraulic gradient values can be assessed through parity plots such as those shown in Fig. 6.4. It can also be quantified by calculating the Mean Absolute Percentage Error (MAPE) over the $\mathcal{N}_{samples}$ sample points as [Messa and Matoušek, 2020]:

$$\text{MAPE}\,(i_m) = \frac{100}{\mathcal{N}_{samples}} \sum_{j=1}^{\mathcal{N}_{samples}} \left| i_{m,j}^{correlation} - i_{m,j}^{\text{exp}} \right| \cdot \frac{2}{i_{m,j}^{correlation} + i_{m,j}^{exp}} \tag{6.5}$$

with $i_m = \Delta p/\varrho_w g L$. The comparison to experimental hydraulic gradient data for a glass-beads slurry is provided in Fig. 6.4a, Fig. 6.4b, and Fig. 6.4c. This experiment [Matoušek et al., 2013] was carried out in a pipe with a diameter of $D = 100$ mm, and the slurry in this case have a solid density of $\varrho_s = 2450$ kg/m^3. The particles have a diameter $d_p = 180$ μm, and the flow velocity ranges from 1 m/s to 5 m/s. Figure 6.4d depicts additional data for hydraulic gradients for a sand-water slurry [Gillies et al., 2004]. The flow is channeled through a pipe

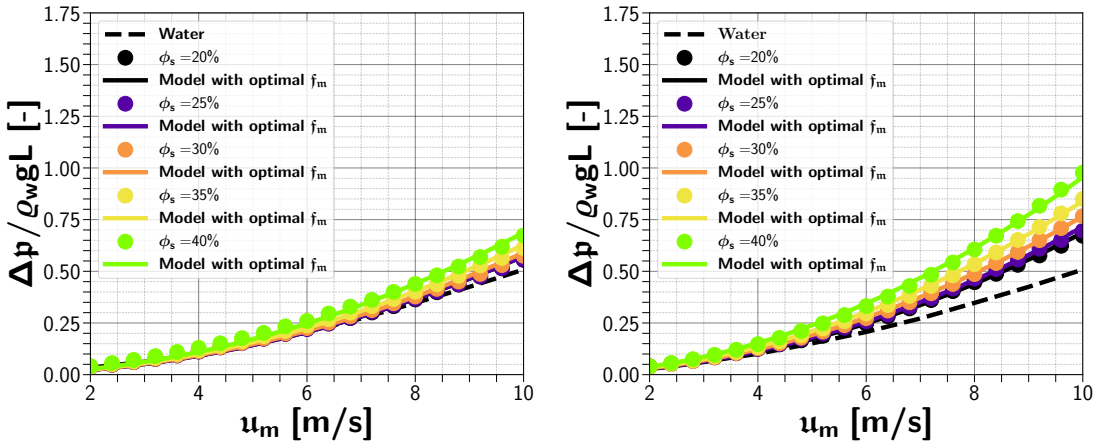

(a) $d_p = 44\ \mu m$ (b) $d_p = 90\ \mu m$

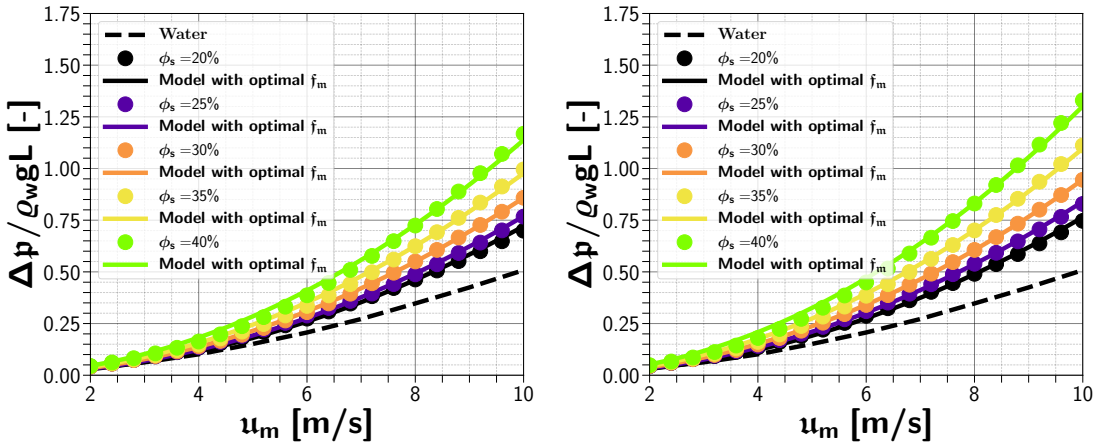

(c) $d_p = 125\ \mu m$ (d) $d_p = 160\ \mu m$

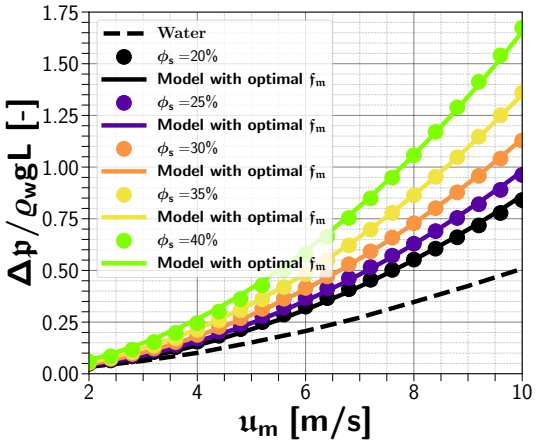

(e) $d_p = 250\ \mu m$

Figure 6.2: The model's fitting results with optimal mixture friction coefficient f_m at different particle diameters and solid concentrations.

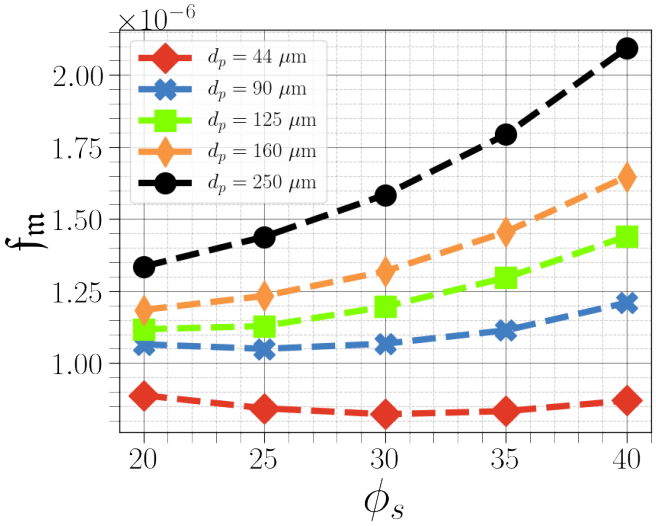

Figure 6.3: The graphical constructed surrogate model for friction coefficient of settling suspensions.

with a diameter of $D = 103$ mm, with a solid density of $\varrho_s = 2650$ kg/m^3 and particles diameter of $d_p = 90$ μm. The flow velocity goes from 1 m/s to 8 m/s.

The present results demonstrate a satisfactory degree of agreement with experimental data. In particular for hydraulic gradients associated with velocities equal to or less than 4 m/s, which corresponds to the operational range of velocities for the intended slurry instance. It is also observed that discrepancies increase when comparing data outside of the surrogate model's calibration range as in Fig. 6.4d in terms of pipe diameter and solid density. Therefore, it is concluded that even a little difference in pipe diameter from the one used to generate the surrogate model can have a significant impact on the outcome. The accuracy of the predictions of the pressure gradient is clearly affected by the resistance reduction effect due to the multi-sized slurry particle size, which is not considered as study parameter in the present evaluation. In fact, one should note that the considered two-fluid Eulerian-Eulerian approach tends to overestimate the pressure gradient when considering "big" particles, while an underestimation is more likely to occur for the "small" ones. If the attention is limited to the latter class, the predictions of pressure gradient basically lie within the interval $[-10\%, 0]$ of the measured value, with significant increase of the reliability of the model. Two reasons may contribute to explain the overestimation which characterizes the "big" particles. Firstly, the considerable dimension of the particles compared to the boundary layer thickness may cast doubt on the assumption that the solid phase behaves as a continuum within the log law region, with mean velocity given by the smooth-wall log law of Launder and Spalding [1983]. Moreover, the lack of a proper hydrodynamic lift closure model leads to noticeable estimate of pressure drop when the center of the particles lies in the log law region [Wilson and Sellgren, 2003], which is precisely the "big" particle case.

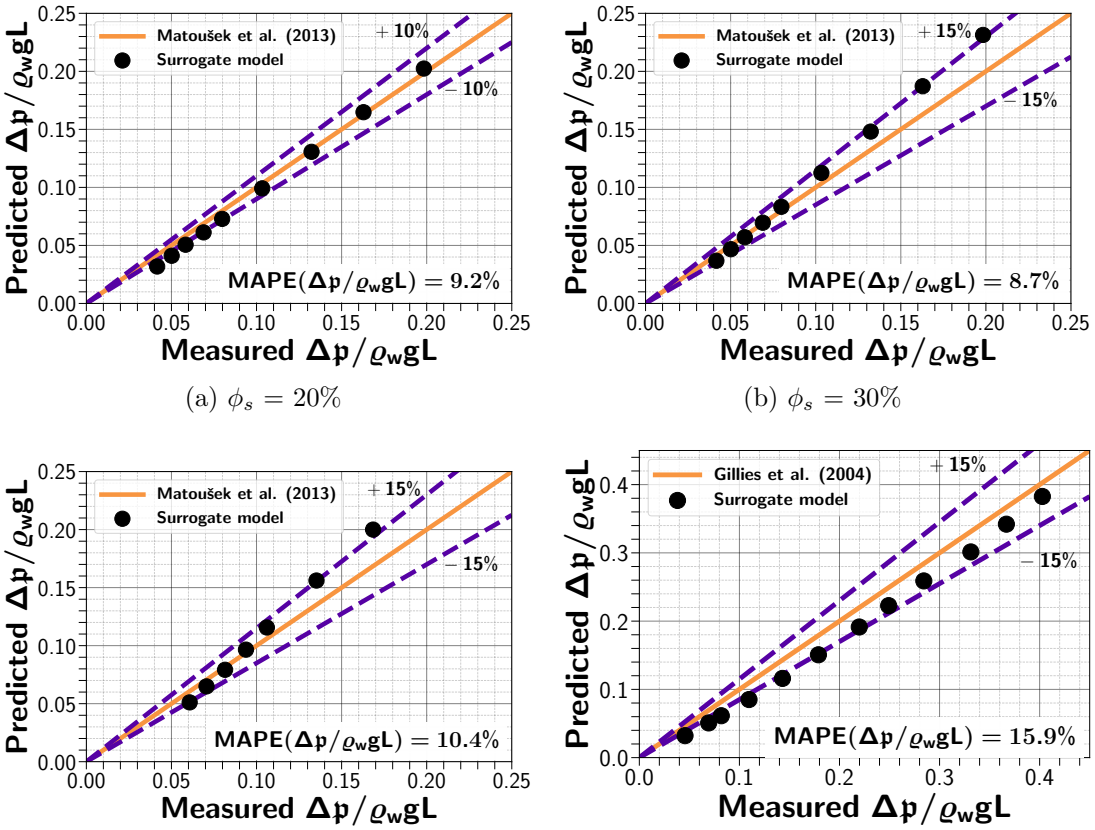

(a) $\phi_s = 20\%$ (b) $\phi_s = 30\%$

(c) $\phi_s = 40\%$ (d) $\phi_s = 24\%$

Figure 6.4: Hydraulic gradient parity graphs between predicted and measured values for different solid concentrations.

6.1.3 Conclusion

A novel CFD-based surrogate model was presented for predicting pressure loss when dealing with settling suspensions. The surrogate model was designed to cover slurry flows with particle sizes ranging from 44 μm to 270 μm, solid concentrations up to 40%, and velocity varying from 2 m/s to 10 m/s. Two transport regimes were identified, when the flow characteristics changes namely heterogeneous flow and stratified flow. It was noticed that the surrogate model outperform when velocities are equal to or less than 4 m/s. However, the model's overall validity was assessed and found to have acceptable agreements of a mean percentage error equal to or less than 15%, which may be examined further using experimental data on slurry phosphate.

The idea of developing a surrogate model using CFD appears to work effectively. The benefit of this approach is that it enables the provision of a surrogate model even in the absence of a large experimental dataset deemed adequate for providing a robust foundation for the pressure drop correlation construction. Furthermore, we demonstrated that the developed model accurately predicts the

pressure loss by at least 85 percent of a real slurry running within the inlet operating conditions for which it was built.

6.2 Experimental validation of phosphate slurry flow

In this section, experimental measurements are presented, which were conducted to validate the pressure drop model developed in Section 6.1.2. The comparison with experimental data can be conducted at either the laboratory or industrial scale. Laboratory scale refers to experimental or process conditions that are conducted in a controlled laboratory environment, typically on a small scale. It helps to investigate fundamental scientific principles, develop new technologies or validate small-scale proof of concepts. On the other hand, industrial scale refers to experimental or process conditions that are conducted on a larger scale, in industrial setting, to test the feasibility, scalability, and economic viability of a particular technology or process before it is implemented on a commercial scale. However, conducting a comparison with experimental data on a large industrial scale can be challenging due to several factors, such as the complexity and variability of the industrial environment, the need to collect and analyze a vast amount of data from multiple sensors, and the difficulty in controlling all operational conditions. Unfortunately, we were unable to set up a laboratory or pilot-scale test loop in this thesis that would have enabled us to thoroughly validate our CFD model by controlling all operational conditions. Thus, the experimental data used to assess our surrogate model for the phosphate slurry is directly obtained from pre-installed sensors at the industrial plant. The schematic diagram in section 2.1.1 provides a detailed illustration of the pipeline system, which incorporates a total of five pressure sensors placed at strategic points along the main pipeline. Notably, the densitometer utilized for concentration measurement is only installed at the pipeline's inlet and outlet points. Due to this limitation, our numerical simulations were solely based on the experimental investigations conducted on the pressure drop of phosphate slurry flowing through a series of horizontal and inclined pipes.

Although we attempted to compare the pressure data obtained from the main pipeline with our CFD numerical model, the significant distance between the sensors made it impossible to achieve a reliable comparison. Moreover, the high computational cost associated with the large-scale industrial system made it infeasible to use the experimental data for validating our model. The application of surrogate modeling proves to be useful in this scenario, as it reduces the computational cost and enables the calculation of pressure drop for slurry flows over long pipe distances. In order to compute the pressure drop in horizontal pipes, two surrogate models were developed. The first model is based on gPC and is extensively discussed in chapter 5. By using the gPC analysis, we obtained a

polynomial model that can accurately compute the pressure drop caused by friction in a specific range of operation. The second model is based on CFD, which predicts the friction coefficient, and is then utilized to compute the pressure drop caused by friction (cf section 6.1.2). Both surrogate models face the issue of requiring scaling up to the industrial scale, as the real pipe diameter is nine times larger than the diameter used to construct our surrogate models. Regarding the polynomial model, it requires a new design of experiment consisting of 1000 samples, for which deterministic simulations must be carried out in the larger pipe. However, repeating the same approach is computationally expensive and requires a significant amount of computational resources. As for the second approach, efforts to scale up the friction coefficient for larger pipe diameters through a similarity study [Hoyt, 2003], did not yield positive results, due to the high non-linear flow behavior. To address the issue of scaling up the friction coefficient for the larger pipe diameter, the second approach was adopted to develop a new mixture friction coefficient, denoted as f_m, that takes into account the relevant physical parameters. However, to reduce the computational burden, the CFD simulations were conducted only for the specific physical parameters of the phosphate slurry flow, in terms of the solid concentration and particle size. The resulting f_m value obtained from this study is 0.028, which will be used in the subsequent comparisons.

It should be noted that the presence of water plugs between the slurry batches can cause variations in the density of the slurry. It is worth mentioning that the surrogate model has been developed assuming a uniform initial solid concentration for each run. Thus, comparing the results obtained from the surrogate model with the data collected from the main pipeline can be challenging due to the dynamic nature of the solid concentration in the actual process. Therefore, to perform a comparison with real data, a secondary pipe was considered. This pipe transports continuous batches of phosphate slurry from the processing plant BeniAmir to the main station. The pipeline stretches for 15 km and follows the natural contours of the terrain, resulting in varying inclinations, as illustrated in Fig. 6.5. In this scenario, pressure sensors are installed at both the entrance and exit of the pipeline. The aim is to compare the pressure drop across the aforementioned pipe network. We monitor the pressure measurements at both the inlet and outlet. We obtain the outlet pressure reading from the sensor and then use it to compute the inlet pressure. The network is divided into 121 elementary pipes based on changes in elevation. An example of the segmentation for the first 2 km of the network is presented in Table 6.2. The analysis starts with the final elementary pipe, denoted as P_{121}, for which the outlet pressure is known. From there, the inlet pressure can be calculated. The calculated inlet pressure of P_{121} becomes the outlet pressure of the preceding elementary pipe, P_{120}, for which the inlet pressure can be computed. This iterative process is repeated for each successive elementary pipe until the inlet pressure at the beginning of the network is obtained.

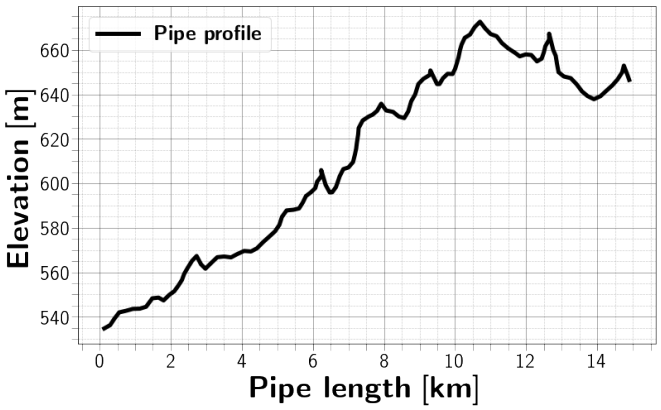

Figure 6.5: BeniAmir Pipe profile

Table 6.2: Samples of the considered pipe segments

Pipe segments	Length (km)	Inclination θ °
P_1	0.13	2.083765743
P_2	0.29	3.846307056
P_3	0.41	4.060335139
P_4	0.55	1.006333062
P_5	0.74	1.166762971
P_6	0.93	0.005341377
P_7	1.13	0.043999938
P_8	1.30	5.245571857
P_9	1.48	0.011907536
P_{10}	1.65	-0.043328083
⋮	⋮	⋮
P_{117}	14.63	3.751768003
P_{118}	14.68	4.365985367
P_{119}	14.78	4.159718342
P_{120}	14.82	-6.111615562
P_{121}	14.90	-2.780785081

Before proceeding to the comparison, it is worth mentioning that the surrogate model developed in this study is only applicable to horizontal pipes and does not consider the effect of pipe inclination. Nevertheless, the global sensitivity analysis presented in section 5.1.5 revealed that pipe inclination does not impact pressure drop due to friction. Therefore, the contribution of the inclination can be added solely to the friction component of pressure drop to determine the total head loss. Hence, the surrogate model employed for this comparison can be presented as follows:

$$\Delta p_{Total} = f_m \frac{\varrho_m L}{D} \frac{u_m^2}{2} + \varrho_m g \sin(\theta) \tag{6.6}$$

The flow properties of the phosphate slurry include a density of $\varrho_s = 2600$ kg/m^3, while the water density is $\varrho_w = 1000$ kg/m^3. The solid concentration in the flow was measured to be approximately $\phi_s = 36\%$. The surrogate model was developed assuming mono-sized particles, with the particles' size specified by their d_{50} value, which is 100 μm in this case. The network has a diameter of $D = 0.492$ m, with a constant relative roughness $\varepsilon = 0.0213$ mm. The slurry flows through it at an average mixture velocity of 2.071 m/s. A graphical user interface (GUI) was developed under *Modelica software* to enable the use of the surrogate model on an industrial scale. The pipe system was discretized into N segments, which included the process components such as pumps and sensors (cf Fig. 6.9). The iterative process described earlier for calculating pressure drop over time was implemented through a C++ code that was coupled with the GUI. The GUI is described in detail in section 6.3. The following findings are derived from actual measurements obtained at OCP during the timeframe of 06:00:00 pm on June 11, 2022, to 10:00:00 am on June 12, 2022. The overall time taken for computing these results using the current surrogate model is approximately 5 minutes. The gathered data from the OCP Group SCADA system comprises over 2000 data points, with a time interval of 30 seconds between each point. Figure 6.6 shows the comparison between the predicted and measured pressure drop results for the pipeline connecting the BeniAmir processing plant and the main station over a period of 16 hours. When it comes to assessing the effectiveness of a predictive model, MAPE (Mean Absolute Percentage Error) is a widely-used metric. This is particularly true when you need to evaluate the model's accuracy relative to the actual values, especially if the target variable varies in scale across different observations.

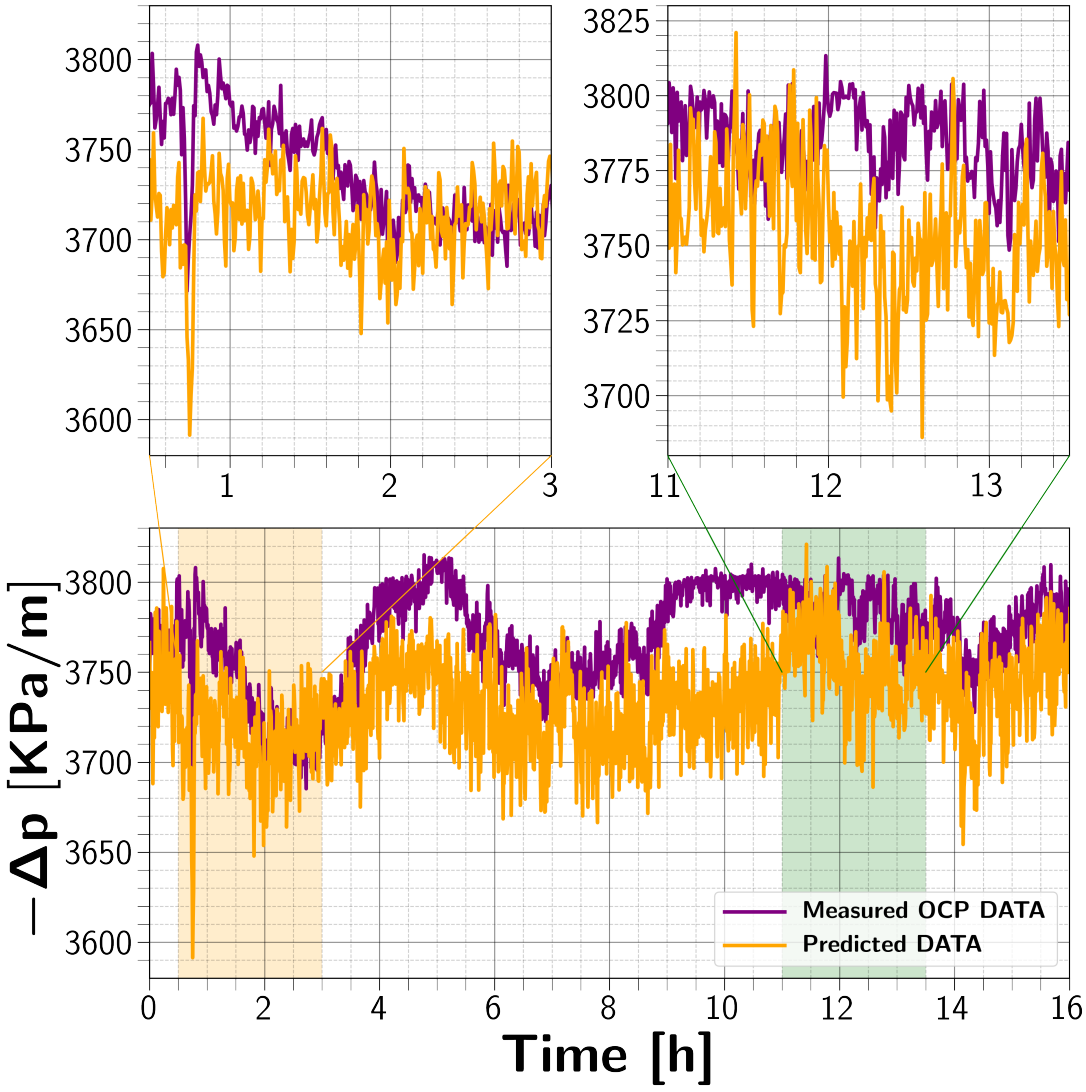

Figure 6.6: Comparison between pressure monitoring sensor data and predicted pressure drop.

The computed pressure drops are in good agreement with the trend observed in the measured data, with a relatively small average absolute error of approximately 6%. This translates to an error of around 180 KPa on average between the predicted values and the actual values. In reality, the slurry density undergoes slight variations over extended distances due to its non-Newtonian behavior. Furthermore, the presence of multi-sized particles in the slurry can have an impact on the flow dynamics, resulting in varying levels of friction that our model, which only accounts for mono-sized particles, fails to capture. It's important to keep in mind that our model doesn't consider the shape of particles, which can impact the amount of drag force they experience in fluid flow. As a result, this can have an effect on the pressure drop in the pipe. Additionally, it is worth

noting that the accuracy of pressure sensors used in the measurements can vary within a range of ±1%. Taken together, these factors can contribute to errors and result in deviations between the predicted and measured results.

6.3 Graphical user interface

The graphical user interface serves as a means of communication between humans and machines. It employs pictograms on the screen to represent the objects that need to be manipulated, thus allowing users to operate them while minimizing the need to manipulate the computer codes developed within the scope of this project. The main objective of the interface is to enable smooth communication between the user and the hydrodynamic code. Under the Modelica software, the various components of the main and BeniAmir pipes system were incorporated. Figure 6.9 illustrates an instance of the main pipeline system. As mentioned earlier, the

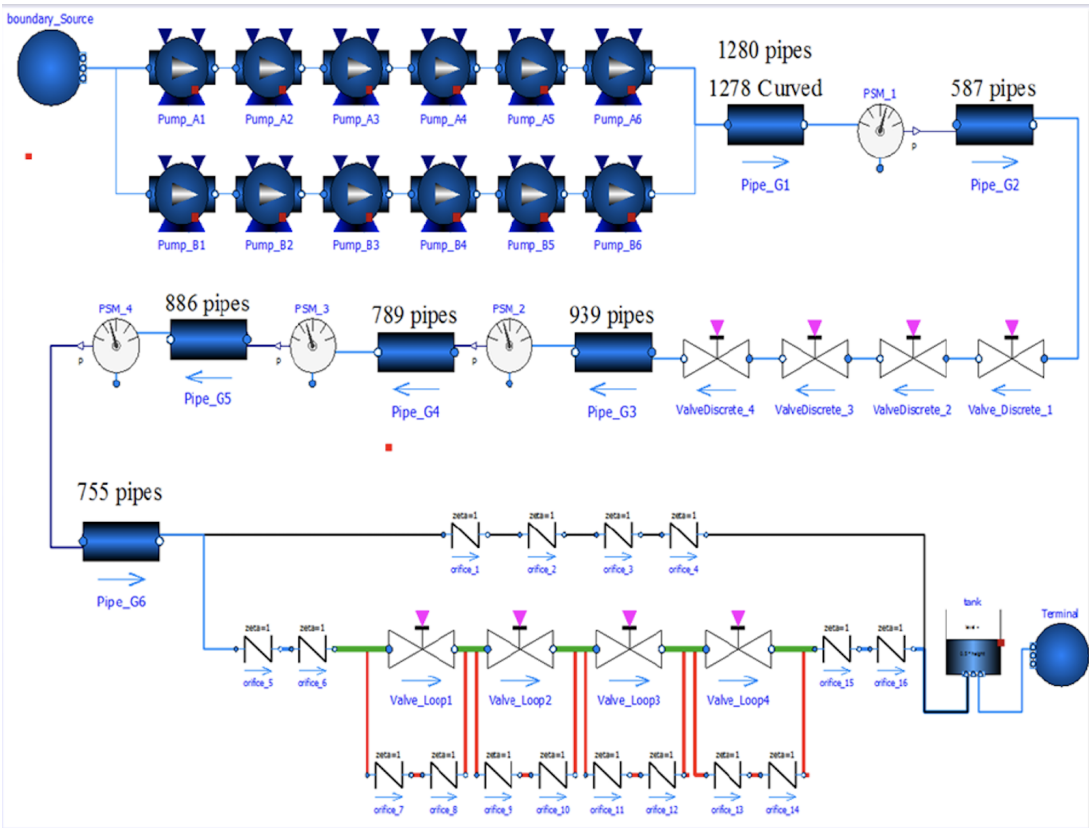

Figure 6.7: Representation of the main pipeline system under *Modelica software*

code is employed to calculate the inlet pressure for each pipe segment using the surrogate model, followed by the determination of pressure losses. Figure 6.9 provides an overview of the graphical interface characteristics that must be entered to execute simulations. As long as the terms, concepts, and methods utilized are

properly comprehended, using this interface is relatively straightforward. The presented in Fig. 6.9 depicts a simulation of a phosphate flow, displaying the total network pressure results at the input.

6.4 Conclusion

The objective of the present chapter is to build a model able to predict the pressure drop of the flow of phosphate slurry through horizontal and inclined pipelines. In this chapter, experimental validation of the developed model for predicting pressure drop in phosphate slurry flows has been performed. As industrial data, a history of 16 hours of the phosphate slurry flow data was used for comparison. The computed pressure drops show good agreement with the trend observed in the measured data, with an average absolute error of approximately 6%. Considering the simplifications made in the model and the underlying assumptions, this level of error is relatively acceptable. The developed model provides a significant reduction in computational time compared to the three-dimensional CFD model, while maintaining a high level of accuracy. It should be noted, however, that although the developed model has been validated, there is still room for improvement. To further improve the model, additional experimental measurements and other flow properties can be taken into account during the model construction process.

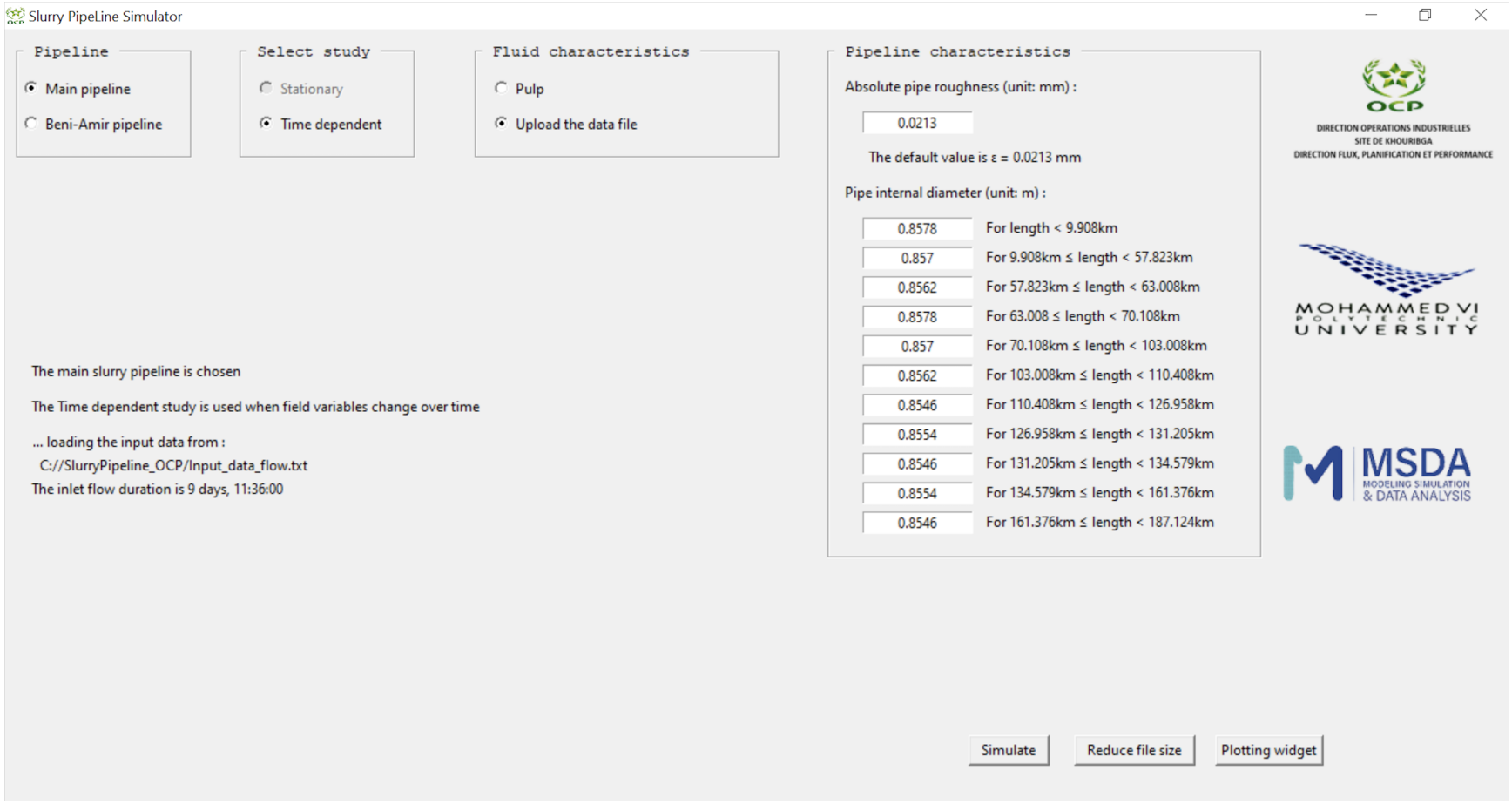

Figure 6.8: The operating conditions that must be provided by the user

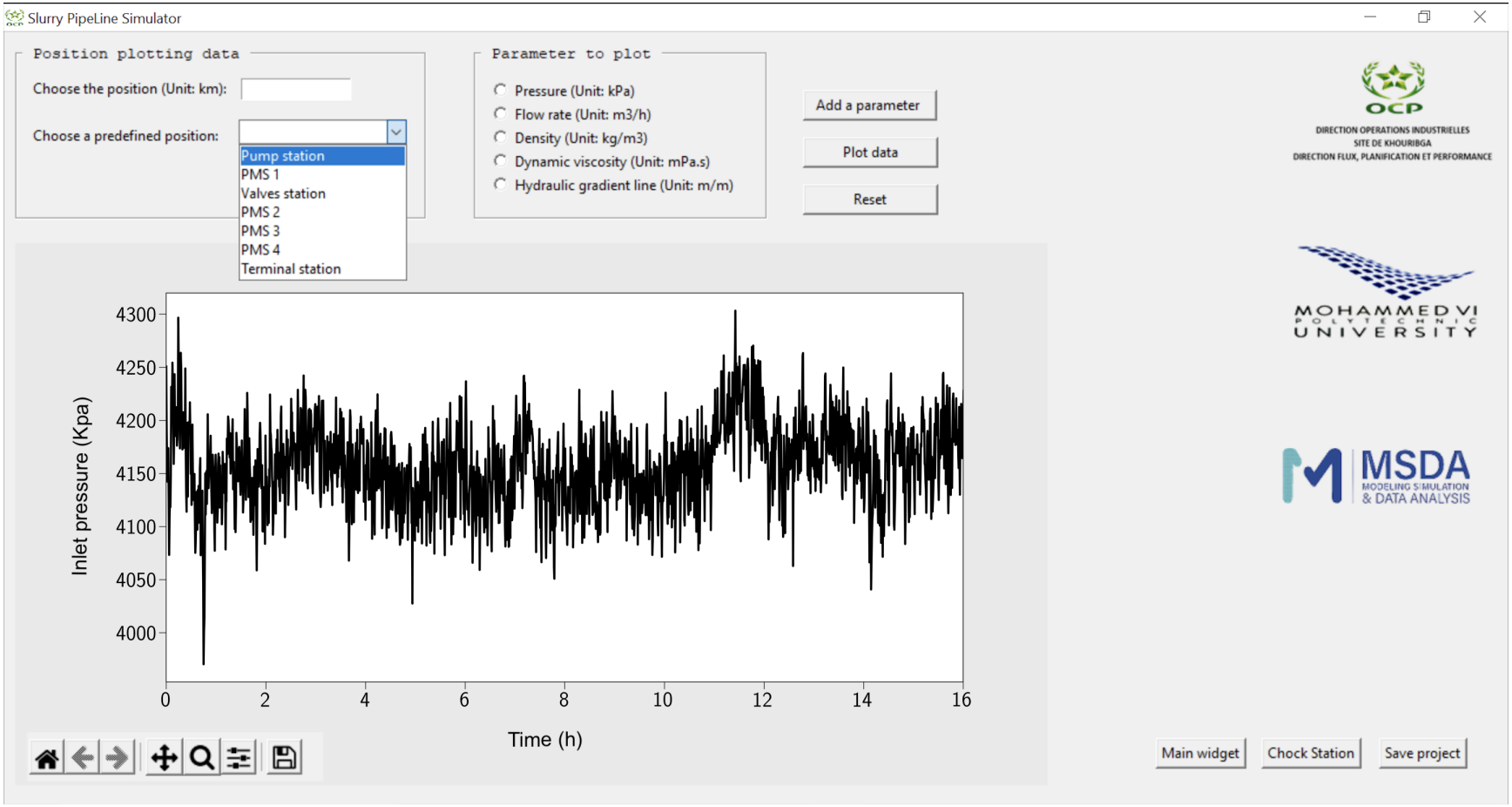

Figure 6.9: Simulation results displayed by the GUI

6

Validation expérimentale par modélisation de substitution

Objectifs:

Dans ce chapitre, l'approche expérimentale utilisée pour valider le modèle CFD biphasique formulé dans le chapitre 4 est présentée. Cependant, la complexité computationnelle associée à la réalisation de simulations CFD multiphases en trois dimensions rend extrêmement difficile la comparaison avec des données expérimentales provenant de longs pipelines industriels réels. Pour surmonter ces défis computationnels, des modèles de substitution sont utilisés pour exécuter la validation expérimentale dans cette thèse. La section 6.1 est dédiée au développement d'un nouveau modèle de substitution basé sur la CFD qui peut prédire avec précision la perte de charge dans les écoulements de boues. La performance de ce nouveau modèle est ensuite évaluée en le comparant aux données expérimentales du flux de phosphate de l'usine industrielle dans la section 6.2.

6.1 La modélisation de substitution

6.1.1 Introduction

La modélisation de substitution est utilisée dans diverses disciplines d'ingénierie et scientifiques où des simulations informatiques complexes ou des expériences physiques sont utilisées. Dans de tels scénarios, l'acquisition de données supplémentaires nécessite la réalisation d'expériences supplémentaires, entraînant des coûts économiques ou matériels importants, ainsi que des opérations informatiquement coûteuses. Il est comparativement plus simple d'obtenir de telles informations à partir d'un modèle de substitution car il entraîne des coûts de calcul significativement inférieurs. Il existe plusieurs approches proposées dans la littérature pour obtenir un modèle de substitution, telles que la régression polynomiale, le krigeage et les réseaux de neurones. ù Le modèle de substitution, également connu sous le nom de méta-modèle ou de modèle de surface de réponse, a été largement appliqué dans de nombreux domaines différents de la science et de l'ingénierie. Ici, le modèle de substitution est utilisé comme représentation mathématique d'un modèle de dynamique des fluides numérique (CFD) qui peut être utilisé pour prédire la sortie du modèle CFD pour un ensemble donné d'entrées. Ces méthodes peuvent être utilisées pour créer différents types de modèles de substitution, y compris des modèles globaux qui peuvent être utilisés pour prédire la sortie du modèle CFD pour n'importe quel ensemble d'entrées, et des modèles locaux qui ne sont précis que pour une région spécifique de l'espace d'entrée. L'objectif est de réduire le coût de calcul de l'exécution d'une simulation CFD, car ils peuvent fournir des prédictions précises avec une charge de calcul beaucoup plus faible que le modèle CFD original.

6.1.2 Un modèle de substitution de la perte de charge

Les modèles de substitution sont de plus en plus utilisés pour la commande et le soutien à la décision dans diverses industries. Dans l'industrie des pipes, la prédiction de la perte de charge du flux le long du tuyau revêt une importance primordiale. En particulier, pour les écoulements de boues à deux phases, un bon contrôle de la perte de charge est essentiel, car il permet d'optimiser d'une part la consommation d'énergie des pompes, et d'éviter d'autre part les problèmes résultant de la sédimentation de la phase solide et de l'obstruction du tuyau. Actuellement, il n'existe aucune méthode théorique pour prédire la perte de charge lorsqu'il s'agit de suspensions en sédimentation. De nombreuses équations empiriques corréler les données dans certaines situations, mais aucune n'a encore été proposée pour fournir des prédictions précises des chutes de pression pour un mélange solide-liquide général.

À la connaissance de l'auteur, les corrélations pertinentes pour calculer les chutes de pression des écoulements de boues suggérées dans la littérature sont soit totalement empiriques, soit semi-empiriques. Les modèles de substitution

sont classés en deux types en fonction de leur stratégie d'approximation : (i) une approche basée sur le modèle ou basée sur la physique ([Durlofsky, 2010]); (ii) une approche basée sur les données ou boîte noire [Kleijnen, 2015]. Les modèles à ordre réduit (ROMs) sont des techniques basées sur le modèle qui approximent les équations d'origine par des équations d'ordre inférieur, réduisant ainsi le coût de calcul. En revanche, les techniques basées sur les données créent le modèle de substitution en utilisant uniquement les données d'entrée et les réponses de sortie, en traitant la simulation CFD comme une boîte noire. Le but de ce travail est d'établir l'évaluation d'un modèle de substitution basé sur le modèle qui peut être utilisé pour estimer la perte de charge d'un écoulement de boue de phosphate. Le modèle d'ordre réduit suggéré, qui vise à approximer le modèle phénoménologique, utilise la formule empirique pour les pertes de pression dues à la friction dans les tuyaux horizontaux, qui se lit comme suit :

$$\Delta p_f = f_m \frac{\varrho_m L}{D} \frac{u_m^2}{2}, \tag{6.1}$$

où la densité et la vitesse sont celles du mélange solide-liquide. Le modèle de substitution sera construit pour estimer le coefficient de frottement du mélange f_m en fonction du diamètre des particules et de la concentration en solides.

Les simulations utiliseront les caractéristiques liées au matériau de la boue de phosphate et à ses paramètres de fonctionnement en transport, y compris la distribution de taille des particules, la concentration en solides et les variations de vitesse. La base de données CFD contient 525 points fonctionnels, avec des valeurs variées de taille des particules, de concentration en solides et de vitesses d'entrée. Une densité des solides de $\varrho_s = 2450$ kg/m^3, et une densité de l'eau de $\varrho_w = 1000$ kg/m^3, sont retenues pour l'écoulement. Les tailles des particules varient de $dp = 44$ μm à $dp = 250$ μm, avec une concentration en solides allant de $\phi_s = 20\%$ à $\phi_s = 40\%$. La boue est transportée via un tuyau d'un diamètre de $D = 100$ mm, et couvre une plage de vitesses de 2 m/s à 10 m/s. Nous cherchons à trouver le facteur de frottement optimal du mélange de boue f_m, qui correspond bien aux résultats de la CFD par le biais d'un processus de minimisation. L'algorithme de Levenberg–Marquardt (LMA) [Levenberg, 1944, Marquardt, 1963], qui est une méthode hybride prenant en charge à la fois les techniques de Gauss–Newton et de descente de gradient pour converger vers une solution optimale, est utilisé pour effectuer ce processus d'optimisation.

La première étape consiste à construire une fonction objectif qui prend les valeurs des variables d'ajustement, calcule les valeurs à minimiser, et renvoie à la fin le coefficient de frottement f_m. Pour un tel problème, la statistique du chi-carré (χ^2) est souvent utilisée :

$$\chi^2 = \sum_i^N \frac{\left[\mathcal{Y}_i^{\text{num}} - \mathcal{Y}_i^{\text{correlation}}(f_m)\right]^2}{\varepsilon_i^2}, \tag{6.2}$$

où $\mathcal{Y}i^{\text{num}}$ est l'ensemble des points de données CFD, $\mathcal{Y}i^{\text{correlation}}(fm)$ est le calcul de la corrélation de la perte de charge et fm est la variable dans la corrélation à optimiser dans l'ajustement, et εi est l'incertitude estimée des données. À cette étape, les prédictions du modèle de substitution sont comparées aux résultats expérimentaux publiés dans la littérature qui ont utilisé les mêmes paramètres physiques et géométriques que cette étude pour tester sa fiabilité. Le degré d'accord entre les valeurs prédites et mesurées du gradient hydraulique peut être évalué à l'aide de graphiques de parité tels que ceux illustrés dans la figure 6.1.

La comparaison des données expérimentales du gradient hydraulique pour une suspension de billes de verre est présentée dans les figures 6.1a et 6.1b. Ces expériences [Matoušek et al., 2013] ont été réalisées dans un tuyau de diamètre $D = 100$ mm, et la suspension dans ce cas avait une densité de solides de $\varrho_s = 2450$ kg/m^3. Les particules avaient un diamètre de $dp = 180$ μm, et la vitesse d'écoulement variait de 1 m/s à 5 m/s. L'écoulement est canalisé à travers un tuyau de diamètre $D = 103$ mm, avec une densité de solides de $\varrho s = 2650$ kg/m^3 et un diamètre de particules de $d_p = 90$ μm. La vitesse d'écoulement varie de 1 m/s à 8 m/s.

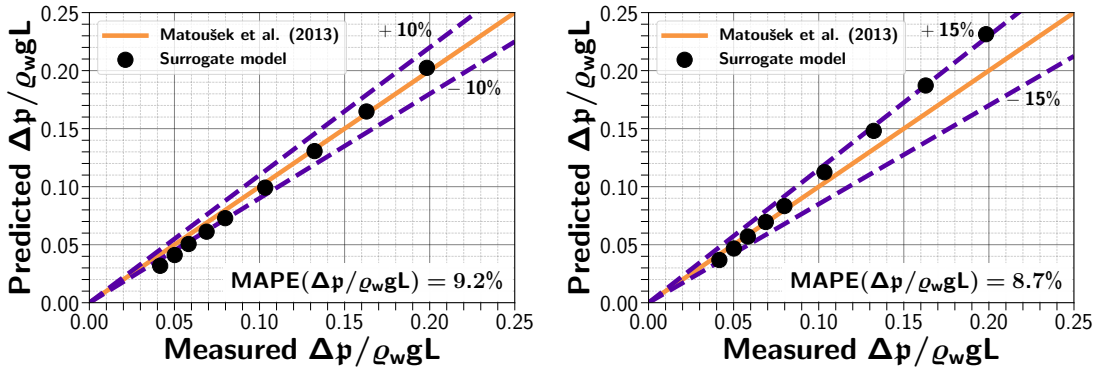

(a) $\phi_s = 20\%$ (b) $\phi_s = 30\%$

Figure 6.1: Graphiques de parité du gradient hydraulique entre les valeurs prédites et mesurées pour différentes concentrations de solides.

6.1.3 Conclusion

Un nouveau modèle de substitution basé sur la CFD a été présenté pour prédire la perte de charge dans le cas de suspensions en sédimentation. Le modèle de substitution a été conçu pour couvrir les écoulements de boues avec des tailles de particules allant de 44 μm à 270 μm, des concentrations en solides allant jusqu'à 40%, et des vitesses variant de 2 m/s à 10 m/s. Cependant, la validité globale du modèle a été évaluée et a montré des accords acceptables avec une erreur moyenne

en pourcentage égale ou inférieure à 10%, ce qui peut être examiné plus en détail à l'aide de données expérimentales sur des boues de phosphate.

L'idée de développer un modèle de substitution utilisant la CFD semble être efficace. L'avantage de cette approche est qu'elle permet de fournir un modèle de substitution même en l'absence d'un grand ensemble de données expérimentales jugé adéquat pour fournir une base solide pour la construction de la corrélation de perte de charge. De plus, nous avons démontré que le modèle développé prédit avec précision la perte de charge pour au moins 85% d'une véritable boue fonctionnant dans les conditions de fonctionnement d'entrée pour lesquelles il a été construit.

6.2 La validation expérimentale de l'écoulement de boue de phosphate.

Dans cette section, les mesures expérimentales sont présentées, qui ont été réalisées pour valider le modèle de perte de charge développé dans la section 6.1.2. Malheureusement, nous n'avons pas pu mettre en place une boucle d'essai à l'échelle du laboratoire ou du pilote dans cette thèse, ce qui nous aurait permis de valider en profondeur notre modèle CFD en contrôlant toutes les conditions opérationnelles. Ainsi, les données expérimentales utilisées pour évaluer notre modèle de substitution pour la boue de phosphate sont directement obtenues à partir des capteurs pré-installés sur le site industriel. En raison de plusieurs limitations, nos simulations numériques étaient basées uniquement sur les investigations expérimentales menées sur la perte de charge de la boue de phosphate s'écoulant à travers une série de tuyaux horizontaux et inclinés. Pour calculer la perte de charge dans les tuyaux horizontaux, deux modèles de substitution ont été développés. Le premier modèle est basé sur l'analyse gPC et est largement discuté dans le chapitre 5. En utilisant l'analyse gPC, nous avons obtenu un modèle polynomial capable de calculer avec précision la perte de charge due à la friction dans une plage d'opération spécifique. Le deuxième modèle est basé sur la CFD, qui prédit le coefficient de friction, et est ensuite utilisé pour calculer la perte de charge due à la friction (voir section 6.1.2). Les deux modèles de substitution sont confrontés au problème de l'adaptation à l'échelle industrielle, car le diamètre réel du tuyau est neuf fois plus grand que le diamètre utilisé pour construire nos modèles de substitution. En ce qui concerne le modèle polynomial, il nécessite une nouvelle conception d'expérience comprenant 1000 échantillons, pour lesquels des simulations déterministes doivent être réalisées dans le tuyau de plus grand diamètre. Cependant, répéter la même approche est coûteux en termes de calculs et nécessite une quantité importante de ressources informatiques. Quant à la deuxième approche, les efforts pour adapter le coefficient de friction aux diamètres de tuyaux plus grands par le biais d'une étude de similarité [Hoyt, 2003] n'ont pas donné de résultats positifs, en raison du comportement

d'écoulement hautement non linéaire. Pour résoudre le problème de l'adaptation du coefficient de friction aux diamètres de tuyaux plus grands, la deuxième approche a été adoptée pour développer un nouveau coefficient de friction pour les mélanges, noté f_m, qui prend en compte les paramètres physiques pertinents. Cependant, pour réduire la charge de calcul, les simulations CFD ont été réalisées uniquement pour les paramètres physiques spécifiques de l'écoulement de boue de phosphate, en termes de concentration en solides et de taille des particules. La valeur de f_m obtenue à partir de cette étude est de 0,028, qui sera utilisée dans les comparaisons ultérieures. Pour des problèmes de variabilité de la concentration dans le pipe principal au cours du transport de la pulpe, les données d'un pipe secondaire on été utilisé. Ce pipeline secondaire transporte des lots continus de boue de phosphate de l'usine de traitement BeniAmir à la station principale, s'étendant sur 15 km en suivant les contours naturels du terrain, ce qui entraîne des inclinaisons variables. Avant de procéder à la comparaison, il convient de noter que le modèle de substitution développé dans cette étude est uniquement applicable aux tuyaux horizontaux et ne prend pas en compte l'effet de l'inclinaison du tuyau. Néanmoins, l'analyse de sensibilité globale présentée dans la section 5.1.5 a révélé que l'inclinaison du tuyau n'affecte pas la perte de charge due à la friction. Par conséquent, la contribution de l'inclinaison peut être ajoutée uniquement au composant de friction de la perte de charge pour déterminer la perte de charge totale. Ainsi, le modèle de substitution utilisé pour cette comparaison peut être présenté comme suit :

$$\Delta p_{Total} = f_m \frac{\varrho_m L}{D} \frac{u_m^2}{2} + \varrho_m g \sin(\theta) \tag{6.3}$$

Les propriétés d'écoulement de la boue de phosphate comprennent une densité de $\varrho_s = 2600$ kg/m^3, tandis que la densité de l'eau est de $\varrho_w = 1000$ kg/m^3. La concentration en solides dans l'écoulement a été mesurée à environ $\phi_s = 36\%$. Le modèle de substitution a été développé en supposant des particules de taille unique, avec une taille de particules spécifiée par leur valeur de d_{50}, qui est de 100 μm dans ce cas. Le réseau a un diamètre de $D = 0.492$ m, avec une rugosité relative constante $\varepsilon = 0.0213$ mm. La boue s'écoule à travers le réseau à une vitesse moyenne du mélange de 2.071 m/s. Les résultats suivants sont dérivés de mesures réelles obtenues à OCP pendant la période de 18h00 le 11 juin 2022 à 10h00 le 12 juin 2022. La Figure 6.6 montre la comparaison entre les résultats de la perte de charge prédits et mesurés pour le pipeline reliant l'usine de traitement de BeniAmir et la station principale sur une période de 16 heures.

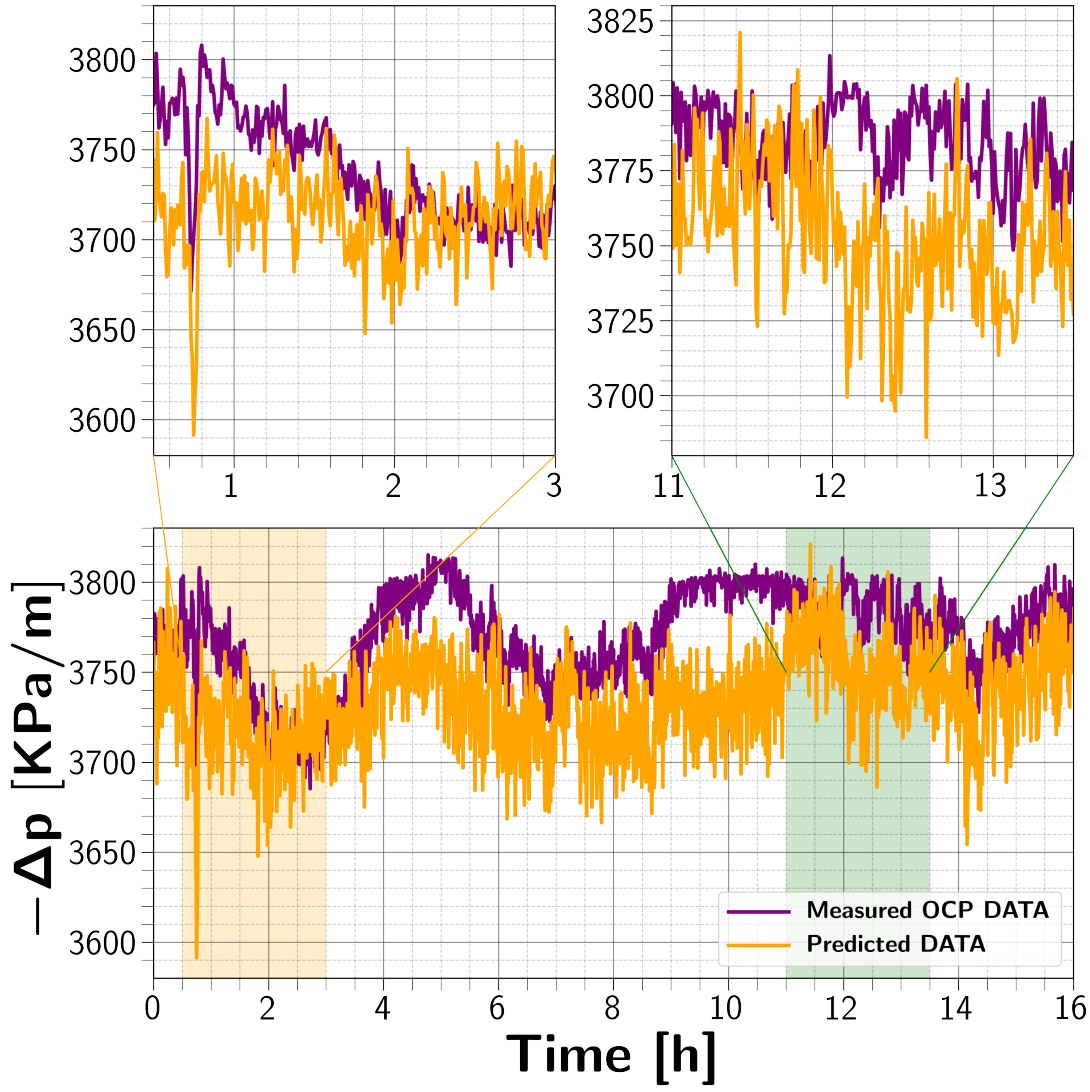

Figure 6.2: Comparaison entre les données du capteur de surveillance de la pression et la perte de charge prédite.

Les chutes de pression calculées sont en bon accord avec la tendance observée dans les données mesurées, avec une erreur absolue moyenne relativement faible d'environ 6%. Cela se traduit par une erreur moyenne d'environ 180 kPa entre les valeurs prédites et les valeurs réelles. En réalité, la densité de la boue subit de légères variations sur de longues distances en raison de son comportement non newtonien. De plus, la présence de particules de différentes tailles dans la boue peut avoir un impact sur la dynamique de l'écoulement, entraînant des niveaux variables de frottement que notre modèle, qui ne prend en compte que des particules de taille unique, ne parvient pas à capturer. Il est important de garder à l'esprit que notre modèle ne prend pas en compte la forme des particules, ce qui peut influencer la quantité de force de traînée qu'elles subissent dans l'écoulement

du fluide. Par conséquent, cela peut avoir un effet sur la perte de charge dans le tuyau. De plus, il convient de noter que la précision des capteurs de pression utilisés dans les mesures peut varier dans une plage de $\pm 1\%$. Pris ensemble, ces facteurs peuvent contribuer aux erreurs et entraîner des écarts entre les résultats prédits et mesurés.

6.3 Conclusion

L'objectif du présent chapitre est de construire un modèle capable de prédire la perte de charge de l'écoulement de la boue de phosphate à travers des pipelines horizontaux et inclinés. Dans ce chapitre, une validation expérimentale du modèle développé pour prédire la perte de charge dans les écoulements de boue de phosphate a été réalisée. Les données industrielles utilisées pour la comparaison sont basées sur un historique de 16 heures de données d'écoulement de boue de phosphate. Les chutes de pression calculées montrent un bon accord avec la tendance observée dans les données mesurées, avec une erreur absolue moyenne d'environ 6%. Compte tenu des simplifications effectuées dans le modèle et des hypothèses sous-jacentes, ce niveau d'erreur est relativement acceptable. Le modèle développé permet une réduction significative du temps de calcul par rapport au modèle CFD tridimensionnel, tout en maintenant un niveau acceptable de précision. Pour améliorer davantage le modèle, des mesures expérimentales supplémentaires et d'autres propriétés d'écoulement peuvent être prises en compte lors du processus de construction du modèle.

7 Conclusions and perspectives

7.1 Conclusions

This work is about modeling slurry flows in pipelines. The primary objective of this thesis was to develop a CFD model for simulating and studying slurry flows, with a specific focus on phosphate slurry. The aim was to contribute to the understanding of the specific physical features of slurry transport in pipelines through numerical simulation. The developed CFD model can be used to predict the physics of the slurry flow, which is crucial for controlling the operation and optimizing the current processes for transporting phosphate slurry. Additionally, it can aid in the design of new integrated and efficient networks.

To begin, a thorough assessment of past numerical investigations of slurry flows in horizontal pipes is conducted to identify the proper modelling methodologies and mathematical models. CFD models are divided into two main categories: those that track each individual particle and those that interpret both phases as interpenetrating continua. Models that track each particle require significant computer resources and are limited to relatively dilute flows. In contrast, the second category of models, which interpret both phases as interpenetrating continua, are the only reasonable solution option for simulating dense flows. On the basis of this state of the art, the two fluid Eulerian model is adopted, as it provides the optimum trade-off between computing cost and the capability to represent the physical behaviors governing slurry pipe flow.

In this thesis, the proposed mathematical model solves a double-averaged formulation of the mass and momentum conservation equations for both phases. The two phases are coupled through interfacial momentum transfer terms. To accurately model the behavior of the solid phase, such as contact pressure and

velocity collisions, closures are necessary to express these behaviors in terms of continuous pressure and viscosity. The Kinetic Theory of Granular Flow (KTGF) was utilized in this study to establish a correlation between the total kinetic energy of a collection of particles moving randomly within the carrier fluid and their fluctuating velocity through the granular temperature concept. The inclusion of these terms accounts for the interactions and transfer of momentum, energy, and species between the two phases and enhances the predictive capabilities of the model. Eddy-viscosity based models are frequently employed to address turbulence in the fluid phase of two-phase flows. Their primary aim is to capture the turbulent characteristics of the fluid phase and they make use of the concept of eddy viscosity to replicate the impacts of turbulence. These models calculate the eddy viscosity in the fluid phase by utilizing the turbulent kinetic energy and dissipation rate.

The development and numerical validation of the model is divided in two steps. Beginning with the single-phase flow scenario, this stage plays a critical role in ensuring precise integration of turbulence models, near-wall treatment parameters, and other essential parameters necessary for succeeding multiphase simulations. The CFD results in this section demonstrate a strong correlation with both the empirical data and theoretical models for pressure loss.

Afterwards, two-phase flow simulations were performed. The two-fluid model (TFM) is now applied to simulate the two-phase flow. The performance of the model is investigated by comparison to experimental data from literature. Two turbulence models, namely standard k-ε and k-ω SST model, are tested and their ability to give accurate results are compared. Calibration and validation of the numerical model is conducted by referencing the chord average in the vertical diameter of solid concentration and velocity profiles. Comparisons between experiment and simulation cover slurry flows with particles concentrations from $\phi_s = 0.19$ to $\phi_s = 0.4$. The particle sizes are in the range between from $d_p = 4$ μ_m to $d_p = 270$ μ_m. CFD results showed a high level of correspondence with the presented experimental data. The performance of the numerical model is more investigated through a comparison of the variation of the pressure drop per unit length with respect to the inlet velocity of the mixture u_m in the range of 2 to 8 (m/s). The overall mean relative errors results of the pressure drops are limited to 10%. This is largely acceptable, and demonstrates the numerical model's validity within the specified range of physical conditions. It is also remarked that the k-ω SST model is slightly better than k-ε model in predicting the pressure drop.

Simulating sediment transport in pipelines using two-phase flow models is a common practice, but due to the numerous input parameters involved, there is a significant amount of uncertainty in the results. Therefore, it is necessary to conduct a comprehensive analysis that includes uncertainty quantification (UQ) and sensitivity analysis (SA) to enhance prediction accuracy and quantify the importance of each input parameter. The study's outcomes shed light on the ef-

fect of system uncertainties on the energy consumption of slurry flow in pipelines and underscore the significance of considering these uncertainties to optimize energy efficiency. In this framework, five parameters are considered as random variables with a given probability distribution over a prescribed range of investigation, based on the operating conditions of the intended phosphate slurry flow. The corresponding analysis concern physical, geometry and modeling properties: (i) Particles sizes, (ii) Initial solid concentration, (iii) Inlet velocity of the flow mixture, (iv) Pipe inclination, (V) Specularity coefficient. Firstly, we have investigated resulting uniform and 1-dimensional quantities of interest (QoIs). The Generalized Polynomial Chaos expansions (PCE) for Uncertainty Quantification (UQ) and GSA, was used to fulfill this task. The Sobol' indices calculated for pressure drop demonstrate that the variability of the latter is heavily influenced by the effects of the mixture velocity, u_m, and particle diameter, d_p, then followed by initial particles concentration ϕ_s. Particle sizes were confirmed that they should be within the optimal range of medium to fine particles. High solid concentrations affects friction, but it strongly depend upon the ratio of the solids concentration to the maximum settled concentration. Furthermore, when operating around the deposition limit velocity u_{dl}, it is possible to increase the solid concentration at the proposed range 40% while ensuring low levels of energy consumption. An interesting and useful finding concern the effect of the pipe inclination θ, we find out that the latter doesn't effect on the pressure drop by frictions. Also, as expected higher specularity coefficient $\mathcal{SC}$ leads to an increase in the pressure drop. A good calibration of this parameter in the numerical validation step is crucial to ensure reliable predictions within slurry flows.

The second part of this study focused on investigating uncertainty quantification (UQ) and global sensitivity analysis (GSA) for a two-dimensional case of phosphate slurry flow. To reduce the cost of constructing the polynomial chaos expansion (PCE) model, we utilized proper orthogonal decomposition (POD) to reduce the dimensionality of the output variables. The reduced-order model was then applied to the two-dimensional two-fluid model (TFM) equations. In addition, a comprehensive global sensitivity analysis and uncertainty quantification were performed for the two-dimensional quantities of interest (QOIs). Distributions of mean and variance of our *QOIs*, demonstrated that the phosphate slurry within these operating conditions is confirmed to be classified as two-layer (stratified) flow. The PCE or PCE-POD techniques shows that the developed model are able to produce acceptable results for our statistical quantities. They proved their effectiveness to reproduce well the behavior of the slurry flow.

Finally, the performance of the developed two-phase CFD model in simulating the phosphate slurry flow is evaluated. However, due to the technical challenges associated with performing pilot-scale experiments, there is a lack of experimental data available for this benchmark case. Therefore, experimental data obtained directly from pre-installed sensors at the industrial plant are used for comparison. The available data includes measurements from five pressure sensors installed

along the pipeline. Consequently, the evaluation of the model is based solely on its ability to predict the pressure drop.

This thesis utilizes surrogate models to address the computational challenges associated with three-dimensional multiphase CFD simulations. A new CFD-based surrogate model was developed to predict pressure loss in settling suspensions. The model is capable of simulating slurry flows with particle sizes ranging from 44 μm to 270 μm, solid concentrations up to 40%, and velocities ranging from 2 m/s to 10 m/s. The accuracy of the surrogate model was assessed using experimental data from literature and demonstrated an acceptable overall validity with a mean percentage error of 10% or less.

To estimate the pressure drop of phosphate slurry flow in both horizontal and inclined pipelines, a scaled-up version of the surrogate model was used to account for the larger pipe diameter. The additional head loss caused by the inclinations of the pipes was included in the total head loss calculation, by adding it solely to the friction component of pressure drop. The new model's performance was evaluated based on 16 hours of data history. The calculated pressure drops show good agreement with the measured data trend, with an average absolute error of about 5%. Given the model's simplifications and underlying assumptions, this level of error is relatively acceptable. The developed model offers a significant reduction in computational time compared to the three-dimensional CFD model, while still maintaining an acceptable level of accuracy.

7.2 Perspectives

Future research may include both modeling and application enhancements. It should be noted, however, that although the developed model has been validated, there is still room for improvement:

- Incorporating particle size distributions for instance that are bimodal or tri-modal in the model can enhance its precision and reflect more closely the behavior of real slurries.

- By taking into account supplementary physical and geometrical parameters, the precision and dependability of UQ and GSA for slurry flows can be enhanced. The shape of solid particles, which has an impact on the drag coefficient and settling velocity, as well as geometrical parameters like pipe diameter, wall roughness, and bends can exert a notable influence on the flow behavior, and as such, should be incorporated into the analysis.

- To account for a larger variation range and generalize the study for other slurry flows, it may be necessary to sample the input parameters over a wider range of values, including extreme values that are less likely to occur but can still have significant effects on the output.

- Studying the pump's energy consumption as a function of different parameters can provide a more representative measure of the energy efficiency of slurry transport.
- Moreover, employing PCE surrogate models to approximate slurry flow behavior and make predictions for specific parameters of interest can be a valuable approach.
- To enhance the accuracy of the surrogate model used for comparison with industrial data, additional experimental measurements can be conducted, and other relevant flow properties can be incorporated during the model construction process.
- Further investigation of the scaling approach to establish a relationship between the evolution of key parameters of interest and the pipe diameter can be highly beneficial in facilitating the construction of surrogate models. By studying the scaling approach, it may be possible to identify trends and patterns in the behavior of the slurry flow as the pipe diameter varies. This information can be used to construct surrogate models that accurately capture the behavior of the slurry flow under different pipe diameters, and enable more accurate predictions of key parameters of interest.
- In addition, understanding the scaling behavior can provide valuable insights into the fundamental physical mechanisms that govern the behavior of the slurry flow. This knowledge can be used to improve the design and operation of slurry flow systems, and help to optimize their performance.
- The real-world phosphate slurry flow utilizes water plugs to segregate different slurry batches. By incorporating the effect of these plugs on the resulting density variation, it may be possible to use the surrogate model to accurately predict the pressure drop along the main pipeline.

All of these enhancements can contribute to achieving the main objective of creating a digital twin of the slurry transport process. Especially create a more accurate and representative one.

7

Conclusions and perspectives

7.1 Conclusions

Ce travail porte sur la modélisation des écoulements de boue dans les pipelines. L'objectif principal de cette thèse était de développer un modèle de CFD pour simuler et étudier les écoulements de boue, en mettant l'accent sur la boue de phosphate. L'objectif était de contribuer à la compréhension des caractéristiques physiques spécifiques du transport de boue dans les pipelines par la simulation numérique. Le modèle de CFD développé peut être utilisé pour prédire la physique de l'écoulement de boue, ce qui est crucial pour le contrôle des opérations et l'optimisation des processus actuels de transport de boue de phosphate. De plus, il peut aider à la conception de nouveaux réseaux intégrés et efficaces.

Pour commencer, une évaluation approfondie des études numériques antérieures sur les écoulements de boue dans les conduites horizontaux est réalisée afin d'identifier les méthodologies de modélisation appropriées et les modèles mathématiques. Les modèles de CFD sont divisés en deux catégories principales : ceux qui suivent chaque particule individuelle et ceux qui interprètent les deux phases comme des continus interpenétrants. Les modèles qui suivent chaque particule nécessitent d'importants moyens informatiques et sont limités aux écoulements relativement dilués. En revanche, la deuxième catégorie de modèles, qui interprète les deux phases comme des continus interpenétrants, est la seule option raisonnable pour simuler les écoulements denses. Sur la base de cet état de l'art, le modèle eulerien à deux fluides est adopté, car il offre un compromis optimal entre le coût de calcul et la capacité à représenter les comportements physiques régissant l'écoulement de boue dans les conduites.

Dans cette thèse, le modèle mathématique proposé résout une formulation

à double moyenne des équations de conservation de la masse et de la quantité de mouvement pour les deux phases. Les deux phases sont couplées par l'intermédiaire de termes de transfert de quantité de mouvement interfaciale. Pour modéliser avec précision le comportement de la phase solide, tels que la pression de contact et les collisions de vélocité, des fermetures sont nécessaires pour exprimer ces comportements en termes de pression et de viscosité continues. La Théorie Cinétique des Écoulements Granulaires (KTGF) a été utilisée dans cette étude pour établir une corrélation entre l'énergie cinétique totale d'un ensemble de particules se déplaçant de manière aléatoire dans le fluide porteur et leur vélocité fluctuante à travers le concept de température granulaire. L'inclusion de ces termes permet de prendre en compte les interactions et les transferts de quantité de mouvement, d'énergie et d'espèces entre les deux phases et améliore les capacités prédictives du modèle. Les modèles basés sur la viscosité turbulente sont fréquemment utilisés pour aborder la turbulence dans la phase fluide des écoulements diphasiques. Leur objectif principal est de capturer les caractéristiques turbulentes de la phase fluide et ils utilisent le concept de viscosité turbulente pour reproduire les effets de la turbulence. Ces modèles calculent la viscosité turbulente dans la phase fluide en utilisant l'énergie cinétique turbulente et le taux de dissipation.

Le développement et la validation numérique du modèle sont divisés en deux étapes. La première étape commence par le scénario d'écoulement monophasique, et joue un rôle crucial pour assurer une intégration précise des modèles de turbulence, des paramètres de traitement près de la paroi et d'autres paramètres essentiels nécessaires pour les simulations multiphases ultérieures. Les résultats CFD de cette section montrent une forte corrélation avec à la fois les données empiriques et les modèles théoriques de perte de charge.

Ensuite, des simulations d'écoulement biphasique ont été réalisées. Le modèle à deux fluides (TFM) est maintenant appliqué pour simuler l'écoulement biphasique. La performance du modèle est étudiée en comparant les résultats aux données expérimentales de la littérature. Deux modèles de turbulence, à savoir le modèle standard k-ε et le modèle k-ω SST, sont testés et leur capacité à fournir des résultats précis est comparée. L'étalonnage et la validation du modèle numérique sont effectués en se référant à la concentration moyenne de particules dans le diamètre vertical et aux profils de vitesse. Les comparaisons entre l'expérience et la simulation portent sur des écoulements de boues avec des concentrations de particules allant de $\phi_s = 0,19$ à $\phi_s = 0,4$. Les tailles de particules se situent dans la plage de $d_p = 4$ μ_m à $d_p = 270$ μ_m. Les résultats CFD ont montré un niveau élevé de correspondance avec les données expérimentales présentées. La performance du modèle numérique est plus investiguée par une comparaison de la variation de la perte de charge par unité de longueur par rapport à la vitesse d'entrée du mélange u_m dans la plage de 2 à 8 (m/s). Les erreurs relatives moyennes globales des pertes de pression sont limitées à 10%. Cela est largement acceptable et démontre la validité du modèle numérique dans la plage

spécifiée de conditions physiques. Il est également remarqué que le modèle k-ω SST est légèrement meilleur que le modèle k-ε pour prédire la perte de charge.

La simulation du transport de sédiments dans les pipelines à l'aide de modèles d'écoulement diphasique est une pratique courante, mais en raison du grand nombre de paramètres d'entrée impliqués, il existe une quantité significative d'incertitude dans les résultats. Il est donc nécessaire de mener une analyse approfondie qui inclut la quantification de l'incertitude (UQ) et l'analyse de sensibilité (SA) pour améliorer la précision des prédictions et quantifier l'importance de chaque paramètre d'entrée. Les résultats de l'étude mettent en lumière l'effet des incertitudes du système sur la consommation d'énergie de l'écoulement de lisier dans les pipelines et soulignent l'importance de prendre en compte ces incertitudes pour optimiser l'efficacité énergétique. Dans ce cadre, cinq paramètres sont considérés comme des variables aléatoires avec une distribution de probabilité donnée sur une plage d'investigation prescrite, basée sur les conditions de fonctionnement de l'écoulement de lisier de phosphate envisagé. L'analyse correspondante concerne les propriétés physiques, géométriques et de modélisation : (i) Tailles des particules, (ii) Concentration solide initiale, (iii) Vitesse d'entrée du mélange d'écoulement, (iv) Inclinaison de la conduite, (v) Coefficient de spécularité. Tout d'abord, nous avons étudié les quantités d'intérêt (QoIs) uniformes et unidimensionnelles résultantes. Les expansions du chaos polynomial généralisé (PCE) pour la quantification de l'incertitude (UQ) et l'analyse de sensibilité (GSA) ont été utilisées pour accomplir cette tâche. Les indices de Sobol' calculés pour la perte de charge perte de chargedémontrent que la variabilité de cette dernière est fortement influencée par les effets de la vitesse du mélange, u_m, et du diamètre des particules, d_p, suivis de près par la concentration initiale des particules ϕ_s. Il a été confirmé que les tailles des particules devraient se situer dans la plage optimale des particules moyennes à fines. Les concentrations solides élevées affectent la friction, mais cela dépend fortement du rapport de la concentration des solides à la concentration maximale déposée. De plus, lorsqu'on opère autour de la vitesse limite de dépôt u_{dl}, il est possible d'augmenter la concentration solide dans la plage proposée de 40% tout en assurant de faibles niveaux de consommation d'énergie. Une découverte intéressante et utile concerne l'effet de l'inclinaison de la conduite θ, nous avons découvert que ce dernier n'affecte pas la perte de charge par friction. De plus, comme prévu, un coefficient de spécularité plus élevé $\mathcal{SC}$ entraîne une augmentation de la perte de charge. Un bon étalonnage de ce paramètre lors de l'étape de validation numérique est essentiel pour garantir des prédictions fiables dans les écoulements de boues.

La deuxième partie de cette étude a porté sur l'analyse de l'incertitude (UQ) et l'analyse de sensibilité globale (GSA) pour un cas bidimensionnel d'écoulement de boue de phosphate. Afin de réduire les coûts de construction du modèle d'expansion du chaos polynomial (PCE), nous avons utilisé la décomposition en composantes orthogonales (POD) pour réduire la dimensionnalité des variables de sortie. Le modèle à ordre réduit a ensuite été appliqué aux équations du mod-

èle à deux fluides bidimensionnel (TFM). De plus, une analyse complète de la sensibilité globale et de l'incertitude a été réalisée pour les grandeurs d'intérêt bidimensionnelles (QOIs). Les distributions de la moyenne et de la variance de nos QOIs ont montré que la boue de phosphate dans ces conditions de fonctionnement est confirmée comme étant un écoulement à deux couches (stratifié). Les techniques PCE ou PCE-POD ont montré que le modèle développé est capable de produire des résultats acceptables pour nos grandeurs statistiques. Elles ont prouvé leur efficacité à reproduire le comportement de l'écoulement de boue.

Finalement, la performance du modèle CFD biphasique développé pour simuler l'écoulement de boue de phosphate est évaluée. Cependant, en raison des défis techniques associés à la réalisation d'expériences à l'échelle pilote, il existe un manque de données expérimentales disponibles pour ce cas d'étude de référence. Par conséquent, les données expérimentales obtenues directement à partir des capteurs pré-installés dans l'usine industrielle sont utilisées pour la comparaison. Les données disponibles comprennent les mesures de cinq capteurs de pression installés le long du pipeline. En conséquence, l'évaluation du modèle est basée uniquement sur sa capacité à prédire la perte de charge.

Cette thèse utilise des modèles de substitution pour aborder les défis computationnels associés aux simulations CFD tridimensionnelles multiphasiques. Un nouveau modèle de substitution basé sur la CFD a été développé pour prédire la perte de charge dans les suspensions en décantation. Le modèle est capable de simuler les écoulements de boues avec des tailles de particules allant de 44 μ_m à 270 μ_m, des concentrations solides allant jusqu'à 40% et des vitesses variant de 2 m/s à 10 m/s. L'exactitude du modèle de substitution a été évaluée en utilisant des données expérimentales de la littérature et a démontré une validité globale acceptable avec une erreur moyenne en pourcentage de 10% ou moins.

Pour estimer la perte de charge d'un écoulement de boue de phosphate dans des pipelines horizontaux et inclinés, une version mise à l'échelle du modèle de substitution a été utilisée pour prendre en compte le plus grand diamètre de la conduite. La perte de charge additionnelle causée par les inclinaisons des conduites a été incluse dans le calcul de la perte de charge totale, en l'ajoutant uniquement à la composante de friction de la perte de charge. La performance du nouveau modèle a été évaluée sur la base de 16 heures de données historiques. Les pertes de pression calculées montrent une bonne concordance avec la tendance des données mesurées, avec une erreur absolue moyenne d'environ 6%. Étant donné les simplifications et les hypothèses sous-jacentes du modèle, ce niveau d'erreur est relativement acceptable. Le modèle développé offre une réduction significative du temps de calcul par rapport au modèle CFD tridimensionnel, tout en maintenant un niveau acceptable de précision.

7.2 Perspectives

Les futures recherches peuvent inclure des améliorations à la fois du modèle et de son application. Cependant, il convient de noter que bien que le modèle développé ait été validé, il reste encore des possibilités d'amélioration :

- L'incorporation de distributions de tailles de particules, par exemple bimodales ou trimodales, dans le modèle peut améliorer sa précision et refléter plus fidèlement le comportement des boues réelles.

- En tenant compte de paramètres physiques et géométriques supplémentaires, la précision et la fiabilité des méthodes d'UQ (Uncertainty Quantification) et GSA (Global Sensitivity Analysis) pour les écoulements de boues peuvent être améliorées.

  La forme des particules solides, qui a un impact sur le coefficient de traînée et la vitesse de décantation, ainsi que les paramètres géométriques tels que le diamètre de la conduite, la rugosité des parois et les coudes peuvent exercer une influence notable sur le comportement de l'écoulement, et doivent donc être incorporés dans l'analyse.

- Pour tenir compte d'une plage de variation plus large et généraliser l'étude à d'autres écoulements de boues, il peut être nécessaire d'échantillonner les paramètres d'entrée sur une plage de valeurs plus large, y compris des valeurs extrêmes qui sont moins susceptibles de se produire mais qui peuvent encore avoir des effets significatifs sur les résultats.

- L'étude de la consommation d'énergie de la pompe en fonction de différents paramètres peut fournir une mesure plus représentative de l'efficacité énergétique du transport de boues.

- De plus, l'utilisation de modèles de substitution PCE (Polynomial Chaos Expansion) pour approximer le comportement de l'écoulement de boues et faire des prédictions pour des paramètres d'intérêt spécifiques peut être une approche précieuse.

- Pour améliorer la précision du modèle de substitution utilisé pour la comparaison avec les données industrielles, des mesures expérimentales supplémentaires peuvent être réalisées et d'autres propriétés d'écoulement pertinentes peuvent être incorporées lors de la construction du modèle.

- Une investigation plus approfondie de l'approche d'échelle pour établir une relation entre l'évolution des paramètres clés d'intérêt et le diamètre de la conduite peut être très bénéfique pour faciliter la construction des modèles de substitution.

- En étudiant le comportement d'échelle, il peut être possible d'identifier des tendances et des motifs dans le comportement de l'écoulement de boues à mesure que le diamètre de la conduite varie.
- Cette information peut être utilisée pour construire des modèles de substitution qui capturent précisément le comportement de l'écoulement de boues sous différents diamètres de conduites, et permettent des prédictions plus précises des paramètres clés d'intérêt.
- De plus, comprendre le comportement d'échelle peut fournir des informations précieuses sur les mécanismes physiques fondamentaux qui gouvernent le comportement de l'écoulement de boues. Cette connaissance peut être utilisée pour améliorer la conception et l'exploitation des systèmes d'écoulement de boues, et aider à optimiser leur performance.
- La réalité du flux de boues de phosphate dans le monde réel utilise des bouchons d'eau pour séparer différentes charges de boues. En incorporant l'effet de ces bouchons sur la variation de densité résultante, il est possible d'utiliser le modèle de substitution pour prédire avec précision la perte de charge le long de la canalisation principale.

Toutes ces améliorations peuvent contribuer à atteindre l'objectif principal de créer un jumeau numérique du processus de transport de boues, en particulier en créant un jumeau numérique plus précis et représentatif.

• Appendices •

A

Phosphate slurry properties

The density value relevant for slurry calculations is the dry density of the solid. OCP phosphate ore, solids density ϱ_s = typically 3.0 t/m^3. For OCP phosphate ore, porosity is typically 20%. It is calculated as follow:

$$P = \frac{V_V}{V_T} \tag{A.1}$$

Where, V_V is voids volume and V_T is the total volume (void + solid). Note that size of pores is « $1\mu_m$, but make up significant fraction of total volume. In the slurry, the pores fill with water which results in an "effective" density as presented bellow:

$$\varrho_{s\text{" effective"}} = (1 - P) \times \varrho_s + P \times \rho_w \tag{A.2}$$

The solids density of the OCP slurry is 3.0 t/m^3 with a porosity of 20%. As a result, the "effective" solids density is 2.6 t/m^3. The shapes of the particles in question are generally non-spherical, and their sizes vary. Granulometric analysis is conventionally used to measure particle sizes, and in this particular case, it was used to measure particles with a diameter greater than 45 μm. The first step in the analysis is to obtain a representative sample of the material to be analyzed. The sample is then dried and sieved through a set of standardized sieves with progressively smaller mesh sizes. The sieves are stacked in order of decreasing mesh size, with the largest mesh size at the top and the smallest at the bottom. Figure A.1 describe the process of the determining the particle size distribution. A dry sample is placed on top of a stack of sieves, with each sieve having an aperture size that determines the mass of particles retained on it. The size distribution of the particles can then be calculated using the weight percentages of each fraction.

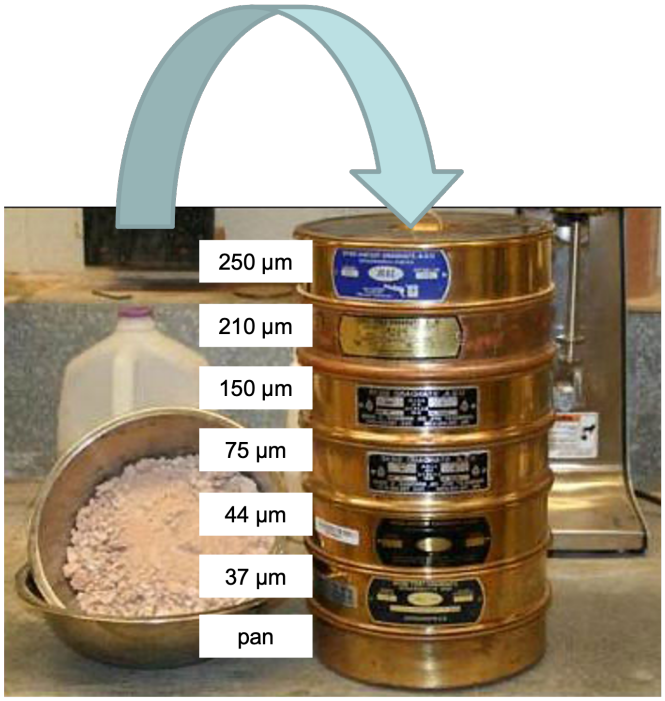

Figure A.1: Classification of particle sizes based on a granulometric analysis

The results on the granulometric analysis is summarized in the table A.1. The

Table A.1: Dry sample granulometric analysis results

Sieve size	Mass retained	% Retained	% Passing
250μm	0 g	0%	100%
210μm	15 g	3%	97%
150μm	115 g	23%	74%
75μm	215 g	43%	31%
44μm	55 g	11%	20%
37μm	15 g	3%	17%
pan	85 g	17%	0%

information gathered from the dry sample granulometric analysis can be used to compute diverse parameters that offer valuable insights into the particle size distribution of the material under investigation. These parameters can assist in comparing experimental data with simulation results. For instance, one can determine the average size of the particles, as well as the median particle size d_{50} and the uniformity coefficient that quantifies the degree of variation in particle sizes.

B

The drag coefficient of a particle in an infinite volume

The drag coefficient of a single sphere in an infinite medium can be described as a function of the particle Reynolds number, denoted as Re_p. As the value of Re_p increases, different regimes can be identified. In the Stokes regime (as Re_p approaches 0), the drag coefficient, denoted as $C_{d,s}$, can be approximated by $24/\mathrm{Re}_p$. There is also an intermediate regime, and a constant drag coefficient regime (when $700 < \mathrm{Re}_p < 2 \times 10^5$).

Various empirical or semiempirical expressions have been proposed in literature to approximate the drag coefficient for a single sphere in an infinite medium Cheng [2009], Clift et al. [2005]. Some of the most commonly-used expressions are listed below.

1. Schiller [1933]

$$C_{d,s} = \begin{cases} 24\left(1 + 0.15\,\mathrm{Re}_p^{0.687}\right)/\mathrm{Re}_p & \text{if } \mathrm{Re}_p \leqslant 1000 \\ 0.44 & \text{if } \mathrm{Re}_p > 1000 \end{cases} \tag{B.1}$$

2. Abraham [1970] [$\mathrm{Re}_p < 6 \cdot 10^3$] :

$$C_{d,s} = 0.2924\left(1 + \frac{9.06}{\mathrm{Re}_p^{1/2}}\right)^2 \tag{B.2}$$

3. Brauer [1971] [$\mathrm{Re}_p < 3 \cdot 10^5$] :

$$C_{d,s} = 0.40 + \frac{4}{\mathrm{Re}_p^2} + \frac{24}{\mathrm{Re}_p} \tag{B.3}$$

4. Cheng [2009] [$\mathrm{Re}_p < 2 \cdot 10^5$] :

$$C_{d,s} = \frac{24}{\mathrm{Re}_p}\left(1 + 0.27\mathrm{Re}_p\right)^{0.43} + 0.47\left[1 - \exp\left(-0.04\mathrm{Re}_p^{0.38}\right)\right] \tag{B.4}$$

5. Dellavalle [1948]

$$C_{d,s} = \left(0.63 + 4.8\sqrt{\frac{1}{\mathrm{Re}_p}}\right)^2 \tag{B.5}$$

6. Singh et al. [2022] [$\mathrm{Re}_p < 10^4$] :

$$C_{d,s} = 0.36 + \frac{5.48}{\mathrm{Re}_p^{0.573}} + \frac{24}{\mathrm{Re}_p} \tag{B.6}$$

7. Lapple and Shepherd [1940] [$\mathrm{Re}_p < 10^3$] :

$$C_{d,s} = \frac{24}{\mathrm{Re}_p}\left(1 + 0.125\,\mathrm{Re}_p^{0.72}\right) \tag{B.7}$$

8. Kürten et al. [1966] [$0.1 < \mathrm{Re}_p < 4 \cdot 10^3$] :

$$C_{d,s} = 0.28 + \frac{6}{\mathrm{Re}_p^{1/2}} + \frac{21}{\mathrm{Re}_p} \tag{B.8}$$

Bibliography

Abd Al Aziz, A. I., and Mohamed, H. I. A study of the factors affecting transporting solid–liquid suspension through pipelines. *Open Journal of Fluid Dynamics*, 2013, 2013.

Abraham, F. F. Functional dependence of drag coefficient of a sphere on reynolds number. *The Physics of Fluids*, 13(8):2194–2195, 1970.

Akhtar, A., Pareek, V., and Tadé, M. CFD simulations for continuous flow of bubbles through gas-liquid columns: Application of vof method. *Chemical Product and Process Modeling*, 2, 01 2007.

Al-Yaari, M. A., and Abu-Sharkh, B. F. CFD prediction of stratified oil-water flow in a horizontal pipe. *Asian Transactions on Engineering*, 1(5):68–75, 2011.

Alghosoun, A., Mocayd, N. E., and Seaid, M. A nonintrusive reduced-order model for uncertainty quantification in numerical solution of one-dimensional free-surface water flows over stochastic beds. *International Journal of Computational Methods*, 19(04):2150073, 2022.

Antaya, C. L., Adane, K. F. K., and Sanders, R. S. Modelling concentrated slurry pipeline flows. In *Fluids Engineering Division Summer Meeting*, volume 44755, pages 1659–1671. American Society of Mechanical Engineers, 2012.

Armenio, V., Piomelli, U., and Fiorotto, V. Effect of the subgrid scales on particle motion. *Physics of Fluids*, 11(10):3030–3042, 1999.

Arolla, S. K., and Desjardins, O. Transport modeling of sedimenting particles in a turbulent pipe flow using Euler–Lagrange large eddy simulation. *International Journal of Multiphase Flow*, 75:1 – 11, 2015.

Ashgriz, N., and Mostaghimi, J. An introduction to computational fluid dynamics. *Fluid flow handbook*, 1:1–49, 2002.

Auton, T. R., Hunt, J. C. R., and Prud'Homme, M. The force exerted on a body in inviscid unsteady non-uniform rotational flow. *Journal of Fluid Mechanics*, 197:241–257, 1988.

Bakker, A., Haidari, A., and Oshinowo, L. Realize greater benefits from CFD. *Chemical Engineering Progress*, 97:45–53, 03 2001.

Balabanov, V., Grossman, B., Watson, L., Mason, W., and Haftka, R. Multifidelity response surface model for hsct wing bending material weight. In *7th AIAA/USAF/NASA/ISSMO Symposium on Multidisciplinary Analysis and Optimization*, page 4804, 1998.

Basirat, S., and Salehi Neyshabouri, S. A. A. Eulerian–Eulerian model application to simulate scouring downstream of sluice gate. *Iranian Journal of Science and Technology, Transactions of Civil Engineering*, 41(2):197–203, 2017.

Benjelloun, S., Desvillettes, L., Ghidaglia, J., and Nielsen, K. Modeling and simulation of thick sprays through coupling of a finite volume euler equation solver and a particle method for a disperse phase. *Note di Matematica*, 32(1): 63–85, 2012.

Berveiller, M. *Eléments finis stochastiques: approches intrusive et non intrusive pour des analyses de fiabilité*. PhD thesis, Université Blaise Pascal-Clermont-Ferrand II, 2005.

Berveiller, M., Sudret, B., and Lemaire, M. Stochastic finite element: a non intrusive approach by regression. *European Journal of Computational Mechanics/Revue Européenne de Mécanique Numérique*, 15(1-3):81–92, 2006.

Blatman, G., and Sudret, B. An adaptive algorithm to build up sparse polynomial chaos expansions for stochastic finite element analysis. *Probabilistic Engineering Mechanics*, 25(2):183–197, 2010.

Blatman, G., and Sudret, B. Adaptive sparse polynomial chaos expansion based on least angle regression. *Journal of Computational Physics*, 230(6):2345–2367, 2011a.

Blatman, G., and Sudret, B. Principal component analysis and least angle regression in spectral stochastic finite element analysis. In *Proc. 11th Int. Conf. on Applications of Stat. and Prob. in Civil Engineering (ICASP11), Zurich, Switzerland*, 2011b.

Bloch, G., and Denoeux, T. Neural networks for process control and optimization: Two industrial applications. *ISA transactions*, 42(1):39–51, 2003.

Bordet, A., Poncet, S., Poirier, M., and Galanis, N. Advanced numerical modeling of turbulent ice slurry flows in a straight pipe. *International Journal of Thermal Sciences*, 127:294–311, 2018.

Bossio, B. M., Blanco, A. J., and Hernandez, F. H. Eulerian-Eulerian modeling of non-newtonian slurries flow in horizontal pipes, 2009.

Boukharfane, R., Er-Raiy, A., Parsani, M., and Chakraborty, N. Structure and dynamics of small-scale turbulence in vaporizing two-phase flows. *Scientific reports*, 11(1):15242, 2021.

Brauer, H. *Grundlagen der Einphasen-und Mehrphasenströmungen*, volume 2. Sauerländer, 1971.

Brennen, C. E., and Brennen, C. E. *Fundamentals of multiphase flow*. Cambridge university press, 2005.

Capecelatro, J., and Desjardins, O. Eulerian–Lagrangian modeling of turbulent liquid–solid slurries in horizontal pipes. *International Journal of Multiphase Flow*, 55:64–79, 10 2013.

Carnahan, N. F., and Starling, K. E. Equation of state for nonattracting rigid spheres. *The Journal of Chemical Physics*, 51:635–0, 1969.

Chauchat, J., Cheng, Z., Nagel, T., Bonamy, C., and Hsu, T.-J. SedFoam-2.0: a 3-D two-phase flow numerical model for sediment transport. *Geoscientific Model Development*, 10:4367–4392, 11 2017.

Chen, L., Duan, Y., Pu, W., and Zhao, C. CFD simulation of coal-water slurry flowing in horizontal pipelines. *Korean Journal of Chemical Engineering*, 26: 1144–1154, 07 2009a.

Chen, L., Duan, Y., Pu, W., and Zhao, C. CFD simulation of coal-water slurry flowing in horizontal pipelines. *Korean journal of chemical engineering*, 26(4): 1144–1154, 2009b.

Chen, R.-C. *Experimental and numerical studies of solid-liquid multiphase flow in pipes*. Case Western Reserve University, 1991.

Cheng, N.-S. Comparison of formulas for drag coefficient and settling velocity of spherical particles. *Powder Technology*, 189(3):395–398, 2009.

Chevreuil, M., and Nouy, A. Model order reduction based on proper generalized decomposition for the propagation of uncertainties in structural dynamics. *International Journal for Numerical Methods in Engineering*, 89(2):241–268, 2012.

Clift, R., Grace, J. R., and Weber, M. E. *Bubbles, drops, and particles*. Courier Corporation, 2005.

Crowe, C. T., Schwarzkopf, J. D., Sommerfeld, M., and Tsuji, Y. *Multiphase flows with droplets and particles*. CRC press, 2011.

Dellavalle, J. Micrometrics: The technology of fine particles. *Pitman: London, UK*, 1948.

Deman, G., Konakli, K., Sudret, B., Kerrou, J., Perrochet, P., and Benabderrahmane, H. Using sparse polynomial chaos expansions for the global sensitivity analysis of groundwater lifetime expectancy in a multi-layered hydrogeological model. *Reliability Engineering & System Safety*, 147:156–169, 2016.

Dinescu, C., Smirnov, S., Hirsch, C., and Lacor, C. Assessment of intrusive and non-intrusive non-deterministic CFD methodologies based on polynomial chaos expansions. *International Journal of Engineering Systems Modelling and Simulation*, 2(1-2):87–98, 2010.

Dixit, S., Kumar, S., Pradhan, A. R., Kumar, S., Kumar, K., Vatin, N. I., Miroshnikova, T., and Epifantsev, K. Numerical simulation of sand–water slurry flow through pipe bend using CFD. *International Journal on Interactive Design and Manufacturing (IJIDeM)*, pages 1–13, 2022.

Drew, D., and Lahey Jr, R. The virtual mass and lift force on a sphere in rotating and straining inviscid flow. *International Journal of Multiphase Flow*, 13(1): 113–121, 1987.

Drew, D. A. Mathematical modeling of two-phase flow. *Annual review of fluid mechanics*, 15(1):261–291, 1983.

Dubreuil, S., Berveiller, M., Petitjean, F., and Salaün, M. Construction of bootstrap confidence intervals on sensitivity indices computed by polynomial chaos expansion. *Reliability Engineering & System Safety*, 121:263–275, 2014.

Dufek, J., and Bergantz, G. W. Suspended load and bed-load transport of particle-laden gravity currents: the role of particle–bed interaction. *Theoretical and Computational Fluid Dynamics*, 21:119–145, 03 2007.

Durand, R. J. Basic relationships of the transportation of solids in pipes-experimental research. *Intern. Assoc. Hydr. Res., 5th Congr. Minneapolis, 1953*, 1953.

Durlofsky, L. J. Use of reduced-order modeling procedures for production optimization. *SPE Journal*, 15(02):426–435, 2010.

Efron, B., Hastie, T., Johnstone, I., and Tibshirani, R. Least angle regression. *The Annals of Statistics*, 32(2):407–499, 2004.

Ekambara, K., Sanders, R. S., Nandakumar, K., and Masliyah, J. H. Hydrodynamic simulation of horizontal slurry pipeline flow using ansys-cfx. *Industrial & Engineering Chemistry Research*, 48:8159–8171, 09 2009.

El Hamra, F. E.-Z., and Boukharfane, R. Development and assessment of algorithms for DEM-LES simulations of fluidized bed. *Particuology*, 2023a.

El Hamra, F. E.-Z., and Boukharfane, R. Numerical study of a single-spout and Z-shaped fluidized bed biomass gasifier. In *Computer Aided Chemical Engineering*, volume 52, pages 139–144. Elsevier, 2023b.

El Moçayd, N., and Seaid, M. Data-driven polynomial chaos expansions for characterization of complex fluid rheology: Case study of phosphate slurry. *Reliability Engineering & System Safety*, 216:107923, 2021.

El Moçayd, N., Ricci, S., Goutal, N., Rochoux, M. C., Boyaval, S., Goeury, C., Lucor, D., and Thual, O. Polynomial surrogates for open-channel flows in random steady state. *Environmental Modeling & Assessment*, 23:309–331, 2018a.

El Moçayd, N., Mohamed, M. S., Ouazar, D., and Seaid, M. Stochastic model reduction for polynomial chaos expansion of acoustic waves using proper orthogonal decomposition. *Reliability Engineering & System Safety*, 195:106733, 2020.

El Mocayd, N., Mohamed, M. S., and Seaid, M. Non-intrusive polynomial chaos methods for uncertainty quantification in wave problems at high frequencies. *Journal of Computational Science*, 53:101344, 2021.

El Moçayd, N., Ricci, S., Goutal, N., Rochoux, M. C., Boyaval, S., Goeury, C., Lucor, D., and Thual, O. Polynomial surrogates for open-channel flows in random steady state. *Environmental Modeling & Assessment*, 23:309–331, 2018b.

Elkarii, M., Bouallou, C., and Ratnani, A. Towards modelling a diphasic flow using the CFD technique to achieve a digital twin of a phosphate slurry piping process. *Chemical Engineering Transactions*, 2020.

Elkarii, M., Boukharfane, R., Benjelloun, S., and Bouallou, C. A CFD-based surrogate model for predicting slurry pipe flow pressure drops. *Particulate Science and Technology*, 41(3):432–442, 2023a.

Elkarii, M., Boukharfane, R., Benjelloun, S., Bouallou, C., and El Moçayd, N. Global sensitivity analysis for phosphate slurry flow in pipelines using generalized polynomial chaos. *Physics of Fluids*, 35(6), 2023b.

Elkarii, M., Boukharfane, R., Benjelloun, S., Bouallou, C., and El Moçayd, N. A gPC-based global sensitivity analysis for phosphate slurry flow in pipelines. In *Computer Aided Chemical Engineering*, volume 52, pages 367–373. Elsevier, 2023c.

Enwald, H., Peirano, E., and Almstedt, A.-E. Eulerian two-phase flow theory applied to fluidization. *International Journal of Multiphase Flow*, 22:21–66, 1996.

Fernandes, F. A. Optimization of fischer-tropsch synthesis using neural networks. *Chemical Engineering & Technology: Industrial Chemistry-Plant Equipment-Process Engineering-Biotechnology*, 29(4):449–453, 2006.

Ghanem, R. G., and Spanos, P. D. *Stochastic finite elements: a spectral approach*. Courier Corporation, 2003.

Gidaspow, D. Multiphase flow and fluidization: Continuum and kinetic theory descriptions. *The Canadian Journal of Chemical Engineering*, 73:784–784, 1994.

Gidaspow, D., Bezburuah, R., and Ding, J. Hydrodynamics of circulating fluidized beds: kinetic theory approach. Technical report, Illinois Inst. of Tech., Chicago, IL (United States). Dept. of Chemical ..., 1991.

Gillies, R. G., Shook, C. A., and Xu, J. Modelling heterogeneous slurry flows at high velocities. *The Canadian Journal of Chemical Engineering*, 82(5):1060–1065, 2004.

Gillies, R. G., and Shook, C. A. Modelling high concentration settling slurry flows. *The Canadian Journal of Chemical Engineering*, 78, 2000.

Gillies, R. G. *Pipeline flow of coarse particle slurries*. Citeseer, 1993.

Gillies, R., Shook, C., and Wilson, K. An improved two layer model for horizontal slurry pipeline flow. *The Canadian Journal of Chemical Engineering*, 69(1): 173–178, 1991.

Giunta, A. A., Balabanov, V., Haim, D., Grossman, B., Mason, W. H., Watson, L. T., and Haftka, R. T. Multidisciplinary optimisation of a supersonic transport using design of experiments theory and response surface modelling. *The Aeronautical Journal*, 101(1008):347–356, 1997.

Gopaliya, M. K., and Kaushal, D. R. Analysis of effect of grain size on various parameters of slurry flow through pipeline using CFD. *Particulate Science and Technology*, 33(4):369–384, 2015.

Gopaliya, M. K., and Kaushal, D. R. Modeling of sand-water slurry flow through horizontal pipe using CFD. *Journal of Hydrology and Hydromechanics*, 64(3): 261, 2016.

Guo, Y., Li, X., Sun, Y., Yang, Y., Fang, Y., and Li, H. Investigation into the flow characteristics of slurry shield pipeline system under sandy pebble stratum: Model test and CFD-DEM simulation. *Powder Technology*, 415:118149, 2023.

Hadinoto, K. Predicting turbulence modulations at different Reynolds numbers in dilute-phase turbulent liquid–particle flow simulations. *Chemical engineering science*, 65(19):5297–5308, 2010.

Hashemi, S. A., Spelay, R. B., Adane, K. F. K., and Sean Sanders, R. Solids velocity fluctuations in concentrated slurries. *The Canadian Journal of Chemical Engineering*, 94:1059–1065, 06 2016a.

Hashemi, S. A., Spelay, R. B., Adane, K. F., and Sean Sanders, R. Solids velocity fluctuations in concentrated slurries. *The Canadian Journal of Chemical Engineering*, 94(6):1059–1065, 2016b.

Hernandez, F. H., Blanco, A. J., and Rojas-Solorzano, L. CFD modeling of slurry flows in horizontal pipes. In *Fluids Engineering Division Summer Meeting*, volume 48401, pages 857–863, 2008.

Hiltunen, K., Jäsberg, A., Kallio, S., Karema, H., Kataja, M., Koponen, A., Manninen, M., and Taivassalo, V. Multiphase flow dynamics. *Theory and Numerics. Tech. Rep*, 722, 2009.

Hoyt, J. Scale-up from laboratory pipe-flow data to large flows. In *Fluids Engineering Division Summer Meeting*, volume 36967, pages 745–749, 2003.

Hrenya, C. M., and Sinclair, J. L. Effects of particle-phase turbulence in gas-solid flows. *AIChE Journal*, 43:853–869, 1997.

Ishii, M. Thermo-fluid dynamic theory of two-phase flow. *NASA Sti/recon Technical Report A*, 75:29657, 1975.

Ishii, M., and Mishima, K. Two-fluid model and hydrodynamic constitutive relations. *Nuclear Engineering and design*, 82(2-3):107–126, 1984.

Jamshidi, R., Angeli, P., and Mazzei, L. On the closure problem of the effective stress in the Eulerian-Eulerian and mixture modeling approaches for the simulation of liquid-particle suspensions. *Physics of Fluids*, 31(1):013302, 2019.

Jiang, Y., and Zhang, P. Pressure drop and flow pattern of slush nitrogen in a horizontal pipe. *AIChE journal*, 59(5):1762–1773, 2013.

Jiang, Y., and Zhang, P. Numerical investigation of slush nitrogen flow in a horizontal pipe. *Chemical Engineering Science*, 73:169–180, 2012.

Jing, L., Kwok, C. Y., Leung, Y. F., and Sobral, Y. D. Extended CFD-DEM for free-surface flow with multi-size granules. *International Journal for Numerical and Analytical Methods in Geomechanics*, 40:62–79, 01 2016.

Johnson, P. C., and Jackson, R. Frictional–collisional constitutive relations for granular materials, with application to plane shearing. *Journal of Fluid Mechanics*, 176:67–93, 1987.

Joshi, T., Parkash, O., and Krishan, G. Slurry flow characteristics through a horizontal pipeline at different prandtl number. *Powder Technology*, 413:118008, 2023.

Kaushal, D., and Tomita, Y. Experimental investigation for near-wall lift of coarser particles in slurry pipeline using γ-ray densitometer. *Powder technology*, 172(3):177–187, 2007.

Kaushal, D., Sato, K., Toyota, T., Funatsu, K., and Tomita, Y. Effect of particle size distribution on pressure drop and concentration profile in pipeline flow of highly concentrated slurry. *International Journal of Multiphase Flow*, 31(7): 809–823, 2005.

Kaushal, D., Thinglas, T., Tomita, Y., Kuchii, S., and Tsukamoto, H. CFD modeling for pipeline flow of fine particles at high concentration. *International Journal of Multiphase Flow*, 43:85–100, 2012.

Kaushal, D., Kumar, A., Tomita, Y., Kuchii, S., and Tsukamoto, H. Flow of mono-dispersed particles through horizontal bend. *International Journal of Multiphase Flow*, 52:71–91, 6 2013.

Kim, J., and Hwangbo, H. Sensor-based optimization model for air quality improvement in home iot. *Sensors*, 18(4):959, 2018.

Klausner, J. F., Fu, F., and Mei, R. A conductance based solids concentration sensor for large diameter slurry pipelines. *J. Fluids Eng.*, 122(4):819–824, 2000.

Kleijnen, J. P. C. Design and analysis of simulation experiments. In *International Workshop on Simulation*, pages 3–22. Springer, 2015.

Krampa, F. N. *Two-fluid modelling of heterogeneous coarse particle slurry flows*. PhD thesis, University of Saskatchewan, 2009.

Kumar, N., Gopaliya, M. K., and Kaushal, D. R. Experimental investigations and CFD modeling for flow of highly concentrated iron ore slurry through horizontal pipeline. *Particulate Science and Technology*, 37(2):232–250, 2019.

Kumar, S., Duduković, M., and Toseland, B. Measurement techniques for local and global fluid dynamic quantities in two and three phase systems. In *Non-invasive monitoring of multiphase flows*, pages 1–45. Elsevier, 1997.

Kumar, U., Mishra, R., Singh, S., and Seshadri, V. Effect of particle gradation on flow characteristics of ash disposal pipelines. *Powder Technology*, 132(1): 39–51, 5 2003.

Kürten, H., Raasch, J., and Rumpf, H. Beschleunigung eines kugelförmigen feststoffteilchens im strömungsfeld konstanter geschwindigkeit. *Chemie Ingenieur Technik*, 38(9):941–948, 1966.

Lahiri, S. K., and Ghanta, K. C. Regime identification of slurry transport in pipelines: A novel modelling approach using ANN & differential evolution. *Chemical Industry and Chemical Engineering Quarterly*, 16(4):329–343, 2010a.

Lahiri, S., and Ghanta, K. Regime identification of slurry transport in pipelines: A novel modelling approach using ann & differential evolution. *Chemical Industry and Chemical Engineering Quarterly*, 16:329–343, 2010b.

Laín, S., and Sommerfeld, M. Euler/Lagrange computations of pneumatic conveying in a horizontal channel with different wall roughness. *Powder Technology*, 184(1):76–88, 2008.

Lapple, C., and Shepherd, C. Calculation of particle trajectories. *Industrial & Engineering Chemistry*, 32(5):605–617, 1940.

Launder, B. E., and Spalding, D. B. The numerical computation of turbulent flows. In *Numerical prediction of flow, heat transfer, turbulence and combustion*, pages 96–116. Elsevier, 1983.

Le Maıtre, O. P., Knio, O. M., Debusschere, B. J., Najm, H. N., and Ghanem, R. G. A multigrid solver for two-dimensional stochastic diffusion equations. *Computer Methods in Applied Mechanics and Engineering*, 192(41-42):4723–4744, 2003.

Levenberg, K. A method for the solution of certain non-linear problems in least squares. *Quarterly of Applied Mathematics*, 2(2):164–168, 1944.

Li, M.-z., He, Y.-p., Liu, Y.-d., and Huang, C. Hydrodynamic simulation of multi-sized high concentration slurry transport in pipelines. *Ocean Engineering*, 163: 691–705, 07 2018.

Lin, C., and Ebadian, M. A numerical study of developing slurry flow in the entrance region of a horizontal pipe. *Computers & Fluids*, 37:965–974, 2008.

Ling, J., Skudarnov, P., Lin, C., and Ebadian, M. Numerical investigations of liquid–solid slurry flows in a fully developed turbulent flow region. *International Journal of Heat and Fluid Flow*, 24:389–398, 2003.

Liu, W., He, Y., Li, M., Chen, Q., Liu, Y., and Huang, C. Computational fluid dynamics modeling of slurry flow in horizontal pipes: Effect of specularity coefficient on hydraulic gradient. *Ocean Engineering*, 238:109–625, 2021.

Loth, E. Particles, drops and bubbles: Fluid dynamics and numerical methods. *Particles, Drops and Bubbles: Fluid Dynamics and Numerical Methods*, 2010.

Lun, C. K. K., Savage, S. B., Jeffrey, D. J., and Chepurniy, N. Kinetic theories for granular flow: inelastic particles in couette flow and slightly inelastic particles in a general flowfield. *Journal of Fluid Mechanics*, 140:223–256, 1984.

Lun, C., and Savage, S. The effects of an impact velocity dependent coefficient of restitution on stresses developed by sheared granular materials. *Acta Mechanica*, 63(1-4):15–44, 1986.

Manninen, M., Taivassalo, V., and Kallio, S. On the mixture model for multiphase flow, 1996.

Marquardt, D. W. An algorithm for least-squares estimation of nonlinear parameters. *Journal of the Society for Industrial and Applied Mathematics*, 11(2): 431–441, 1963.

Matousek, V. Concentration distribution in pipeline flow of sand-water mixtures. *Vodohospodarsky Casopis*, 48(3):180–196, 2000.

Matousek, V. Pressure drops and flow patterns in sand-mixture pipes. *Experimental thermal and fluid science*, 26(6-7):693–702, 2002.

Matoušek, V., Krupička, J., Konfršt, J., and Pěník, V. Internal structure of settling-slurry flows: solids distribution and friction in horizontal pipe. In *Proc. of 16th International Conference on Transport and Sedimentation of Solid Particles, September*, pages 18–20, 2013.

Matoušek, V., Krupička, J., and Kesely, M. A layered model for inclined pipe flow of settling slurry. *Powder Technology*, 333:317–326, 2018.

Matoušek, V., Krupička, J., Konfršt, J., and Penik, V. Internal structure of settling-slurry flows: solids distribution and friction in horizontal pipe, 09 2013.

Matoušek, V., Visintainer, R., Furlan, J., and Sellgren, A. Pipe-size scale-up of frictional head loss in settling slurry flows using predictive models: Experimental validation. In *Fluids Engineering Division Summer Meeting*, volume 83723, page V002T04A026. American Society of Mechanical Engineers, 2020.

Meert, K., and Rijckaert, M. Intelligent modelling in the chemical process industry with neural networks: a case study. *Computers & chemical engineering*, 22:S587–S593, 1998.

Mendygarin, Y., Rojas-Solórzano, L. R., Kussaiyn, N., Supiyev, R., and Zhussupbekov, M. Eulerian-Eulerian multiphase modeling of blood cells segregation in flow through microtubes. In *ASME International Mechanical Engineering Congress and Exposition*, volume 58363, page V003T04A020. American Society of Mechanical Engineers, 2017.

Messa, G. V., Malin, M., and Malavasi, S. [asme asme 2013 pressure vessels and piping conference - paris, france (sunday 14 july 2013)] volume 4: Fluid-structure interaction - numerical prediction of pressure gradient of slurry flows in horizontal pipes, 2013.

Messa, G. V., Yang, Q., Adedeji, O. E., Chára, Z., Duarte, C. A. R., Matoušek, V., Rasteiro, M. G., Sanders, R. S., Silva, R. C., and de Souza, F. J. Computational fluid dynamics modelling of liquid–solid slurry flows in pipelines: State-of-the-art and future perspectives. *Processes*, 9(9):1566, 2021.

Messa, G. V., and Matoušek, V. Analysis and discussion of two fluid modelling of pipe flow of fully suspended slurry. *Powder Technology*, 9 2020.

Molinaro, A. M., Simon, R., and Pfeiffer, R. M. Prediction error estimation: a comparison of resampling methods. *Bioinformatics*, 21(15):3301–3307, 2005.

Moré, J. J. The Levenberg–Marquardt algorithm: Implementation and theory. In *Numerical Analysis*, pages 105–116. Springer, 1978.

Nimana, B., Verma, A., Di Lullo, G., Rahman, M. M., Canter, C. E., Olateju, B., Zhang, H., and Kumar, A. Life cycle analysis of bitumen transportation to refineries by rail and pipeline. *Environmental Science & Technology*, pages 680–691, 11 2016.

Ofei, T. N., Irawan, S., and Pao, W. CFD method for predicting annular pressure losses and cuttings concentration in eccentric horizontal wells. *Journal of Petroleum Engineering*, 2014:1–16, 2014.

Ofei, T. N., and Ismail, A. Y. Eulerian-Eulerian simulation of particle-liquid slurry flow in horizontal pipe. *Journal of Petroleum Engineering*, 2016:1–10, 2016.

Ohira, K., Nakagomi, K., Takahashi, K., and Aoki, I. Pressure-drop reduction and heat-transfer deterioration of slush nitrogen in square pipe flow. *Physics Procedia*, 67:681–686, 2015.

Palmer, K., and Realff, M. Metamodeling approach to optimization of steady-state flowsheet simulations: Model generation. *Chemical Engineering Research and Design*, 80(7):760–772, 2002.

Peker, S., Helvacı, S., Yener, H., Ikizler, B., and Alparslan, A. 4—motion of particles in fluids. *Solid-Liquid Two Phase Flow; Elsevier: Amsterdam, The Netherlands*, pages 245–289, 2008.

Pham Van Bang, D., Lefrançois, E., Sergent, P., and Bertrand, F. Expérimentation par irm et modélisation par éléments finis de la sédimentation-consolidation des vases. *La Houille Blanche*, pages 39–44, 06 2008.

Piminchumo Marinos, O. R., and others, . *numerical simulation of liquid-solid slurry flow using the Eulerian-Eulerian two-fluid model*. PhD thesis, University of Saskatchewan, 2020.

Portela, L. M., and Oliemans, R. V. Eulerian–Lagrangian DNS/LES of particle–turbulence interactions in wall-bounded flows. *International journal for numerical methods in fluids*, 43(9):1045–1065, 2003.

Prosperetti, A., and Tryggvason, G. *Computational methods for multiphase flow*. Cambridge university press, 2009.

Pullum, L., McCarthy, D., and others, . Ultra high concentration and hybrid hydraulic transport systems. In *4th International Conference on Bulk Materials, Storage, Handling and Transportation: 7th International Symposium on Freight Pipelines*, pages 91–95, 1992.

Rabhi, A., Chkifa, A., Benjelloun, S., and Latifi, A. Surrogate-based modeling in flotation processes. *Computer Aided chemical engineering*, 43:229–234, 2018.

Raisee, M., Kumar, D., and Lacor, C. A non-intrusive model reduction approach for polynomial chaos expansion using proper orthogonal decomposition. *International Journal for Numerical Methods in Engineering*, 103(4):293–312, 2015.

Reagana, M. T., Najm, H. N., Ghanem, R. G., and Knio, O. M. Uncertainty quantification in reacting-flow simulations through non-intrusive spectral projection. *Combustion and Flame*, 132(3):545–555, 2003.

Reyes, C., and Ihle, C. F. Numerical simulation of cation exchange in fine-coarse seawater slurry pipeline flow. *Minerals Engineering*, 117:14–23, 2018.

Roco, M. C., and Shook, C. A. Modeling of slurry flow: The effect of particle size. *The Canadian Journal of Chemical Engineering*, 61:494–503, 1983a.

Roco, M., and Shook, C. Modeling of slurry flow: The effect of particle size. *The Canadian Journal of Chemical Engineering*, 61(4):494–503, 1983b.

Rusconi, J., Lakhouaja, A., and Kopuz, M. The design and engineering of the 187 km khouribga to Jorf Lasfar phosphate slurry pipeline. *Procedia Engineering*, 138:142–150, 2016.

Sadeghi, M., Li, S., Zheng, E., Sontti, S. G., Esmaeili, P., and Zhang, X. CFD simulation of turbulent non-newtonian slurry flows in horizontal pipelines. *Industrial & Engineering Chemistry Research*, 61(15):5324–5339, 2022.

Saltelli, A., and Tarantola, S. On the relative importance of input factors in mathematical models: safety assessment for nuclear waste disposal. *Journal of the American Statistical Association*, 97(459):702–709, 2002.

Saltelli, A., Ratto, M., Tarantola, S., and Campolongo, F. Sensitivity analysis practices: Strategies for model-based inference. *Reliability Engineering & System Safety*, 91(10-11):1109–1125, 2006.

Sanders, R., Sun, R., Gillies, R., McKibben, M., Litzenberger, C., and Shook, C. Deposition velocities for particles of intermediate size in turbulent flow. In *Hydrotransport*, volume 16, pages 429–442, 2004.

Schaan, J., Sumner, R. J., Gillies, R. G., and Shook, C. A. The effect of particle shape on pipeline friction for newtonian slurries of fine particles. *The Canadian Journal of Chemical Engineering*, 78, 2000a.

Schaan, J., Sumner, R. J., Gillies, R. G., and Shook, C. A. The effect of particle shape on pipeline friction for newtonian slurries of fine particles. *The Canadian Journal of Chemical Engineering*, 78(4):717–725, 2000b.

Schiller, L. A drag coefficient correlation. *Zeit. Ver. Deutsch. Ing.*, 77:318–320, 1933.

Seong, Y., Park, C., Choi, J., and Jang, I. Surrogate model with a deep neural network toevaluate gas–liquid flow in a horizontal pipe. *Energies*, 13:968, 2020.

Shook, C., and Bartosik, A. Particle—wall stresses in vertical slurry flows. *Powder Technology*, 81:117–124, 1994.

Silva, R., Faia, P., Garcia, F., and Rasteiro, M. Characterization of solid–liquid settling suspensions using electrical impedance tomography: A comparison between numerical, experimental and visual information. *Chemical Engineering Research and Design*, 111:223–242, 07 2016.

Simon, F., Guillen, P., Sagaut, P., and Lucor, D. A gPC-based approach to uncertain transonic aerodynamics. *Computer Methods in Applied Mechanics and Engineering*, 199(17-20):1091–1099, 2010.

Sinclair, J. L., and Jackson, R. Gas-particle flow in a vertical pipe with particle-particle interactions. *AIChE Journal*, 35:1473–1486, 1989.

Singh, H., Kumar, S., and Mohapatra, S. K. Modeling of solid-liquid flow inside conical diverging sections using computational fluid dynamics approach. *International Journal of Mechanical Sciences*, 186:105909, 2020a.

Singh, M. K., Kumar, S., and Ratha, D. Computational analysis on disposal of coal slurry at high solid concentrations through slurry pipeline. *International Journal of Coal Preparation and Utilization*, 40(2):116–130, 2020b.

Singh, N., Kroells, M., Li, C., Ching, E., Ihme, M., Hogan, C. J., and Schwartzentruber, T. E. General drag coefficient for flow over spherical particles. *AIAA journal*, 60(2):587–597, 2022.

Skudarnov, P., Lin, C., and Ebadian, M. Double-species slurry flow in a horizontal pipeline. *J. Fluids Eng.*, 126(1):125–132, 2004.

Sobol, I. M. Sensitivity analysis for non-linear mathematical models. *Mathematical Modelling and Computational Experiment*, 1:407–414, 1993.

Sobol, I. M. Global sensitivity indices for nonlinear mathematical models and their Monte Carlo estimates. *Mathematics and Computers in Simulation*, 55 (1-3):271–280, 2001.

Sontti, S. G., Sadeghi, M., Zhou, K., Zheng, E., and Zhang, X. Computational fluid dynamics investigation of bitumen residues in oil sands tailings transport in an industrial horizontal pipe. *Physics of Fluids*, 35(1):013340, 2023.

Spelay, R., Gillies, R., Hashemi, S., and Sanders, R. Kinematic friction of concentrated suspensions of neutrally buoyant coarse particles. In *Proceedings of the 20th International Conference on Hydrotransport, Melbourne, Australia*, pages 3–5, 2017.

Sudret, B. Global sensitivity analysis using polynomial chaos expansions. *Reliability Engineering & System Safety*, 93(7):964–979, 2008.

Swamee, P. K., and Jain, A. K. Explicit equations for pipe-flow problems. *Journal of the Hydraulics Division*, 102(5):657–664, 1976.

Swamy, M., Díez, N. G., and Twerda, A. Numerical modelling of the slurry flow in pipelines and prediction of flow regimes. *WIT Trans Eng Sci*, 89(2015): 311–322, 2015.

Syamlal, M., Rogers, W., and O'Brien, T. J. Mfix documentation theory guide, 12 1993a.

Syamlal, M., Rogers, W., and O'Brien, T. J. MFIX documentation: Volume 1, theory guide. national technical information service, springfield, va. Technical report, DOE/METC-9411004, NTIS/DE9400087, 1993b.

Turian, R. M., and Yuan, T.-F. Flow of slurries in pipelines. *AIChE Journal*, 23 (3):232–243, 1977.

Uzi, A., and Levy, A. Flow characteristics of coarse particles in horizontal hydraulic conveying. *Powder Technology*, 12 2017.

Versteeg, H. K., and Malalasekera, W. An introduction to computational fluid dynamics: the finite volume method, 2007.

Wan, C., Xiao, S., Zhou, D., Zhu, H., Bao, Y., Kakanda, K., and Han, Z. Numerical simulation on transportation behavior of gradated coarse particles in deep-sea vertical pipe transportation. *Physics of Fluids*, 2023.

Wang, J., Wang, S., Zhang, T., and Liang, Y. Numerical investigation of ice slurry isothermal flow in various pipes. *International Journal of Refrigeration*, 36, 1 2013.

Wang, Y., Hu, K., Ren, L., and Lin, G. Optimal observations-based retrieval of topography in 2d shallow water equations using pc-enkf. *Journal of Computational Physics*, 382:43–60, 2019.

Weber, M. Improved Durand-equation for multiple application. In *International Symposium on Slurry Flows*, 1986.

Weller, H. G., Tabor, G., Jasak, H., and Fureby, C. A tensorial approach to computational continuum mechanics using object-oriented techniques. *Computers in Physics*, 12(6):620–631, 1998.

Wen, C. Y., and Yu, Y. H. A generalized method for predicting the minimum fluidization velocity. *AIChE Journal*, 12(3):610–612, 1966.

Wilcox, D. C. Reassessment of the scale-determining equation for advanced turbulence models. *AIAA Journal*, 26(11):1299–1310, 1988.

Wilcox, D. C. *Turbulence modeling for CFD*, volume 2. DCW industries La Canada, CA, 1998.

Wilson, K. C., and Sellgren, A. Interaction of particles and near-wall lift in slurry pipelines. *Journal of Hydraulic Engineering*, 129(1):73–76, 2003.

Wilson, K. Deposition limit nomograms for particles of various densities in pipeline flow. In *Proc. Hydrotransport*, volume 6, pages 1–12. BHRA Fluid Engineering Bhubaneswar, India, 1979.

Wilson, K. C., Addie, G. R., Sellgren, A., and Clift, R. *Centrifugal Pumps*. Springer, 2006.

Wu, J., Graham, L., Wang, S., and Parthasarathy, R. Energy efficient slurry holding and transport. *Minerals Engineering*, 23(9):705–712, 2010.

Xiu, D., and Karniadakis, G. E. The Wiener–Askey polynomial chaos for stochastic differential equations. *SIAM journal on Scientific Computing*, 24(2):619–644, 2002.

Yamazaki, W., Kato, T., Homma, T., Shimoyama, K., and Obayashi, S. Stochastic tsunami inundation flow simulation via polynomial chaos approach. *Journal of Fluid Science and Technology*, 13(4):JFST0025–JFST0025, 2018.

Yilmaz, F., and Gundogdu, M. Y. Analysis of conventional drag and lift models for multiphase CFD modeling of blood flow. *Korea-Australia Rheology Journal*, 21(3):161–173, 2009.

Yu, K., Lau, K., and Chan, C. Numerical simulation of gas-particle flow in a single-side backward-facing step flow. *Journal of computational and applied mathematics*, 163(1):319–331, 2004.

Zhang, M., Kang, Y., Wei, W., Li, D., and Xiong, T. CFD investigation of the flow characteristics of liquid–solid slurry in a large-diameter horizontal pipe. *Particulate Science and Technology*, 39(6):712–725, 2021.

Zhong, H., Lan, X., Gao, J., Zheng, Y., and Zhang, Z. The difference between specularity coefficient of 1 and no-slip solid phase wall boundary conditions in cfd simulation of gas–solid fluidized beds. *Powder Technology*, 286:740–743, 2015.

Zhou, H., Guo, J., Zhang, T., Li, M., Tang, T., and Gou, H. Eulerian multifluid simulations of proppant transport with different sizes. *Physics of Fluids*, 2023.

Zhou, M., Kuang, S., Luo, K., Zou, R., Wang, S., and Yu, A. Modeling and analysis of flow regimes in hydraulic conveying of coarse particles. *Powder Technology*, 373:543–554, 2020.

RÉSUMÉ

Le transport de boues par pipelines est une méthode courante dans diverses industries en raison de son efficacité et de son caractère écologique. Cela est particulièrement vrai pour le transport de phosphate brut, qui est acheminé des sites d'extraction vers les usines de transformation en engrais. Pour concevoir des systèmes de canalisation de boues efficaces, il est essentiel de comprendre les caractéristiques physiques spécifiques du transport des boues et de pouvoir prédire la dynamique de l'écoulement des boues. La dynamique des fluides numérique (CFD) est devenue une méthode largement utilisée dans les industries pour éviter les coûts et les contraintes techniques des essais expérimentaux, ainsi que les limitations des modèles simplifiés basés sur la physique. Cette thèse a un double objectif. Premièrement, elle vise à développer un modèle généralisé d'écoulement des boues à l'aide de la CFD pour améliorer notre compréhension de l'écoulement des boues de phosphate et essayer de l'approcher par le biais d'une simulation numérique directe. Les modèles CFD bi-fluides sont le seul moyen possible de simuler les écoulements de boues denses, mais leur simulation est difficile et coûteuse. Par conséquent, le développement de modèles de substitution peut être utile pour la simulation et le contrôle des opérations. Une nouvelle corrélation de la perte de charge pour les écoulements solide-liquide basée sur des calculs numériques est proposée, et sa performance est évaluée par des comparaisons avec des données expérimentales provenant de l'industrie OCP. Cette approche a permis d'intégrer le modèle développé au niveau industriel. Deuxièmement, un étalonnage minutieux et une compréhension des différents paramètres physiques ainsi que de leur interaction pour minimiser la consommation d'énergie sont cruciaux pour optimiser et sécuriser les opérations de pipeline. De plus, les solutions numériques pour les écoulements de suspensions sont souvent soumises à des incertitudes découlant des conditions initiales et des conditions aux limites dans les modèles mathématiques utilisés. Dans cette étude, des expansions en chaos polynomial sont proposées pour estimer l'incertitude inhérente à l'écoulement souhaité de la suspension et effectuer une analyse de sensibilité de l'efficacité énergétique de l'écoulement. Les résultats révèlent que les variations de la vitesse du mélange et de la taille des particules jouent un rôle essentiel dans la détermination de l'efficacité énergétique. Par conséquent, le contrôle de ces facteurs représente une étape critique pour assurer le transport efficace et sécurisé de la suspension à travers les pipelines.

MOTS CLÉS

Écoulement de Phosphate, Simulation Numérique, Quantification de l'Incertitude, Analyse de Sensibilité

ABSTRACT

The transportation of slurries through pipelines is widely used in various industries due to its high efficiency and environmentally friendly nature. This is particularly true for the transportation of raw phosphate, which is conveyed from extraction points to fertilizer processing plants. To design effective slurry pipeline systems, it is essential to have a thorough understanding of the specific physical features of slurry transport and to be able to predict the physics of the slurry flow. In recent years, Computational Fluid Dynamics (CFD) has become a commonly-used approach due to the technical and economic burden of experimental tests, and the limited generalizability of many simplified physically-based models. The aim of this thesis is twofold. Firstly, it aims to develop a generalized slurry flow model using CFD to improve our understanding of phosphate slurry flow and approach it through direct numerical simulation. The two-fluid CFD models are the only possible way to simulate dense slurry flows, however, simulating real slurry pipe flows is challenging due to their high computational costs. Therefore, developing surrogate models can be useful in operations simulation and monitoring tools. A new two-phase pressure drop correlation based on numerical computations is proposed, and its performance is assessed via comparisons with experimental data from the industrial plant. Secondly, careful calibration and understanding of several physical parameters and their interplay to minimize energy losses is crucial to optimize and secure pipeline operations. Moreover, numerical solutions for slurry flows are frequently subject to uncertainties arising from the initial and boundary conditions in the mathematical models employed. In this study, polynomial chaos expansions (PCE) are proposed to estimate the uncertainty inherent in the desired slurry flow and perform a sensitivity analysis of flow energy efficiency. This comprehensive analysis that addresses uncertainty quantification (UQ) and sensitivity analysis (SA) is essential to improve prediction reliability. The findings reveal that variations in slurry velocity and particle size play a pivotal role in determining energy efficiency. Therefore, controlling these factors represents a critical step in ensuring the efficient and safe transportation of slurry through pipelines.

KEYWORDS

Phosphate Slurry Flow, CFD Simulation, Surrogate Modeling, Uncertainty Quantification, Sensitivity Analysis